THE UNIVERSITY OF WARWICK

Library Declaration and Deposit Agreement

1. STUDENT DETAILS

Please complete the following:

Full name: Gun Antonia Evelina Nilsson Lock

University ID number: 0227973

2. THESIS DEPOSIT

2.1 I understand that under my registration at the University, I am required to deposit my thesis with the University in BOTH hard copy and in digital format. The digital version should normally be saved as a single pdf file.

2.2 The hard copy will be housed in the University Library. The digital version will be deposited in the University's Institutional Repository (WRAP). Unless otherwise indicated (see 2.3 below) this will be made openly accessible on the Internet and will be supplied to the British Library to be made available online via its Electronic Theses Online Service (EThOS) service.
[At present, theses submitted for a Master's degree by Research (MA, MSc, LLM, MS or MMedSci) are not being deposited in WRAP and not being made available via EthOS. This may change in future.]

2.3 In exceptional circumstances, the Chair of the Board of Graduate Studies may grant permission for an embargo to be placed on public access to the hard copy thesis for a limited period. It is also possible to apply separately for an embargo on the digital version. (Further information is available in the *Guide to Examinations for Higher Degrees by Research*.)

2.4 *If you are depositing a thesis for a Master's degree by Research, please complete section (a) below. For all other research degrees, please complete both sections (a) and (b) below:*

(a) Hard Copy

I hereby deposit a hard copy of my thesis in the University Library to be made publicly available to readers (please delete as appropriate) EITHER immediately ~~OR after an embargo period of ..... months/years as agreed by the Chair of the Board of Graduate Studies.~~

I agree that my thesis may be photocopied. YES / ~~NO~~ (*Please delete as appropriate*)

(b) Digital Copy

I hereby deposit a digital copy of my thesis to be held in WRAP and made available via EThOS.

Please choose one of the following options:

EITHER My thesis can be made publicly available online. YES /~~NO~~ (*Please delete as appropriate*)

~~OR My thesis can be made publicly available only after…..[date] (Please give date)~~
~~YES / NO (*Please delete as appropriate*)~~

~~OR My full thesis cannot be made publicly available online but I am submitting a separately identified additional, abridged version that can be made available online.~~
~~YES / NO (*Please delete as appropriate*)~~

~~OR My thesis cannot be made publicly available online. YES / NO (*Please delete as appropriate*)~~

3. GRANTING OF NON-EXCLUSIVE RIGHTS

Whether I deposit my Work personally or through an assistant or other agent, I agree to the following:

Rights granted to the University of Warwick and the British Library and the user of the thesis through this agreement are non-exclusive. I retain all rights in the thesis in its present version or future versions. I agree that the institutional repository administrators and the British Library or their agents may, without changing content, digitise and migrate the thesis to any medium or format for the purpose of future preservation and accessibility.

4. DECLARATIONS

(a) I DECLARE THAT:

- I am the author and owner of the copyright in the thesis and/or I have the authority of the authors and owners of the copyright in the thesis to make this agreement. Reproduction of any part of this thesis for teaching or in academic or other forms of publication is subject to the normal limitations on the use of copyrighted materials and to the proper and full acknowledgement of its source.

- The digital version of the thesis I am supplying is the same version as the final, hard-bound copy submitted in completion of my degree, once any minor corrections have been completed.

- I have exercised reasonable care to ensure that the thesis is original, and does not to the best of my knowledge break any UK law or other Intellectual Property Right, or contain any confidential material.

- I understand that, through the medium of the Internet, files will be available to automated agents, and may be searched and copied by, for example, text mining and plagiarism detection software.

(b) IF I HAVE AGREED (in Section 2 above) TO MAKE MY THESIS PUBLICLY AVAILABLE DIGITALLY, I ALSO DECLARE THAT:

- I grant the University of Warwick and the British Library a licence to make available on the Internet the thesis in digitised format through the Institutional Repository and through the British Library via the EThOS service.

- If my thesis does include any substantial subsidiary material owned by third-party copyright holders, I have sought and obtained permission to include it in any version of my thesis available in digital format and that this permission encompasses the rights that I have granted to the University of Warwick and to the British Library.

5. LEGAL INFRINGEMENTS

I understand that neither the University of Warwick nor the British Library have any obligation to take legal action on behalf of myself, or other rights holders, in the event of infringement of intellectual property rights, breach of contract or of any other right, in the thesis.

Please sign this agreement and return it to the Graduate School Office when you submit your thesis.

Student's signature: .....  ..... Date: 02-07-2012

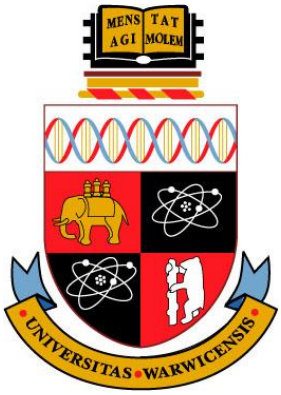

Mutational and Computational Characterization of Transmembrane Domains in the Fungal G Protein-Coupled Pheromone Receptors STE2 and Mam2

by

Gun Antonia Evelina Nilsson Lock

A thesis submitted to the

Molecular Organization and Assembly in Cells Doctoral Training Centre

University of Warwick

For the degree of Doctor of Philosophy

Supervisors: Dr Graham Ladds and Dr. Ann Dixon

September 2011

DECLARATION OF AUTHORSHIP

The work presented in this thesis is original and was conducted by the author unless otherwise specified, under the supervision of Dr. Graham Ladds at the Warwick Medical School and Dr. Ann Dixon at the Department of Chemistry, University of Warwick.

This research was funded by the EPSRC through the doctoral training centre Molecular Organisation and Assembly in Cells (MOAC).

All sources of information have been acknowledged by means of a reference.

ABSTRACT

G protein-coupled receptors (GPCRs) comprise the largest family of cell-surface receptors involved in sensing a multitude of ligands and are consequently attractive pharmacological targets. Their study is complicated by cross-talk between signalling pathways and altered receptor pharmacology due to, for instance, receptor oligomerization. Difficulties in obtaining structural information of the receptors hinder the understanding of oligomerization and therefore it is desirable to develop alternative approaches in which to study this phenomenon.

The fungal pheromone GPCRs, STE2 and Mam2, from *Saccharomyces cerevisiae* and *Schizosaccharomyces pombe* respectively are both known to oligomerize and a GxxxG motif in the first transmembrane (TM) domain of STE2 has previously been shown to mediate receptor oligomerization. Previous work on polytopic proteins suggest that individual TM helices may be treated as individually stable domains, and it may therefore be possible to study oligomerization via single TM peptides as opposed to full-length receptor. This thesis describes the use of STE2 and Mam2 to explore TM helix oligomerization and the effects of mutations on receptor trafficking, localization and cellular signalling. The development of a luminescent reporter assay for *Sz. pombe*, which proved more sensitive than previously used assays and is capable of generating high-throughput data, is also discussed.

It was found that STE2 could couple to the *Sz. pombe* pheromone-response pathway and mutations in the GxxxG dimerization motif affected both signalling and trafficking. Expression of the first TM GxxxG containing domain of STE2 was insufficient for oligomerization, in line with previous reports suggesting that the presence of the second domain is required for receptor oligomerization. In Mam2, a motif was identified that appeared homologous to the STE2 dimerization motif and mutations of this motif also affected trafficking and signalling. This domain could oligomerize in isolation, and mutations of the motif abolished oligomerization. In contrast the study of more polar TM domains appeared more complicated. These findings suggest that relatively hydrophobic TM domains can be studied as individually stable units, whereas more polar domains may require the presence of other TM domains.

ACKNOWLEDGEMENTS

I am immensely grateful to a number of people without whom this thesis would not have been possible.

First and foremost I would like to thank my two supervisors Dr. Graham Ladds and Dr. Ann Dixon for giving me the opportunity to carry out the work presented in this thesis, for their supervision and guidance throughout my research, and for their contagious passion and enthusiasm for their respective research fields. I especially want to thank Dr. Graham Ladds for his above and beyond commitment to my success, well-being and ensuring my safe-escape from both phenol:chloroform induced mishaps and apartment entrapments!

I am immensely grateful to Professor Alison Rodger for help and support throughout my PhD, partly for letting me use her research facilities but also for her endless patience, personal support and offering me a place on the MOAC course. I would also like to thank all the people at MOAC, in particular Dr. Dorothea Mangels and the 2005 cohort, and MOAC and the EPSRC for funding.

I am also very grateful to Dr. Joanne Oates for showing me the ropes around the lab in my first year and for everyone else in the Dixon and Ladds groups, past and present, for help and support. I would in particular like to thank Professor John Davey, Dr. Andrew Beevers, Dr. Matthew Hicks, Dr. Joanne Oates, Dr. Eilish McCann, Michael Bond, Wayne Croft and Cate Weston for useful discussions and guidance.

Special thanks to Dr. Stefano Costanzi for help with the homology models and to Wayne Croft for helping me with confocal microscopy. Many thanks also go to Professor Sanjiv Gambhir and to Professor Donald Engelman for providing the Rluc8 and TOXCAT plasmids. I would also like to thank Anthony Lock for help with the computer scripts.

Finally I would like to thank my two families for making sure I always have somewhere in the world to call home and for always being fully behind me in whatever I choose to do. In particular I would like to thank my husband without whom this thesis would not have a table of contents, but also for his love and support during the ups and downs that working towards a PhD brings. Lastly I would like to dedicate this thesis to the memory of my great-aunt Ruth Bringle.

TABLE OF CONTENTS

LIST OF FIGURES

LIST OF TABLES

ABBREVIATIONS

AA	Amino acid
Amp	Ampicillin
AGS	Activators of G protein Signalling
ARF	ADP-Ribosylation Factor
AUC	Analytical Ultracentrifugation
BAR	Bin–Amphiphysin–Rvs
BiFC	Bimolecular Fluorescence Complementation
BRET	Bioluminescence Resonance Energy Transfer
cAMP	Cyclic AMP
CAM	Constitutively Active Mutant
CAT	Chloramphenicol Acetyl-Transferase
CBP	CREB Binding Protein
CDC	Cell Division Control
CHI	CNS (Crystallography and NMR Searching) of Helix Interactions
CME	Clathrin Mediated Endocytosis
CoA	Coenzyme A
CREB	cAMP Response Element Binding
CRLR	Calcitonin Receptor-Like Receptor
DAG	Diacylglycerol
EC_{50}	Median Effective Concentration
ERAD	ER Associated Degradation
DAG	Diacylglycerol
DMM	Defined Minimal Media
DNA	Deoxyribonucleic Acid
dodecylphosphocholine	Dodecylphosphocholine
ECM	Extracellular Matrix
EGF	Epidermal Growth Factor
E. coli	*Escherichia coli*
EDTA	Ethylenediaminetetraacetic Acid
ER	Endoplasmic Reticulum
FACS	Fluorescence Activated Cell Sorting
FOA	5-Fluoro-Orotic Acid

FRET	Fluorescence Resonance Energy Transfer
GABA	Metabotrophic γ-Aminobutyric Acid Receptor
GAP	GTPase Accelerating Protein
GDI	Guanosine Nucleotide Dissociation Inhibitors
GDP	Guanosine Diphosphate
GEF	Guanine nucleotide Exchange Factor
GFP	Green Fluorescent Protein
G protein	Guanosine nucleotide-binding protein
GTP	Guanosine Triphosphate
GpA	Glycophorin A
GRK	G protein-coupled Receptor Kinase
GTP	Guanosine Triphosphate
GPCR	G Protein-Coupled Receptor
HMG	High Mobility Group
IP_3	Inositol Triphosphate
kb	kilo bases
kDa	kilo Dalton
LB	Luria-Bertani Broth
MAP	Mitogen Activated Protein
MAPK	Mitogen Activated Protein Kinase
MAPKK	Mitogen Activated Protein Kinase Kinase
MAPKKK	Mitogen Activated Protein Kinase Kinase Kinase
MBP	Maltose Binding Protein
MCS	Multi-Cloning Site
MW	Molecular Weight
NMR	Nuclear Magnetic Resonance
OD	Optical Density
ONPG	o-Nitrophenyl-β-D-galactoside
PAGE	Polyacrylamide Gel Electrophoresis
PAK	p21 Activating Kinase
PBS	Phosphate Buffered Saline
PCA	Protein fragment Complementation Assay
PCR	Polymerase Chain Reaction
PDB	Protein Data Bank

pEC_{50}	Negative natural logarithm of EC_{50}
PF	Periplasmic Fraction
PKA	Protein Kinase A / cAMP Dependent Protein Kinase
PKC	Protein Kinase C
PLC	Phospholipase C
PM	Plasma Membrane
PVDF	Polyvinylidene Fluoride
RAMP	Receptor Activity-Modifying Protein
RET	Förster Resonance Energy Transfer
RGS	Regulator of G protein Signalling
Rluc	*Renilla* luciferase
RMSD	Root Mean Square Deviation
Sc. cerevisiae	*Saccharomyces cerevisiae*
S.D	Standard Deviation
SDS	Sodium Dodecyl Sulphate
SDS-PAGE	Sodium Dodecyl Sulphate Polyacrylamide Gel Electrophoresis
S.E.M	Standard Error of the Mean
SF	Spheroplast Fraction
SPF	Spheroplast Proteolysis Fraction
Sz. pombe	*Schizosaccharomyces pombe*
TM	Transmembrane
UTR	Untranslated Region
WHIM	Warts, Hypogammaglobulinemia, Infections and Myelokathexis
WT	Wild-Type
w/v	Weight per volume
YE	Yeast Extract

AMINO ACID ABBREVIATIONS

Figure i-1 show the 20 amino acids encoded by the genetic code with their one letter and three letter abbreviations and structure. The R-group is highlighted in blue.

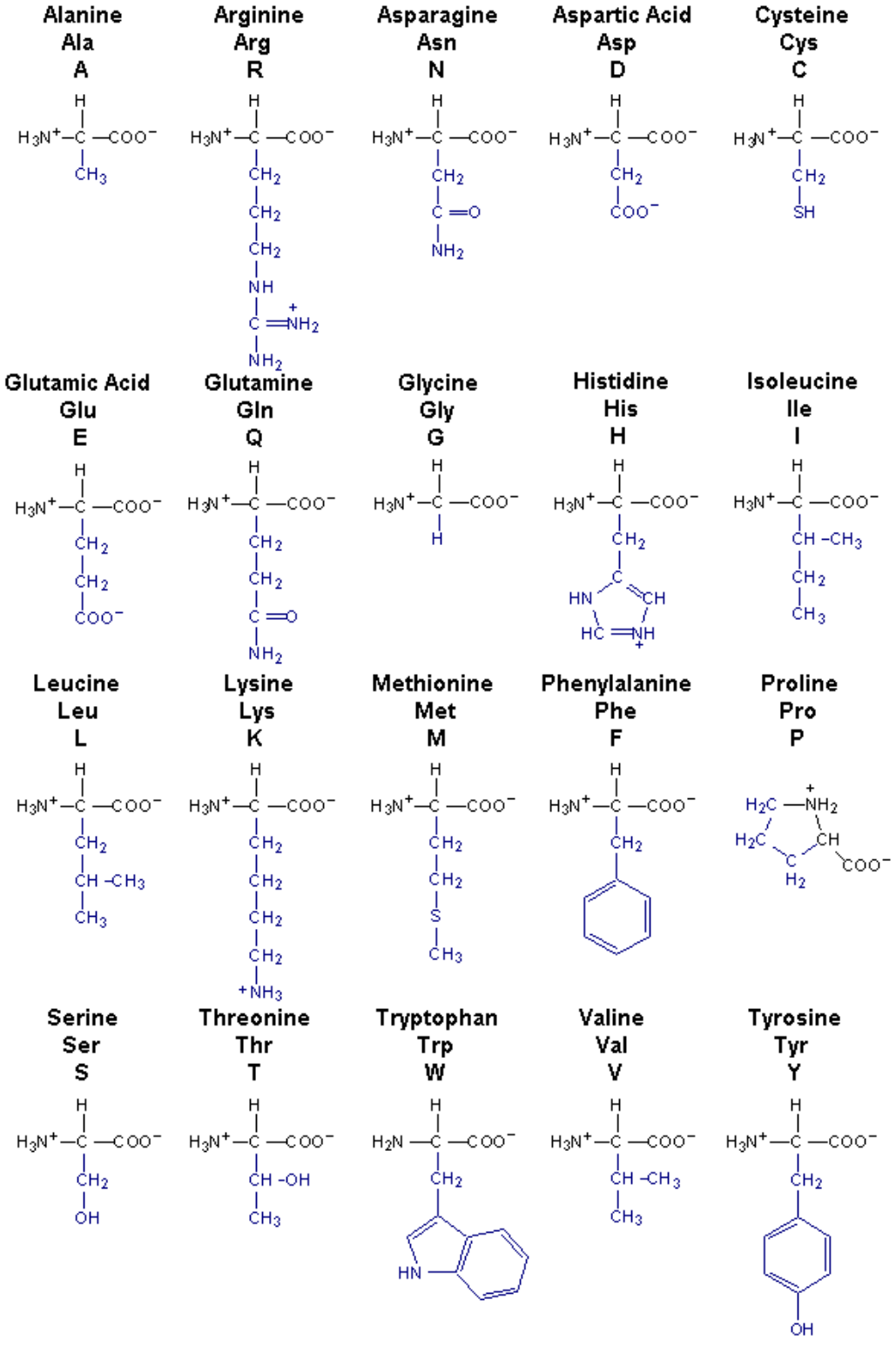

Figure i-1: The 20 amino acids encoded by the genetic code

1 GENERAL INTRODUCTION

1.1 Main Objectives

This thesis concerns the study of the oligomerization of G protein coupled receptors (GPCRs) and how specific amino acid interactions facilitate receptor interactions. In order to realize this objective, individual TM domains from two different GPCRs were studied, compared and contrasted using a range of diverse approaches. The development and optimization of a novel bioluminescent reporter assay is also discussed.

1.2 Membrane Proteins

Membrane proteins are involved in a range of biologically indispensable processes including; the transport of small molecules and ions, cell signalling, structural stability and cell-to-cell adhesion. Their correct functioning is critical to cells and organisms as implied by several diseases caused by malfunctioning membrane proteins, such as autoimmunity, diabetes and cancer (Sanders and Myers 2004; Bocharov, Volynsky et al. 2010). Membrane proteins targeted to the plasma membrane bridge the boundary between the exterior and interior of the cell and they are therefore amenable pharmacological targets. A remarkable ~60% of drugs are known to bind to the surface of cells (Overington, Al-Lazikani et al. 2006) with the majority binding to targets that include; GPCRs, ligand-gated ion channels, voltage-gated ion channels or protein kinases. The further understanding of membrane protein structure and function is therefore immensely important for pharmacological and economical reasons.

1.2.1 Integral Membrane Proteins

Integral membrane proteins span the lipid bilayer at least once and remain permanently attached to the membrane. The highly apolar environment of the membrane means that membrane proteins lose their 3D structure upon solubilisation, and consequently techniques used for the structural study of globular proteins are not readily applied to membrane proteins. Despite challenges in the structural characterization of membrane proteins, two main classes of integral membrane proteins have been described to date. These include the β-barrel class of membrane proteins and the α-helical class of membrane proteins. The α-helical class is the largest which is reflected by their relative abundance in the Protein Data Bank (PDB) database where 86% of membrane protein structures are of α-helical proteins (http://pdbtm.enzim.hu/ 2011).

1.2.2 The Membrane Environment

Biological membranes provide a boundary between the exterior and interior of cells as well as compartmentalizing intracellular organelles. The membrane is a highly heterogenous environment; the plasma membrane contains ~50% phospholipids and ~50% protein and other structures such as steroids and carbohydrates also associate with the membrane. The fluid mosaic model describes the current view of membrane organization (Singer and Nicolson 1972) and is illustrated in Figure 1-1. In this model phospholipids provide the fundamental structural organization of the membrane. Phospholipids consist of a hydrophilic phosphate-containing head-group linked to two fatty acid hydrocarbon tails. Due to their amphipathic nature, phospholipids can spontaneously form lipid bilayers in solution. The lipid:water interface does not provide a sharp division between a hydrophobic and a hydrophilic environment. Rather, an interfacial region exists spanning ~15 Å, which is thick enough to accommodate an amphipathic helix (White and Wimley 1999). The thickness of the hydrophobic core is ~30 Å (White 2003) but can vary depending on the lipid composition of the bilayer (Lewis and Engelman 1983). An appropriately thick bilayer surrounding a membrane protein is important due to the cost of exposing hydrophobic residues to water. It has therefore been proposed that lipids may stretch or compress to match the span of membrane proteins, and conversely membrane proteins may also structurally adjust to shield hydrophobic residues, for instance via tilting of transmembrane (TM) domains (Lee 2004).

Integral membrane proteins traverse the membrane, whereas peripheral membrane proteins only associate with one face of the bilayer; either the side facing the extracellular matrix (ECM) or the cytosol. Carbohydrates associate with the bilayer on the extracellular face, via lipid domains or glycoproteins, and may serve a role in cell-cell interactions. Steroids also insert into the membrane and are involved in maintaining membrane fluidity and rigidity. In the fluid mosaic model, individual components of the membrane are allowed to freely diffuse. This can be exemplified by the fission yeast *Schizosaccharomyces pombe* (*Sz. pombe*) protein kinase Pom1p. *Sz. pombe* exhibit polarized growth, and a gradient of Pom1p at the cell-tip contributes to maintaining sites of cytokinesis, cell polarity and control of cell length. The cortical gradient of the kinase is achieved by insertion of the kinase at the cell tip, diffusion of molecules throughout the cortex, followed by its removal from the membrane (Padte, Martin et al. 2006; Pan, Saunders et al. 2011) resulting in higher densities of the kinase at the cell-tip compared to other areas of the membrane. The simplicity of the fluid mosaic model has recently been challenged by a more complex picture in which membranes are compartmentalized into regions of separate membrane domains, as previously reviewed

(Lindner and Naim 2009), although their roles, location and existence is debated. In another view, certain proteins favour interactions with certain lipids, although difficulties in determining the transient protein-lipid interactions make this phenomenon challenging to study (Lee 2004).

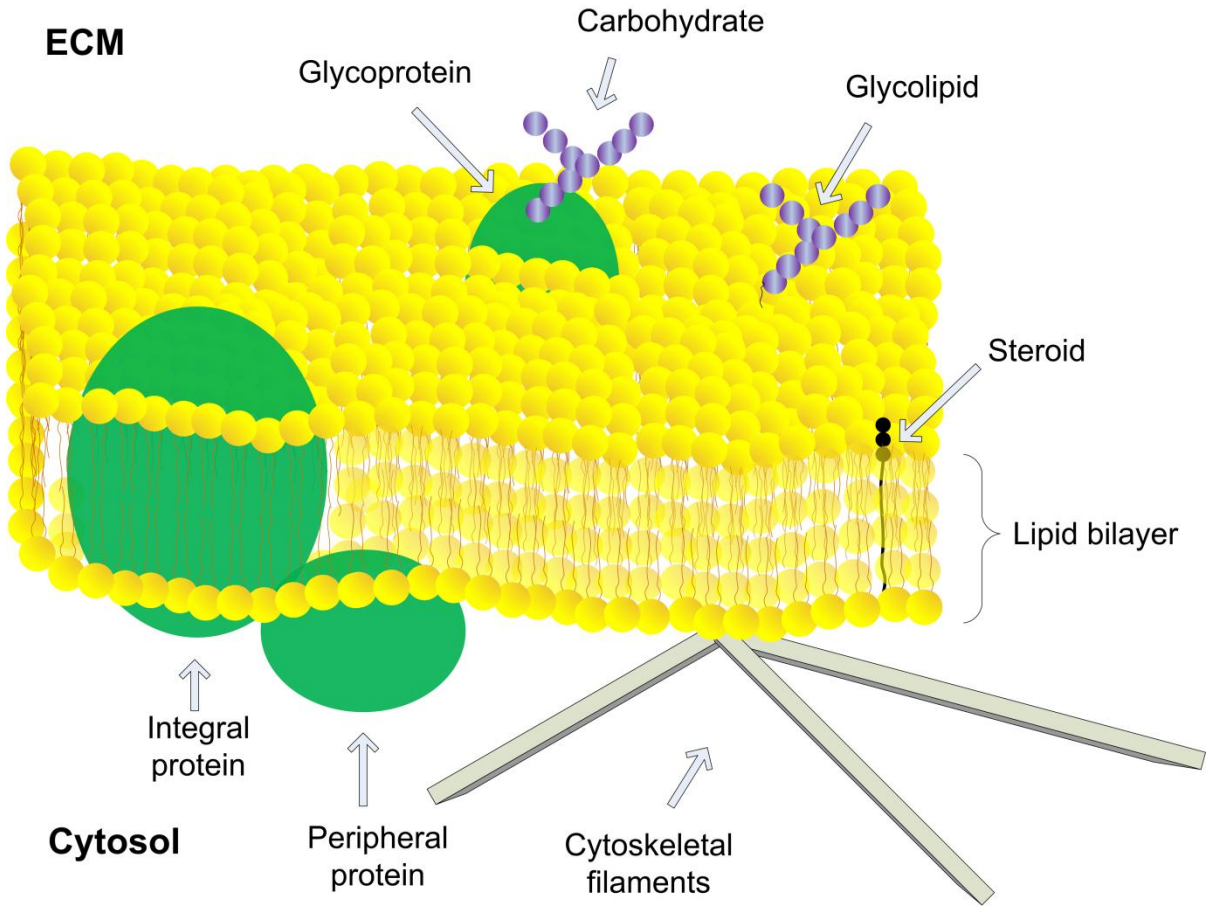

Figure 1-1: The fluid mosaic model of biological membranes

Biological membranes represent a heterogeneous environment containing various types of lipids associated with different proteins, which can either be integral to the lipid bilayer or peripheral. Carbohydrates are often associated with the membrane on the side facing the extracellular matrix (ECM), either via a lipid domain or via a glycoprotein. Steroids are also associated with the membrane, such as cholesterol in animals or ergosterol in fungi. On the cytosolic side the membrane is connected to the interior of the cell via cytoskeletal filaments, which serve a role in transport of molecules and structural support.

1.2.3 Membrane Protein Biogenesis and Exit to the Plasma Membrane

1.2.3.1 The Endoplasmic Reticulum

Not all biological membranes are able to translocate and integrate newly synthesised membrane proteins. Membranes that can include these of the endoplasmic reticulum (ER), mitochondria, chloroplasts and peroxisomes, whereas the plasma membrane and endocytic organelles are unable to do so (von Heijne 1990). Cells have therefore developed a secretory pathway that serves as a gateway for proteins destined for these organelles.

Polytopic membrane proteins (i.e. proteins that span the membrane multiple times) are synthesised by ribosomes attached to the cytosolic side of the ER and enter the ER co-translationally via the Sec61 translocation complex to which they associate via hydrophobic targeting sequences. Orientation signals within the protein (Higy, Junne et al. 2004) as well as molecular and lipid chaperones (van Voorst and De Kruijff 2000; Krebs, Noorwez et al. 2004) aid the correct insertion, folding and orientation of the membrane protein, and proteins may undergo certain post-translational modifications such as disulfide-bond formation in the ER (Achour, Labbe-Jullie et al. 2008). Incorrectly folded membrane proteins however are exported to the ER-associated degradation pathway (ERAD) in the cytosol for degradation (Tsai, Ye et al. 2002).

There is evidence that plasma-membrane signalling complexes may form in the ER. For instance the $GABA_{B1}$ receptor forms a complex with the Gβγ subunits of G proteins and the potassium channel Kir3 prior to reaching the plasma membrane, and this complex may form as early as the ER (David, Richer et al. 2006). Variations in complex formation may influence the pharmacology of the protein. In the case of the calcitonin receptor-like receptor (CRLR), interactions with receptor activity-modifying protein 1 (RAMP1) in the ER yields a receptor specific for binding calcitonin gene-related peptide at the cell surface whereas interactions with RAMP2/3 in the ER yields a receptor specific for binding adrenomedulin at the plasma membrane (McLatchie, Fraser et al. 1998; Ittner, Koller et al. 2005). Complex formation is essential for targeting of RAMPs to the plasma membrane because monomers display an ER retention signal, which is masked upon complex-formation (Steiner, Muff et al. 2002). Several other proteins have been found to chaperone membrane proteins to the plasma membrane and complex-formation is in some, but not all, cases essential for transport (Dong, Filipeanu et al. 2007).

1.2.3.2 Targeting to the Golgi Apparatus and Plasma Membrane

Export from the ER occurs at ER "exit sites" in a coat protein II (COPII)-dependent manner (Achour, Labbe-Jullie et al. 2008). Proteins destined for the Golgi accumulate at these sites that form buds when coated with the COPII associated proteins Sar1, Sec23-Sec24 and Sec13-Sec31. It has been proposed that integral membrane proteins interact with domains of Sar1 and Sec23-24 which labels them for transport (Barlowe 2003). Interaction sites vary but may involve a di-acidic motif composed of the amino acids DxE, a double phenylalanine motif, or other more complicated motifs, and is a rate-limiting step in COPII bud formation (Dong, Filipeanu et al. 2007). Multiple binding sites on Sec23 have been identified, which supports the theory that different interaction motifs on separate membrane proteins can bind to the same transport molecule (Miller, Beilharz et al. 2003).

Following budding, the COPII transport vesicles are transported and fused to the Golgi apparatus and subsequently migrate through the network of flattened cisternae; from the cis-Golgi network to the trans-Golgi network via the medial-Golgi and endo-Golgi. Each of these regions contain different enzymes involved in selective post-translational modification of cargo, such as glycosylation (Alberts, Johnson et al. 2002). N-linked glycosylation may be important for the transport of some proteins from the Golgi to the plasma membrane, although for others it is less clear what the target signals are (Dong, Filipeanu et al. 2007). It's been suggested that in some cases, the same motifs involved in targeting proteins from the ER to the Golgi may be involved in targeting proteins from the Golgi to the plasma membrane, as has been found for the di-acidic motif (Nishimura, Plutner et al. 2002).

1.2.3.3 Regulation of the Secretory Pathway

The correct targeting and fusion of transport vesicles with membranes involves the inclusion of a V-SNARE inside the vesicle, which is specific to the target membrane and acts co-operatively with a T-SNARE which is integral to the transport membrane (Lodish, Berk et al. 2000). Timing of vesicle fusion is thought to be achieved through the accumulation of Rab-GTP (part of the Ras superfamily of monomeric G proteins) although the exact mechanism is not known (Lodish, Berk et al. 2000; Dong, Filipeanu et al. 2007). There is however evidence that the secretory pathway may regulate storage of proteins, thereby playing a role in regulating the levels of proteins at the cell surface. For example the dopamine D1 receptor is stored in Golgi-derived vesicles and is only released to the plasma membrane following the activation of cell-surface expressed receptors (Brismar, Asghar et al. 1998; Kruse, Adachi et al. 2003). This has also been observed for the thrombin receptor and is separate from the recycling phenomenon that is seen in other cell surface receptors, because thrombin

receptors are irreversibly activated and targeted to lysosomes following activation (Hein, Ishii et al. 1994). Thrombin is retained in the Golgi by another membrane protein, p24A, and following activation of G protein-bound receptor at the cell surface, the G protein dissociates and targets p24A to trigger the release of Golgi-bound thrombin (Luo, Wang et al. 2007). For other receptors in contrast, such as the β2-adrenergic receptor, plasma membrane expression following the secretory pathway is constitutive (Hein, Ishii et al. 1994).

1.2.4 Membrane Protein Internalization

1.2.4.1 Endocytosis

Endocytosis acts as a regulator of signalling through controlling the lipid-protein composition of the membrane. Three distinct cellular compartments are associated with the endocytic pathways; the early endosomes, late endosomes and lysosomes (or vacuoles in fungi). Internalized molecules first encounter the early endosomes. The mildly acidic pH of the lumen of these structures can cause ligands to dissociate from receptors, and receptors may therefore be recycled from the early endosomes via tubular structures back to the plasma membrane. Early endosomes mature into late endosomes, in which the lumen becomes increasingly acidic and there is a loss of the tubular structures needed for recycling, ultimately determining the fate of cargo for degradation by the lysosome (Lodish, Berk et al. 2000). Actin filaments have been strongly implicated in the movement of vesicles between these compartments in yeast and in some, but not all, mammalian cell types (Kaksonen, Sun et al. 2003; Gachet and Hyams 2005). Endosomal cargo destined for degradation is targeted to the lysosome where contents are broken down into component parts such as amino acids from proteins, or cholesterol and fatty acids from cholesterol esters (Lodish, Berk et al. 2000).

1.2.4.2 Pathways Mediating Endocytosis

Several different pathways for endocytic uptake in cells are known to exist. These include clathrin-mediated endocytosis (CME) where clathrin-coated pits develop, and progressive invagination of the pit ultimately leads to scission from the plasma membrane, and the formation of clathrin-coated vesicles. Adaptor proteins mediate bud formation and recruit Clathrin, which forms a lattice around the vesicle. Bin–Amphiphysin–Rvs (BAR) domain-containing proteins in turn recruit dynamin and together they form the neck of the bud, and vesicles are ultimately formed by fission of the bud from the plasma membrane by the GTPase dynamin (Doherty and McMahon 2009). The clathrin-coat is subsequently lost from the vesicle before fusion with the target early endosomes. Much research has focused on

CME and it has been extensively reviewed in the literature (Mousavi, Malerod et al. 2004; Traub 2005; Roth 2006).

The most commonly reported non-clathrin coated buds are known as caveolae. These flask-shaped invaginations are rich in cholesterol, sphingolipids and the protein caveolin and are often observed in clusters, which can occupy as much as a third of plasma membrane area (Mayor and Pagano 2007). Caveolae are believed to perform multiple functions in the cell including lipid storage, responding to mechanical stress, and to play a role in cell signalling events such as Ca^{2+} signalling (Parton and Simons 2007). Caveolae can exist as immobile plasma membrane domains (Thomsen, Roepstorff et al. 2002) but can also couple to the endocytic pathway through internalization of vesicles coated with caveolin; a process that can be exploited by pathogens to gain entry into cells (Pelkmans, Kartenbeck et al. 2001). Other endocytic pathways also exist (Sandvig, Pust et al. 2011) which may involve coat proteins other than caveolin and clathrin, flotilin is another example, or different GTPases; for instance RhoA, cell division control protein 42 (CDC42) or ADP-ribosylation factor 6 (ARF6). The mechanisms appear to vary greatly between cell-types making it difficult to propose specific general pathways (Mayor and Pagano 2007).

1.2.4.3 Regulation of Internalization

Internalization of membrane proteins may be constitutive or triggered by cellular activities (Mousavi, Malerod et al. 2004). Signals triggering the internalization of membrane proteins are diverse, and several pathways may internalize the same protein through different signals. The epidermal growth factor (EGF) receptor kinase for instance is internalized by CME (Willingham and Pastan 1982) but may be internalized via caveolin-dependent endocytosis in response to high doses of ligand (Sigismund, Woelk et al. 2005). It has been proposed that CME promotes recycling of the EGF receptor, to prolong signalling, whereas the clathrin-independent pathway targets the receptor for degradation (Sigismund, Argenzio et al. 2008). Signals for CME include tyrosine or leucine-based motifs in the C-terminal cytoplasmic tail of proteins, and some components of clathrin-coated pits also contain ubiquitin-binding domains (Mousavi, Malerod et al. 2004). Ubiquitylation, i.e. the conjugation of ubiquitin to a target protein, has also been implicated as a signal for caveolin dependent endocytosis (Sigismund, Woelk et al. 2005). Adaptor proteins mediate ubiquitylation and these may recognize their targets by a variety of methods including proteins that have become phosphorylated or the presence of polar TM domains in the target protein (Leon and Haguenauer-Tsapis 2008).

1.2.5 Protein Folding in the Membrane

1.2.5.1 Integration of Proteins into the Membrane

The process by which membrane proteins are integrated into lipid bilayers is currently not fully understood. Mothes and colleagues (1997) proposed a model in which membrane proteins laterally integrate into the ER membrane via the ribosome-translocon channel. In this model, the appearance of a hydrophobic stretch of polypeptide within the translocon causes a closing of the channel, and the segment moves laterally into the bilayer. This process may be repeated when translating a polytopic protein (Mothes, Heinrich et al. 1997). The hydrophobic stretches found in membrane proteins and adjacent residues appear sufficient to drive the integration of a protein into the membrane, partly because the introduction of a TM domain into cytosolic proteins can convert them into membrane proteins and also because model peptides will only partition into the membrane if they are sufficiently hydrophobic (MacKenzie 2006). The structural comparison of the translocon in a peptide-bound form and inactive form provided further evidence for a lateral gate present in the translocon (Martinez-Gil, Sauri et al. 2011).

Membrane proteins insert into the membrane because it is energetically favourable to bury hydrophobic residues, even though dehydrating the hydrophilic backbone comes at a cost. For example, the free energy for the insertion of the α-helical protein glycophorin A (GpA) is estimated to be -36 kcal/mol^{-1} due to burial of hydrophobic residues. Conversely the cost of dehydrating the backbone of GpA is +26 kcal/mol^{-1} (White 2003). Therefore, there is favourable net free energy of 10 kcal/mol^{-1} when inserting the helix into the membrane compared to leaving it in the cytosol (White 2003). The formation of secondary structures within the membrane is also energetically favourable, and most integral membrane proteins adopt α-helical structures across the lipid bilayer. The cost of transferring a non-H-bonded peptide bond from a hydrophilic to hydrophobic environment is +6.4 kcal/mol^{-1} whereas transferring an H-bonded peptide bond to a hydrophobic environment is only +2.1 kcal/mol^{-1}. There is thus a free energy cost of +4 kcal/mol^{-1} of disrupting a single H-bond in the membrane, meaning that the secondary structure is inherently stable and carries a lower energetic cost (White 2003). A typical transmembrane α-helix is right-handed and each residue contributes to a 100° turn and a 0.15 nm rise of the helix. The hydrophobic core of a lipid bilayer is ~30 Å thick meaning that typically 20 amino acids would be involved in spanning the hydrophobic core. This is not necessarily always true however; as previously discussed the lipids may influence bilayer thickness to some extent to accommodate longer or shorter helices. The helices themselves may also conform to bilayer thickness by tilting in

the membrane, and side-chain to main-chain hydrogen bonding may also increase the length of the helix (Lee 2004).

1.2.5.2 The Two-Stage Model of Membrane Protein Folding

The two-stage model of membrane protein folding provides an important conceptual framework in which to understand protein folding into the membrane (Popot and Engelman 1990). According to the two-stage model (Figure 1-2) membrane proteins fold in two thermodynamically distinct stages. In the first stage, hydrophobic sequences insert into the lipid bilayer and form independently stable domains. This is driven by the hydrophobic effect. In the second stage, helical domains laterally interact to form the fully folded tertiary structure of the protein. This may be driven by energetically favoured bond-formation and packing between helices.

Although the two-stage model appears simplistic, early studies on bacteriorhodopsin supported the model. Bacteriorhodopsin is a 7TM spanning proton pump involved in sensing light in archaea. Fragments of the receptor will fold independently, and will form the fully functional native structure upon mixing (Popot, Gerchman et al. 1987; Kahn and Engelman 1992; Kataoka, Kahn et al. 1992). Since then, fragments of several other polytopic proteins have shown to integrate into membranes and fold independently of the full-length protein, and to form subsequent lateral interactions with each other via their TM domains, including lactose permease (Bibi and Kaback 1990), rhodopsin (Ridge, Lee et al. 1995), the red cell anion exchanger protein (Groves and Tanner 1995) and the yeast α-factor receptor (Martin, Leavitt et al. 1999). A third stage was later added to account for protein quaternary structures and interactions with co-factors, lipids and water (Engelman, Chen et al. 2003).

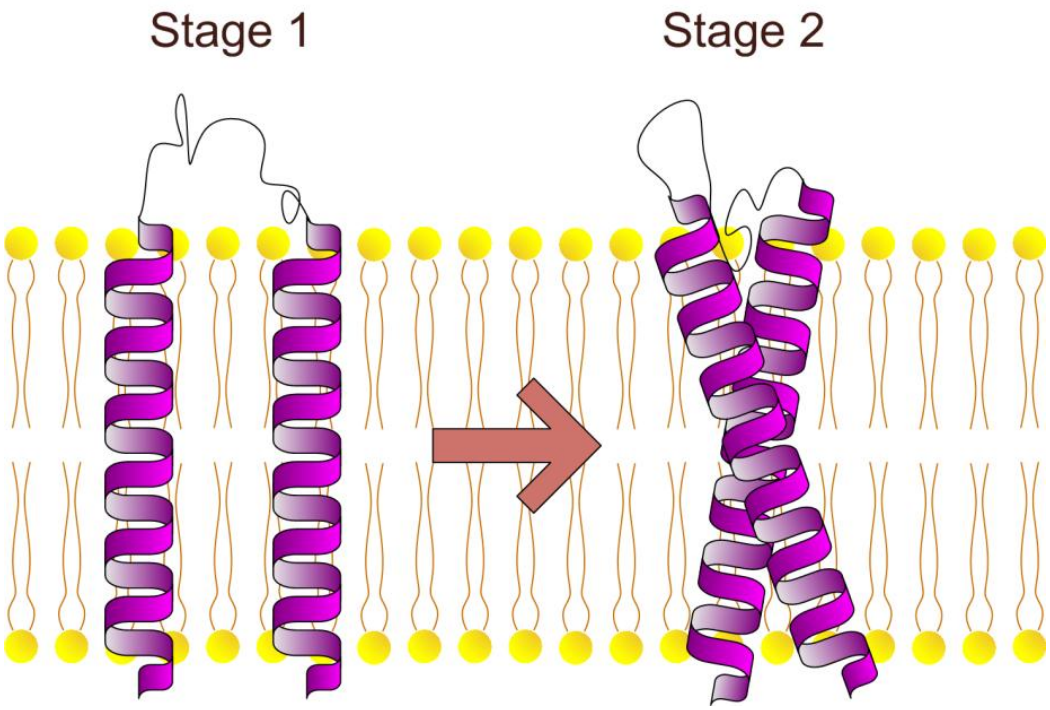

Figure 1-2: The two-stage model of membrane protein folding

The two-stage model of membrane protein folding was proposed by Popot and Engelman in 1990. In the first stage, independently stable trans-bilayer helices form in response to the hydrophobic effect and main-chain hydrogen bonds form in the non-aqueous environment. In the second stage helices interact to form the tertiary fold of the protein that may be driven by energetically favorable polar contacts between helices, or packing.

1.2.6 Transmembrane Domain Interactions

The two-stage model predicts that individual TM domains initially form independently stable structures, before laterally interacting to form a polytopic protein or form quaternary structures. The model does not however postulate how lateral interactions are formed. The hydrophobic effect is an important force driving the folding of globular proteins (Tanford 1978), but due to the low dielectric environment of the membrane other forces must drive the lateral association of membrane proteins. The study of the interactions within polytopic and/or oligomeric membrane proteins is not trivial and remains one of the biggest challenges in protein chemistry to this day. In the PDB only 2% of structures represent membrane proteins (http://pdbtm.enzim.hu/ 2011), however membrane proteins are believed to constitute 20-25% of all proteins (Boyd, Schierle et al. 1998; von Heijne 1999). Considering their pharmacological and economical importance, the lack of structural information of membrane proteins clearly reflects the challenges presented to structural biologists.

1.2.6.1 The Structural Importance of Transmembrane Domains

The TM spanning regions of membrane proteins were traditionally believed to merely anchor the protein to the membrane. Early studies on fragmented bacteriorhodopsin however showed that this is not the case. In bacteriorhodopsin a functional protein can be reconstituted only if all 7TM domains are expressed, and in contrast four of the six loop regions found outside of the hydrophobic core are dispensable, although they do influence folding stability and kinetics (Luneberg, Widmann et al. 1998; Marti 1998). This demonstrated that the transmembrane segments do not merely anchor membrane proteins to the lipid bilayer, but serve a purpose in maintaining protein structure.

1.2.6.2 Motifs Known to Mediate Membrane Protein-Protein Interactions

1.2.6.2.1 Motifs of Two Small Residues

The study of single-spanning membrane proteins and designed peptides has contributed to much of our current understanding in how transmembrane domains interact, and several motifs have been identified that appear important in driving associations. For instance, the single TM-spanning protein GpA which is expressed in erythrocytes, dimerizes via a motif of two glycines spaced four residues apart (GxxxG) (Lemmon, Flanagan et al. 1992; Adams, Engelman et al. 1996). Due to their relative spacing in the primary sequence, the two glycines appear on the same side of the α-helix. The small size of the glycine side-chains allows two helices to come in close proximity and form stabilizing van der Waals interactions

by a “ridges-into-grooves” packing of adjacent β-branched residues into the grooves created by the glycine residues (MacKenzie, Prestegard et al. 1997). The ridges-into-grooves, or knobs-into-holes, packing of residues is illustrated in Figure 1-3. Statistical analysis revealed that the GxxxG motif is overrepresented in genomes (Russ and Engelman 2000) and since its discovery it’s been found to mediate the dimerization of several other membrane proteins including the *Heliobacter pylori* vacuolating toxin (McClain, Iwamoto et al. 2003), the yeast α-factor receptor (Overton, Chinault et al. 2003), Carnitine palmitoyltransferase 1 (Jenei, Borthwick et al. 2009), the Major Histocompatibility Complex Class II and invariant chain (King and Dixon 2010), among others. Sequence context is important to allow the ridges-into-grooves packing and therefore large hydrophobic residues are often found immediately adjacent to the GxxxG motif and/or on the same face to assist interactions (Senes, Gerstein et al. 2000; Schneider and Engelman 2004). As a consequence, not all GxxxG motifs are involved in dimerization (McClain, Iwamoto et al. 2003). Since the discovery of the GxxxG motif, other variations have been found termed smallxxxsmall motifs because they all involve small residues (G, S, A) spaced four residues apart (Senes, Gerstein et al. 2000; Escher, Cymer et al. 2009).

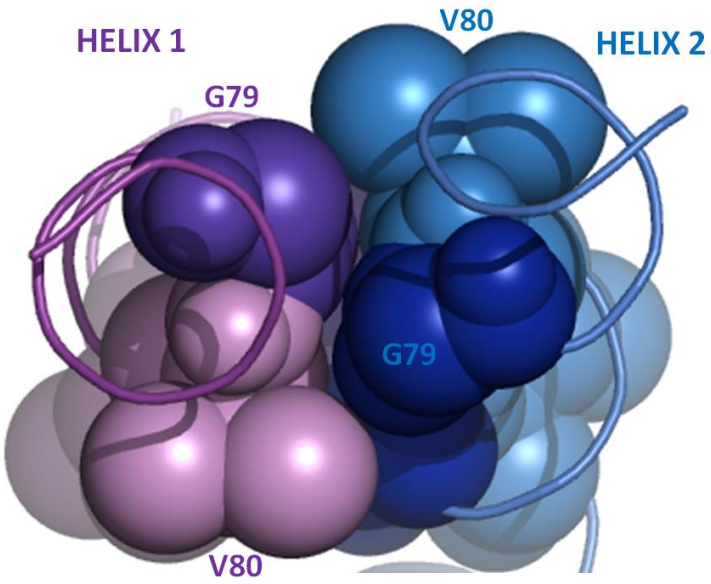

Figure 1-3: Ridges-into-grooves packing of residues in dimeric glycophorin A

The structure of the transmembrane dimer Glycophorin A exemplifies the ridges-into-grooves, or knobs-into-holes, packing of the GxxxG motif found in many membrane proteins. In the model shown here each helix in the dimer is represented by purple and blue respectively and a top-down view is shown for clarity. The residues involved in packing are shown as van der Waals spheres. The "groove" formed by the two G79 residues allow the V80 residues on the opposite helix to come in very close proximity to form a "ridges-into-grooves" interaction. A similar interaction occurs between G83 on each helix to V84 on the opposite helix. The model was created using the CHI software suite.

1.2.6.2.2 Heptad Repeats

Heptad repeat motifs also drive the association of membrane proteins. In contrast to the GxxxG motif mainly found in right-handed helix interactions, this motif is generally found in left-handed helix interactions. The heptad motif is driven by repeats of seven residues and helices ultimately achieve a knobs-into-holes packing (Langosch and Heringa 1998; MacKenzie 2006).

1.2.6.2.3 Polar Amino Acids

The presence of polar amino acids in the hydrophobic core of a membrane is energetically unfavourable but can be compensated for by the surrounding hydrophobic residues. The high energetic cost of breaking H-bonds in the hydrocarbon core of a bilayer means that polar contacts provide a strong stabilising force for helix association. For instance, the introduction of a single asparagine residue into a hydrophobic model peptide can transform the peptide from monomeric species to dimeric species both in an *in vitro* and in an *in vivo* system (Zhou, Cocco et al. 2000). The strongly polar amino acids, including histidine, glutamic acid, arginine and aspartic acid, show the highest propensity to form inter-helical H-bonds in the membrane (Sodt and Head-Gordon 2010). Other polar amino acids also induce oligomerization, including asparagine and glutamine (Choma, Gratkowski et al. 2000; Zhou, Cocco et al. 2000; Zhou, Merianos et al. 2001). Threonine and serine residues tend to be overrepresented in transmembrane domains compared to other polar residues (Curran and Engelman 2003), however these residues, together with tyrosine, only appear to have a moderate effect on transmembrane domain oligomerization (Gratkowski, Lear et al. 2001; Zhou, Merianos et al. 2001). As with the smallxxxsmall motif, sequence context is important for associations. The membrane protein BNIP3 for instance, dimerizes strongly via a histidine residue but BNIP3 also contains a GxxxG motif on the same face of the helix as the histidine residue. Mutations of the GxxxG motif disrupts dimerization by not allowing the two monomers to come into close enough proximity for histidine to hydrogen bond (Sulistijo, Jaszewski et al. 2003; Lawrie, Sulistijo et al. 2010).

1.2.6.2.4 Aromatic Residues

Aromatic residues such as phenylalanine, threonine or tyrosine can also contribute to energetically favourable interactions between TM helices. Pairs of aromatic residues can π-π stack, or the π electrons of the aromatic ring of a single aromatic residue can form a cation-π interaction to a positively charged residue such as arginine, lysine or histidine. Cation-π interactions and π-π stacking has been found both in model peptides and in native

membrane proteins and interactions can be four-fold stronger than those arising from knobs-into-holes packing (Dougherty 1996; Johnson, Hecht et al. 2007). For each of these interactions two possible conformations are possible. For the interaction of two aromatic residues, the interaction can either be stacking or edge-to-face, the former typically involving extensive van der Waals contact whereas the latter involve a CH-π interaction. For the cation-π interaction the positively charged residue can either be perpendicular or parallel to the aromatic ring (Johnson, Hecht et al. 2007). Cation-π interactions are interesting because they allow a polar, yet hydrophobic, interaction in the membrane i.e. they can bind ions but are composed of hydro-carbons (Dougherty 1996). This type of interaction is not exclusive to membrane protein-membrane protein interactions, but has also been observed between receptor and ligand (Tantry, Ding et al. 2010).

1.2.6.3 Effects of Proline Residues on Membrane Protein Structure

Prolines present in the transmembrane domains can also influence helix packing and their importance in membrane proteins is reflected by the phenotypic consequences of mutating prolines in human membrane proteins (Partridge, Therien et al. 2004). The amide nitrogen of proline cannot form backbone hydrogen bonds and proline residues therefore introduce distinct kinks in transmembrane domains. Proline is present at 60% of transmembrane helix deformation sites and it has been proposed that in cases where proline is not present, the proline could have been lost with time as the kink became stabilized by other molecular forces (Yohannan, Faham et al. 2003). Proline residues in transmembrane domains are most often found in the middle of the helices (Barlow and Thornton 1988).

On a molecular level, prolines are believed to reduce the stability and rigidity of transmembrane helices due to the loss of the NH···O=C bond. In one specific class of integral membrane proteins, the 7TM spanning GPCR receptors, this allows a rotational switch upon activation (Elling, Frimurer et al. 2005). In this model, upon receptor activation the extracellular side of the receptor undergoes an inward movement which closes the ligand-binding site whereas the cytoplasmic side opens up to allow downstream signalling. This movement is achieved via a see-saw motion of TM6 and TM7 which pivots about the centre of the helices, and it has been suggested the pivoting is achieved via the proline residues (Schwartz, Frimurer et al. 2006). Mutations of transmembrane proline residues have been shown to have an effect on both ligand-binding and activation of GPCRs (Ladds, Davis et al. 2005; Reis, Santos et al. 2007; Mazna, Grycova et al. 2008)

These studies show that lateral interactions between membrane spanning domains are most likely driven by non-covalent interactions (van der Waals forces, electrostatic interactions

and hydrogen bonding) and the presence of certain motifs and residues in transmembrane domains can be strong predictors of transmembrane helix-helix interactions.

1.2.7 Methods for Studying Transmembrane Helix Interactions

1.2.7.1 Membrane Protein Structural Determination

Many biophysical techniques exist to study interactions between transmembrane peptides *in vitro*. These techniques include, among others, sodium dodecyl sulphate polyacrylamide gel-electrophoresis (SDS-PAGE), analytical ultracentrifugation (AUC), chemical cross-linking, solution-state nuclear magnetic resonance (NMR), or solid-state NMR and are often performed in detergent micelles or synthetic lipid bilayers (MacKenzie, Prestegard et al. 1997; Fisher, Engelman et al. 1999; Liu, Crocker et al. 2003; Doura, Kobus et al. 2004; Jenei, Borthwick et al. 2009). The biophysical characterization of polytopic proteins provides an even greater challenge. X-ray crystallography is the only currently available method for obtaining full-length polytopic membrane protein structures (Henderson, Baldwin et al. 1991) although it may be possible to piece together structural information on receptor fragments from NMR to generate an image of the full-length protein (Toyoshima, Nakasako et al. 2000).

Apart from being highly artificial systems, these biophysical techniques come with other challenges. Detergent micelles can destabilize helices for instance, through interactions between amino acids and the polar head-groups of the detergent, thereby allowing increased side-chain flexibility in the amino acid chain or disrupting inter-helical bonds thereby distorting the structure (Langosch, Brosig et al. 1996; MacKenzie 2006). Furthermore, only a handful of structures of large polytopic proteins have been solved to date by X-ray crystallography. This is largely due to difficulties in obtaining large quantities of protein and purifying them in their native form. Much research is therefore currently focused on improving techniques (Bill, Henderson et al. 2011).

1.2.7.2 Reporter Systems to Study Protein-Protein Interactions in the Membrane

A range of indirect techniques has been developed to investigate interactions in biological membranes. These include an array of different luminescence-based techniques, for instance the Förster resonance energy transfer (RET) techniques including bioluminescence resonance energy transfer (BRET) and fluorescence resonance energy transfer (FRET) as well as protein fragment complementation assays (PCA) such as bimolecular fluorescence

complementation (BiFC) (Overton, Chinault et al. 2003; Milligan and Bouvier 2005; Gehret, Bajaj et al. 2006). Recently RET and PCA techniques have been combined to monitor the formation of large protein complexes (Vidi and Watts 2009). The BRET technique has also been used to monitor changes in protein conformation upon ligand binding (Percherancier, Yamina et al. 2005).

Oligomerization of single transmembrane spanning domains can be readily studied using the TOXCAT assay (Russ and Engelman 1999). In this technique a TM domain of interest is expressed as an MBP-TM-ToxR chimera in the *E. coli* inner membrane. The maltose binding protein (MBP) drives the construct to the membrane and ensures its correct orientation. Interaction of two TM domains bring their ToxR domains in close proximity, leading to expression of chloramphenicol acetyl-transferase (CAT), (Figure 1-4) and levels of CAT expression can directly be quantified by its activity on a substrate. Since TOXCAT can only measure interactions between the same domains ("homo-oligomerization") an alternative technique was developed to allow the studying of "hetero-oligomers" i.e. oligomers formed by the interaction of different transmembrane domains (Schneider and Engelman 2003). Other assays involving protein fusions and reporter complementation also exist, such as the split-ubiquitin assay (Johnsson and Varshavsky 1994).

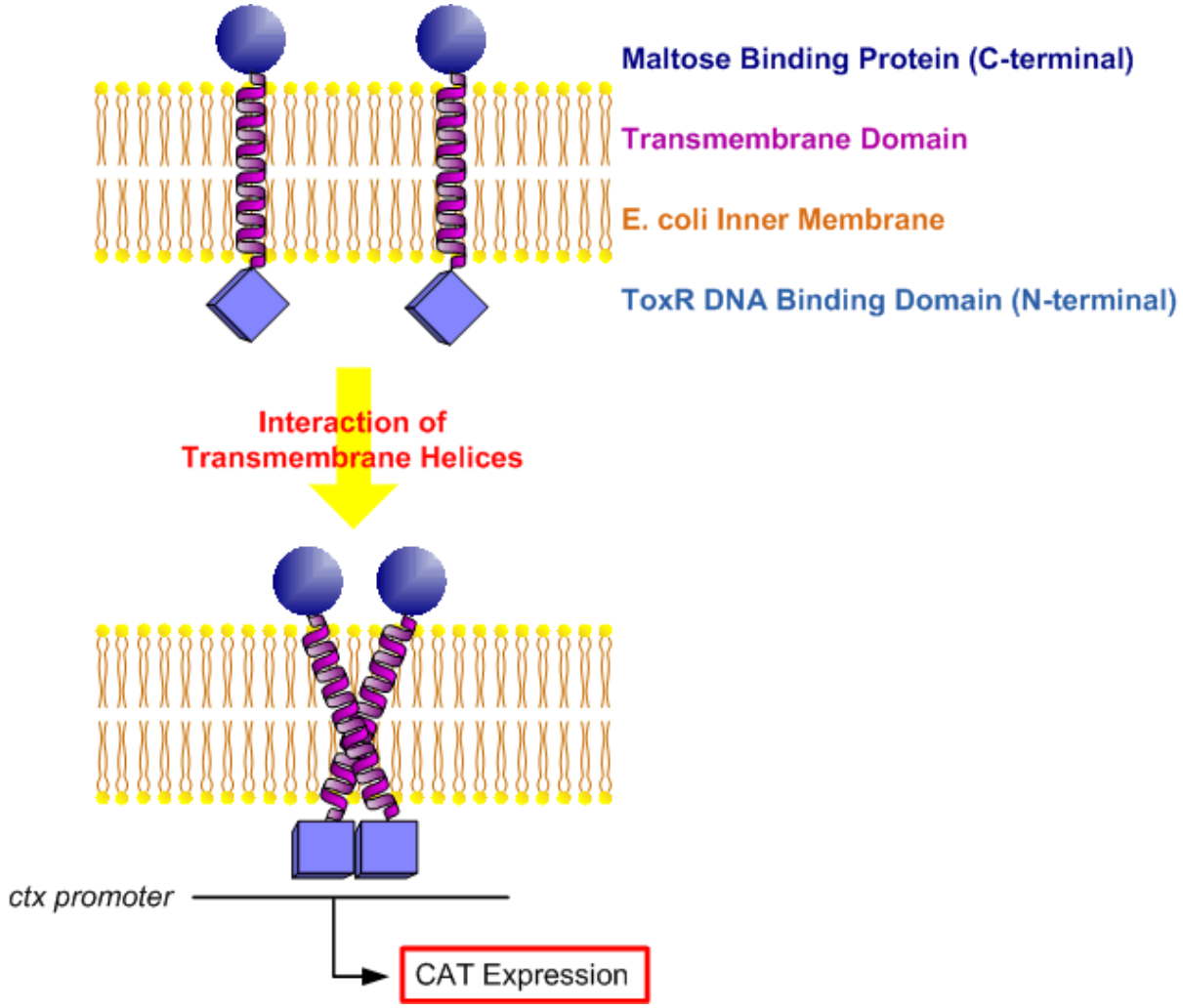

Figure 1-4: Principles of the TOXCAT assay.

A protein chimera is expressed in *E. coli* consisting of the TM domain of interest, flanked by the ToxR DNA binding domain at the N-terminus, and the maltose binding protein (MBP) at the C-terminus. The MPB drives and anchors the TM to the membrane. If the two TM domains come in close proximity their respective ToxR DNA binding domains are brought together. ToxR dimers, but not monomers, bind the operator region of the *ctx* operon and activate the transcription of CAT. CAT confers chloramphenicol resistance by acetylating chloramphenicol.

1.3 Cell to Cell Communication

The ability of cells to sense their environment and respond with appropriate cellular responses is crucial to survival. Social and multi-cellular organisms additionally require inter-cellular communication in order to formulate coordinated responses. Vast arrays of cellular pathways have evolved to sense and respond to stimuli as diverse as nutrients, stress or developmental information. Some signalling pathways may involve the passive diffusion of signalling molecules into cells; estrogen for instance can cross the lipid bilayer. Most signalling pathways however rely on membrane bound receptors to sense external stimuli and to induce the appropriate response. In some cases, such as ligand- and voltage-gated ion channels or receptor tyrosine kinases, the receptor itself is involved in actively inducing the desired response. In other cases, such as GPCR signalling, the receptors merely relay the signal intracellularly.

Many diseases that plague modern society are associated with the disruption of normal cell-to-cell communication. These include, among many others, autoimmune disease, where an individual's immune system fails to recognise its own constituent parts, type-2 diabetes, where cells do not respond to insulin properly or cancer, where cells do not to respond to normal homeostatic control. The study of cell-to-cell communication is therefore important for understanding how to detect, and combat, such diseases.

1.3.1 G Protein-Coupled Receptors

GPCRs form a large ubiquitous family of signalling receptors; humans alone encode ~800 GPCRs (Fredriksson, Lagerstrom et al. 2003) and they are found in all eukaryotic organisms. Although GPCRs do not share a high degree of sequence similarity they do share a highly conserved topology. GPCRs are involved in sensing a wide array of stimuli, or ligands, including light, odours, proteins, peptides, lipids, sugars, nucleotides and ions, and the extracellular signal is typically relayed within the cell via the G protein to promote a response.

1.3.1.1 Conformational States of G Protein-Coupled Receptors

GPCRs exist in a state of dynamic equilibrium between conformational states where receptors are in an "on" or an "off" state termed R* and R respectively (Kenakin 2002). Full agonists stabilize the "on" state R* and inverse agonists stabilize the "off" state R. Antagonists in contrast do not shift the equilibrium but block the binding of other ligands. Most receptors exist in a state shifted towards R in the absence of ligands; however

examples of receptors that are constitutively active do exist, for instance the sphingosine-1-phosphate receptors (Uhlenbrock, Gassenhuber et al. 2002) or the Mas and angiotensin II type 1 receptors (Kostenis, Milligan et al. 2005; Canals, Jenkins et al. 2006).

1.3.1.2 G Protein-Coupled Receptor Families

Due to the sheer size of the GPCR super-family, a classification system was created to subdivide the family. This classification scheme is based on homology, with receptors within the same group sharing ~25% sequence similarity in the TM core (Bockaert and Pin 1999; Pierce, Premont et al. 2002; Vroling, Sanders et al. 2010). The class A receptors is the largest class and include the well-studied GPCRs rhodopsin and β2-adrenergic receptors. These receptors may bind small ligands in their TM domains, such as light or odours, or peptides that mainly bind to the N-terminal region and extracellular loops. It also includes receptors that bind glycoprotein hormones and these have large extracellular domains to which the ligand binds. The class B receptors comprise a much smaller group of receptors and include the secretin-like receptors. These receptors are also characterized by their large extracellular domains to which large peptide hormones bind. Class C receptors include the metabotropic glutamate receptors, GABA-B, and receptors involved in sensing calcium. A number of additional small groups exist that are classified according to their respective organisms rather than sequence similarity, for instance the Class D yeast pheromone receptors, the Class E *Dictyostelium discoideum* cAMP receptors or the class F frizzled/smoothened group from *Drosophila melanogaster*.

1.3.1.3 G Protein-Coupled Receptor Signalling

GPCRs typically reside in the membrane in the inactive R state bound to the inactive heterotrimeric Gαβγ-GDP complex (Figure 1-5). Ligand binding promotes a rotation about TM6 and TM3, leading to R to R* isomerisation, typically triggered by a tryptophan residue in TM6 located two residues prior to a highly conserved proline residue (Gether, Lin et al. 1997; Shi, Liapakis et al. 2002; Xu, Wu et al. 2011). Receptors may acquire constitutively active mutations (CAMs) that stabilize the R* state (Ladds, Davis et al. 2005), and many human disease states are associated with CAMs (Seifert and Wenzel-Seifert 2002). In the activated R* state, GPCRs function as guanine nucleotide exchange factors (GEFs) and promote the dissociation of GDP and subsequent association of GTP on the Gα-subunit (Pierce, Premont et al. 2002). This frees the Gα and Gβγ complex from the receptor and the subunits are free to regulate downstream signalling effectors. Hydrolysis of Gα-GTP to GDP, either by intrinsic Gα-GTPase activity or by regulator of G protein signalling (RGS) proteins causes the re-association of Gαβγ-GDP with receptor and return to the R state.

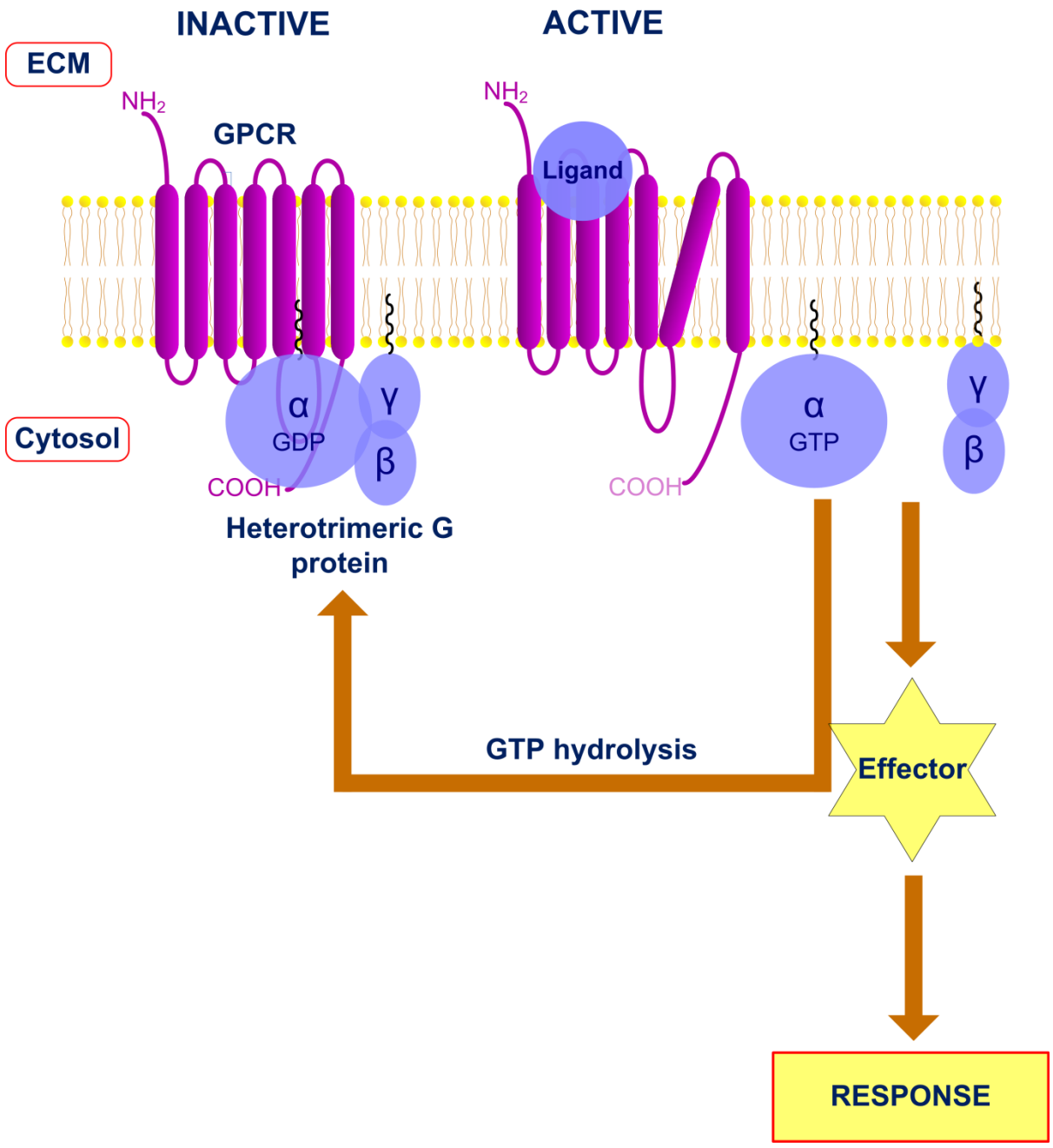

Figure 1-5: Generalized schematic of G protein-coupled receptor signalling

Ligands bind to regions of the GPCR located on the extracellular side. Binding of ligand activates the receptor through inducing conformational changes. This promotes intrinsic GEF activity in the receptor thereby promoting GDP for GTP exchange on the associated Gα subunit. Gα and Gβγ can then interact with intracellular effector proteins to bring about a cellular response. The signalling response is terminated upon Gα-GTP hydrolysis and reformation of the complete inactive heterotrimeric Gαβγ protein. Gα often contains intrinsic GTPase activity but hydrolysis of GTP may be enhanced by RGS proteins.

1.3.2 G Protein-Coupled Receptor Structure

1.3.2.1 Conserved Topology of G Protein-Coupled Receptors

Knowledge of the 3D structure of proteins is of utmost importance to the pharmaceutical industry because it enables the computerized screening and design of drugs, thereby reducing the cost and time-frame for drug development (Costanzi 2010). As mentioned in section 1.2.7, few structures of GPCRs have been solved to date but advances are being made (Bill, Henderson et al. 2011). The overall topology of GPCRs consists of seven TM spanning domains connected by three intracellular loops (IC) and three extracellular loops (EC). The N-terminus is positioned in the ECM and the C-terminus in the cytoplasm (Figure 1-6). Some GPCRs contain an additional amphipathic helix in the C-terminal tail (helix 8 or H8 in the diagram) and they may contain post-translational modifications such as disulphide bonds, shown to connect EC2 and TM3 in Figure 1-6.

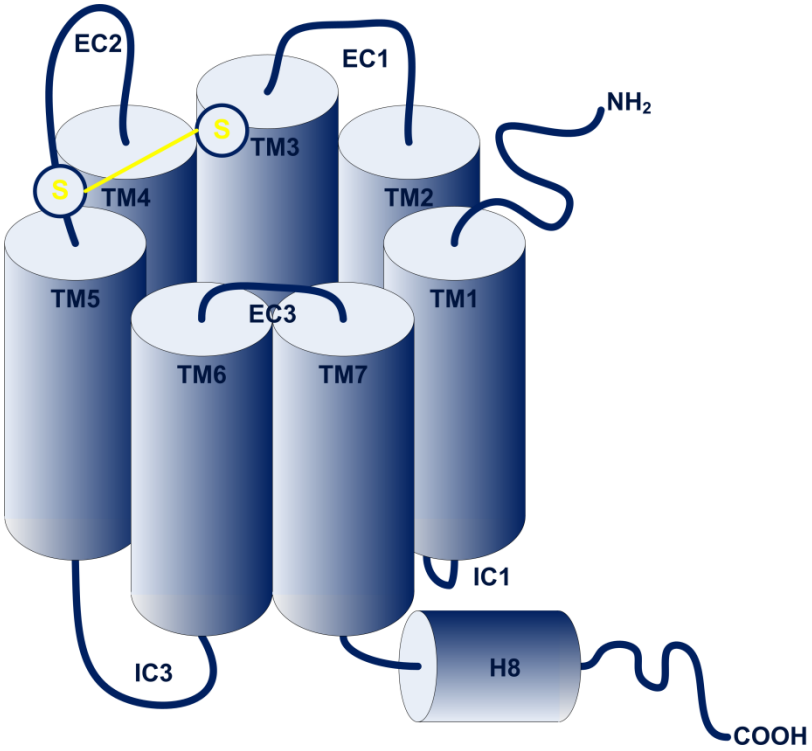

Figure 1-6: Topology of G protein-coupled receptors

G protein-coupled receptors contain seven transmembrane α-helical domains, denoted TM1-7 in the schematic. The TM domains are connected by three intracellular (IC) and three extracellular (EC) loops. The N-terminus is positioned on the extracellular side and the C-terminus is positioned in the cytosol. GPCRs may also contain an amphipathic helix in the C-terminal tail (H8) and post-translational modifications such as disulphide bonds (illustrated in yellow).

1.3.2.2 Crystal Structures of Inactive G Protein-Coupled Receptors

Rhodopsin when bound to its inverse agonist 11-cis retinal, was the first GPCR to be sequenced and to have its structure solved to atomic resolution (Hargrave, McDowell et al. 1983; Palczewski, Kumasaka et al. 2000). This was possible largely due to its high expression levels in retinal rod cells enabling the purification of large amounts of protein, and consequently the study of rhodopsin has pioneered much research in the GPCR field. Since then, a handful of other inactive GPCR structures have been solved to atomic resolution including (but not limited to); human β_2-adrenergic receptor in complex with the inverse agonist carazolol (Cherezov, Rosenbaum et al. 2007; Rasmussen, Choi et al. 2007), the turkey β_1-adrenergic receptor bound to the antagonist cyanopindolol (Warne, Serrano-Vega et al. 2008), human adenosine A_{2A} receptor in complex with the antagonist ZM241385 (Jaakola, Griffith et al. 2008), human dopamine D3 receptor in complex with the antagonist eticlopride (Chien, Liu et al. 2010) and human CXCR4 chemokine receptor bound to the antagonist peptide IT1t (Wu, Chien et al. 2010).

Sequence conservation between these class A GPCRs is highest within the TM core and the overall fold of the TM bundles are highly similar with root mean square deviations (RMSD) ranging from 0.7 for the β1- and β2-adrenergic receptors to 2.4 Å for rhodopsin and the adenosine A_{2A} receptor (Hanson and Stevens 2009). Some differences can be found in the tilt and length of TM domains, which may reflect the ability of the GPCRs to bind highly diverse ligands. The binding pocket of the β-adrenergic receptors are similar to that of rhodopsin where the long axis of the ligand is parallel to the membrane and makes contact with TM3, TM5, TM6 and TM7. In these structures cyanopindolol and carazolol do not make contact with the tryptophan residue involved in the rotational switch in activation of the β-adrenergic receptors (see section 1.3.1.3), retinal in contrast does make contact with this residue (Rosenbaum, Cherezov et al. 2007). In contrast, the binding pocket of the adenosine A_{2A} receptor is quite different, and the ligand binds perpendicular to the membrane rather than parallel and mainly contacts the EC2 loop (Hanson and Stevens 2009). Rhodopsin and the β-adrenergic receptors differ greatly in their extracellular region. In rhodopsin there is extensive structure to this region that serves to exclude solvent from the binding site, whereas the β-adrenergic receptors adopt a more open conformation, possibly to allow the ligand access to the binding site (Hanson and Stevens 2009).

Interestingly, the crystal structure of the CXCR4 chemokine receptor reinforced data suggesting that this receptor forms dimeric complexes (Wu, Chien et al. 2010). Homo- and hetero-dimerization of the CXCR4 receptor is believed to have pharmacological effects important to human disease states. For instance WHIM syndrome (warts,

hypogammaglobulinemia, infections and myelokathexis) result from the heterozygous expression of mutant CXCR4 receptor unable to internalize and wild-type receptor, where dimerization is believed to cause the dominance of mutant CXCR4 over the wild-type receptor (Balabanian, Lagane et al. 2005; Lagane, Chow et al. 2008). Surprisingly the dimeric interface of the CXCR4 GPCR did not involve the core of the TM bundle, which is implicated in the dimerization of many membrane proteins including some GPCRs, but instead appeared to be driven by hydrophobic interactions at the extracellular side of TM5 and TM6 (Wu, Chien et al. 2010).

Comparisons between the intracellular regions are hindered by the addition of T4 lysozyme in the IC3 loop area of all solved structures except rhodopsin. This enzyme was added because IC3 is highly flexible thereby allowing helices to move and the introduction of T4 lysozyme restricts the movement of helices whilst maintaining the polar surface needed for crystallization (Rosenbaum, Cherezov et al. 2007). Rhodopsin, but not the β-adrenergic receptors and adenosine A_{2A} receptor, was found to contain an ionic lock formed by a salt-bridge between a highly conserved E/DRY motif in TM3 and a glutamate residue in TM6. This ionic lock is believed to keep the receptor in an inactive state, and mutations of these residues in the β_2-adrenergic receptor result in a CAM phenotype. It was therefore surprising that the ionic lock is absent from the structure of the β-adrenergic receptors and adenosine A_{2A} receptor, and two possible explanations were proposed. Either the ionic lock is absent altogether from these receptors, which could explain their higher basal activity compared to rhodopsin (but does not explain why mutations induce the CAM phenotype) or is because the T4 lysozyme interferes with the residues that form the ionic lock (Rosenbaum, Rasmussen et al. 2009). In contrast the crystal structure of the human dopamine D3 receptor revealed that this receptor contains an ionic lock despite the presence of T4 lysozyme (Chien, Liu et al. 2010).

1.3.2.3 Crystal Structures of Activated G Protein-Coupled Receptors

Recently, several structures of activated receptors have been published. These include the activated form of rhodopsin “opsin” and its active metarhodopsin II intermediate (Park, Scheerer et al. 2008; Scheerer, Park et al. 2008; Choe, Kim et al. 2011). The most notable changes compared to rhodopsin include two openings in the retinal binding pocket, which may allow the dissociation of retinal upon activation. The tryptophan residue implicated in the rotation of TM6 has moved into space previously occupied by retinal (Rosenbaum, Rasmussen et al. 2009). The ionic lock is also lost and the arginine residue on TM3 involved in forming the ionic lock instead appear to interact with a Gα-derived peptide included in the structure (Scheerer, Park et al. 2008).

The structure of adenosine A_{2A} receptor bound to an adenosine derivative was recently released (Xu, Wu et al. 2011). In this structure, ligand binding was much more extensive compared to when bound to the structurally smaller antagonist ZM241385, thereby stabilizing the active state. Rotation about the conserved tryptophan residue in TM6 was also observed in this receptor, allowing extensive remodelling of TM5 and TM7. In both opsin and adenosine A_{2A} there is a conserved NPxxY motif in TM7, which also undergoes a rotational switch upon activation. In the adenosine A_{2A} receptor, movement was much more pronounced than for opsin, and involved extensive tilting of TM7. Furthermore, the residues that may be involved in the ionic lock (but were not resolved in the inactive structure) were observed to move apart.

These studies all reflect the structural diversity among the class A GPCR family, despite their relatively high sequence conservation. It will be interesting to see how similar, or dissimilar, the other classes of GPCRs are compared to these receptors and the release of more structures will aid the computational modelling of receptor:drug interactions.

1.3.3 G proteins and Effector Systems

1.3.3.1 G Protein Activity

Guanosine nucleotide binding proteins (G proteins) represent a diverse family of signalling proteins involved in the regulation of many cellular processes such as secretion, motility or transcription, by regulating proteins such as transporters, ion channels, or metabolic enzymes (Neves, Rarn et al. 2002). G Proteins are involved in both relaying the message from an activated GPCR, as well as regulating GPCR signalling pathways.

G proteins contain an α-helical domain involved in upstream protein specificity and a GTPase domain involved in nucleotide binding and effector specificity. G proteins function as molecular switches; when bound to GDP they are “off” and when bound to GTP they are “on” (illustrated in Figure 1-7). GEFs facilitate the dissociation of GDP thus allowing the more cellularly abundant GTP to bind, and thereby promoting the “on” state. When switched on G proteins can bind downstream effectors to promote the cellular response (Gulbins, Coggeshall et al. 1994; Lambright, Noel et al. 1994). Most G proteins contain some level of intrinsic GTPase activity to turn off activity, although intrinsic activity tends to be slower than needed for rapid physiological changes and hydrolysis can be accelerated ~1000 fold by GTPase accelerating proteins (GAPs) (Ahmadian, Stege et al. 1997). G proteins with intrinsic GTPase activity contain a conserved arginine residue which is inserted into the G protein catalytic site to promote hydrolysis of GTP and convert the G protein to the “off”

state, and GAPs may stabilize this conformation. In G proteins with no intrinsic GTPase activity, the GAP itself may contain and insert this “arginine finger” (Ahmadian, Stege et al. 1997; Resat, Straatsma et al. 2001). G proteins may be held in the inactive state by guanosine nucleotide dissociation inhibitors (GDIs).

1.3.3.2 Monomeric G Proteins

Many G proteins can exist as stable monomers including the Ras oncogenes, or the Ras-like families of GTPases ARF and Rab (mentioned previously in sections 1.2.3.3 and 1.2.4.2), or Rho. Rac1 is an example of the Rho family of GTPases and is involved in cell adhesion, endocytosis, the immune response, transcription and the cell cycle (Bosco, Mulloy et al. 2009). Its numerous involvements in cellular processes clearly emphasize the importance of monomeric G proteins to cellular function.

1.3.3.3 Heterotrimeric G Proteins

G proteins can also exist in a heterotrimeric arrangement of three subunits; Gα, Gβ and Gγ that associate with GPCRs to relay signals. This complex can be viewed as a dimer, because signalling can either occur via the Gα subunit or the Gβγ subunits, and dissociation of the Gβγ subunit can often only occur under denaturing conditions (Neves, Rarn et al. 2002). In GPCR signalling, GEF activity in the receptor, which may involve remodelling of the ionic lock to incur changes in the G protein (Scheerer, Park et al. 2008), results in the activated heterotrimeric G protein exposing effector binding sites. The activated G protein may dissociate to propagate the signal, or may exist in scaffolded signalling complexes (Wang, Golebiewska et al. 2009). In addition to the GPCR, heterotrimeric G protein activation may also be achieved via monomeric G proteins that function as GEFs; for example Rab3 (Cismowski 2006). Signalling is terminated upon GTP hydrolysis, which promotes the reassociation of Gαβγ and return to the inactive state (Figure 1-5).

1.3.3.3.1 Gα-Families

In human cells, 16 genes encode for more than 20 different Gα subunits that share 35-95% sequence identity and are divided into four distinct families that affect a range of targets, which may be overlapping (Khafizov, Lattanzi et al. 2003). The G_s family includes G proteins that are activated by many GPCRs, notably including the olfactory receptors, and primarily stimulate Ca^{2+} channels and adenylyl cyclase, though they may have an inhibitory role on Na^{+} channels. The G_i family in contrast has an inhibitory role on adenylyl cyclase, and may close Ca^{2+} channels but stimulate K^{+} channels. Both G_s and G_i may stimulate the tubulin

GTPases, indicating the functional overlap between classes of G proteins. The G_i family also include G_t which is activated by vertebrate rhodopsin to stimulate phosphodiesterase 6 in vision (Neves, Rarn et al. 2002). The invertebrate squid rhodopsin in contrast, signals via a G protein from the G_q family, which activates phospholipase C (PLC) (Murakami and Kouyama 2008). Finally, the $G_{12/13}$ family of G proteins activate many monomeric G proteins such as Rho and Ras (Neves, Rarn et al. 2002). Although the effector proteins appear relatively specific to the various types of Gα, the same is not observed for the targets of Gβγ or even the Gα subunit that they couple to (Wang, Golebiewska et al. 2009).

In addition to signalling via the Gα, GPCR signalling cascades may also be activated by the Gβγ heterodimer. This is for instance observed in the yeast *Saccharomyces cerevisiae* (*Sc. cerevisiae*) pheromone-response signalling cascade where Gβγ activates the mitogen activated protein kinase (MAPK) cascade and the Gα subunit instead adopts an inhibitory role on signalling (Dohlman 2002). Signalling cascades may also be activated independently of the G protein altogether, which has been observed in β2-adrenergic receptor upon binding arrestin (Shenoy, Drake et al. 2006).

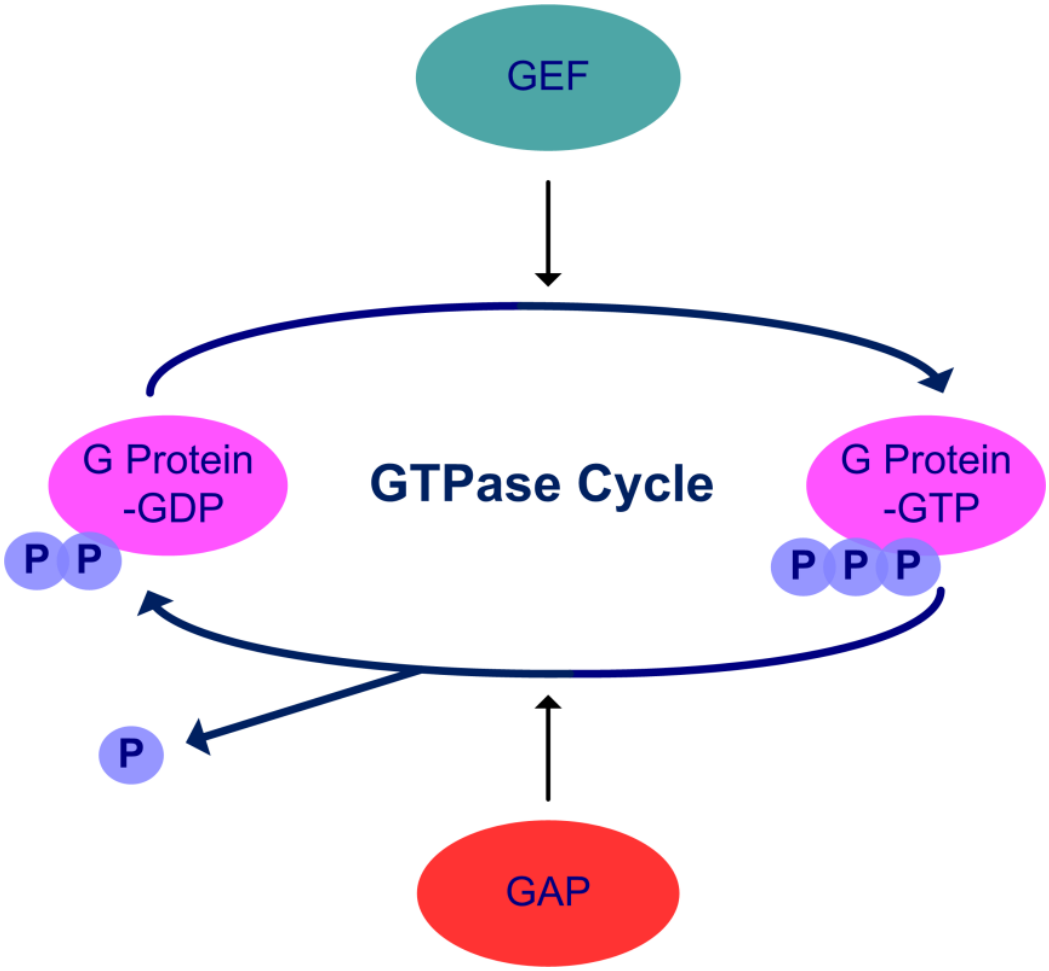

Figure 1-7: The GTPase cycle

Schematic of the G protein GTPase cycle. GEFs stimulate the GDP for GTP exchange on the G protein. Many G proteins contain intrinsic GTPase activity and can hydrolyse the γ-phosphate thus returning to the GDP-bound conformation. Hydrolysis can be accelerated by a GAP.

1.3.3.4 Second Messengers

The effector molecules themselves affect "second messenger" levels. PLC for instance cleaves fatty acids to produce the second messengers DAG (diacylglycerol) and IP_3 (inositol triphosphate). IP_3 can then diffuse through the cytosol and activate IP_3 receptors. Targets of IP_3 receptors include calcium channels in the ER, which cause cytosolic calcium levels to increase and lead to further changes in the cell. DAG in turn remains bound to the membrane and may activate protein kinase C (PKC) together with the increased levels of Ca^{2+}, and upon activation PKC phosphorylates other molecules. The direct binding of G proteins to ion channels in contrast can affect the membrane potential, or have a direct effect on calcium levels (Lodish, Berk et al. 2000).

The second messenger cyclic AMP (cAMP) is produced from adenylyl cyclase and broken down by cAMP phosphodiesterases. Different isoforms of adenylyl cyclase in mammals are regulated either by G proteins or by Ca^{2+} (and as mentioned in the previous paragraph, both G_s and G_i may affect Ca^{2+} levels, as well as directly regulating adenylyl cyclase). Upon adenylyl cyclase activation, there is a rise in cellular cAMP and consequently there is a rise in activated protein kinase A (PKA) (as illustrated in Figure 1-8), the target of cAMP. Released subunits of PKA move into the nucleus, where they phosphorylate the cAMP regulatory element binding protein (CREB; several different subtypes exist). CREB recruits the co-activator CREB binding protein (CBP) and together they stimulate transcription. Different cell types may respond differently to increasing levels of cAMP, and this pathway regulate the transcription of many genes including hormone synthesis in endocrine cells or proteins in the brain involved in long term memory. Furthermore, many ligands may activate adenylyl cyclase in the same cell type. Despite this diversity, the same cell type may respond in the same way independent of ligand type. For instance, four different hormones that all stimulate cAMP production in adipose cells all lead to the breakdown of triacylglycerol to fatty acids (Lodish, Berk et al. 2000; Alberts, Johnson et al. 2002).

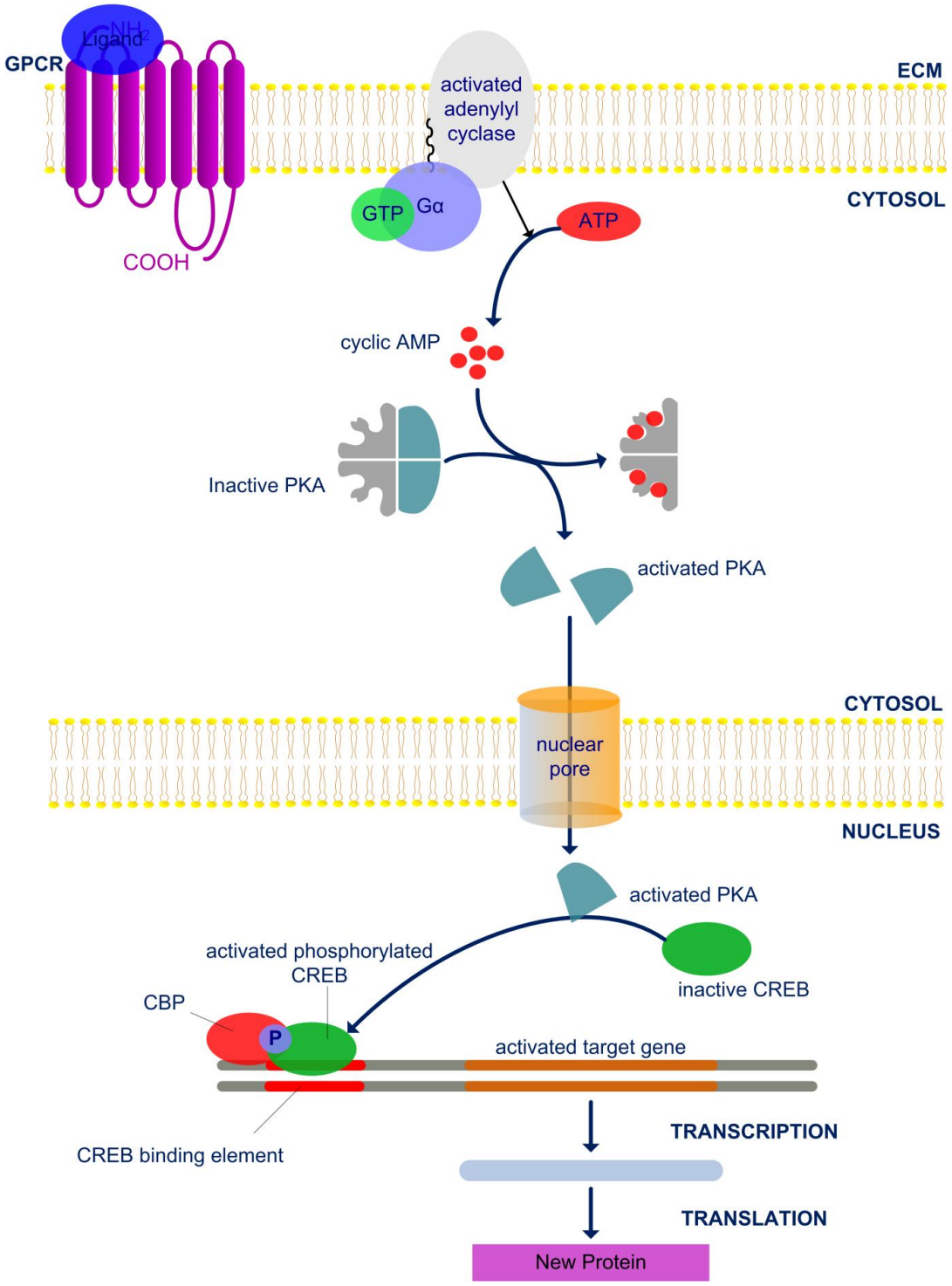

Figure 1-8 Regulation of gene transcription by G protein stimulated adenylyl cyclase

Activation of the G_S protein following the activation of the GPCR leads to activated adenylyl cyclase. Activated adenylyl cyclase rapidly converts ATP to 3'5'-AMP. Increased levels of AMP leads to increased levels of activated PKA (protein kinase A) in the cytosol. PKA consists of two regulatory and two catalytic subunits, which are separated upon cAMP binding. Upon activation the catalytic subunits dissociate and are free to move into the nucleus and phosphorylate CREB (cAMP regulatory element binding protein). CREB can in its phosphorylated form recruit the co-activator CBP and together they up-regulate gene transcription.

1.3.4 Regulators of G Protein-Coupled Receptor Signalling

1.3.4.1 Regulation of G Protein-Coupled Receptor Expression

GPCR signalling is regulated on many levels. GPCRs and associated signalling molecules may be up- or down-regulated at a transcriptional level through transcription factor activity (Sugimoto, Iino et al. 1991; Pashkov, Huang et al. 2011) and some GPCRs may even regulate their own transcription through a positive feedback loop. This is seen, for instance, with the *Sz. pombe* transcription factor Ste11, which is activated through the MAP Kinase cascade triggered by the activated GPCR Mam2, and up-regulates *Mam2* transcription to achieve increased sensitivity of the receptor (Kjaerulff, Lautrup-Larsen et al. 2005; Wood, Kwon et al. 2011). Mam2 mRNA may further be stabilized by the RNA binding protein Csx1 and because Mam2 is needed for mating *Csx1*$^{-}$ mutants are sterile (Matia, Sotelo et al. 2011). Instead of up-regulating GPCR plasma membrane expression at a transcriptional level, some GPCRs may be stored in intracellular compartments and released to the plasma membrane following agonist activation (Hein, Ishii et al. 1994; Brismar, Asghar et al. 1998), thereby sensitizing the pathway (Achour, Labbe-Jullie et al. 2008).

1.3.4.2 Binding of Ligand

One GPCR may bind several different ligands, and the type of ligand may alter the coupling that the GPCR has for different G proteins (Ladds, Davis et al. 2003). This may be attributed to the many molecular switches that can occur in GPCR activation, and ligands may trigger different switches, leading to altered G protein specificity and ultimately altered cellular responses (Ahuja and Smith 2009). Ligand-specificity in turn may be controlled, as discussed in section 1.2.3.1 through the single transmembrane spanning proteins RAMP (McLatchie, Fraser et al. 1998). RAMPs regulate many additional aspects of GPCR signalling (Kuwasako, Shimekake et al. 2000) including chaperoning trafficking during endocytosis (Kuwasako, Shimekake et al. 2000) and trafficking from ER to Golgi (Bouschet, Martin et al. 2005). For some receptors RAMP expression is absolutely necessary for trafficking explaining difficulties in expressing some GPCRs in heterologous systems (Parameswara and Spielman 2006).

1.3.4.3 Activators of G Protein Signalling

Heterotrimeric G proteins may achieve activation in the absence of receptor, a mechanism mediated by activator of G protein signalling (AGS) proteins, and these proteins may be subdivided into three distinct functional groups (Blumer, Cismowski et al. 2005; Cismowski

2006; Sato, Blumer et al. 2006). Group one currently has two members which act as GEFs and activate heterotrimeric G proteins independently of GPCRs but inhibit signalling via the Gβγ complex (Hill, Goddard et al. 2009). Group two comprise a larger group with four members which act as GDIs and prevent signalling via Gα but allow the Gβγ complex to dissociate. The third group has three members and all bind the Gβγ complex in the absence of receptor, and facilitate interactions with effectors.

1.3.4.4 Receptor Internalization

GPCRs may be down-regulated via endocytosis as discussed in section 1.2.4. For GPCRs specifically, endocytosis may occur in the presence of ligand or constitutively and can be mediated by CME or non-CME pathways (Scarselli and Donaldson 2009). Phosphorylation of serine and threonine residues in the IC3 loop or C-terminal tail-region is a common mechanism to target the receptor for internalization. Phosphorylation may be mediated by G protein-coupled receptor kinases (GRKs) or the second messengers protein kinase A (PKA) or protein kinase C (PKC), and different kinases may phosphorylate different sites in the receptors (Tobin, Butcher et al. 2008). One function of GRK phosphorylation is to increase the rate of arrestin recruitment to the GPCR, and phosphorylation by different GRKs result in variations in the rate of recruitment to the β2-adrenergic receptor (Violin 2006). Phosphorylation by PKA in contrast does not lead to arrestin recruitment to the β2-adrenergic receptor. This can possibly be explained by that phosphorylation by GRKs increase the negative charge at the arrestin binding site, which might be needed to promote arrestin binding. Phosphorylation at sites other than the arrestin binding site may therefore not affect arrestin binding (Violin 2006).

Arrestin binding has two effects on GPCR signalling; it occludes the binding site for the heterotrimeric G protein thereby preventing its activation, and it links the receptor to CME (Figure 1-9). Arrestin binding to a receptor exposes a binding site for clathrin and AP2. Following internalization the arrestin may rapidly dissociate, as observed with the β2-adrenergic receptor, or remain tightly bound, as seen with the vasopressin type II receptor. The biological significance of the different dissociation rates is unclear, but it may play a role in delaying receptor recycling (Oakley, Laporte et al. 1999) or it has been speculated that some receptors that remain bound to their heterotrimeric G proteins may continue to signal from the endosomes (Jalink and Moolenaar 2010) although this hypothesis is controversial (DeFea 2011).

Arrestins do not solely function as signal terminators, but may also serve as scaffolds for signalling via many pathways, including amongst many others the MAPK cascade,

independently of heterotrimeric G proteins (Shenoy, Drake et al. 2006) although this does not appear to be typical (DeFea 2011). Like with many GPCR regulating mechanisms, the precise mechanism determining the fate of arrestin-bound receptors; be it recycling, degradation or G protein independent signalling, are unclear.

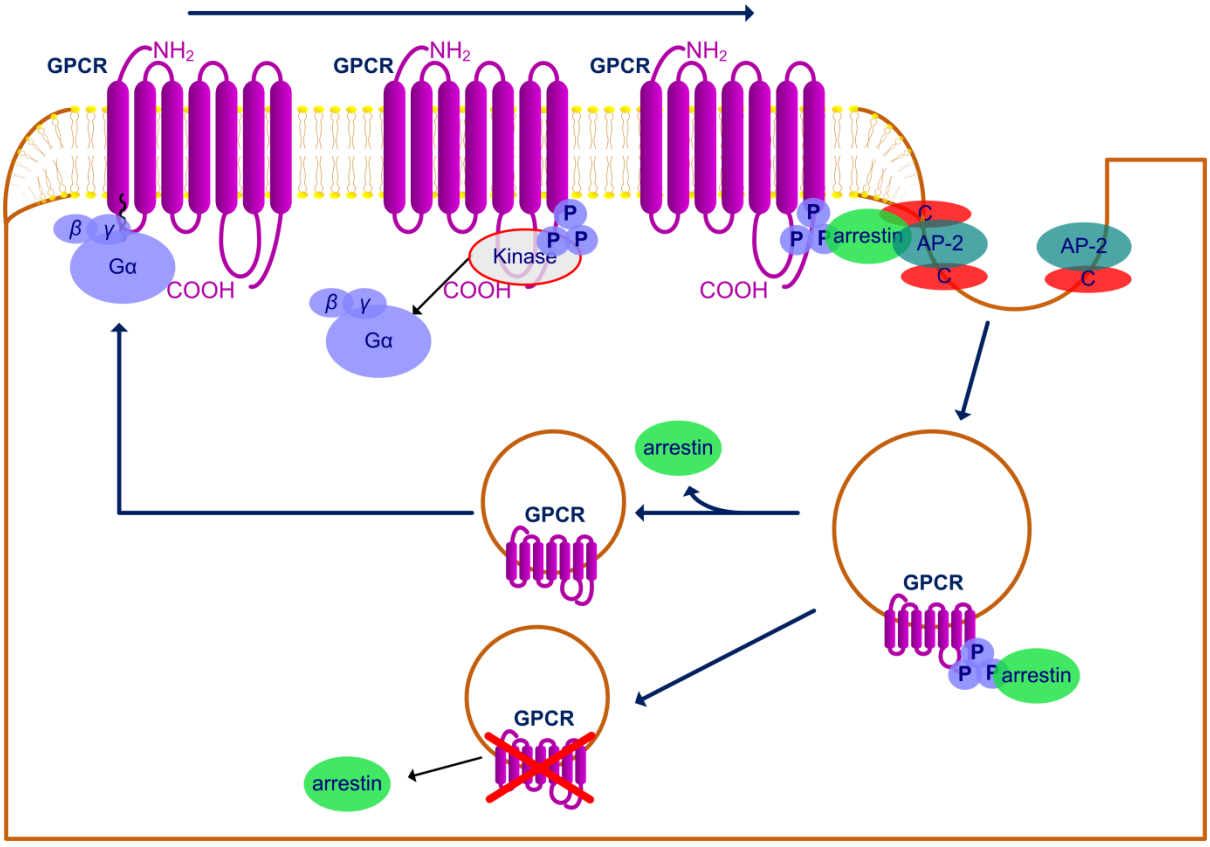

Figure 1-9: G protein-coupled receptor internalization via β-arrestin

The GPCR is initially expressed at the plasma membrane. Following phosphorylation by a protein kinase the heterotrimeric G protein is displaced by arrestin. Association of arrestin with the GPCR expose a clathrin/AP2 binding domain and the complex is recruited into clathrin coated pits. Upon budding of the pit, clathrin is lost. Following arrestin dissociation, the GPCR may be recycled back to the plasma membrane or be degraded in lysosomes.

1.3.5 G Protein-Coupled Receptor Oligomerization

An additional layer adding to the complexity of GPCR regulation is the notion that some GPCRs are capable of forming homo- or hetero-oligomers. Although the area has been surrounded by some controversy (Chabre and le Maire 2005) it is now generally accepted that some GPCRs form oligomeric complexes of functional importance. The formation of these complexes play a role in a number of cellular functions including receptor trafficking, ER quality control, signal amplification, trans-activation, ligand sensitivity, G protein specificity, internalization or pharmacology, and has been extensively reviewed in the literature (Park, Filipek et al. 2004; Terrillon and Bouvier 2004; Skrabanek, Murcia et al. 2007; Gurevich and Gurevich 2008; Ferré, Baler et al. 2009).

1.3.5.1 A Functional Role for Receptor Oligomerization

The chemokine receptors provide an interesting case study for GPCR oligomerization. The chemokine receptors represent a family of 19 GPCRs in humans involved in chemotaxis of many cell types, for instance leukocytes, and they primarily signal through a $G\alpha_i\beta\gamma$ complex (Moser, Wolf et al. 2004). Chemokine receptor signalling involves activation of PLC and promote the release of calcium from intracellular stores via DAG and IP_3 (see section 1.3.3), which activate a MAPK cascade and lead to chemotaxis. The crystal structure of the chemokine receptor CXCR4 indicate that this receptor exist in a dimeric form (Wu, Chien et al. 2010) and is the only crystal structure of a dimeric GPCR to date. CXCR4 is also able to form hetero-dimers with other chemokine receptors and ligand binding does not promote or dissociate either homo- or hetero-oligomers (Percherancier, Yamina et al. 2005). The CXCR7 receptor can bind the same chemokine ligand as CXCR4, however it cannot couple to G_i and for this reason it was initially classified as an orphan receptor. A recent study demonstrated that CXCR7 can hetero-oligomerize with CXCR4 to form a complex that constitutively signal via arrestin whereas G_i signalling is suppressed. Cells signalling via this pathway show enhanced chemotaxis compared to when signalling via CXCR4 alone (Decaillot, Kazmi et al. 2011) demonstrating a distinct functional role for receptor hetero-association.

GPCR hetero-dimerization is also implied in GPCR transport, for instance in the case of GABABR1. When expressed alone, the GABABR1 receptor is retained in the ER but when co-expressed with GABABR2, GABABR1 is released from the ER and is transported to the cell surface. Hetero-dimerization of the two receptors masks an RxR-based ER-retention signal in the GABABR1 tail, thereby allowing its export from the ER (White, Wise et al. 1998).

1.3.5.2 Effects of Oligomerization on the R* State

The importance of homo-dimer formation on GPCR function is not yet fully understood, but different ligands may influence the dimeric state. For instance in the β2-adrenergic receptor, agonist binding stabilizes the dimeric form whereas binding of inverse agonist favours the monomeric form (Hebert, Moffett et al. 1996). One hypothesis is that oligomer formation may be involved in allosteric regulation (Maurice, Kamal et al. 2011). For instance, in the dopamine D_2 receptor, agonist binding to one protomer in a dimer induces activation of both receptors. When another agonist is introduced into the second protomer, the functional response is inhibited whereas introduction of an inverse agonist enhance signalling. Binding of inverse agonist to the second protomer appear to stabilize the R* state (which is shifted towards R* due to binding of agonist to the first protomer and conformational changes in the first protomer are translated to the second), in contrast, binding of a second agonist has negative allosteric effects, possibly due to incompatibility between the different structural conformations adopted by the protomers when bound to different ligands. Although these structural conformations each alone can signal, they may not cooperatively be able to (Han, Moreira et al. 2009). This same effect has been observed in homo-dimers of oxytocin (Albizu, Cottet et al. 2010) and heterodimers of adenosine A_{2A}-μ-opioid receptors (Vilardaga, Nikolaev et al. 2008).

1.3.5.3 Interactions Governing Receptor Oligomerization

Despite the abundance of data supporting the existence of GPCR oligomers, little information is available on the mechanism for interactions, and predictions are often restricted to whole TM domains rather than specific amino acids. For instance there is evidence to suggest that some GPCRs interact via TM1-TM1 interactions as well as TM4 and/or TM5, for instance the C5a receptor (Klco, Lassere et al. 2003), STE2 (Wang and Konopka 2009), the mouse delta opioid receptor (Johnston, Aburi et al. 2011) or rhodopsin (Liang, Fotiadis et al. 2003), although the occurrence of rhodopsin oligomers is debated (Edrington, Bennett et al. 2008). The specific residues involved in the interactions however are largely unknown.

For some receptors however, individual residues have been shown to be involved in oligomerization. For instance, there is evidence for TM6-TM6 interactions in the β2-adrenergic receptor via a GxxxG motif (Hebert, Moffett et al. 1996) and there is also evidence that the STE2 pheromone receptor dimerizes via a GxxxG motif in TM1 (Overton, Chinault et al. 2003). Not all dimerization events are mediated by transmembrane interactions; the metabotrobic glutamate receptors for instance dimerizes via a disulphide

bond in the extracellular domain (Romano, Yang et al. 1996; Kunishima, Shimada et al. 2000). The CXCR4 receptor also dimerizes via interactions outside of the TM bundle although in this receptor interactions appear to be driven via the hydrophobic effect, involving the extracellular regions of TM5 and TM6 (Wu, Chien et al. 2010).

1.4 Yeast Models

GPCR signalling is difficult to study in mammalian systems for a number of reasons. In humans, ~1000 GPCRs couple to ~20 Gα, 5 Gβ, and 12 Gγ subunits in various combinations as well as coupling to many different regulators. Furthermore, different receptors may be activated by the same ligands, and substantial cross-talk can occur throughout the signalling cascades (Zaugg and Schaub 2004). This makes it extremely challenging to study individual component parts of the signalling pathways. Metazoa are additionally relatively difficult to study *per se*, and research is therefore often done in cell lines as opposed to whole organisms. Mammalian cell lines in turn are difficult to handle, meaning that much research is performed *in vitro* using cell extracts.

Many cellular events are conserved between yeast and higher eukaryotes. In contrast to higher eukaryotes, yeast are relatively easy to manipulate, simple to culture and are fast-growing; making it an excellent model organisms in which to study eukaryotic cellular processes. Yeast are unicellular eukaryotic organisms that may grow by budding, as observed with *Sc. cerevisiae*, or by binary fission, as observed in *Sz. pombe*. Despite both of these yeasts being unicellular ascomycete fungi, they are not closely related. Estimates of their divergence range from 330-420 million years ago, making fission yeast and budding yeast as distantly related to each other as mammals are to either yeast (Sipiczki 2000). Their relative evolutionary distance is reflected in their genome content where 75% of fission yeast genes are conserved in budding yeast, compared to 71% conserved to metazoan genes (Wood 2006). Most house-keeping genes are conserved between fungi and metazoa and differences are mainly found in organism-specific processes such as spore-formation in fungi or development in metazoa. Sequence identity between fission yeast and budding yeast range from 60-90% which is similar to the metazoan homologs (Moreno, Klar et al. 1991), although some metazoan processes appear more similar in *Sz. pombe* compared to *Sc. cerevisiae*, for instance cell-cycle control, centromere structure, cytokinesis or mitochondrial maintenance and regulation (Kuhl, Dujeancourt et al. 2011; Wood 2011). The similarities of these two fungi to metazoa make them suitable model organisms for many higher eukaryotic processes, and their relative difference makes the study of both valuable.

1.4.1 Studying G Protein-Coupled Receptor Signalling in Budding Yeast

Sc. cerevisiae has extensively been used as a model organism to overcome the difficulties of studying GPCR signalling systems in mammalian cells. *Sc. cerevisiae* contain two GPCR signalling pathways; one involved in glucose-sensing, and one involved in mating. Several important findings about GPCR signalling were discovered in *Sc. cerevisiae* including signalling via Gβγ (Whiteway, Hougan et al. 1989) and the existence of RGS and AGS proteins (Dohlman and Thorner 1997; Cismowski, Takesono et al. 1999). *Sc. cerevisiae* has also been utilized to investigate many human GPCR signalling components, discoveries including ligands for orphan GPCRs (Ladds, Goddard et al. 2005). There are however limitations to studying GPCR signalling in *Sc. cerevisiae*. For example, budding yeast signal via the Gβγ subunit in the pheromone-response pathway, and the Gα has a negative regulating role (Dohlman 2002). This may create problems when expressing human components in the yeast such as RGS proteins to investigate Gα function, because they will regulate a negative regulator rather than a stimulatory Gα. Furthermore, only ~50% of heterologous GPCRs couple to the pheromone pathway in *Sc. cerevisiae* (Dowell and Brown 2002) which may reflect difficulties in coupling to Gα, incorrect protein folding, incorrect post-translational modifications, issues with trafficking, or an inability of the ligand to cross the cell wall (Ladds, Goddard et al. 2005).

1.4.2 Studying G Protein-Coupled Receptor Signalling in Fission Yeast

Similar to *Sc. cerevisiae*, *Sz. pombe* contain two distinct GPCR signalling pathways; one involved in glucose-sensing via the GPCR Git3 and the activation of adenylate cyclase (Welton and Hoffman 2000; Ivey and Hoffman 2005) and one involved in pheromone-sensing via the GPCR Mam2 or Map3 and activation of a MAP kinase cascade (Davey 1992; Tanaka, Davey et al. 1993). Activation of the glucose-sensing pathway prevents the activation of the pheromone-responsive pathway through repression of the transcription factor Ste11 by activated PKA (Maeda, Mochizuki et al. 1990), but apart from this regulation there is no known cross-talk between the two signalling cascades (see (Davey 1998; Hoffman 2005) for reviews). Unlike in *Sc. cerevisiae*, signal propagation in the *Sz. pombe* GPCR signalling pathways are mainly achieved via the Gα subunits meaning that they resemble the majority of metazoan GPCR signalling pathways more closely. Heterologous GPCRs and downstream signalling components have in many cases been successfully investigated in *Sz. pombe* via the pheromone-sensing pathway (Ladds, Davis et al. 2003;

Ladds, Goddard et al. 2005; Ladds, Goddard et al. 2007) although without Gα modifications (Ladds, Davis et al. 2003) human GPCRs may fail to couple to the *Sz. pombe* signalling cascade despite high expression levels (Sander, Grünewald et al. 1994; Arkinstall, Edgerton et al. 1995; Ficca, Testa et al. 1995).

1.4.2.1 The Fission Yeast Pheromone-response

Sz. pombe exist in one of two mating states; M (minus) or P (plus). During vegetative growth cells exist in a haploid state but under conditions of nitrogen starvation, cells arrest in G1 and mating of cells of opposite phenotype is initiated, resulting in the formation of diploid zygotes (Nielsen 2004), followed by meiosis and sporulation (Yamamoto 2004). M cells express the GPCR Mam2 which sense P-factor, secreted by P cells. P cells in turn sense M-factor through the GPCR Map3, which is secreted by M cells. Both M-factor and P-factor are short polypeptide pheromones, 9 and 23 amino acids long respectively (Davey 1992; Imai and Yamamoto 1994).

Stimulation of Map3 or Mam2 by pheromone promotes activation of the Gα subunit Gpa1 (Obara, Nakafuku et al. 1991). Unlike in the glucose-sensing pathway, there is no confirmed Gβγ complex coupling to the pheromone-response pathway. A putative Gβ-subunit has been described in the literature however and although it is not required to propagate the signalling response it acts as a negative regulator of signalling. The deletion phenotype of this gene can be rescued by the expression of human Gβ-subunits (Goddard, Ladds et al. 2006). The activation of the *Sz. pombe* pheromone-response leads to the induction of two individual cellular response-pathways; one resulting in the transcription of genes involved in mating and one resulting in morphological changes in the cell (Figure 1-10). At the initiation point of the pheromone-response, the G protein-coupled receptor Mam2 or Map3 is activated upon binding of ligand, and conformational changes in the receptor cause a GDP for GTP exchange in the G protein Gpa1 (Ladds, Davis et al. 2005). The immediate downstream target of Gpa1 is yet uncharacterized but results in activation of the monomeric G protein Ras1 via one of the GEFs Ste6 or Efc25, which are believed to be in competition with each other. Activation of Ras1 via Ste6 leads to the transcriptional response whereas activation of Ras1 via Efc25 results in morphological changes in the cell (Sipiczki 1988; Papadaki, pizon et al. 2002; Forfar 2007).

In the transcriptional response, Ras1 activate the MAP kinase kinase kinase (MAPKKK) Byr2. Activated Byr2 in turn phosphorylate the MAP kinase kinase (MAPKK) Byr1, whose target is the MAP kinase (MAPK) Spk1. Activated Spk1 is translocalized to the nucleus where it activates the transcription factor Ste11, partly by direct phosphorylation of the

transcription factor and partly by inhibiting the regulatory Pat1 kinase (Kjaerulff, Lautrup-Larsen et al. 2005). The high mobility group (HMG) box transcription factor Ste11 is responsible for the increased expression of most of the 163 proteins upregulated in response to pheromone and binds A-rich DNA regions (Sugimoto, Iino et al. 1991; Xue-Franzen, Kjaerulff et al. 2006)

Activation of Ras1 via the GEF Efc25 in contrast, leads to morphological changes in the cell starting with the activation of Scd1. Scd1 is the exchange factor for Cdc42 – a Rho-like GTPase, which phosphorylates the p21 activating kinase (PAK) Shk1. Activated Shk1 phosphorylates a number of proteins including Orb6 and Tea1 (Kim, Yang et al. 2003) and the Rho-GAP Rga8 involved in negative regulation of the Shk1 mediated growth pathway (Yang, Qyang et al. 2003), which aid controlling changes in cell morphology by modulating microtubule activity and the actin cytoskeleton. Orb6 is a serine/threonine kinase involved in cytoskeleton organization and cell cycle control (Verde, Wiley et al. 1998). Tea1 establishes growth at the cell tips (Glynn, Lustig et al. 2001) together with other proteins including Pom1 and Tea3 (Niccoli, Arellano et al. 2003). Morphological changes in the cell as a result of the pheromone-response include growing from the tip of the cell towards the source of pheromone, resulting in elongated, ‘shmooing’, cells with increased cell volume (Davey 1991).

The shmoo response brings cells of opposite mating type into physical contact, resulting in hydrogen bond formation between the mating-type specific agglutinins Mam3 (expressed by M-cells) and Map4 (expressed by P-cells) at the cell tips (Sharifmoghadam, Bustos-Sanmamed et al. 2006). Agglutination results in fusion of the two cells and their nuclei, thereby producing a diploid. Four spores are then formed by meiosis, containing haploid nuclei.

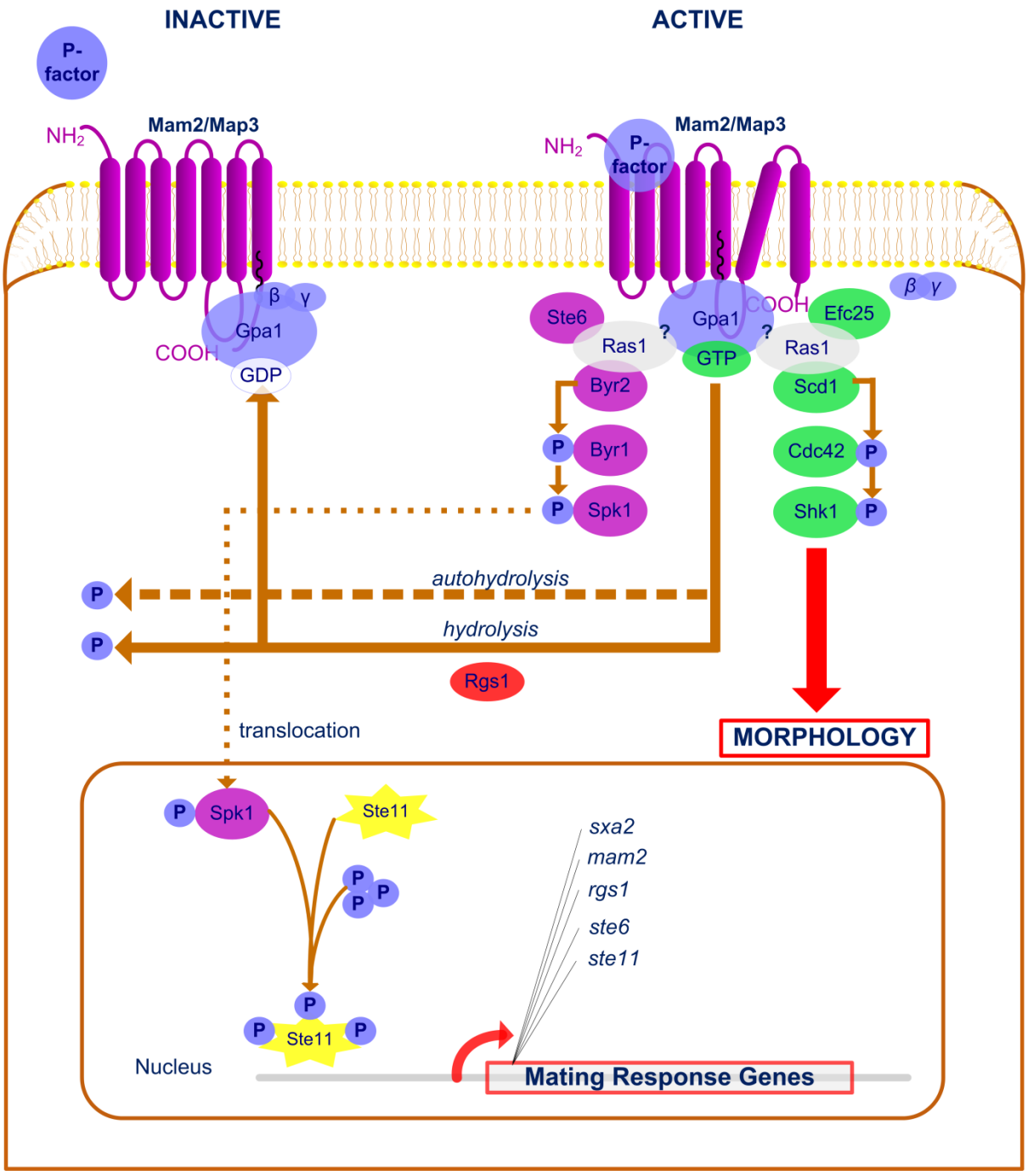

Figure 1-10: The *Sz. pombe* pheromone-response

The G protein Gpa1, consisting of a GDP-bound Gα-subunit and a possible Gβγ-complex, forms a complex with the inactive GPCR Mam2 or Map3. Binding of pheromone to the receptor promotes the GDP for GTP exchange on the Gα-subunit Gpa1, and its subsequent dissociation from the Gβγ-complex. Gpa1-GTP activates a downstream effector leading to Ras1 activation. Interactions of activated Ras1 with the Ste6 GEF stimulate the transcriptional response through a MAPK cascade and activation of transcription factor Ste11. Interactions of activated Ras1 with the Efc25 GEF in contrast stimulate the morphological response leading to chemotropic elongation (shmooing) and other changes in cell morphology. Attenuation of the pheromone-response can be achieved at several levels.

1.4.2.2 Regulation of the Fission Yeast Pheromone-response

Several mechanisms exist to regulate the *Sz. pombe* pheromone-response and allow cells unable to find a mating partner to resume mitotic growth (Davey and Nielsen 1994; Imai and Yamamoto 1994). The RGS protein Rgs1 for instance has been shown to have a dual role in the regulation of signalling in both M and P-cells. Rgs1 attenuates the pheromone-response by enhancing the intrinsic GTPase activity of the Gα Gpa1 (Watson, Davis et al. 1999; Pereira and Jones 2001). Via the same mechanism it also acts as a positive regulator of pheromone-signalling because Gα-GTP may only activate effectors at a 1:1 stoichiometry per activation round, and deactivation thus releases Gα back to the pool of possible activators (Smith, Hill et al. 2009). Attenuation of the pheromone-response may also occur further downstream in the signalling pathway. The MAP kinase phosphatase Pmp1 for instance is needed to dephosphorylate Spk1, and cells lacking Pmp1 have a prolonged recovery rate in resuming mitotic growth (Didmon, Davis et al. 2002).

An extracellular regulatory mechanism also exists whereby M-cells secrete the peptidase Sxa2, which removes the C-terminal leucine residue of P-factor, inhibiting its binding to receptor. Expression of *sxa2* is under the control of the transcription factor Ste11 making it an integral part of the pheromone-response (Imai and Yamamoto 1992; Ladds, Rasmussen et al. 1996; Ladds and Davey 2000). In fact, the expression of both *sxa2* and *rgs1* is positively regulated by the pheromone-response. Interestingly, cells that lack Rgs1 are sterile because they cannot form conjugates despite being hyper-sensitive to pheromone and Sxa2 may be required for zygote formation. This suggests that down-regulation of the pheromone-response may be pre-requisite for successful completion of mating, aside from allowing recovery upon failure to mate (Pereira and Jones 2001). Other regulatory mechanisms of the pheromone-response are likely to exist. *Sc. cerevisiae* for instance internalizes receptor in response to pheromone (Hicke and Riezman 1996; Hicke, Sanolari et al. 1998) but this has not yet been characterized in *Sz. pombe*.

1.4.3 *Schizosaccharomyces pombe* Reporter Systems

Several methods exist for quantifying the *Sz. pombe* pheromone response. Early quantitative studies of the *Sz. pombe* pheromone-response pathway included measuring the morphological response via cell volume measurements (Davey 1991) and northern blot analysis (Davey and Nielsen 1994). In comparison to reporter assays however, which quantify the transcription of genes under the control of a promoter, these assays can be time-consuming or less sensitive. The identification of the *sxa2* gene provided a suitable site for the incorporation of an endogenous reporter of the pheromone-response in *Sz. pombe*

(Imai and Yamamoto 1992). As previously discussed, Sxa2 is a serine carboxypeptidase up-regulated in response to pheromone, that degrade extracellular P-factor by removal of the C-terminal leucine residue (Ladds and Davey 2000), and this site has extensively been exploited for reporter-purposes. The creation of a *sxa2>lacZ* reporter strain allowed the quantification of the time and pheromone dependent transcriptional pheromone-response (Didmon, Davis et al. 2002). The sensitivity of the *lacZ* reporter is however limited by protein quantity; lower amounts of β-galactosidase available result in a reduced rate of formation of functional tetramer units, and endogenous cellular activity can cleave the substrate for β-galactosidase generating background noise (Nichtl, Buchner et al. 1998). The assay is also time-consuming and not suitable for high-throughput generation of data. An *Sxa2>GFP* reporter was subsequently created to allow continuous time-resolved measurements of cells (Smith 2009). Detection of the pheromone-response using the GFP reporter however appeared less sensitive than the β-galactosidase reporter and required higher concentrations of pheromone despite the relative brightness of GFP. The signal also appeared to increase linearly with time, rather than reflecting the down-regulation of the pheromone-response with time, or display the typical dose-response sigmoidal curve. This could reflect the long maturation process of GFP due to post-translational modifications (Tsien 1998), low sensitivity at low expression levels due to high background activity, the long half-life of GFP, or other problems with the assay.

1.4.3.1 The Role of Individual Transmembrane Domains in Yeast 7TM Receptors

To date, there are no crystal structures of full-length yeast GPCR receptors. Due to the difficulties in resolving the structure of full-length GPCR's to atomic resolution, techniques have been developed to study 7TM receptors using receptor fragments. Work utilizing this approach emerged in the 1980's and focussed on the Archaean 7TM receptor bacteriorhodopsin (Popot, Gerchman et al. 1987). Early discoveries included the observation that most TM helices when expressed independently of the rest of the receptor would reconstitute a functional protein fold even in the absence of extracellular loops (Kahn, Engelman et al. 1992; Kataoka, Kahn et al. 1992) lending support to the two-stage model of membrane protein folding (Popot and Engelman 1990) and credibility to the concept of studying TM domains from polytopic proteins individually. Peptide fragments are now widely used for the biophysical study of specific regions of polytopic integral membrane proteins.

This approach has to date been utilized in yeast for the study of the *Sc. cerevisiae* α-factor GPCR STE2. Experiments performed in dodecylphosphocholine (DPC) and SDS micelles

revealed that the TM domains of the α–factor receptor indeed adopt a α–helical structure capable of forming higher order oligomers (Neumoin, Arshava et al. 2007; Cohen, Arshava et al. 2008). Although certain TM domains have been implicated in the oligomerization of the receptor (Overton and Blumer, 2002) and biochemical analysis indicate a role for ligand binding in stabilization of the oligomeric form of the receptor (Shi, Paige et al. 2009; Wang and Konopka 2009), the nature of the interactions between receptors on an atomic, or even an amino acid based level remain elusive. More extensive, mutational analysis of individually epressed TM domains may therefore shed light on the nature of these interactions.

1.5 Aims of the Work Presented in this Thesis

The overall aims of the work presented in this thesis were to gain further insight into the role of receptor oligomerization during GPCR signalling in the fission yeast *Sz. pombe*. In order to realize these aims, work was undertaken to characterize the oligomerization-motif GxxxG in the first transmembrane domain of the *Sc. cerevisiae* GPCR STE2 expressed in *Sz. pombe*. Specifically, mutational effects of this motif were investigated in order to elucidate its influence on full-length receptor oligomerization, TM-TM oligomerization, receptor localization, and its overall effects on pheromone signalling in *Sz. pombe*. Findings in STE2 were contrasted to mutational studies on small residues found in the *Sz. pombe* pheromone receptor Mam2, in order to investigate whether a motif with similar functional consequences could be identified in the fission yeast receptor.

A second aim of this thesis was to produce a novel *Sz. pombe* pheromone reporter strain, using the ultra-sensitive *Renilla reniformis* luciferase gene, under the control of the *sxa2* promoter. The intention behind this strain development was to create a reporter strain that allowed a highly sensitive read-out of the pheromone response and that also allowed quantitative, high-throughput generation of data.

2 MATERIALS AND METHODS

2.1 Materials

2.1.1 General Laboratory Reagents

The general laboratory reagents were supplied by Sigma-Aldrich Co. Ltd. (Poole, Dorset, UK) and Merck BDH Laboratory Supplies (Poole, Dorset, UK). All were of analytical grade.

2.1.2 Molecular Biology Reagents

Restriction enzymes, T4 DNA ligase, T4 DNA kinase, Taq DNA polymerase (from *Thermus Aquaticus*) and all oligonucleotides were supplied by Invitrogen Ltd (Paisley, Scotland, UK). FastStart DNA polymerase and alkaline phosphatase was supplied by Roche Diagnostics Ltd.

2.1.3 Electrophoresis Reagents

Ultrapure type-I Agarose was supplied by Invitrogen Ltd (Paisley, Scotland, UK).

2.1.4 Pheromones

The *Sz. pombe* P-factor pheromone was synthesized by AltaBioscience, Birmingham, UK. The *Sc. cerevisiae* α-factor pheromone was synthesized by Keck Biotechnology Research Laboratory, Connecticut, USA.

2.1.5 Growth Media

All media was made using reverse osmosis (RO grade) H_2O. Components for Defined Minimal Medium (DMM; Davey et al. (1995)) and yeast Amino Acid selective medium (AA) were supplied by Sigma Aldrich Co. Ltd. Yeast extract, Luria Broth and Select Agar were supplied by Invitrogen Ltd (Paisley, Scotland, UK). Rich Yeast Extract (YE) media was used supplemented with adenine, leucine and uracil (250 µg/mL) as required. Plates were made with 1.5% select agar.

2.1.5.1 Yeast Defined Minimal Medium

DMM (per litre):

NH_4Cl	5 g
Na_2HPO_4	2.2 g
Phthalic Acid	3 g
Glucose	20 g
Salts 50x stock)	10 mL
Vitamins (1,000x stock)	1 mL
Minerals (10,000x stock)	100 µL

50x stock salts (per litre):

$MgCl_2.6H_2O$	52.5 g
$CaCl_2.2H_2O$	735 mg
KCl	50 g
Na_2SO_4	2 g

1000x stock solution of vitamins (per 100 mL):

Nicotinic acid	1 g
Inositol	1 g
Pantothenic acid	100 mg
Biotin	1 mg

10000x stock solution of minerals (per 100 mL):

Citric acid	1 g
Boric acid	500 mg
$MnSO_4.H_2O$	500 mg
$ZnSO_4.7H_2O$	400 mg
Molybdic acid	305 mg
$FeCl_3.6H_2O$	200 mg
KI	100 mg
$CuSO_4.5H_2O$	40 mg

2.1.5.2 Yeast Amino Acid Selective Medium

Yeast Amino Acid Selective Medium (AA) (per litre):

Yeast nitrogen base (without amino acids)	6.7 g
Glucose	20 g
Amino acid mix	1.5 g
Select amino acid mix	0.5 g

Amino acid mix:

L-alanine	2 g
L-arginine	2 g
L-asparagine	2 g
L-cysteine	2 g
L-glutamine	2 g
L-glutamate	2 g
L-glycine	2 g
L-isoleucine	2 g
L-lysine	2 g
L-phenylalanine	2 g
L-proline	2 g
L-serine	2 g
L-threonine	2 g
L-tryptophan	2 g
L-tyrosine	2 g
L-valine	2 g
myo-inositol	2 g
para-amino benzoic acid	0.4 g

Select amino acid mix (components omitted as required for selection):

Adenine	2 g
L-histidine	2 g
L-leucine	4 g
Uracil	2 g
L-methionine	2 g

2.1.5.3 Yeast Extract Medium

Yeast Extract Medium (per litre):

Yeast extract	5 g
Glucose	30 g

2.1.6 Bacterial Strains

General cloning was performed using *Escherichia coli* (*E. coli*) strain DH5α (*supE44 hsdR17 endA96 thi-1 relA1 recA1 gyrA96*) supplied by Stratagene (Cambridge, UK).

TOXCAT assays were performed using *E. coli* strain NT326 (*F−(argF-lac)U169, rpsL150, relA1, rbsR, flbB5301,ptsF25, thi-1, deoC1, ΔmalE444, recA, srlA+, Strep25 resistance*) kindly provided by Professor Donald M. Engelman (Yale University).

2.1.7 *Schizosaccharomyces pombe* Strains

Genes and gene products from the two yeasts studied were distinguished between by the use of upper-case or lower case letters. *Sz. pombe* genes were denoted in the style *yfg1* and proteins Yfg1. *Sc. cerevisiae* genes are denoted *YFG1* and proteins YFG1.

Standard nomenclature has been used to describe the *Sz. pombe* strains used in this study. A gene deletion is referred to as *yfg1-D10* where 1000 base pairs (bp) of the *yfg1* locus have been deleted. The disruption of a gene using the selectable *ura4* cassette (Davis, Pateman et al. 1999) is referred to as *yfg1*::*ura4+*. Creation of reporter strains in which expression of a reporter gene is linked to the promoter of an endogenous gene at the original locus are termed *pro1>rep1*.

Strain	Genotype
JY522	*mat1-M, Δmat2/3::LEU2-, leu1-, ade6-M216, ura4-D18, cyr1-D51, sxa2::ura4+*
JY544	*mat1-M, Δmat2/3::LEU2-, leu1-32, ade6-M216, ura4-D18, cyr1-D51, sxa2>lacZ (Didmon, Davis et al. 2002)*
JY1169	*mat1-M, Δmat2/3::LEU2-, leu1-32, ade6-M216, ura4-D18, cyr1-D51, mam2-D10, sxa2>lacZ (Ladds, Davis et al. 2003)*
JY1552	*mat1-M, Δmat2/3::LEU2-, leu1-32, ade6-M216, ura4-D18, cyr1-D51, mam2-D10, sxa2>Rluc*
JY1553	*mat1-M, Δmat2/3::LEU2-, leu1-32, ade6-M216, ura4-D18, cyr1-D51, mam2-D10, sxa2>Rluc8*

The constructs used in this study were *cyr1* deletion mutants, The *cyr1* gene product is adenylyl cyclase and the absence of this protein removes the requirement for nitrogen starvation in order to induce the pheromone-response (Maeda, Mochizuki et al. 1990; Davey and Nielsen 1994).

The *sxa2* gene product is a serine carboxypeptidase responsible for degrading extracellular P-factor (Ladds, Rasmussen et al. 1996; Ladds and Davey 2000). Deletion of this gene decreases down-regulation of the pheromone-response thereby prolonging the pheromone dependent response and increase functionality of reporter strains (Didmon, Davis et al. 2002).

The *mat1-M*, *Δmat2/3* genotype is an M-cell incapable of switching mating type. Deleting the silent cassettes *mat2* and *mat3* prevent switching of mating type. Similarly, the *mat1-P*, *Δmat2/3* genetype encodes a P-cell incapable of switching mating type (Klar and Miglio 1986).

JY544 refers to the *sxa2>lacZ* reporter strain where exposure of cells to P-factor lead to the production of β-galactosidase as part of the pheromone-response.

JY1169 is a variant of JY544 where the endogenous *mam2* open reading frame (ORF) has been deleted.

JY1552 refers to the *Δmam2, sxa2>Rluc* reporter strain created from JY544 where exposure of cells to P-factor lead to the production of *Renilla* luciferase as part of the pheromone-response.

JY1553 refers to the *Δmam2, sxa2>Rluc8* reporter strain created from JY544 where exposure of cells to P-factor lead to the production of a modified version of *Renilla* luciferase termed Rluc8 (Loening, Fenn et al. 2006) as part of the pheromone-response.

2.1.8 Plasmids and Constructs

The *Rluc* reporter was purchased from Promega (Promega Corporation, Southampton, UK). The *Rluc8* reporter was kindly donated by Professor Sanjiv S. Gambhir (Stanford University, USA). The TOXCAT plasmid was kindly donated by Professor Donald M. Engelman (Yale University, USA).

2.2 Methods

2.2.1 Cloning Techniques

General DNA manipulations were performed as described in (Sambrook, Fritsch et al. 1989). Restriction enzymes, alkaline phosphatase, T4 DNA kinase, T4 DNA ligase and other modifying enzymes were used according to manufacturers' guidelines. 1.5% Agarose gels containing 0.5 µg/mL ethidium bromide were used to analyse DNA fragments by electrophoresis. DNA fragments were recovered from agarose gels using the QIAquick Gel Extraction Kit supplied by Qiagen (Qiagen House, West Sussex, UK).

2.2.2 Transformations

2.2.2.1 Transformations of *Schizosaccharomyces pombe*

Sz. pombe were transformed with circularised plasmid DNA or linear DNA fragments using the lithium acetate protocol as described by (Okazaki, Okazaki et al. 1990).

2.2.2.2 Transformations of *Escherichia coli*

Transformation competent cells were prepared using the calcium chloride method described in Sambrook and Russell (Sambrook and Russel 2001). 10 mL of a mid-exponential phase culture (OD_{600}=0.6) was pelleted and re-suspended in 10 mL of 100 mM $MgCl_2$ and incubated on ice for 5 min. The cells were then pelleted and re-suspended in 1 mL of 100 mM $CaCl_2$. Cells were incubated for 16 h at 4°C before use.

Typically, 2 µL of plasmid DNA or 10 µL of a ligation mix was added to 0.1 mL of competent *E. coli* and incubated on ice for 30 min. The cells were then heat shocked at 42°C in a water bath for 90 sec, after which 0.5 mL of LB was added and the cells incubated at 37°C for 30 min. The cells were pelleted and resuspended in 100 µL of LB before being spread on to agar plates containing ampicillin followed by incubation overnight at 37°C.

2.2.2.3 DNA Sequencing

The pREP series of plasmids were sequenced by the Molecular Biology Service at the University of Warwick. The pccKan series of plasmids were sequenced by GATC Biotech AG (Konstanz, Germany).

2.2.3 Polymerase Chain Reaction

Taq DNA Polymerase was used to colony screen bacterial and yeast strains. FastStart high fidelity enzyme blend (Roche Diagnostics Ltd.) was used to amplify cloning fragments and for bipartite polymerase chain reaction (PCR). Hot-Start Pfu-TURBO™ DNA polymerase (Stratagene, UK) was used for QuikChange mutagenesis. All polymerases were used according to the manufacturers' guidelines.

2.2.3.1 Bipartite Polymerase Chain Reaction Using a Purified DNA Template

Faststart high fidelity enzyme blend (Roche Diagnostics Ltd.) was used according to the manufacturer's guidelines to generate mutations in the pREP plasmids. The reaction was performed in 50 µL volumes using 38 µL filter sterilized dH_2O, 0.5 µL template DNA, 2 µL of each (forward, reverse) primer (10 µM), 1 µL of dNTP mix (containing 10 mM of each dNTP), 5 µL of Faststart 10x PCR reaction buffer, 1 µL DMSO, and 0.5 µL of Faststart DNA polymerase (Roche Diagnostics Ltd.). A typical PCR reaction contained 29 cycles of the following three steps: denaturation at 95°C for 30 sec, annealing at 55°C for 1 min, and extension at 72°C for 2 min.

2.2.3.2 QuikChange Mutagenesis Using a Purified DNA Template

The PCR methods for creating deletion and single amino acid QuikChange mutations were carried out according to the Stratagene site directed mutagenesis kit manual (Stratagene, UK). The reaction was performed in 50 µL volumes using 40 µL filter sterilized dH_2O, 1 µL wild type template DNA, 1 µL of each quick change (forward, reverse) primer (10 µM), 1 µL of dNTP mix (containing 10 mM of each dNTP), 5 µL of Hot-Start Pfu-TURBO™ 10x PCR reaction buffer and 1 µL of Hot-Start Pfu-TURBO™ DNA polymerase (Stratagene, UK). A typical PCR reaction contained 18 cycles of the following three steps: denaturation at 95°C for 30 sec, annealing at 55°C for 1 min, and extension at 68°C for 2 min.

2.2.3.3 Colony Screens of Bacterial Cells

Taq DNA polymerase (Invitrogen Ltd, Paisley, Scotland, UK) was used to screen bacterial and yeast colonies to check for insertion of linear DNA fragments into the genetic material of the organism i.e. plasmids or genome. A single colony was suspended in 100 µL of H_2O. 1 µL of this suspension was used in a 10 µL final volume PCR reaction.

2.2.3.4 *Schizosaccharomyces pombe* Integration Strains

The *ura4* cassette was disrupted in order to create strains JY1552 and JY1553. Cells lacking *ura4* were isolated by growth on AA medium incorporating limited uracil and 5' fluoro-orotic acid (FOA; purchased from Toronto Research Chemicals Inc., Ontario, Canada). FOA is converted by Ura4 into the toxic compound 5' fluoro-uracil (Grimm, Kohli et al. 1988).

2.2.3.5 Screening Crude Preparations of Yeast Genomic DNA by Polymerase Chain Reaction

2.2.4 Preparation of Yeast Genomic DNA

Genomic DNA was isolated from *Sz. pombe* using a previously described method (Hoffman and Winston 1987). Cells were grown to mid-log phase and harvested by centrifugation. This was followed by a wash step in distilled water, and finally resuspended in 200 µL blue buffer (2% Triton X-100, 1% Sodium docecyl sulphate (SDS), 100 mM NaCl, 10 mM Tris-HCl pH 8.0 and 1 mM ethylenediaminetetraacetic acid (EDTA)). This was followed by the addition of 200 µL of a 1:1 phenol:chloroform solution and 400 µL acid-washed beads (425-600 µm diameter, provided by Sigma-Aldrich Co. Ltd.). The tubes were then vortexed for 3 minutes and 200 µL Tris-EDTA (TE) buffer pH 7.5 was immediately added and the tubes centrifuged for 5 minutes at 13000 rpm, 4°C. The aqueous phase was transferred to 1 mL ice-cold ethanol, mixed by inversion and centrifuged for 2 minutes at 13000 rpm, 4°C. The pellet was then washed with 70% ethanol, allowed to air-dry and resuspended in 50 µL TE buffer pH 7.5. This method typically yields 10-20 ng of genomic DNA.

2.2.5 Detection of Orotidine 5'-decarboxylase Activity

Orotidine 5'-decarboxylase (Ura4) activity was detected in *Sz. pombe* using plate-based viability assays (Grimm, Kohli et al. 1988). Cells possessing Ura4 activity were selected via their ability to grow on AA medium lacking uracil. A counter selection for cells not expressing Ura4 was achieved by selecting colonies on AA medium containing uracil and FOA (purchased from Toronto Research Chemicals Inc., Ontario, Canada). FOA is converted into the toxic compound 5' fluoro-uracil by Ura4, and cells producing Ura4 do not survive (Grimm, Kohli et al. 1988).

2.2.6 Cell Number and Size Analysis

Cell density and median cell volume of cultures were determined with a Z2 Coulter Particle Count and Size Analyzer, using Isoton II Azide-free electrolyte. These were supplied by Beckman Coulter (Luton, Bedfordshire, UK).

2.2.7 β-galactosidase Assay

Sz. pombe pheromone dose-response β-galactosidase assays were performed using an adapted method (Dohlman, Apaniesk et al. 1995). *Sz. pombe* cells were cultured to a density of $1x10^6$ cells/mL in AA media lacking thiamine. In the case of Mam2, 500 µL samples of culture were transferred to 2mL Safe-Lock Eppendorf tubes containing 0 or 10^{-9}-10^{-4} M P-factor pheromone dissolved in HPLC-grade MeOH. For STE2, tubes contained 0 or 10^{-9}-10^{-4} M α-factor pheromone dissolved in RO grade H_2O. Tubes were incubated on a rotating wheel at 29°C for 16h unless otherwise stated. 50 µL from each tube was subsequently transferred to 750 µL fresh Z-buffer (made with RO grade H_2O) containing 2.25mM o-nitrophenyl-D-galactoside (ONPG; purchased from Sigma-Aldrich Co. Ltd.) and incubated for a further 90 minutes at 29°C on a rotating wheel. ONPG production was inhibited by the addition of 200 µL 2M Na_2CO_3. β-galactosidase production was then calculated as the ratio of ONPG product formed (detected by optical density (OD) measurement at 420 nm using an Ultrospec 3000; Pharmacia Biotech, Uppsala, Sweden) per number of assayed cells, which was determined using a Coulter Channelyser; (Beckman Coulter, Luton, Bedfordshire, UK) using the formula $OD420/10^6$ assayed cells.

Z-buffer:

0.1M $NaPO_4$ (pH 7.0)

10mM KCl

1mM $MgSO_4$

50mM β-mercaptoethanol

0.5% (w/v) chloroform

0.005% (w/v) SDS

2.2.7.1 Analysis of Dose-response Curves

The GraphPad Prism suite version 4.0 (San Diego, CA, USA) was used to calculate the non-linear regression of the dose-response data. The sigmoidal dose response curve (variable slope) was calculated using the Hill's equation, defined in Equation 1 where Y is the measured response as a function of the dose X and the four parameters: Bottom (the value

of Y at the minimal curve asymptote), Top (the value of Y at the maximum curve asymptote), logEC_{50} (the log of the half maximal effective concentration) and the Hill slope (denting the slope of the curve).

Equation 1: The Hill's equation

2.2.8 Western Blot Analysis

2.2.8.1 Preparation of *Escherichia coli* Whole Cell Extracts

E. coli NT326 expressing TOXCAT chimera from the pccKan plasmids were grown to OD_{600} =0.6. Samples were diluted to OD_{600} =0.1 and a 1 mL sample was centrifuged and resuspended in 80 µL SDS loading buffer and analysed by SDS-PAGE.

2.2.8.2 Preparation of *Schizosaccharomyces pombe* Whole Cell Extracts

20 mL of yeast culture was incubated at 29°C to mid-log phase in AA. Cells were harvested by centrifugation (3000 rpm for 5 min) and washed once with TEN buffer (100 mM Tris pH 6.8, 10 mM EDTA, 150 mM NaCl). The cells were then resuspended in 50 µL TEN buffer containing a dissolved Complete Mini protease inhibitor tablet (Roche Diagnostics Ltd.). Cells were homogenized by vortexing together with 425-600 µm diameter acid-washed beads after which 50 µL TEN buffer and 100 µL sample buffer (125 mM Tris (pH 6.8), 8% glycerol, 5% SDS, 1% β-mercaptoethano, 0.02% bromophenol blue) was added.

2.2.8.3 Sodium Dodecyl Sulphate Polyacrylamide Gel Electrophoresis

SDS polyacrylamide gels were cast and run using the vertical Bio-Rad Mini Protean II gel electrophoresis system (Bio-RAD, CA, USA) according to the manufacturer's recommendations based on a previously described method (Laemmli 1970). 17% separating gels were cast (acrylogel 2.6 (40%) solution (BDH)); 375 mM Tris-HCl pH 8.8, 0.1% SDS, 0.02% APS, 0.06% TEMED), topped with water and left to set for 30 minutes. The separating gel was then topped with a stacking gel (5% acrylogel solution, 125 mM Tris-HCl

pH 6.8, 0.1% SDS, 0.6% APS, 0.06% TEMED). Samples were prepared by mixing with SDS sample loading buffer (125 mM Tris-HCl pH 6.8, 20% glycerol, 4% SDS, 0.02% bromophenol blue, 5% β-mercaptoethanol) and boiled for 10 minutes. Gels were run in a running buffer (25 mM tris; 250 mM glycine; 0.1% SDS) until the dye front migrated off the gel, typically around 3 h at 35 mA.

2.2.8.4 Transfer of Protein to Polyvinylidene Fluoride Membrane

Proteins were transferred from the acrylamide gels to polyvinylidene fluoride (PVDF) membrane (Amersham Biosciences, UK) using a semi-dry Western blotting system (Sigma Aldrich, UK) with Towbin transfer buffer (Towbin, Staehelin et al. 1979). The PVDF membrane was prepared by soaking in methanol and then in Towbin transfer buffer. Transfer was carried out by applying a constant current of 200 mA for 1.5 h.

2.2.8.5 Detection of Maltose Binding Protein

Following protein transfer, membranes were blocked in TTBS (30 mM Tris-HCl, 140 mM NaCl, 3 mM KCl, 0.1% Tween-20, pH 7.4) containing 3% milk for 1 h (or overnight at 4°C). This was followed by three 5 min wash-steps with TTBS. Membranes were then incubated for 1 h with the primary antibody anti-MBP (Sigma-Aldrich, UK), diluted 1/4000 with TTBS containing 3% milk. The wash step was then repeated. The secondary antibody, anti-mouse IgG (Sigma-Aldrich, UK), was used in a 1/10000 dilution with TTBS + 3% milk and incubated for 1 h, followed by washing. Finally, to detect MBP and its fusion proteins, one tablet from the SigmaFast™ BCIP/NBT kit (Sigma-Aldrich, UK) was dissolved in ionized water. Membranes were incubated with the solution for 10 min, and upon visualization of bands, the membrane was scanned.

2.2.8.6 Detection of *Renilla* Luciferase

Following protein transfer, membranes were blocked in PBS (140 mM NaCl, 2.7 mM KCl, 10.1 mM Na_2HPO_4, 1.8 mM KH_2PO_4, pH 7.2) containing 10% skimmed milk for 1 h (or overnight at 4°C). Membranes were then incubated for 1h with the primary antibody anti-Rluc (Caltag-MedSystems Ltd., UK), diluted 1/1000 with PBS containing 1% milk, for 1h. This was followed by three 5 min washes with PBS-T (0.05% Tween-20 in PBS). The secondary antibody, anti-rabbit IgG (Caltag-MedSystems Ltd., UK), was used in a 1/10000 dilution with PBS containing 1% skimmed milk and incubated for 1h, The wash step was then repeated. Finally, an enhanced chemiluminescence (ECL) western blotting substrate (Syngene, UK) was used to detect Rluc.

2.2.8.7 Coomassie Staining

Following electrophoresis, the gel was placed in InstantBlue (Expedeon, Harston, Cambridgeshire, UK) and allowed to develop until the protein bands were visible. Gels were visualised and images were taken using a G:Box iChemi gel documentation system with GeneTools analysis software (Syngene, Cambridge, UK).

2.2.9 TOXCAT Assays

2.2.9.1 The *malE* Complementation Assay

E. coli NT326 cells were transformed with pccKan plasmids encoding the TOXCAT chimeras. Cells were grown to mid-log phase at 37°C and streaked onto plates containing Maltose Minimal Media (M9 salts (48 mM Na_2HPO_4, 22 mM KH_2PO_4, 8.6 mM NaCl, 18.7 mM NH_4Cl), 2 mM $MgSO_4$, 100 µM $CaCl_2$; 0.4% maltose; 15% (w/v) agar) and incubated at 37ºC for 3 days. Cells able to express the chimera and transport and insert it into the inner membrane in the correct orientation are able to grow on maltose as a sole carbon source.

2.2.9.2 The Quantitative Chloramphenicol Acetyl-Transferase Assay

E. coli NT326 expressing TOXCAT chimera from the pccKan plasmids were grown to OD_{600} = 0.6. 200 µL aliquots were pelleted and resuspended in 500 µL 100 mM Tris-HCl pH 8.0. Cells were lysed by adding 20 µL lysis buffer (100 mM EDTA, 100 mM DTT, 50 mM Tris-HCl pH 8.0) and a drop of toluene and were then incubated at 30ºC for 30 min. The lysed cells were then diluted 10-fold and a 60 µL sample was taken. The levels of CAT expression were assayed using the FAST CAT® Green (deoxy) Chloramphenicol Acetyltransferase assay kit (Invitrogen Ltd, Paisley, Scotland, UK) according to the manufacturer's instructions. The fluorescence of the samples was determined using a Perkin Elmer LS50B fluorimeter. Samples were excited at 495 nm and emission at 525 nm was recorded. The fluorescence was normalised using to the positive control GpA.

2.2.10 Fluorescence Microscopy

Strains were cultured in the appropriate medium to a density of $1x10^6$ cells/mL. 1 mL of culture was harvested via centrifugation at 2,000 rpm for 3 min and the cells washed twice in fresh growth medium. Cells were resuspended in 20 µL of H_2O. 2µL of cell suspension was transferred to poly-lysine-coated slides (Sigma-Aldrich Co. Ltd., Poole, Dorset, UK) and viewed using a Personal DeltaVision (Applied Precision, Inc).

2.2.10.1 Image Analysis

The software suite ImageJ (Abramoff, Magalhaes et al. 2004) was used to analyse fluorescent images of individual cells. Cell segmentation was achieved using the BOA plugin for ImageJ which is part of the QuimP (Quantitative Imaging of Membrane Proteins) package (Dormann, Libotte et al. 2002; Zimmer, Zhang et al. 2006) modified by R. Tyson and W. Croft. Using the software, the cortex boundary was manually modified to calculate pixel intensity at the membrane and the interior of the membrane.

2.2.11 Luminescence Assays Using Multi-well Microplate Reader

2.2.11.1 Liquid Assays

Cultures of *Sz. pombe* cells were grown to mid-log phase (cell density specified for each experiment) at 29°C and 135 µl samples were treated with concentrations of pheromone and for lengths of time as specified for each experiment. 60 µM EnduRen (Promega Corporation, Southampton, UK) was added 2 h prior to assaying unless otherwise stated. Prior to measurements, cells were transferred to a 96-well microplate (Berthold Technologies, UK). Plates were then installed into a Berthold Mithras LB940 BRET multimode microplate reader (Berthold Technologies (UK) Ltd, Harpenden, Hertfordshire, UK) preheated to 30°C. Using the accompanying MicroWin 2000 software, measurement times of 1 s were taken at intervals as specified for each experiment. Baseline measurements were taken for wells containing cell samples but no EnduRen. The baseline luminescence was subtracted from luminescence measurements and where appropriate, the corrected luminescence reading was divided by the amount of cells in the sample.

2.2.11.2 Agarose-plug Assays

24-well black clear-bottom microplates were prepared by adding 1.5% agarose dissolved by heating and mixing in AA media. The agar media was cooled to 50°C and pheromone was added at the specified concentration unless otherwise stated. 2.5 mL media was added to each well in the microplate and allowed to set in an aseptic flow cabinet. Cells were added and spread evenly onto each plugs at the concentrations and amounts specified for each experiment. Cells were cultured to densities as specified in each experiment at 29°C. 60 µM EnduRen was added to the specified amount of culture and spread evenly onto each agar plug. The baseline was determined using cultures not treated with EnduRen spread onto an agar well and this number was subtracted from the sample luminescence measurement. Plates were then installed into the measurement chamber of the Berthold Mithras LB940

BRET multimode microplate reader (Berthold Technologies (UK) Ltd, Harpenden, Hertfordshire, UK) preheated to 30°C. Using the accompanying MicroWin 2000 software, measurement times of 1s were taken at intervals as specified for each experiment

2.2.12 Flow Cytometry

The Invitrogen Live/Dead® FungaLight Yeast Viability Kit (Invitrogen Ltd, Paisley, Scotland, UK) was used to analyse cell viability. *Sz. pombe* was cultured to a density of $1x10^6$ cells per mL in AA media. 1 mL of culture was then incubated with 0, 10^{-7} M or 10^{-4} M P-factor for 16 h on a rotating wheel. Cultures were washed once with 1 mL PBS (140 mM NaCl, 2.7 mM KCl, 10.1 mM Na_2HPO_4, 1.8 mM KH_2PO_4, pH 7.2) and then resuspended in 1 mL PBS. This was followed by the addition of 0.5 µL 20 mM propidium iodide in DMSO and 0.5 µL 3.34 mM SYTO9® in DMSO. The dye propidium iodide only labels cells with damaged membranes, whereas SYTO9® stains all cells. Viable cells are only stained with SYTO9® and fluoresce green whereas FRET between the two dyes present in dead cells results in red fluorescence. Flow cytometry was performed using an LSR II flow cytometer (BD Biosciences, Oxford, UK). Excitation of both dyes was achieved using a 488 nm blue laser, and emission was detected using a 550 nm long pass filter with a 575/26 nm band pass filter for propidium iodide and a 505 nm long pass filter with a 530/30 nm band pass filter for SYTO® 9.

2.2.13 Computational Methods

2.2.13.1 Transmembrane Helix Predictions

Transmembrane domains were predicted using the freely available online software TMHMM (Krogh, Larsson et al. 2001) accessible at http://www.cbs.dtu.dk/services/TMHMM/.

2.2.13.2 CHI Modelling

The software suite crystallography and nuclear magnetic resonance searching of helix interactions (CHI) was used to compute oligomeric GPCR TM domain structures (Adams, Arkin et al. 1995; Adams, Engelman et al. 1996; Brunger, Adams et al. 1998). The calculations were performed using an 8 node dual 2.66 GHz Xenon processor Linux cluster (Streamline Computing, Warwick). CHI uses an implicit membrane solvent with a dielectric constant of 1. The starting geometries of each monomer were calculated as a canonical α-helix with 3.6 residues per turn. The dimers incorporated both right-handed (-25°) and left-handed (25°) crossing angles and an axis-to-axis distance between the helices of 10.4 Å.

Full searches were performed and helices were simultaneously rotated about their central axis with a sampling step size of 45°, from 0°-360°. For each oligomer, four trials were carried out for each rotation and crossing angle conformation using simulated annealing of all atomic coordinates during which rotation- and crossing angles were free to vary. Energy minimization of structures was carried out both before and after MD simulations. Groups of structures with a backbone RMSD of ≤1 Å were placed in clusters of 10 or more members, followed by a calculation of an average structure.

3 CREATION OF DNA CONSTRUCTS

3.1 Generation of TOXCAT Constructs

To investigate the propensity of individual TM helices from STE2 and Mam2 to form homo-oligomers various lengths and frames of the transmembrane domains were cloned into the pccKan expression vector. The pccKan expression vector contains the ORF for MBP and ToxR that flank the transmembrane domain cloned into the plasmid upon expression of the construct. The pccKan vector (see Figure 3-1) incorporates the constitutively expressed *ToxR* promoter immediately upstream of the *toxR* ORF, and a *Bam*HI site at the end of *toxR*. This is followed by the kanamycin resistance marker (*aminoglycoside 3'-phosphotransferase*) and *malE*, encoding MBP. The *malE* region contains a *Nhe*I site near the N-terminal end. The pccKan vector also contains an ampicillin marker (encoding Beta Lactamase) allowing selection for expression of this plasmid on media containing Amp, and *cat* (encoding chloramphenicol acetyl transferase) to confer resistance to chloramphenicol if *toxR* is expressed, correctly transported to the membrane and in an oligomerized state.

In order to express individual TM domains from Mam2 and STE2 the pccKan vector was digested with *Bam*HI and *Nhe*I allowing the kanamycin resistance gene to drop out and thus yield the linearised pcc plasmid. One forward and one reverse oligonucleotide encoding the TM domain of interest and incorporating the same restriction sites were phosphorylated and hybridised. The primer dimer and the linear pcc plasmid were then ligated to yield a circularized plasmid containing the genetic TOXCAT chimera (as illustrated in Figure 3-1). Plasmids were sequenced for verification. The primers cloned into the pccKan plasmid are listed in Table 3-1 for STE2 constructs and Table 3-2 for Mam2 constructs.

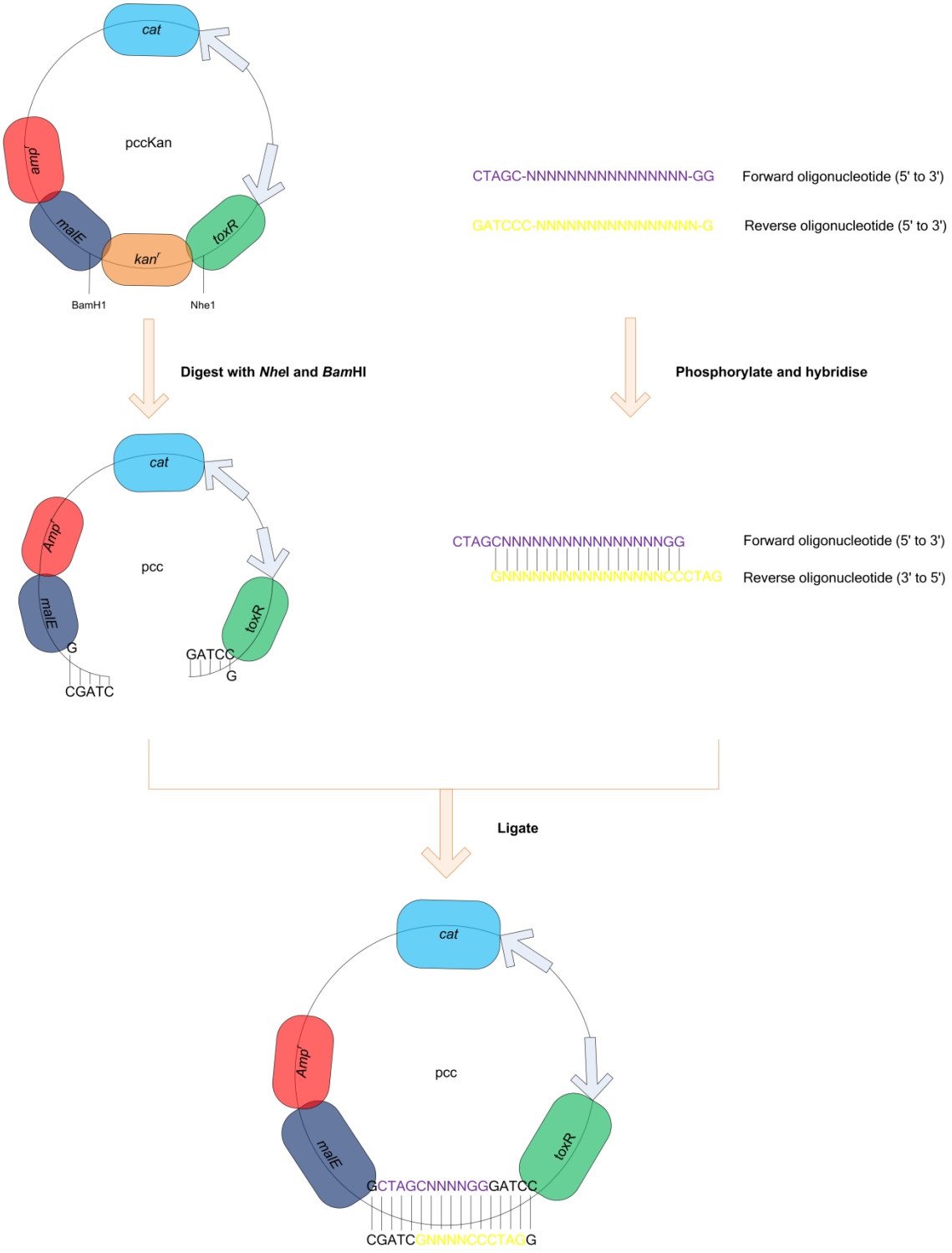

Figure 3-1: Insertion of oligonucleotide sequences corresponding to GPCR TM domains into the pccKan expression vector

The restriction enzymes *NheI* and *BamHI* were used to digest the pccKan vector, resulting in a 1736 bp dropout of the kanamycin resistance gene. A forward and reverse oligonucleotide, corresponding to a transmembrane domain were phosphorylated and hybridized. The resulting pcc vector was ligated together with the oligonucleotide dimer to yield a vector expressing a ToxR-TM-MBP chimera. The vector also contains the ampicillin resistance gene *bla* as well as the *ctx* promoter, which when bound to a ToxR dimer leads to the expression of chloramphenicol acetyl transferase.

TM	Name	Expression Frame	Forward Oligonucleotide Reverse Oligonucleotide
1	1S13	A_{52}-L_{64}	ctagcGCTATTATGTTCGGTGTTCGTTGTGGTGCTGCTGCTTTAgg gatcccTAAAGCAGCAGCACCACAACGAACACCGAACATAATAGCg
1	1S16	T_{50}-T_{65}	ctagcACTCAAGCTATTATGTTCGGTGTTCGTTGTGGTGCTGCTGCTTTAACTgg gatcccAGTTAAAGCAGCAGCACCACAACGAACACCGAACATAATAGCTTGAGTg
1	1S16A	V_{49}-L_{64}	ctagcGTTACTCAAGCTATTATGTTCGGTGTTCGTTGTGGTGCTGCTGCTTTAgg gatcccTAAAGCAGCAGCACCACAACGAACACCGAACATAATAGCTTGAGTAACg
1	1S18	I_{53}-W_{70}	ctagcATCATGTTCGGAGTACGCTGCGGAGCAGCAGCATTAACATTAATCGTAATGTGGgg gatcccCCACATTACGATTAATGTTAATGCTGCTGCTCCGCAGCGTACTCCGAACATGATg
1	1S19	V_{49}-I_{67}	ctagcGTTACTCAGGCCATTATGTTTGGTGTCCGCTGTGGTGCAGCTGCTTTGACTTTGATTgg gatcccAATCAAAGTCAAAGCAGCTGCACCACAGCGGACACCAAACATAATGGCCTGAGTAACg
1	1S20	Q_{51}-W_{70}	ctagcCAGGCCATTATGTTTGGTGTCCGCTGTGGTGCAGCTGCTTTGACTTTGATTGTAATGTGGgg gatcccCCACATTACAATCAAAGTCAAAGCAGCTGCACCACAGCGGACACCAAACATAATGGCCTGg
1	1S25	T_{50}-R_{74}	ctagcATGACATCGCGGACTCAAGCTATTATGTTCGGTGTTCGTTGTGGTGCTGCTGCTTTAACTTTAATCGTAATGTGGgg gatcccCCACATTACGATTAAAGTTAAAGCAGCAGCACCACAACGAACACCGAACATAATAGCTTGAGTCCGCGATGTCATg
2	2S18	F_{81}-Y_{I97}	ctagcTTCATCATCAACCAAGTATCATTATTCTTAATCATCTTACACTCAGCATTATACgg gatcccGTATAATGCTGAGTGTAAGATGATTAAGAATAATGATACTTGGTTGATGATGAAg
3	3S22	I_{133}-F_{154}	ctagcATCATCCAAGTATTATTAGTAGCATCAATCGAAACATCATTAGTATTCCAAATCAAAGTAATCTTCgg gatcccGAAGATTACTTTGATTTGGAATACTAATGATGTTTCGATTGATGCTACTAATAATACTTGGATGATg
4	4S20	G_{163}-I_{82}	ctagcGGATTAATGTTAACATCAATCTCATTCACATTAGGAATCGCAACAGTAACAATGTACTTCGG gatcccGAAGTACATTGTTACTGTTGCGATTCCTAATGTGAATGAGATTGATGTTAACATTAATCCg
5	5S23	T_{208}-I_{230}	ctagcACAATCTTATTAGCATCATCAATCAACTTCATGTCATTCGTATTAGTAGTAAAATTAATCTTAGCAATCgg gatcccGATTGCTAAGATTAATTTTACTACTAATACGAATGACATGAAGTTGATTGATGATGCTAATAAGATTGTg
6	6S19	F_{244}-F_{262}	ctagcTTCCACATTTTATTAATTATGTCATGTCAATCATTATTAGTTCCTTCAATTATTTTCgg gatcccGAAAATAATTGAAGGAACTAATAATGATTGACATGACATAATTAATAAAATGTGGAAg
6	6S23	F_{244}-Y_{266}	ctagcTTCCACATCTTATTAATCATGTCATGCCAATCATTATTAGTACCATCAATCATCTTCATCTTAGCATACgg gatcccGTATGCTAAGATGAAGATGATTGATGGTACTAATAATGATTGGCATGACATGATTAATAAGATGTGGAAg
7	7S21	V_{276}-A_{296}	ctagcGTATTAACAACAGTAGCAACATTATTAGCAGTATTATCATTACCATTATCATCAATGTGGGCAgg gatcccTGCCCACATTGATGATAATGGTAATGATAATACTGCTAATAATGTTGCTACTGTTGTTAATACg

Table 3-1: List of STE2 wild-type single TM domain TOXCAT constructs

The forward (sense) and reverse (antisense) oligonucleotides are detailed for insertion into the TOXCAT toxR-TM-MBP constructs of STE2 wild-type TM domains. The hybridised oligonucleotides were cloned into a *Bam*HI/*Nhe*I site and the overhang bases are denoted in lower-case letters. Constructs were named *XYZ* such that X refers to the number of the TM domain in question, Y refers to the protein from which the TM insert is based on: S for STE2 and M for Mam2, and Z refers to the length of the TM construct. I.e. 1S13 is a 13 amino acid long insert from the first TM domain of STE2.

TM	Name	Expression Frame	Forward Oligonucleotide Reverse Oligonucleotide
1	1M13	G_{49}-L_{61}	ctagcGGTATGACTTTATCAGCTCAATTAGCTTTAGGTGTTTTAgg gatcccTAAAACACCTAAAGCTAATTGAGCTGATAAAGTCATACCg
1	1M13A	R_{45}-A_{57}	ctagcCGGTTATTAACTGGTATGACTTTATCAGCTCAATTAGCTgg gatcccAGCTAATTGAGCTGATAAAGTCATACCAGTTAATAACCGg
1	1M16	L_{46}-L_{61}	ctagcTTATTAACTGGTATGACTTTATCAGCTCAATTAGCTTTAGGTGTTTTAgg gatcccTAAAACACCTAAAGCTAATTGAGCTGATAAAGTCATACCAGTTAATAAg
1	1M18	L_{46}-I_{63}	ctagcTTATTAACTGGTATGACTTTATCAGCTCAATTAGCTTTAGGTGTTTTAACTATTgg gatcccAATAGTTAAAACACCTAAAGCTAATTGAGCTGATAAAGTCATACCAGTTAATAAg
1	1M20	L_{46}-M_{65}	ctagcTTATTAACTGGTATGACTTTATCAGCTCAATTAGCTTTAGGTGTTTTAACTATTCTGATGgg gatcccAATAGTTAAAACACCTAAAGCTAATTGAGCTGATAAAGTCATACCAGTTAATAACATCAGg
1	1M25	R_{45}-L_{69}	ctagcCGGTTATTAACTGGTATGACTTTATCAGCTCAATTAGCTTTAGGTGTTTTAACTATTCTGATGGTGTGCGACGACgg gatcccGTCGTCGCACACAATAGTTAAAACACCTAAAGCTAATTGAGCTGATAAAGTCATACCAGTTAATAACATCAGCCGg
2	2M23	V_{79}-I_{101}	ctagcGTTTTCGTTTTCAATTCAGCTTCAATTGTTGCTATGTGTTTACGTGCTATTTTAAATATTGTTACTATTgg gatcccAATAGTAACAATATTTAAAATAGCACGTAAACACATAGCAACAATTGAAGCTGAATTGAAAACGAAAACg
3	3M20	Y_{122}-A_{141}	ctagcTATGTTCACGTTTTCAATATTTTAATTTTATTATTAGCTCCTGTTATTATTTTCACTGCTgg gatcccAGCAGTGAAAATAATAACAGGAGCTAATAATAAAATTAAAATATTGAAAACGTGAACATAg
4	4M17	I_{162}-W_{178}	ctagcATTATGACTGTTATTTCAGCTTGTTTAACTGTTTTAGTTTTAGCTTTCTGGgg gatcccCCAGAAAGCTAAAACTAAAACAGTTAAACAAGCTGAAATAACAGTCATAATg
5	5M19	Y_{207}-F_{225}	ctagcTATTTCATTGCTAAAATTTTATTCGCTTTCTCAATTATTTTCCACTCAGGTTCATATgg gatcccATATGAACCTGAGTGGAAAATAATTGAGAAAGCGAATAAAATTTTAGCAATGAAATAg
6	6M19	C_{249}-I_{267}	ctagcTGTATTTTAGTTATTTCATGTCAATGTTTAATTGTTCCTGCTACTTTCACTATTATTgg gatcccAATAATAGTGAAAGTAGCAGGAACAATTAAACATTGACATGAAATAACTAAAATACAg
7	7M19	F_{277}-W_{295}	ctagcTTCTCATCAATGACTCAATGTTTATTAATTATTTCATTACCTTTATCATCATTATGGgg gatcccCCATAATGATGATAAAGGTAATGAAATAATTAATAAACATTGAGTCATTGATGAGAAg

Table 3-2: List of Mam2 wild-type single TM domain TOXCAT constructs

The forward (sense) and reverse (antisense) oligonucleotides are detailed for insertion into the TOXCAT toxR-TM-MBP constructs of Mam2 wild-type TM domains. The hybridized oligonucleotides were cloned into a *Bam*HI/*Nhe*I site and the overhang bases are denoted in lower-case letters. Constructs were named *XYZ* such that X refers to the number of the TM domain in question, Y refers to the protein from which the TM insert is based on: S for STE2 and M for Mam2, and Z refers to the length of the TM construct. I.e. 1S13 is a 13 amino acid long insert from the first TM domain of STE2.

3.2 Creation of Constructs Used in the β-galactosidase Assay

Four vectors are used in this thesis for the expression of receptors in *Sz. pombe*. pKS is the vector pBluescript KS(-) that has been digested with *Pvu*II and ligated with a PCR product containing the multi-cloning site (MCS) of a modified pREP3x vector. The modified pREP3x vector incorporates an *Eco*RV site in the MCS and will be referred to as pREP3x throughout this thesis. The pREP4x vector is similar to pREP3x but contain an *ura4* marker in place of the *LEU2* marker on pREP3x. The pKS vector in contrast is smaller than both pREP3x and pREP4x, and is therefore more amenable to ORF manipulations was therefore used throughout this study as the templates for creation of Mam2 and STE2 variants.

3.2.1 Creation of pREP3x-Receptor Point Mutants Using Outward PCR

Outward PCR was utilized in order to create the Mam2 point mutants incorporating the A57G and A57L mutations that were investigated using the β-galactosidase assay. JD3218 (pKS-Mam2) was used as a template for outward PCR together pairs of forward and reverse primers; JO2602 (GAATGACTTTGTCTGCCCAACTTGGTTTAGGAGTCCTTAC) and JO2606 (CAGTTAAAAGTCTATCTCTTTCATATGCAT) for the A57G mutation and JO2600 (GAATGACTTTGTCTGCCCAACTTCTTTTAGGAGTCCTTACC) and JO2606 (CAGTTAAAAGTCTATCTCTTTCATATGCAT) for the A57L mutation. The forward primers contained the desired mutations. The PCR product was then digested with Dpn1, phosphorylated and ligated. After confirmation of incorporation of mutation in the receptor by sequencing, receptors were excised from the pKS vector using a double *Xho*I and *Bam*HI digest. Similarly, pREP3x vector was digested with *Xho*I and *Bam*HI and the two cut products were ligated to yield a pREP3x-Receptor fusions with the A57G or A57L mutation in the Mam2 receptor. See Figure 3-2 for a schematic.

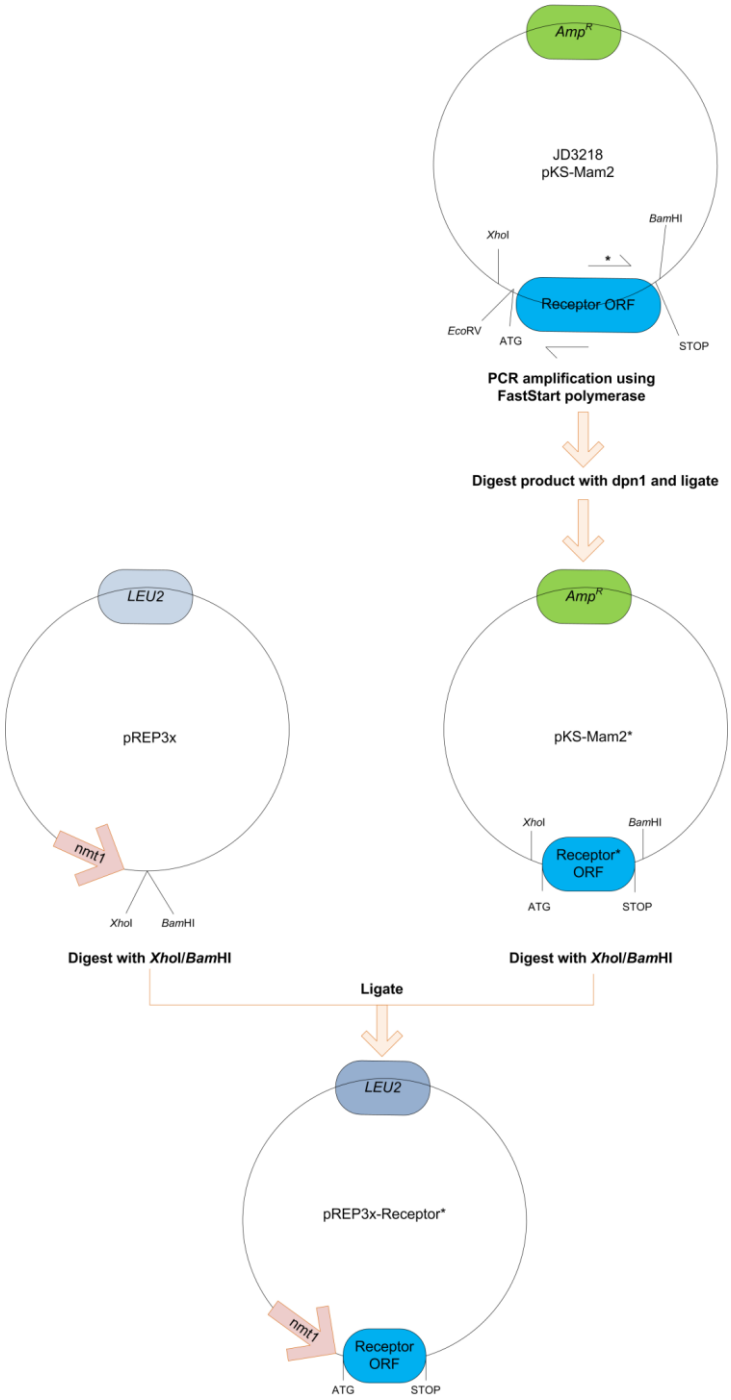

Figure 3-2: Generation of point mutations in the Mam2 receptor

Outward PCR was utilized in order to create the point mutations A57G and A57L in the Mam2 receptor in the pKS vector (JD3218) using forward primers JOJO2602 (GAATGACTTTGTCTGCCCAACTTGGTTTAGGAGTCCTTAC) and JO2606 (CAGTTAAAAGTCTATCTCTTTCATATGCAT) for the A57G mutation and JO2600 (GAATGACTTTGTCTGCCCAACTTCTTTTAGGAGTCCTTACC) and JO2606 (CAGTTAAAAGTCTATCTCTTTCATATGCAT) for the A57L mutation. The resulting PCR products were self-ligated prior to digestion with *Xho*I and *Bam*HI, and the digests were subsequently ligated together with *Xho*I and *Bam*HI digested pREP3x.

3.2.2 Creation of pREP-3x-Receptor-GFP Constructs

To label mutated Mam2 receptors with GFP, the pREP3x construct containing the desired receptor (JD3591 for the Mam2 A57G mutation and JD3592 for the Mam2 A57L mutation) was digested with *Eco*RV and *Bam*HI. This resulted in a 900 bp dropout fragment due to an internal *Eco*RV site in the receptor. JD2232 containing pKS-Mam2-GFP was also digested with *Eco*RV and *Bam*HI and the dropout fragment from this construct (containing C-terminal receptor and GFP) was ligated together with pREP3x containing the N-terminal part of the receptor with the desired mutation, to generate pREP3x-Receptor-GFP fusions. See Figure 3-3 for a schematic.

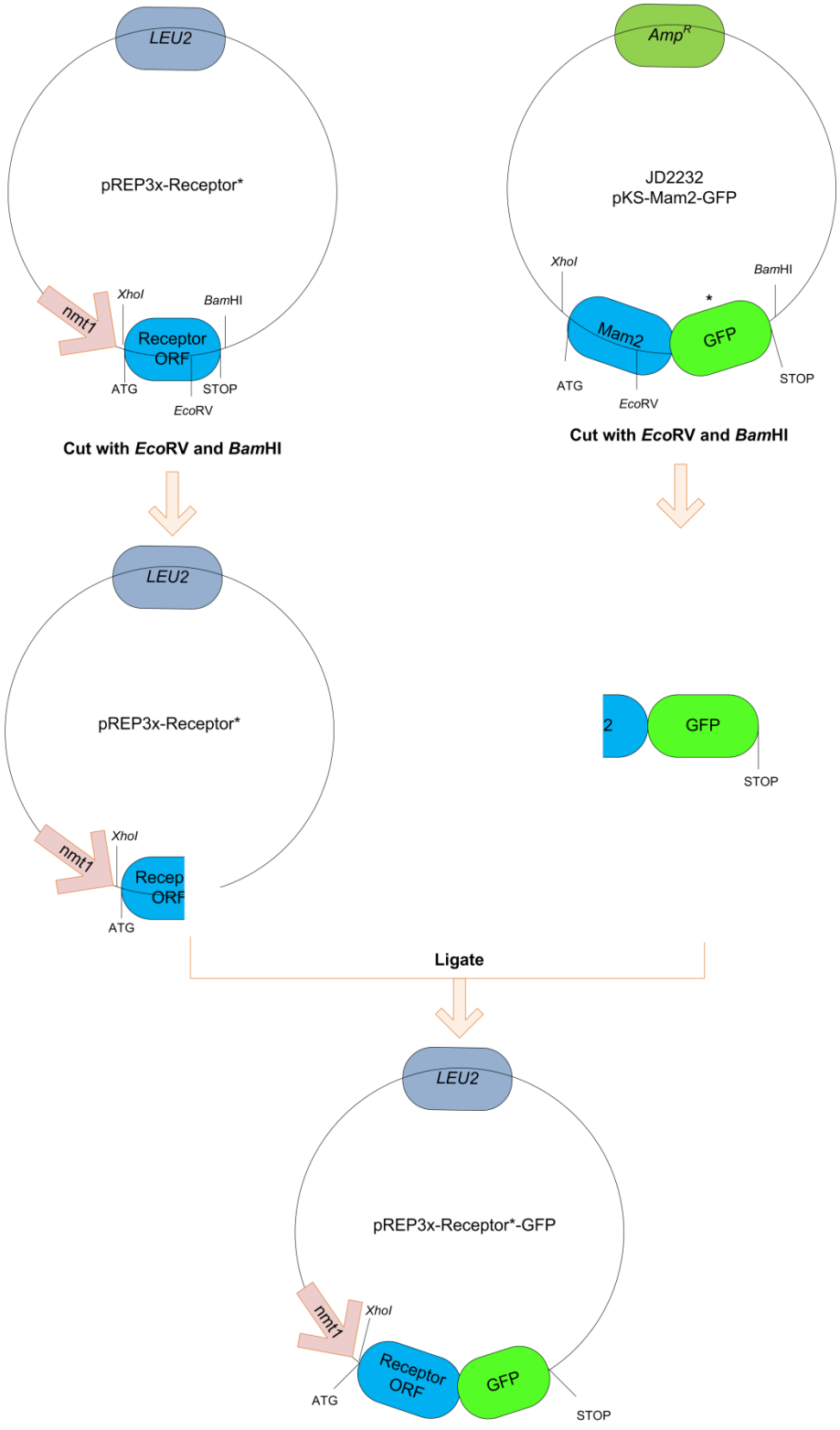

Figure 3-3: GFP-tagging of mutated pREP3x-Mam2 constructs

JD3591 and JD3592 containing the A57G and A57L mutations in Mam2 respectively were digested with *Eco*RV and *Bam*HI to drop out the region of the receptors downstream of the mutations. Likewise, JD2232 was digested with *Eco*RV and *Bam*HI to drop out the corresponding downstream region of wild-type Mam2 fused to GFP. These fragments were then ligated to yield pREP3x constructs containing mutated receptors fused to GFP.

3.3 Creation of Bioluminescence Resonance Energy Transfer Constructs

3.3.1 Generation of pKS-Rluc and pKS-Rluc8

To label receptors with Rluc for BRET assays, Rluc was first cloned into the pKS vector. Template *Rluc* was amplified from the pRL-SV40 vector (Promega Corporation, Southampton, UK) containing *Rluc* using sense primer JO2627 (aaatctagaacgtcagctgATGACTTCGAAAGTTTATGATCCAG) and antisense primer JO2628 (aaaaagatctggatccttagatgatatcTTGTTCATTTTTGAGAACTCGCTC). The sense primer contains a full *Xba*I site and *Pvu*II site and the antisense primer contains a full *Eco*RV, *Bam*HI and *Bgl*II site. The *Xba*I and *Bgl*II sites were used to ligate the *Rluc* ORF into the pKS vector digested with *Xba*I and *Bam*HI (illustrated in Figure 3-4). The resulting construct was called JD3454.

The same strategy was used to create a pKS-Rluc8 construct. Rluc8 is a modified version of Rluc. This construct was created using forward primer JO2689 (aaatctagaacgtcagctgATGGCTTCCAAGGTGTACGACCCC) and reverse primer JO2690 (aaaaagatctggatccttagatgatatcGTCGACCTGCTCGTTCTTCAGCAC). The resulting construct was called JD3513.

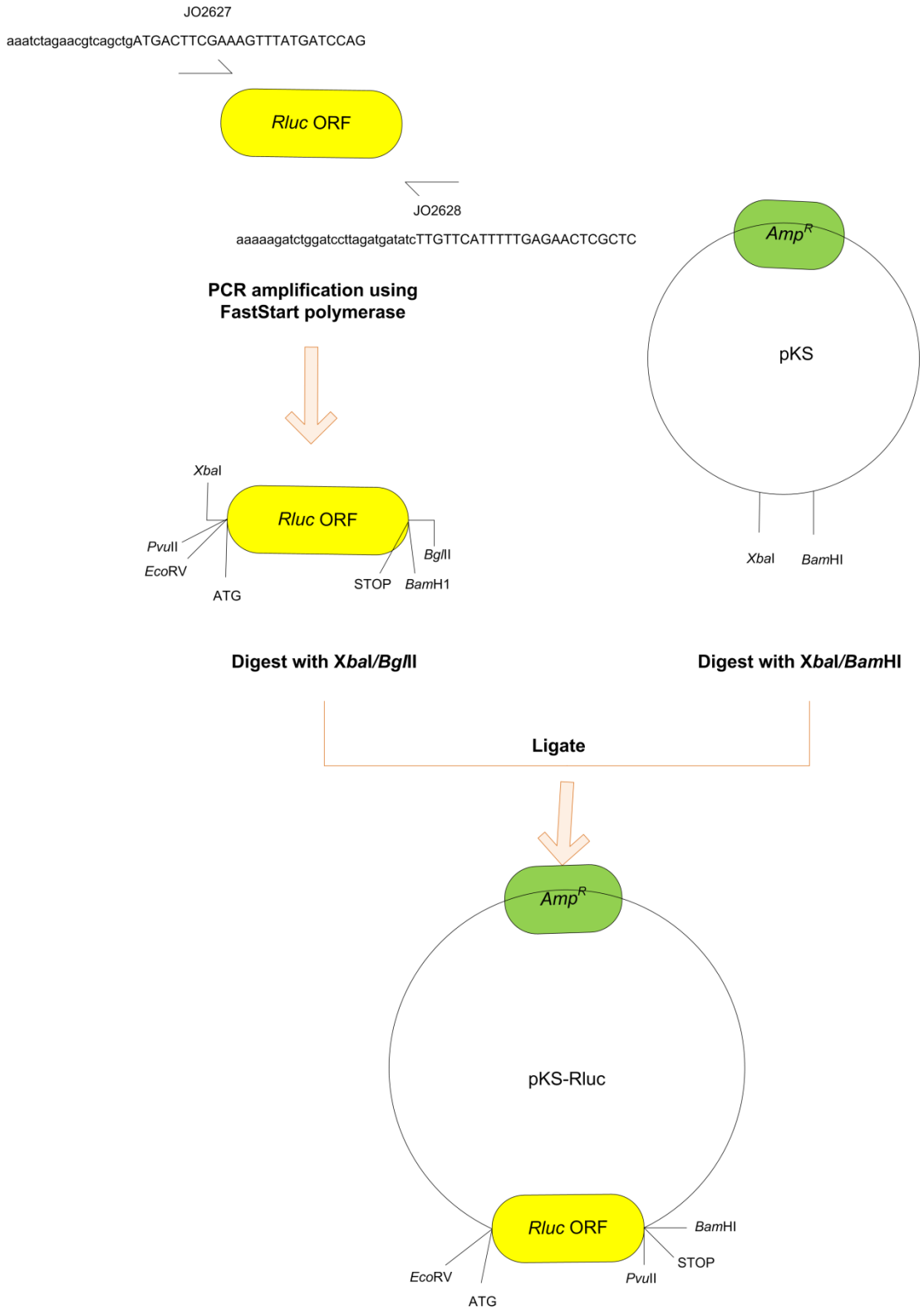

Figure 3-4: Creation of pKS-Rluc

The Rluc ORF was amplified with the sense oligonucleotide JO2627 and antisense oligonucleotide JO2628 using template JD3648. This yielded a fragment flanked by an *Xba*I site and a *Bgl*II site which were used for ligation into the pKS vector digested with *Bam*HI and *Xba*I. The resulting pKS-Rluc plasmid contains a *Pvu*II site for N-terminal tagging, and an *Eco*RV site for C-terminal tagging.

3.3.2 Generation of Receptor-Rluc Fusions

Fusions of receptors with Rluc to be used as donors in BRET assays were made by cloning receptors into the pKS-Rluc construct and subsequent incorporation into the pREP3x vector. Receptor ORFs were amplified from pKS vectors without their stop codons (see Table 3-3 for oligonucleotide sequences). The resulting PCR products were ligated into *Eco*RV digested JD3454 (pKS-Rluc) where the *Eco*RV site immediately precedes Rluc. This generated pKS-receptor-Rluc fusions.

These fusions were then cloned into the pREP3x vector. The pKS-Receptor-Rluc construct was first digested with *Pvu*I, which cuts in the Amp^R region. This was followed by a *Xho*I/*Bam*HI digest which generated two small and one large fragment, the large fragment corresponding to Receptor-Rluc. The isolated Receptor-Rluc fragment was then ligated into *Xho*I/*Bam*HI digested pREP3x vector (JD3387) to generate pREP3x-Receptor-Rluc constructs (Figure 3-5). A pREP3x-Rluc construct was also created using the same method but without incorporating a receptor.

	Forward primer		Reverse primer		
Receptor	**JO #**	**Oligonucleotide sequence**	**JO #**	**Oligonucleotide sequence**	**Construct**
Mam2 JD1627	1508	ATGAGACAACCATGGTGG	1509	CGTCCACTTTTTAGTTTCAG	JD3562
STE2 JD2343	1372	ATGTCTGATGCGGCTCCTTC	2108	TAAATTATTATTATCTTCAGTCCAGAAC	JD3511
$Mam2^{G49A}$ JD2753	1508	ATGAGACAACCATGGTGG	1509	CGTCCACTTTTTAGTTTCAG	JD3602
$Mam2^{G49A,S53A}$ JD2757	1508	ATGAGACAACCATGGTGG	1509	CGTCCACTTTTTAGTTTCAG	JD3603
$Mam2^{G49L,S53L}$ JD2781	1508	ATGAGACAACCATGGTGG	1509	CGTCCACTTTTTAGTTTCAG	JD3604

Table 3-3 Sequence of oligonucleotides to create Receptor-Rluc fusions

3.3.3 Generation of pREP4x Receptor-GFP Fusions

Fusions of receptors with GFP to be used as acceptors in BRET assays were made by subcloning *Xho*I/*Mlu*I fragments from the pREP3x-Receptor-GFP constructs and incorporating them into *Xho*I/*Mlu*I cut pREP4x vector.

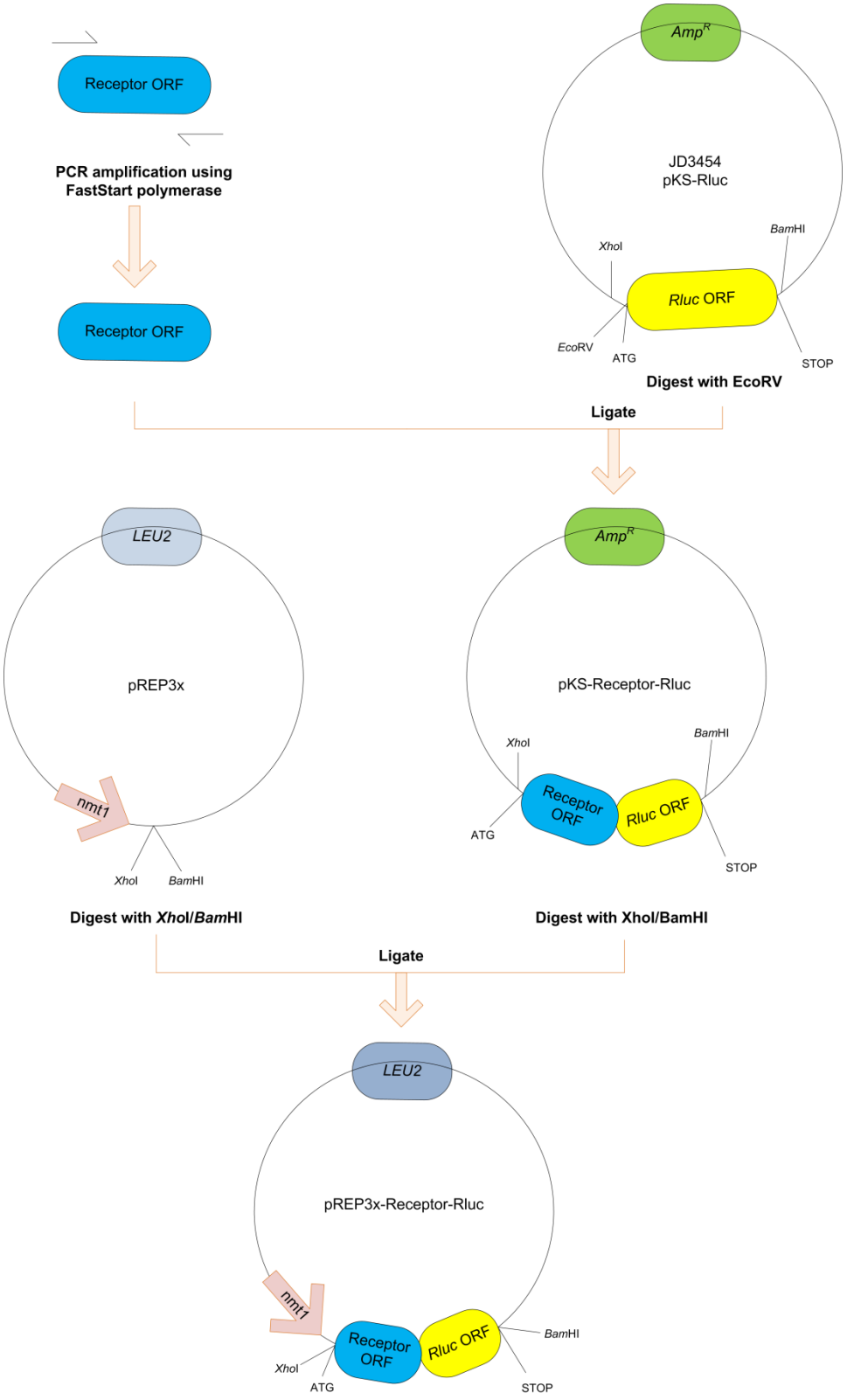

Figure 3-5: Generation of Receptor-Rluc fusion constructs

Receptor ORFs were amplified without the stop codon. The resulting PCR product was ligated into EcoRV digested JD3454 (pKS-Rluc) to generate Receptor-Rluc fusions. This was digested with Pvu1 and then *Xho*I and *Bam*HI with the coding region ligated into *Xho*I and *Bam*HI digested pREP3x to generate pREP3x-Receptor-Rluc fusions.

3.4 Creation of Constructs to Integrate *Rluc* and *Rluc8* into the *Schizosaccharomyces pombe* genome

Two *Sz. pombe* strains were created that incorporated the bioluminescent reporters *Rluc* or *Rluc8* into the genome at the *sxa2* locus. In order to integrate *Rluc* and *Rluc8* into the *Sz. pombe* genome, *Rluc* and *Rluc8* were amplified by PCR from plasmids JD3648 and JD3650 using forward primer JO2681 (ggggatccATGACTTCGAAAGTTTATGATCCAG) and reverse primer JO2628 (aaaaagatctggatccttagatgatatcTTGTTCATTTTTGAGAACTCGCTC) for *Rluc* and forward primer JO2691 (ggggatccATGGCTTCCAAGGTGTACGACCCC) and reverse primer JO2690 (aaaaagatctggatccttagatgatatcGTCGACCTGCTCGTTCTTCAGCAC) for *Rluc8*. The PCR products were cut with *Bam*HI and cloned into the pSP72 vector JD854 (created by Dr. Alan Goddard, University of Warwick) cut with *Bgl*II. In JD854 the 5' and 3' untranslated regions (UTRs) of *Sxa2* flank the *Bgl*II site meaning that inserts are part of an insertion cassette that can be integrated into the genome (see Figure 3-6). This generated the constructs pSP72-*sxa2*UTR-*Rluc-sxa2*UTR (named JD3649) and pSP72-*sxa2*UTR-*Rluc8-sxa2*UTR (named JD3647).

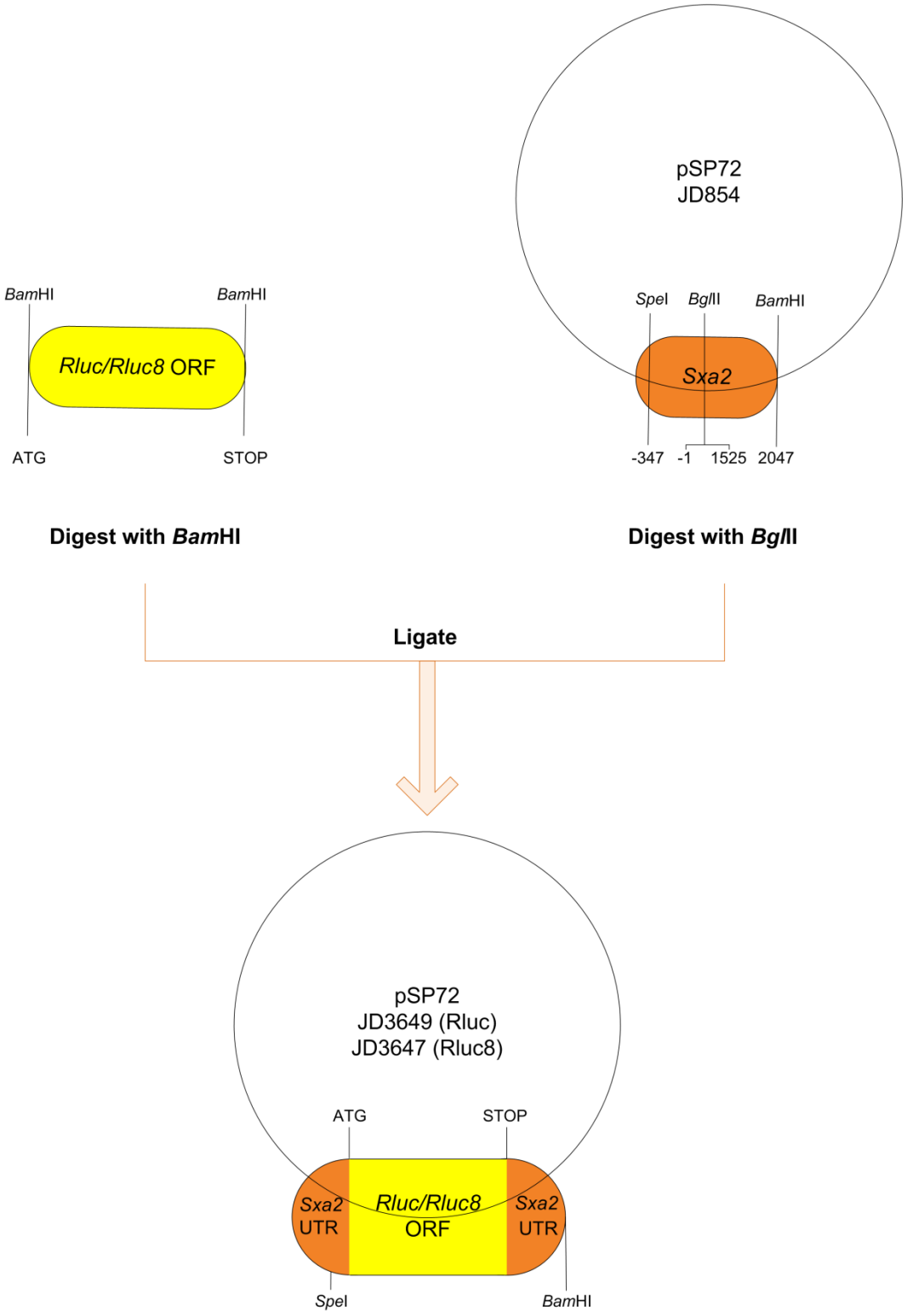

Figure 3-6: Creation of the *Rluc-Sxa2* and *Rluc8-Sxa2* insertion cassettes

The JD854 construct created by Dr. Alan Goddard (University of Warwick) was used to introduce the *Rluc* and *Rluc8* ORFs into the *Sxa2* locus of yeast strain JY522. The *Rluc* and *Rluc8* ORFs were digested with *Bam*HI and ligated into *Bgl*II cut JD854 (pSP72-*sxa2* UTRs, created by Dr. Alan Goddard, University of Warwick) to create JD3649 and JD3647. A *Spe*I/*Bam*HI digest can be performed to excise the *Rluc* or *Rluc8* ORFs flanked by the 5' and 3' UTRs of *sxa2*.

4 EFFECT OF MUTATIONS ON THE FIRST TRANSMEMBRANE DOMAIN OF STE2 AND MAM2

4.1 Background

The existence of GPCR oligomers is now widely accepted within the research community (Milligan, Ramsay et al. 2003; Park, Filipek et al. 2004; Ferré, Baler et al. 2009). GPCR oligomerization may affect biological processes as diverse as receptor trafficking to the membrane (White, Wise et al. 1998), receptor internalization (Rocheville, Lange et al. 2000) or receptor pharmacology (Jordan and Devi 1999; Waldhoer, Fong et al. 2005; Ciruela, Gomez-Soler et al. 2011). The pharmacological implications of GPCR oligomerization makes it an important research area since a better understanding of the phenomenon may lead to the development of more specific therapeutics.

The *Sz. pombe* GPCR Mam2 has previously been shown to form dimers as well as higher order oligomers, and these oligomers appear to be of functional importance as receptors can activate each other *in trans* (Ladds, Davis et al. 2005). The *Sc. cerevisiae* STE2 pheromone receptor has also been shown to oligomerize, and receptor-receptor interactions seem to form between the first transmembrane domains (Overton and Blumer 2000; Overton and Blumer 2002; Overton, Chinault et al. 2003; Gehret, Bajaj et al. 2006). The first transmembrane domain of STE2 contain a GxxxG motif, common to many membrane proteins that oligomerize, and disruption of this motif cause a loss of STE2 oligomerization as well as altered signalling dynamics (Overton, Chinault et al. 2003). Altered signalling dynamics in oligomerization defective GPCR mutants is common to many GPCRs (Jordan and Devi 1999; Jordan, Trapaidze et al. 2001; Overton, Chinault et al. 2003; Ciruela, Gomez-Soler et al. 2011).

The Mam2 receptor also contains a motif of two small residues in its first transmembrane domain, however the functional importance of this motif is not known. The work described in this chapter sought to characterize mutations in the smallxxxsmall motif in the Mam2 receptor, and compare this to the effects of mutations in the GxxxG motif in the first transmembrane domain of STE2, expressed in *Sz. pombe*. This was achieved by quantifying the pheromone-signalling response by means of a reporter gene, and through a novel quantitative analysis of the cellular localization of receptors. The significance of the transmembrane motif was contrasted between the two receptors.

4.2 Effect of Expressing Fluorescently Tagged Receptors from Vectors

4.2.1 Expression of Mam2 from the pREP3x Vector

The GPCRs investigated in this chapter were expressed from the pREP3x vector under the control of the repressible *nmt1* (no message in thiamine) promoter (Maundrell 1993). The pREP3x vector contains the selectable marker *LEU2* from *Sc. cerevisiae*. Plasmids expressed in the JY544 strain (*sxa2>lacZ*) or JY1169 (*sxa2>lacZ, Mam2*$^{-}$) can therefore be maintained through the exclusion of substrates from media because these strains have a nutritional requirement for leucine in the absence of *LEU2* (see section 2.1.7 for full genotype). The large size of the *Sz. pombe* centromeres prevent their incorporation into shuttle vectors and consequently a 1:1 plasmid to cell copy number cannot be maintained. It was therefore of interest to see whether strain JY1169 expressing Mam2 from the pREP3x plasmid displayed altered pheromone-response signalling dynamics to the strain JY544 expressing Mam2 under its endogenous promoter.

The strains JY544, transformed with pREP3x, and JY1169, transformed with pREP3x-Mam2, were grown to a density of $5x10^6$ cells in AA media. Cells were incubated with $0\text{-}10^{-4}$ M P-factor pheromone and incubated on a rotating wheel for 16 h. Figure 4-1A shows the transcriptional pheromone-response and Figure 4-1B shows the morphological pheromone-response of cells. Figure 4-1C shows the change in cell volume calculated as the increase above the median cell volume of unstimulated cells. The pEC_{50} values (the negative logarithm of the EC_{50} value which represents the concentration of pheromone at which 50% of the cells in the population have responded) are shown in Figure 4-3D together with the maximal value (Top) calculated using the Hill equation defined in section 2.2.7.1.

The dose-response curve generated by JY1169 transformed with pREP3x-Mam2 resembled that of JY544 transformed with pREP3x. The maximum of the dose-response curve was slightly elevated for the JY1169 strain, however this difference was not statistically significant as calculated by an unpaired two-tailed t-test ($p>0.05$). This suggests that the Mam2 receptor can be expressed heterologously with minimal effect on the pheromone-response. Interestingly the response appeared to decrease towards the higher concentrations of pheromone ($>10^{-6}$ M), which may reflect down-regulation of the pheromone-response.

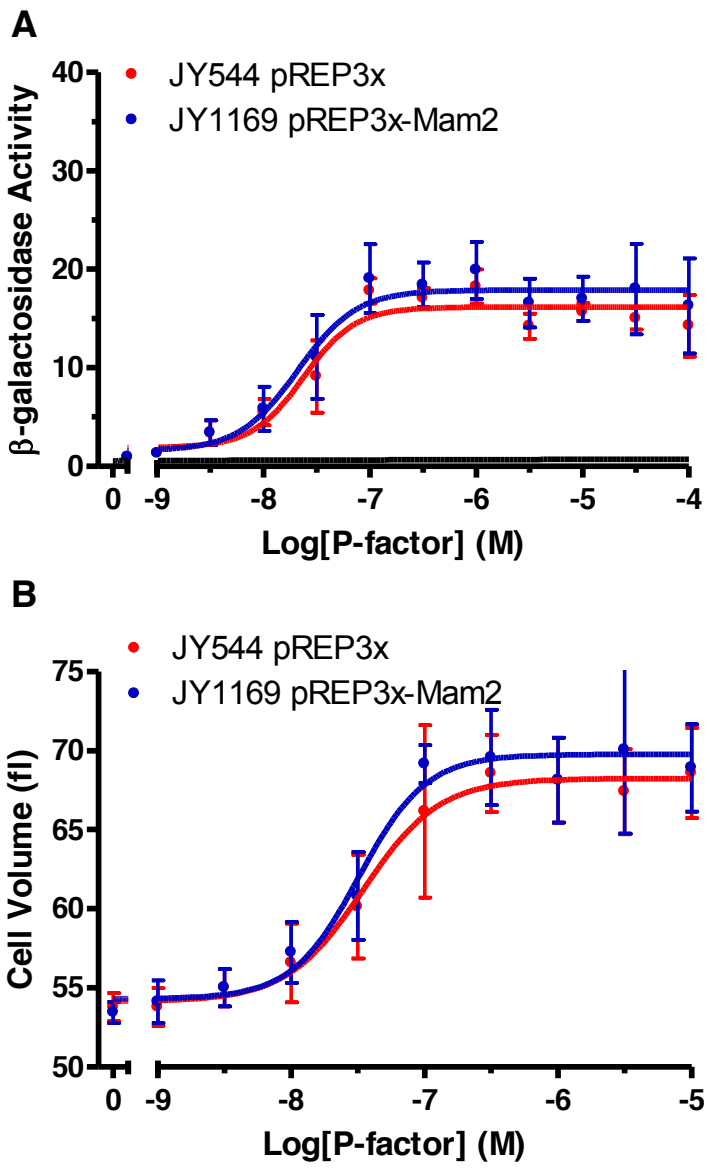

D

	pEC_{50}		Maximum	
	Transcription	Shmoo	Transcription	Shmoo
JY544 pREP3x	7.6±0.1	7.5±0.2	17.2±0.8	25.8±1.8
JY1169 pREP3x-Mam2	7.7±0.2	7.5±0.2	19.1±1.1	27.4±2.5

Figure 4-1: Comparison of endogenous and heterologous Mam2 activity

The strain JY544 (*sxa2>lacZ)* was transformed with pREP3x and JY1169 (*sxa2>lacZ, mam2*$^{-}$*)* was transformed with pREP3x-Mam2. Cells were cultured in AA media to a density of $5x10^6$ cells/mL and incubated with 0 to 10^{-4} M P-factor. Results shown are means of triplicate independent determinations ±SE. **A:** The β-galactosidase activity ($OD_{420}/10^6$ cells) of transformants to measure the transcriptional response. **B:** Median cell volumes of transformants to quantify the morphological response. **C:** Change in cell volume calculated as the increase above the median cell volume of unstimulated cells. **D:** pEC_{50} and maximal signalling values calculated from the dose-response curves in A and C.

4.2.2 A Fluorescent Tag has Little Effect on Receptor Function

GPCRs analysed in this chapter were tagged with green fluorescent protein (GFP) for cell localization purposes. Additionally, the GFP tag can be used as the acceptor for BRET experiments. To investigate whether the fluorescent tag has an effect on receptor function, the pheromone-response of cells expressing Mam2 from the pREP3x vector was compared to cells expressing Mam2-GFP from the pREP3x vector.

The *Sz. pombe* reporter strain JY1169 *(sxa2>lacZ, Mam2⁻)* was transformed with pREP3x, pREP3x-Mam2 or pREP3x-Mam2-GFP under the control of the repressible *nmt1* promoter (Maundrell 1993). Cells were grown to mid log-phase in selective AA media and incubated with $0\text{-}10^{-4}$ M pheromone on a rotating wheel for 16 h before assays were performed. Figure 4-2A shows the β-galactosidase activity to measure the activation of the transcriptional pathway, Figure 4-2B the median cell volumes to measure the shmoo response in the morphological pathway and Figure 4-2C the change in cell volume calculated as the increase above the median cell volume of unstimulated cells. The pEC_{50} and maximal signalling values as calculated from the dose-response are shown in Figure 4-3D.

With respect to the transcriptional response, Mam2 and Mam2-GFP exhibited comparable pEC_{50} values. The maximal signalling response calculated was however slightly lower for Mam2-GFP than for Mam2 alone, but this difference was not statistically significant as calculated by an unpaired two-tailed t-test ($p>0.05$). Cells transformed with vector alone did not respond to pheromone, as was expected. The transcriptional response appeared to decrease when cells were exposed to the higher concentrations of pheromone ($\geq 10^{-6}$ M), which can possibly be attributed to the down-regulation of the pheromone-response as discussed in section 1.4.2.2.

The morphological response was also similar in the two receptors, although very slightly higher for cells expressing Mam2 alone. The maximal increase in median cell volume was 30.80% for cells transformed with Mam2 compared to 26.45% for cells transformed with Mam2-GFP, however this difference was not found to be statistically significant by an unpaired two-tailed t-test ($p>0.05$). These experiments therefore suggest that the GFP tag has little effect on Mam2 function.

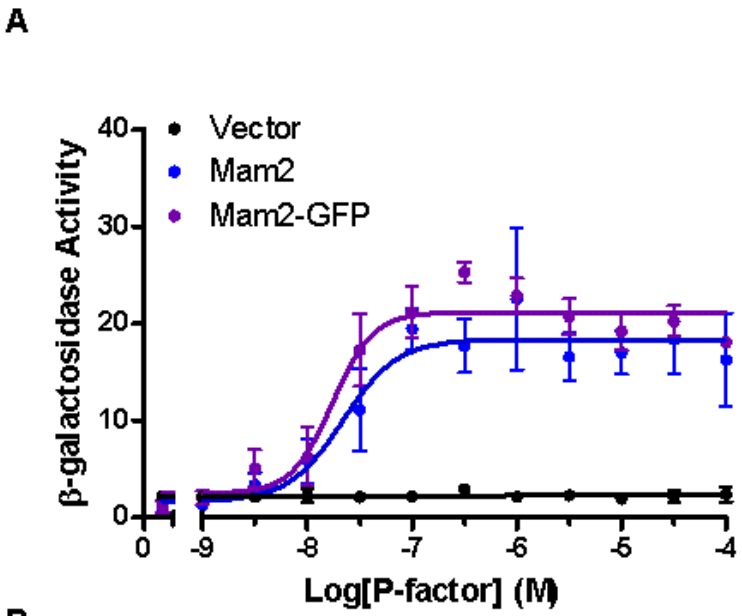

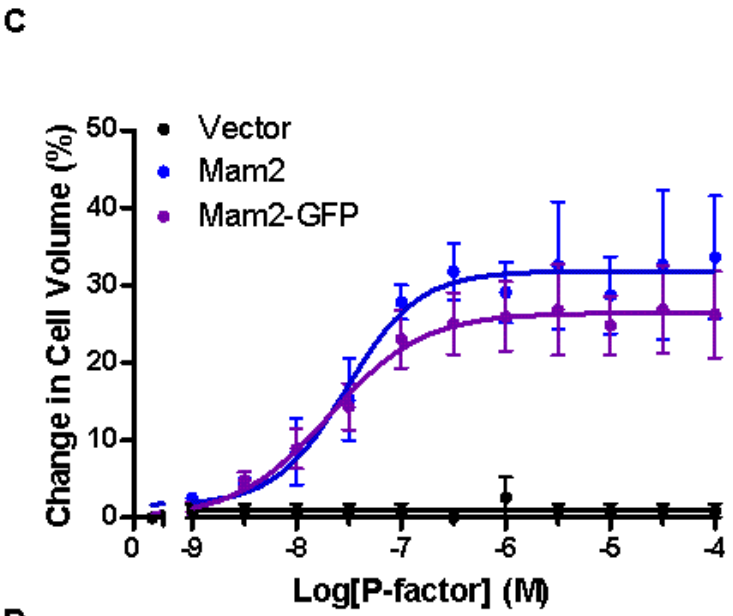

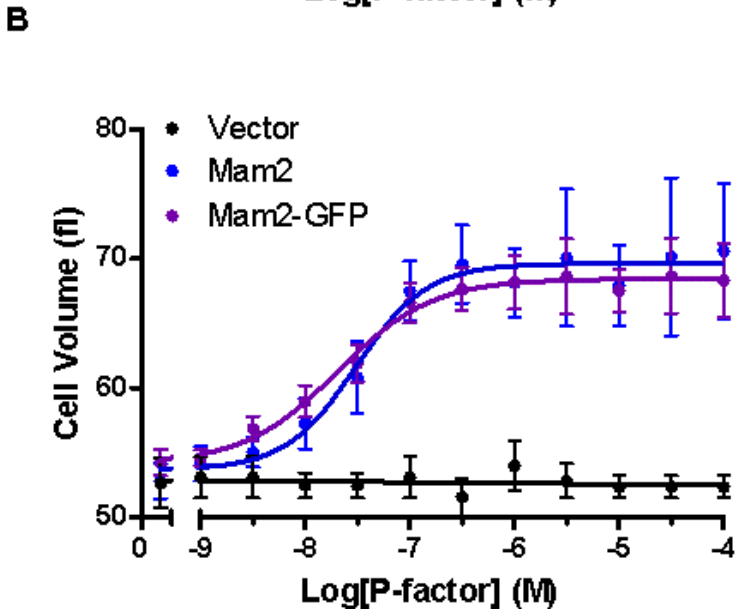

D

	pEC_{50}		Maximum	
	Transcription	Shmoo	Transcription	Shmoo
Vector	N/A	N/A	N/A	N/A
Mam2	7.7±0.2	7.5±0.2	18.4±1.2	30.8±2.1
Mam2-GFP	7.7±0.1	7.7±0.2	21.2±0.8	26.5±1.7

Figure 4-2: Comparison of the activity of Mam2 and Mam2-GFP

JY1169 (*sxa2>lacZ, mam2⁻*) was transformed with pREP3x, pREP3x-Mam2 or pREP3x-Mam2-GFP. Cells were cultured in AA media to a density of ~$5x10^6$ cells/mL and incubated with 0 to 10^{-4} M P-factor. Results shown are means of triplicate independent determinations ±SE. **A:** The β-galactosidase activity ($OD_{420}/10^6$ cells) of transformants to measure the transcriptional response. **B:** Median cell volumes of transformants to quantify the morphological response. **C:** Change in cell volume calculated as the increase above the median cell volume of unstimulated cells. **D:** pEC_{50} and maximal signalling values calculated from the dose-response curves in A and C.

4.2.3 STE2 Activates the Pheromone-Response Similarly to Mam2 when Expressed in *Schizosaccharomyces pombe*

This chapter will discuss the effects of mutations in the *Sc. cerevisiae* STE2 receptor when expressed in *Sz. pombe*. The behaviour of cells transformed with wild-type STE2-GFP, Mam2-GFP or GFP alone was therefore compared to validate expressing STE2-GFP in *Sz. pombe*. Receptors were expressed from the pREP3x plasmid under the control of the repressible *nmt1* promoter (Maundrell 1993) and plasmids were transformed into the JY1169 strain (*sxa2>lacZ, mam2*$^-$). STE2 has previously been shown to couple to the *Sz. pombe* pheromone-response pathway by binding its native α-factor ligand and coupling to the *Sz. pombe* G-protein (Forfar 2007). However it is not known whether the signalling efficiency of the STE2 receptor is similar to the efficiency of Mam2. It was therefore of interest to compare the activity of wild-type STE2 and Mam2 expressed in *Sz. pombe* to see that expressing STE2-GFP instead of Mam2-GFP does not adversely affect the signalling response.

Figure 4-3 shows the pheromone dose-response profiles of *Sz. pombe* cells transformed with pREP3x-Mam2-GFP, pREP3x-STE2-GFP and pREP3x-GFP. Cells were incubated with concentrations of pheromone (α-factor or P-factor) ranging from 0 to 10^{-4} M. Cells transformed with vectors containing STE2-GFP were treated with α-factor and cells transformed with vectors containing Mam2-GFP were treated with P-factor. Cells were grown to mid log-phase and exposed to pheromone on a rotating wheel for 16 h before assays were performed. Figure 4-3A shows the β-galactosidase activity to measure the activation of the transcriptional pathway, Figure 4-3B the median cell volumes in to measure the shmoo response in the morphological pathway and Figure 4-3C the change in cell volume calculated as the increase above the median cell volume of unstimulated cells. The pEC_{50} and maximal signalling values calculated from the dose-response are shown in Figure 4-3D. Both the transcriptional and the morphological response of cells transformed with STE2-GFP and Mam2-GFP were observed to decrease in response to pheromone concentrations in excess of 10^{-6} M. This may be attributable to down-regulation of the pheromone-response. As expected, cells transformed with GFP alone did not respond.

In the transcriptional response the pEC_{50} values (Figure 4-3D) of the two receptors were indistinguishable. Interestingly, the maximal signalling measured appeared different for the two receptors with 16.6 β-galactosidase units per 10^6 cells for STE2-GFP and 21.2 for Mam2-GFP. This difference was found to be statistically significant by an unpaired two-tailed t-test ($p<0.05$). Similarly, maximal shmoo formation in cells expressing STE2-GFP was

significantly different from shmoo formation in cells expressing Mam2-GFP (calculated by an unpaired two-tailed t-test, $p<0.05$). This implies that although Mam2-GFP and STE2-GFP initiate the transcriptional response at similar levels of pheromone, STE2-GFP does not drive the transcriptional response as efficiently as Mam2.

This could be due to a number of reasons including an inability to couple efficiently to other components involved in the pheromone-response. For instance, STE2 is unable to bind the Rgs1 protein (McCann 2010). Although Rgs1 has a role in attenuating the pheromone-response, it is also involved in its positive regulation (Smith, Hill et al. 2009). The positive regulatory function arises from the inability of Gα-GTP to activate the effector more than once per activation round. Deactivation via GTP hydrolysis mediated by Rgs1 thus release the Gα back to the pool of possible activators. This may also explain why the pEC_{50} values are comparable for cells expressing either receptor; Mam2-GFP and STE2-GFP initiate the transcriptional response at similar levels of pheromone when Gα is unlimited, however, cells expressing STE2-GFP cannot sequester Gα-GTP as quickly as cells expressing Mam2-GFP and consequently STE2-GFP does not drive the response as efficiently as Mam2.

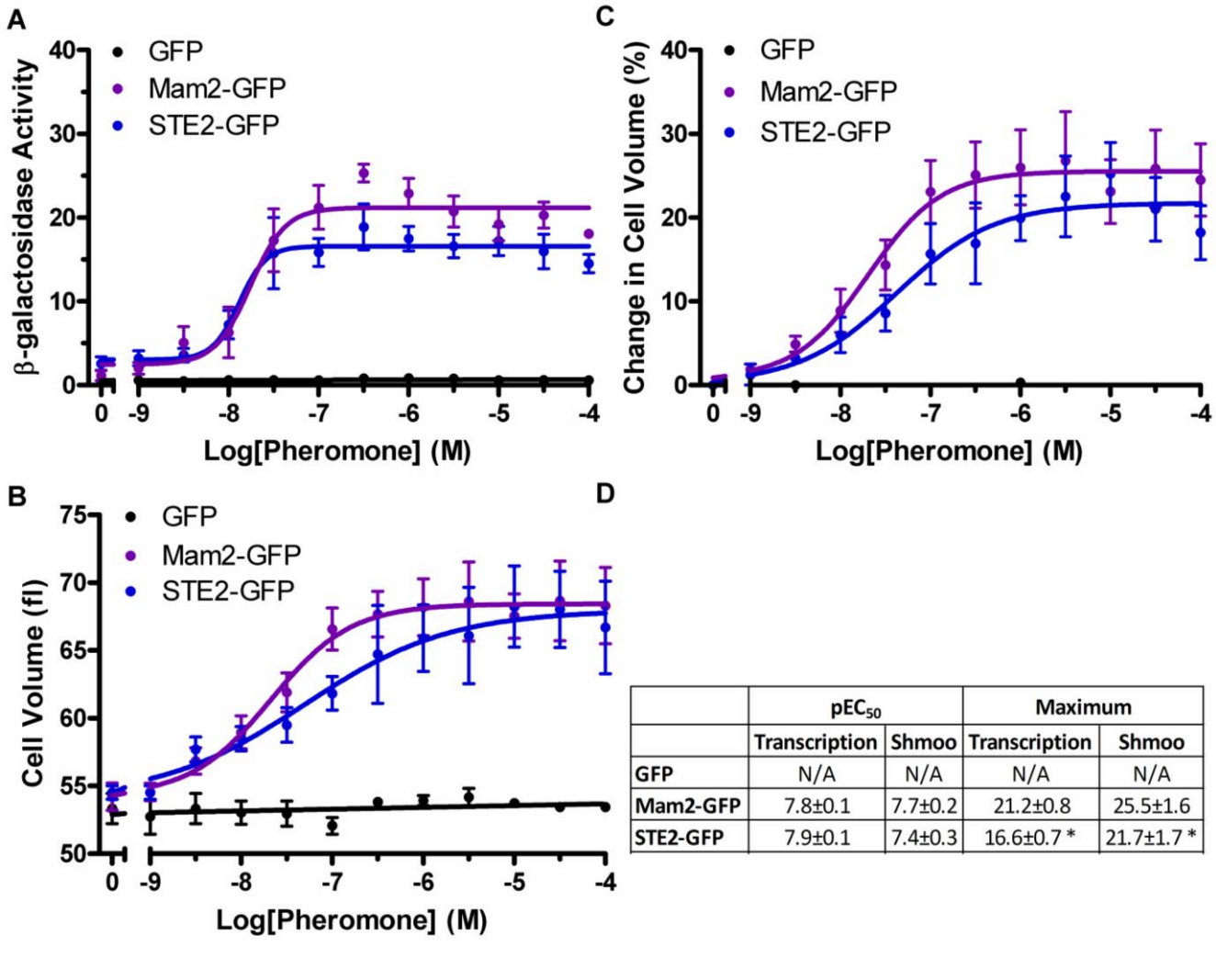

	pEC_{50}		Maximum	
	Transcription	Shmoo	Transcription	Shmoo
GFP	N/A	N/A	N/A	N/A
Mam2-GFP	7.8±0.1	7.7±0.2	21.2±0.8	25.5±1.6
STE2-GFP	7.9±0.1	7.4±0.3	16.6±0.7 *	21.7±1.7 *

Figure 4-3: Comparison of the activity of Mam2-GFP and STE2-GFP expressed in *Sz. Pombe*

JY1169 (*sxa2>lacZ, mam2⁻*) was transformed with pREP3x-GFP, pREP3x-Mam2-GFP or pREP3x-STE2-GFP. Cells were cultured in AA media to a density of ~$5x10^6$ cells/mL and incubated with 0 to 10^{-4} M pheromone. Cells transformed with STE2 were exposed to α-factor and cells transformed with Mam2 were exposed to P-factor. Results shown are means of triplicate independent determinations ±SE. **A:** The β-galactosidase activity ($OD_{420}/10^6$ cells) of transformants to quantify the transcriptional response. **B:** Median cell volume in transformants to measure the morphological response. **C:** Change in cell volume calculated as the increase above the median cell volume of unstimulated cells. **D:** pEC_{50} and maximal signalling values calculated from the dose-response curves in A and C. Statistically significant differences between Mam2-GFP and STE2-GFP are denoted by asterisks. The number of asterisks reflects the p-value such that *=p<0.05, **=p<0.01, ***=p<0.001.

4.2.4 STE2-GFP Accumulates in Cells

Following the functional analysis of receptors tagged with GFP, their sub-cellular localization was determined using confocal microscopy. This was of interest in order to compare the cellular localization of STE2 and Mam2, as well as to determine whether the signalling mutants characterized later in the chapter were mis-localized. JY1169 (*sxa2>lacZ, mam2*⁻) was transformed with pREP3x-GFP, pREP3x-STE2-GFP or pREP3x-Mam2-GFP. Cells were cultured in AA media lacking leucine to mid-exponential phase and examined using confocal microscopy.

Figure 4-4 shows confocal images of representative cells expressing GFP (A), STE2-GFP (B) and Mam2-GFP (C) with visible organelles marked out as; ER (endoplasmic reticulum), N (nucleus), PM (plasma membrane) and V (vacuole). GFP when expressed alone is not targeted to a specific compartment within the cell but is found throughout the cytoplasm and nucleus, with the exception of a number of spherical structures where fluorescence is absent. These structures have previously been described as vacuoles (Takegawa, Iwaki et al. 2003; Ladds, Goddard et al. 2005). The absence of GFP from the plasma membrane is expected as GFP lacks a plasma membrane targeting signal. This also explains its absence from the vacuoles as vacuoles are made up from fusions of internalized plasma membrane (Brooker, Widmaier et al. 2007).

An ImageJ/QuimP10 analysis was performed to quantify the amount of receptor on the membrane, as well as the ratio of receptor on the membrane to the interior of the cell (Figure 4-5A and B respectively). The average pixel intensity at the plasma membrane and the average percentage of fluorescence found at the plasma membrane compared to the interior of the cell is displayed in Figure 4-5C. The images of cells expressing STE2-GFP and Mam2-GFP show that both receptors are present on the plasma membrane. From the QuimP10 analysis of the images it appears as though there is more STE2-GFP found at the cell cortex compared to Mam2-GFP (Figure 4-5A), however this difference was not found to be statistically significant (calculated by an unpaired two-tailed t-test, $p<0.05$). This agrees with the findings from the pheromone-response assay where STE2-GFP and Mam2-GFP displayed comparable reporter activities.

The fluorescence microscopy images suggest that the two receptors predominantly localize to different intracellular compartments. Mam2-GFP internal to cells appears to predominantly localize to the ER of the cells (Figure 4-4B). STE2-GFP internal to cells in contrast appears to associate with structures resembling endosomes and/or vacuoles (Figure 4-4C). Furthermore, there was a statistically significant difference of the amount of receptor internal

to cells when expressing Mam2-GFP compared to when expressing STE2-GFP (Figure 4-5A and calculated by an unpaired, two-tailed t-test, $p<0.05$). Increased amounts of STE2 in endosomes or vacuoles may be due to ineffective targeting of STE2 for degradation. Like in the pheromone-response, this may again be due to an inability of STE2 to couple to the *Sz. pombe* cellular machinery effectively. In *Sc. cerevisiae* STE2 has previously been shown to get trapped in the late endosomal stage if successful protein-protein interactions cannot be formed (Gabriely, Kama et al. 2007) and it is possible that a similar effect is observed when the receptor is expressed in *Sz. pombe*.

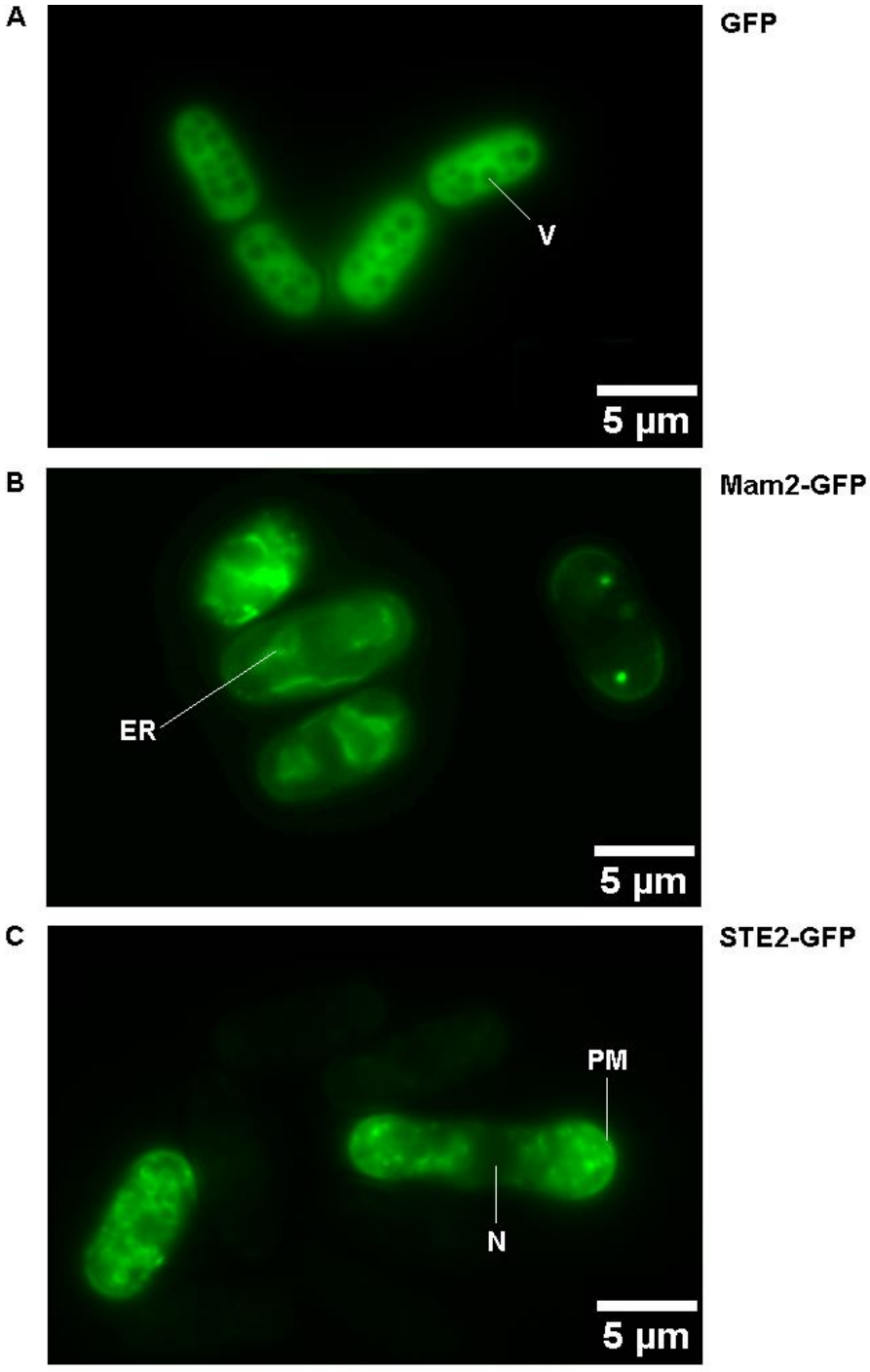

Figure 4-4: Representative images showing the localization of GFP, Mam2-GFP and STE2-GFP in *Sz. pombe*

JY1169 (*sxa2>lacZ, mam2*$^{-}$) was transformed with the pREP3x vectors containing GFP (A), Mam2-GFP (B) or STE2-GFP (C). Cells were cultured in AA media lacking leucine to mid-exponential phase and examined using confocal microscopy. Organelles apparent in the images are marked ER for endoplasmic reticulum, N for nucleus, PM for plasma membrane and V for vacuoles. Images were generated using a Personal DeltaVision (Applied Precision, Inc).

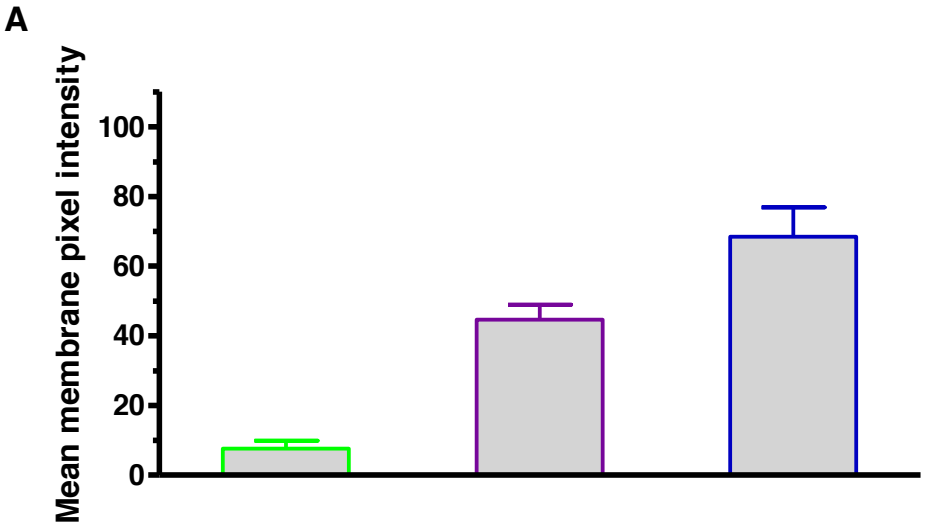

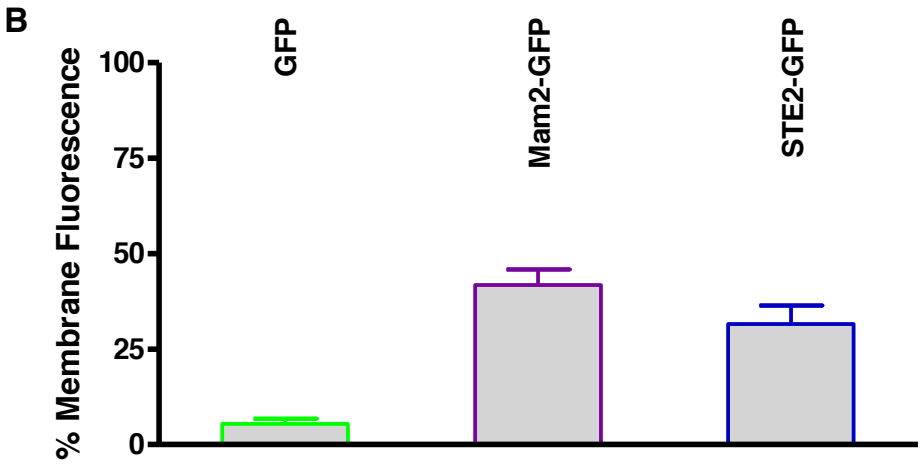

C

	PM intensity	% Membrane localization
GFP	7.6±2.4	5.4±1.4
Mam2-GFP	44.7±4.2	41.8±4.0
STE2-GFP	68.4±8.5	31.6±4.9 *

Figure 4-5: Measured fluorescence intensities at the cell membrane of GFP, STE2-GFP and Mam2-GFP

JY1169 (*sxa2>lacZ, mam2*¯) was transformed with pREP3x-GFP, pREP3x-STE2-GFP or pREP3x-Mam2-GFP. Cells were cultured in AA media lacking leucine to mid-exponential phase and examined using confocal microscopy. Images were generated using a Personal DeltaVision (Applied Precision, Inc) and the intensity of cytoplasm and membrane fluorescence was determined using the software QuimP10. Values shown are means ±SEM of 30 independent representative cells. A statistically significant difference ($p<0.05$) between Mam2-GFP and STE2-GFP is denoted by an asterisk. **A:** The mean individual pixel intensity at the membrane. **B:** The percentage membrane fluorescence of cells calculated from the total cell fluorescence. **C:** The average plasma membrane (PM) intensity and % membrane localization calculated from A and B.

4.3 Effects of Mutations in the SmallxxxSmall Motif on Cell Signalling

4.3.1 SmallxxxSmall Motifs

A motif of two small residues spaced one turn of the helix apart is implicated in the oligomerization of many membrane proteins (Lemmon, Flanagan et al. 1992; McClain, Iwamoto et al. 2003; Li, Gorelik et al. 2004; Jenei, Borthwick et al. 2009; King and Dixon 2010). This is because small residues such as glycine, serine and alanine permit close contact between transmembrane helices to allow extensive van der Waals interactions (MacKenzie and Engelman 1998; Javadpour, Eilers et al. 1999). The importance of the smallxxxsmall motif in TM domains is reflected by its statistical over-representation in membrane proteins (Senes, Gerstein et al. 2000).

4.3.2 STE2 and Mam2 Both Contain Motifs of Small Residues within Their First Transmembrane Domains

The *Sc. cerevisiae* GPCR STE2 contain a GxxxG motif in its first transmembrane domain formed by residues G56 and G60 (Figure 4-6A). Previous studies have implied that this motif is involved in interactions between receptors and that disrupting this motif affects pheromone signalling and transport of the receptor to the plasma membrane (Overton, Chinault et al. 2003). It has also been shown that the phenotype of a tailless GFP tagged version of the receptor, which is deficient in endocytosis, can be rescued by co-expression with the full-length receptor, suggesting that interactions between receptors play a role in internalization (Overton and Blumer 2002). BRET experiments on whole cell lysate later confirmed the ability of full-length STE2 to form dimers (Gehret, Bajaj et al. 2006). To date there is no crystal structure of the receptor, meaning that the exact nature of interactions is not precisely characterized. A homology model presented in section 6.1.4 however shows that the GxxxG motif potentially maps to the lipid-facing side of the transmembrane domain (rather than being involved in intra-helical interactions within the protein), further supporting the theory that the motif could be involved in oligomerization of the receptor.

There is evidence suggesting that Mam2 also forms oligomeric complexes (Ladds, Davis et al. 2005) although the reasons for oligomerization remains unknown. The sequence of Mam2 TM1 as predicted by the TMHMM algorithm (Krogh, Larsson et al. 2001) is shown in Figure 4-6B. Mam2 contain two putative smallxxxsmall motifs in its first transmembrane domain: G49xxxS53 and S53xxxA57. The residue G49 lies just outside of the region

predicted to be within the membrane, however, theoretically defined boundaries do not always agree with experimentally defined boundaries. Figure 4-6C shows an alignment between STE2 and Mam2 TM1 centred about the G56xxxG60 motif in STE2 and the putative smallxxxsmall motifs G49xxxS53 and S53xxxA57 in Mam2, with the log odds score of changing the amino acid in STE2 to the aligned amino acid in Mam2 shown underneath.

The log odds score (Jones, Taylor et al. 1994), is a measure of how conserved specific mutations of residues found in the membrane are between homologous proteins. Negative log odds values indicate 'disfavoured' mutations and positive values mean that the mutation is 'favoured'. In Figure 4-6C negative log odds scores are shown in blue, positive or neutral scores in yellow and residues that are unchanged are shown in green. With regards to the log odds score of changing amino acids in a transmembrane protein, it appears as though aligning the Mam2 residues S53xxxA57 to the STE2 G56xxxG60 motif conserves the sequence better than when aligning the Mam2 G49xxxS53 residues to STE2 G56xxxG60. If Mam2 functions similarly to STE2 then mutations to these residues might potentially have similar effects on cells when mutated.

4.3.3 Mutations Investigated in this Chapter

Two types of mutations were made in the smallxxxsmall motif of STE2 and Mam2 to investigate the effects to cell localization and cell signalling; conservative (changing a small residue to another small residue) and disfavoured (changing a small residue to a structurally larger residue). The log odds score penalty of conservative mutations is lower than for disfavoured mutations, for instance glycine to alanine is 1 or serine to alanine is 2. In contrast, the penalty of changing glycine to leucine is -4 and serine to leucine is -2. Although conservative mutations tend to have a smaller effect on proteins than disfavoured mutations, they can have detrimental effects. For instance, glycine to alanine mutations in the GxxxG motif found in the *Heliobacter pylori* toxin VacA abolishes protein function (McClain, Iwamoto et al. 2003).

Three conservative mutations were investigated in the STE2 G56xxxG60 motif; G56A, G60A and the double mutant G56A,G60A. The same disfavoured mutations studied were the same residues mutated to leucine instead of alanine. Four conservative mutations were investigated in Mam2. These were G49A, S53A, A57G and the double mutant G49A,S53A. The disfavoured mutations investigated were G49L, S53L,A57L and the double mutant G49L,S53L.

A **STE2** Q_{51} A I M F G_{56} V R C G_{60} A A A L T L I V M W M T S_{73}

B **Mam2** M_{50} T L S A Q L A L G V L T I L M W C L L S S S_{72}

C

STE2 GxxxG	V	T	Q	A	I	M	F	**G_{56}**	V	R	C	**G_{60}**	A	A	A	L	T	L	I	V	M	W	M	T	S
Mam2 SxxxA	L	L	T	G	M	T	L	**S_{53}**	A	Q	L	**A_{57}**	L	G	V	L	T	I	L	M	W	C	L	L	S
Log odds score	0	-1	-2	1	1	0	1	1	0	6	-1	1	-2	1	0	3	3	1	1	1	2	1	1	-1	3
Mam2 GxxxS	E	R	D	R	L	L	T	**G_{49}**	M	T	L	**S_{53}**	A	Q	L	A	L	G	V	L	T	I	L	M	W
Log odds score	-2	-1	2	-1	1	1	-2	6	1	-1	-1	1	2	-2	-2	-2	-1	-4	2	0	0	-3	1	0	-3

Figure 4-6: Sequences of STE2 and Mam2 transmembrane domain 1

A: Showing the amino acid sequence of STE2 TM1 as predicted by TMHMM. The two glycines G56 and G60 that form the smallxxxsmall motif in this domain are marked with residue numbers. **B:** Showing the amino acid sequence of Mam2 TM1 as predicted by TMHMM. **C:** Showing the log odds scores between Mam2 and STE2 TM1 with two different alignments, one centering S53xxxA57 in Mam2 and one centring G49xxxS53 in Mam2. A blue background represents negative log odds scores, yellow neutral or favoured. A green background indicates amino acids that are unchanged between the two proteins. Consequently the top alignment appears more conserved than the bottom alignment.

4.3.4 Conservative Mutations in the GxxxG motif of STE2 Transmembrane Domain 1 Affects the Pheromone-response

The pheromone response assay was performed to investigate the effects of conservative mutations in the STE2 GxxxG motif on signalling. JY1169 (*sxa2>lacZ, mam2*$^{-}$) was transformed with pREP3x-STE2-GFP, pREP3x-STE2^{G56A}-GFP, pREP3x-STE2^{G60A}-GFP or pREP3x-STE2^{G56A,G60A}-GFP. Cells were grown to mid log-phase and incubated with 0-10^{-5} M α-factor pheromone for 16 h. Figure 4-7A show the transcriptional pheromone-response and Figure 4-7B the shmoo response of the different transformants. Figure 4-7C shows the change in cell volume calculated as the increase above the median cell volume of unstimulated cells. The pEC_{50} and maximal signalling values calculated from the dose-response in A and C are shown in Figure 4-7D. For both the transcriptional response and the morphological response, the dose-response was observed to decrease at high pheromone concentrations, which may be attributable to down-regulation of the pheromone-response.

When exposed to pheromone, the mutants displayed characteristically different dose-response patterns compared to STE2-GFP. The Ste2^{G56A}-GFP mutant appeared slightly more sensitive to pheromone than STE2-GFP, and both Ste2^{G56A}-GFP and STE2^{G60A}-GFP mutants displayed slightly higher maximal signalling in the transcriptional response than STE2-GFP. These differences were however not statistically significant (calculated using an unpaired two-tailed t-test, $p<0.05$). In contrast, a 2-fold decrease in the maximal transcriptional and morphological dose-response was observed for the STE2^{G56A,G60A}–GFP double mutant. This difference compared to wild-type GFP tagged receptor was statistically significant (calculated using an unpaired two-tailed t-test, $p<0.05$).

The negative genetic interaction observed in the double-alanine mutant is interesting, especially as the signalling efficiency of each single alanine mutant was slightly elevated compared to wild-type. Although the structural conformation of the α-helix is largely determined by the symmetrical protein backbone, the amino acid side-chains can influence it to some extent thereby influencing the overall fold of the receptor. It seems unlikely however, that the fold of this double-mutant receptor is greatly affected as ligand-binding studies have demonstrated that it has a similar affinity to α-factor as wild-type receptor (Overton, Chinault et al. 2003). Another possible explanation for the differences observed is that the double mutant, but not each single mutant, affects protein oligomerization which may affect signalling.

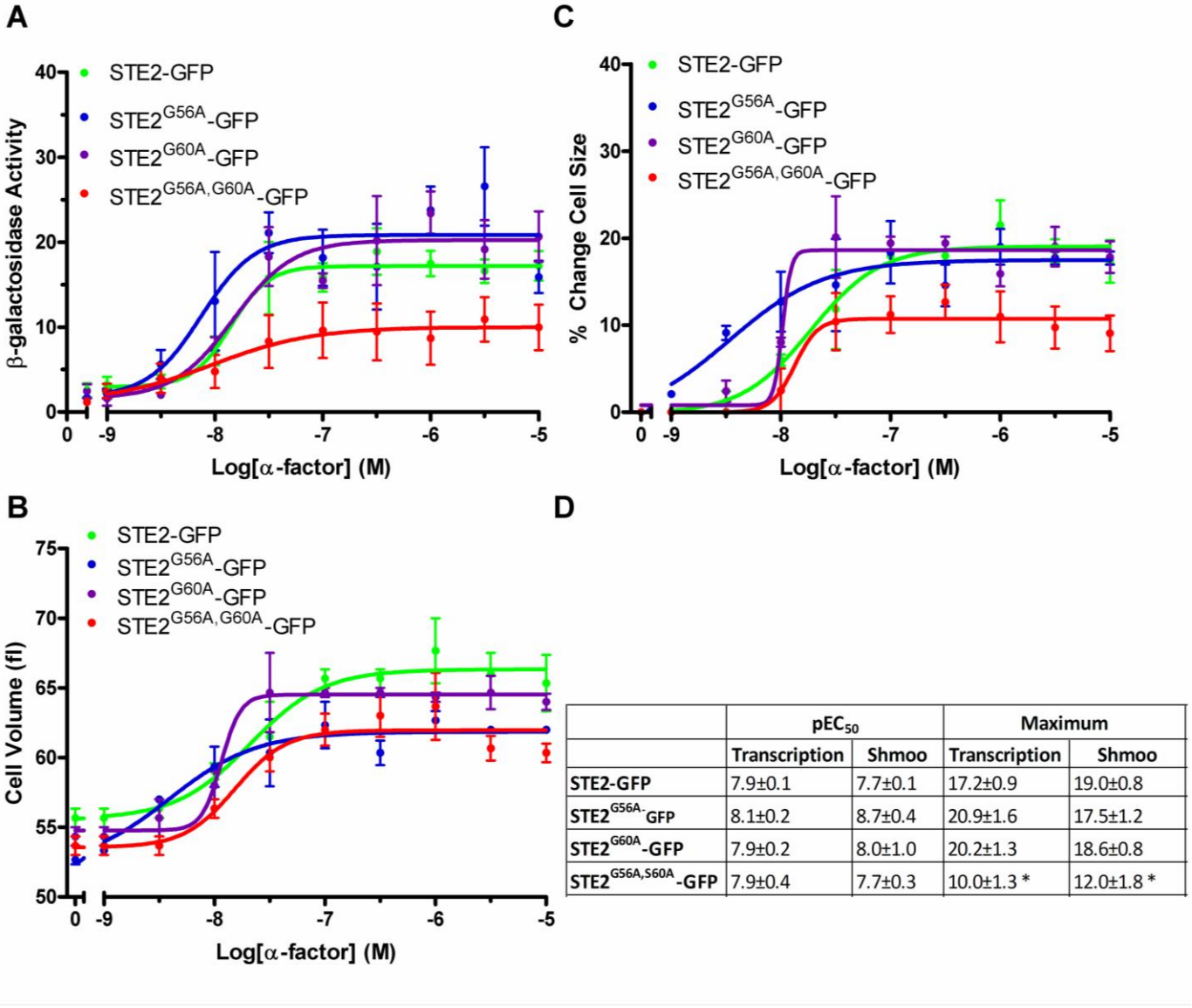

	pEC50		Maximum	
	Transcription	Shmoo	Transcription	Shmoo
STE2-GFP	7.9±0.1	7.7±0.1	17.2±0.9	19.0±0.8
STE2G56A-GFP	8.1±0.2	8.7±0.4	20.9±1.6	17.5±1.2
STE2G60A-GFP	7.9±0.2	8.0±1.0	20.2±1.3	18.6±0.8
STE2G56A,S60A-GFP	7.9±0.4	7.7±0.3	10.0±1.3 *	12.0±1.8 *

Figure 4-7: Effect of conservative mutations in STE2 on the pheromone-response

JY1169 (*sxa2>lacZ, mam2*) was transformed with pREP3x–STE2-GFP, pREP3x-STE2^{G56A}-GFP, pREP3x-STE2^{G60A}-GFP or pREP3x-STE2^{G56A,G60A}-GFP. Cells were cultured in AA to a density of ~5x10^6 cells/mL and incubated with 0 to 10^{-4} M α-factor. Results shown are means of triplicate independent determinations ±SE. **A:** The β-galactosidase activity (OD$_{420}$/10^6 cells) of transformants to measure the transcriptional response. **B:** Median cell volumes of transformants to quantify the morphological response. **C:** Change in cell volume calculated as the increase above the median cell volume of unstimulated cells. **D:** pEC$_{50}$ and maximal signalling values calculated from the dose-response curves in A and C. Statistically significant differences between STE2-GFP and mutants are denoted by asterisks. The number of asterisks reflects the p-value such that * =p<0.05, **=p<0.01, ***=p<0.001.

4.3.5 Effects of Conservative Mutations in STE2-GFP on Receptor Localization

The subcellular localization of STE2-GFP and the alanine STE2-GFP mutants was determined using confocal microscopy. JY1169 (*sxa2>lacZ, mam2*$^{-}$) was transformed with pREP3x-STE2-GFP, pREP3x-STE2^{G56A}-GFP, pREP3x-STE2^{G60A}-GFP or pREP3x-STE2^{G56A,G60A}-GFP. Cells were cultured in AA media lacking leucine to mid-exponential phase and examined using confocal microscopy. Figure 4-8 shows images of representative cells expressing each construct. An ImageJ/QuimP10 analysis was performed to quantify the amount of receptor on the membrane, as well as the ratio of receptor on the membrane to the interior of the cell (Figure 4-9A and B respectively). The average pixel intensity at the plasma membrane and the average percentage of fluorescence found at the plasma membrane compared to the interior of the cell is displayed in Figure 4-9C.

Consistent with the functional analysis of the receptor, the subcellular localization of the STE2^{G56A}-GFP and STE2^{G60A}-GFP mutants resembled that of wild-type receptor, although the STE2^{G56A} mutant appeared to display larger vacuoles (highlighted with a V in Figure 4-8B). The STE2^{G56A,G60A}-GFP double-mutant in contrast displayed a 2-fold reduction of receptor at the plasma membrane and this difference was found to be statistically significant (calculated by an unpaired two-tailed t-test, $p<0.05$), providing an explanation for the reduced signalling observed for this mutant in the pheromone response assay. The plasma membrane localization of this receptor is visibly reduced (compare Figure 4-8 A and D). It is not possible to determine the cause of the reduction in STE2^{G56A,G60A}-GFP abundance but expression may be affected at any stage of the regulation of expression including transcription, translation, trafficking or receptor degradation.

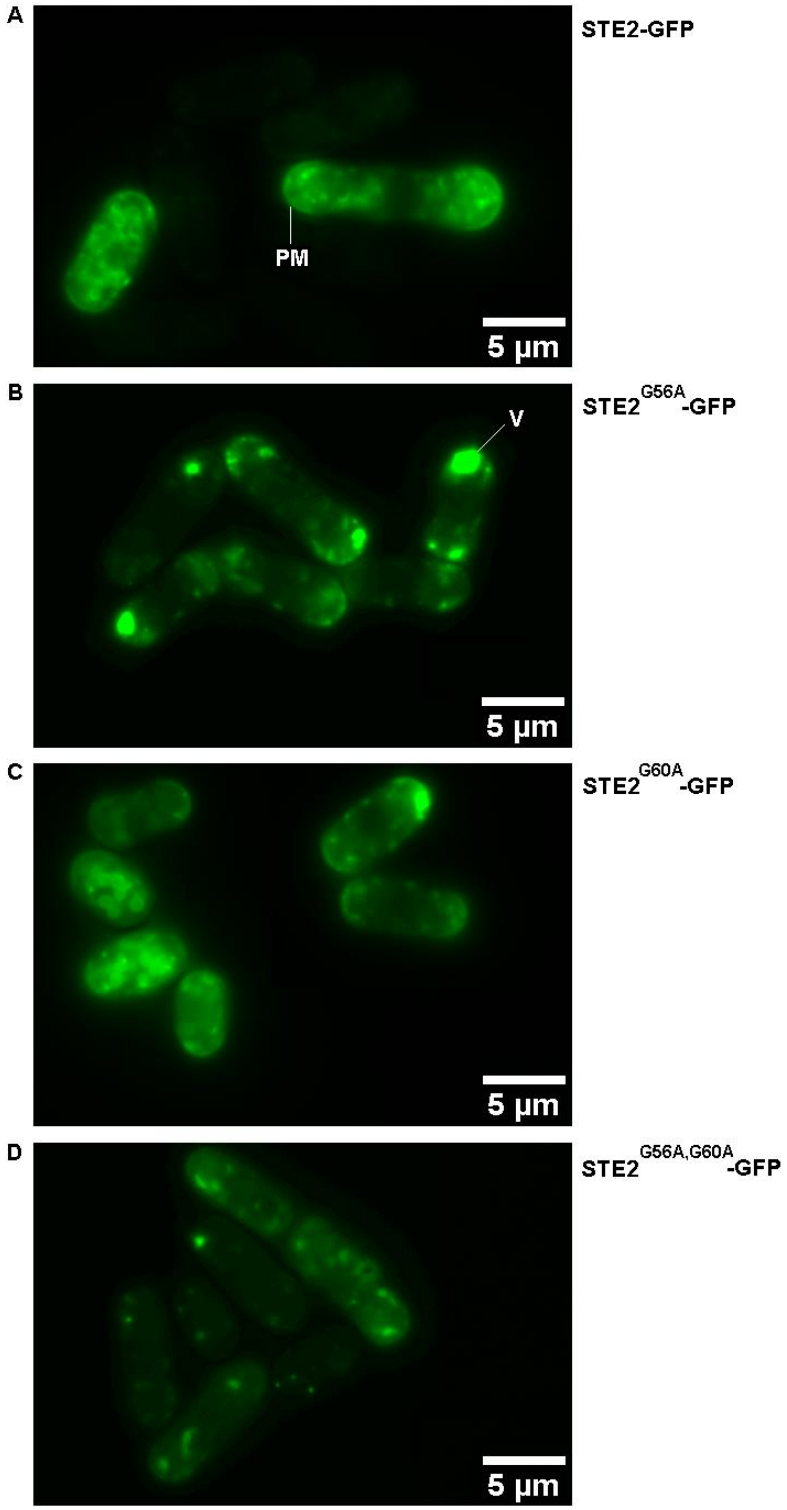

Figure 4-8: Representative images showing the localization of the conservatively mutated STE2-GFP receptors in *Sz. pombe*

JY1169 (*sxa2>lacZ, mam2*$^{-}$) was transformed with **A:** pREP3x-STE2-GFP **B:** pREP3x-STE2^{G56A}-GFP **C:** pREP3x-STE2^{G60A}-GFP or **D:** pREP3x-STE2^{G56A,G60A}-GFP. Cells were cultured in AA media lacking leucine to mid-exponential phase and examined using confocal microscopy. Images were generated using a Personal DeltaVision (Applied Precision, Inc). Plasma membrane (PM) and vacuoles (V) are highlighted.

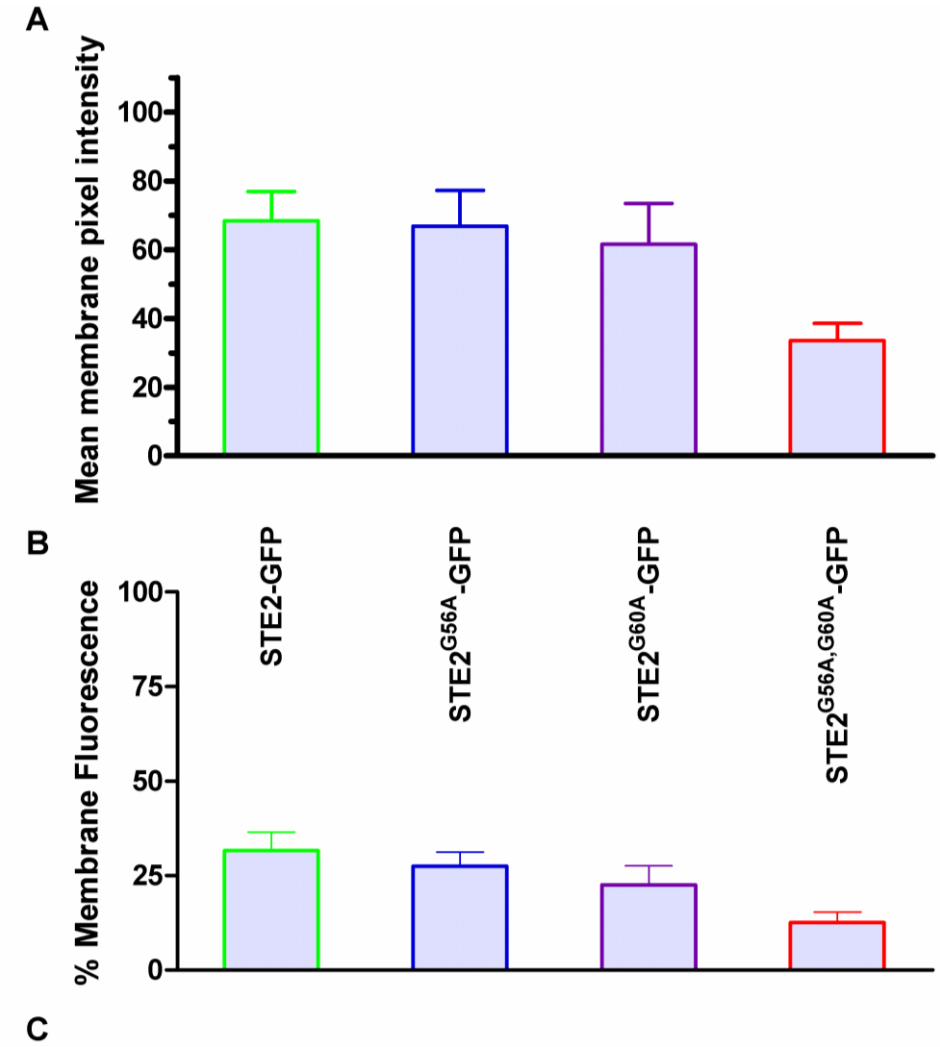

C

	PM intensity	% Membrane localization
STE2-GFP	68.4±8.5	31.6±4.9
$STE2^{G56A}$-GFP	66.8±10.4	27.5±3.7
$STE2^{G60A}$-GFP	61.6±11.9	22.6±5.0
$STE2^{G56A,G60A}$-GFP	33.6±5.0 *	12.5±2.8 *

Figure 4-9: Measured fluorescence intensities at the cell membrane of STE2-GFP and the STE2-GFP constructs containing conservative mutations

JY1169 (*sxa2>lacZ, mam2*) was transformed with pREP3x-STE2-GFP, pREP3x-$STE2^{G56A}$-GFP, pREP3x-$STE2^{G60A}$-GFP or pREP3x-$STE2^{G56A,G60A}$-GFP. Cells were cultured in AA media lacking leucine to mid-exponential phase and examined using confocal microscopy. Images were generated using a Personal DeltaVision (Applied Precision, Inc) and the intensity of cytoplasm and membrane fluorescence was determined using the software QuimP10. Values shown are means ±SEM of 30 independent representative cells. A statistically significant difference ($p<0.05$) between wild-type and mutants is denoted by an asterisk. **A:** The mean individual pixel intensity at the membrane. **B:** The percentage membrane fluorescence of cells calculated from the total cell fluorescence. **C:** The average plasma membrane (PM) intensity and % membrane localization calculated from A and B.

4.3.6 Conservative Mutations in the First Transmembrane Domain of Mam2 Have Varying Effects on the Pheromone-response

The effects of conservative mutations in the first transmembrane domain of Mam2 were also assessed using the pheromone response assay. JY1169 (*sxa2>lacZ, mam2*$^{-}$) was transformed with pREP3x-Mam2-GFP, pREP3x-Mam2^{G49A}-GFP, pREP3x-Mam2^{S53A}-GFP, pREP3x-Mam2^{A57G}-GFP or pREP3x-Mam2^{G49A,S53A}-GFP. Cells were grown to mid log-phase and incubated with 0-10^{-4} M P-factor pheromone for 16 h. The results are shown in Figure 4-10; Figure 4-10A show the transcriptional pheromone-response and Figure 4-10B the shmoo response of the different transformants. Figure 4-10C shows the change in cell volume calculated as the increase above the median cell volume of unstimulated cells. The pEC_{50} and maximal signalling values calculated from the dose-response in A and C are listed in Figure 4-10D.

In the absence of pheromone, the transcriptional signalling activity was similar for wild-type Mam2 and the Mam2 mutants, however the base-line cell volumes fluctuated (Figure 4-10B). In the presence of pheromone the response of the mutants differed from the pheromone-response in wild-type Mam2. The Mam2^{G49A}-GFP mutant had a transcriptional response similar to wild-type Mam2 but displayed a two-fold reduction in maximal morphological response (Figure 4-10C). This difference was not found to be statistically significant however. The Mam2^{A57G}-GFP and Mam2^{G49A,S53A}-GFP mutants displayed the opposite trend with a reduced maximal transcriptional response but a similar maximal morphological response compared to wild-type Mam2 and this difference was statistically significant (calculated using an unpaired two-tailed t-test, $p<0.01$ for the A57G mutation and $p<0.05$ for the G49A,S53A mutation). Differences in the activation of the transcriptional and morphological response when expressing heterologous signalling components has previously been observed in *Sz. pombe* (Ladds, Goddard et al. 2007). This phenomenon cannot however be explained by the current model of the interactions between receptor and downstream signalling component. In the current model, Ras1 is activated downstream of the Gpa1 Gα-subunit, which interacts with the receptor. Ras1 then either interact via the GEF Efc25 to activate the morphological response, or Ste6 to activate the transcriptional response. The exact details of the protein-protein interactions and how one pathway but not the other can be activated are to date unknown.

The Mam2^{S53A}-GFP mutant displayed the strongest signalling phenotype with an apparent reduced response in both the transcriptional and the morphological pathway. A statistical analysis was performed (using an unpaired two-tailed t-test) and the differences observed in

the transcriptional response were significant ($p<0.01$), but not the morphological response. The dose-response was again observed to decrease towards higher concentrations of pheromone, indicative of down-regulation of signalling or cell death.

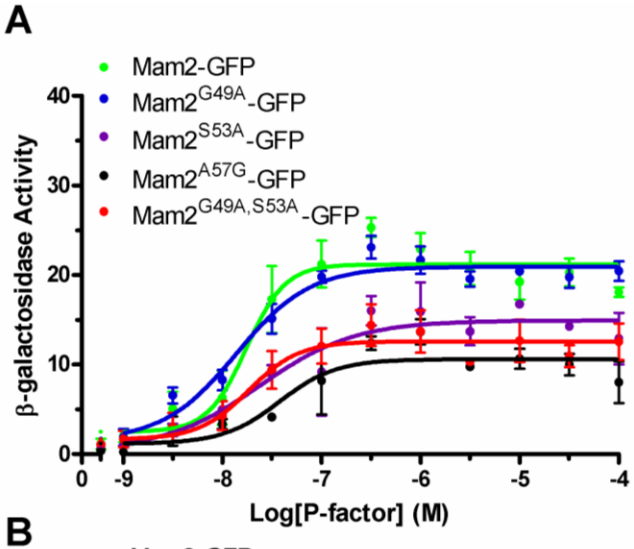

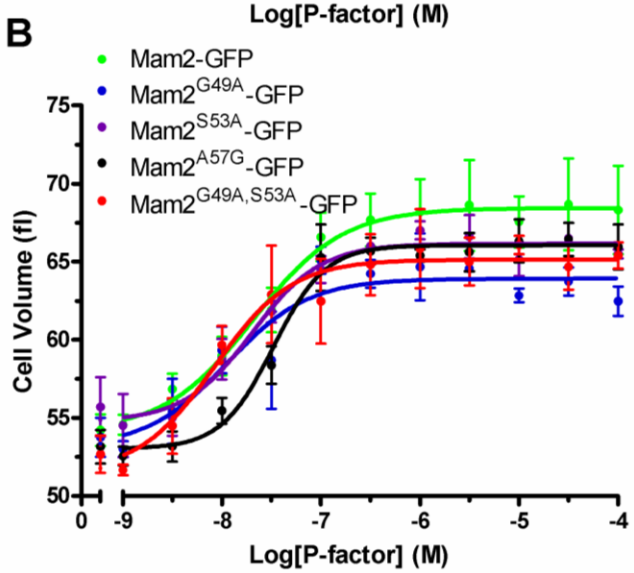

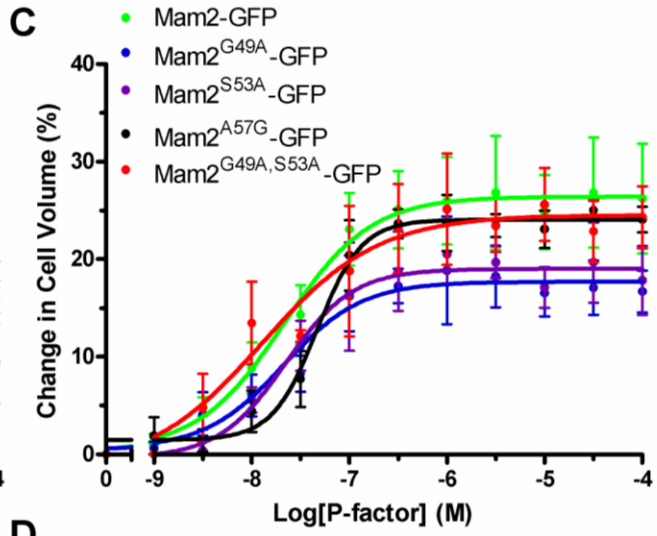

D

	pEC50		Maximum	
	Transcription	Shmoo	Transcription	Shmoo
Mam2-GFP	7.8±0.10	7.7±0.2	21.2±0.8	26.4±1.7
Mam2G49A-GFP	7.90±0.09	7.9±0.4	21.0±0.5	17.7±1.5
Mam2S53A-GFP	7.62±0.24	7.7±0.2	15.0±1.0 **	19.0±1.1
Mam2A57G-GFP	7.42±0.20	7.3±0.1	10.6±0.7 ***	19.0±1.1
Mam2G49A,S53A-GFP	7.73±0.16	8.1±0.3	12.6±0.7 **	19.0±1.1

Figure 4-10: Effect of conservative mutations in Mam2 on the pheromone-response

JY1169 (*sxa2>lacZ, mam2*$^-$) was transformed with pREP3x-Mam2-GFP, pREP3x-Mam2^{G49A}-GFP, pREP3x-Mam2^{S53A}-GFP, pREP3x-Mam2^{A57G}-GFP or pREP3x-Mam2^{G49A,S53A}-GFP. Cells were grown in AA media to a density of ~5x10^6 cells/mL and incubated with 0-10^{-4} M P-factor. Results shown are means of triplicate independent determinations ±SE. **A:** The β-galactosidase activity (OD_{420}/10^6 cells) of transformants to measure the transcriptional response. **B:** Median cell volumes of transformants to quantify the morphological response. **C:** Change in cell volume calculated as the increase above the median cell volume of unstimulated cells. **D:** pEC_{50} and maximal signalling values calculated from the dose-response curves in A and C. Statistically significant differences between Mam2-GFP and mutants are denoted by asterisks. The number of asterisks reflects the p-value such that * =p<0.05, **=p<0.01, ***=p<0.001.

4.3.7 Effects of Conservative Mutations in Mam2-GFP on Receptor Localization

The subcellular localization of Mam2-GFP and the alanine Mam2-GFP mutants was determined using confocal microscopy. JY1169 (*sxa2>lacZ, mam2*$^{-}$) was transformed with pREP3x-Mam2-GFP, pREP3x-Mam2^{G49A}-GFP, pREP3x-Mam2^{S53A}-GFP, pREP3x-Mam2^{A57G}-GFP or pREP3x-Mam2^{G49A,S53A}-GFP. Cells were cultured in AA media lacking leucine to mid-exponential phase and examined using confocal microscopy. Figure 4-11 shows images of representative cells expressing each construct. An ImageJ/QuimP10 analysis was performed to quantify the amount of receptor on the membrane, as well as the ratio of receptor on the membrane to the interior of the cell (Figure 4-12A and B respectively). The average pixel intensity at the plasma membrane and the average percentage of fluorescence found at the plasma membrane compared to the interior of the cell is displayed in Figure 4-12C.

Surprisingly, despite their altered signalling behaviour, the conservative Mam2 mutants Mam2^{G49A}-GFP, Mam2^{S53A}-GFP, Mam2^{A57G}-GFP and Mam2^{G49A,S53A}-GFP all localized to the plasma membrane in higher quantities than wild-type Mam2 labelled with GFP. For all mutants, this difference was statistically significant (calculated using an unpaired two-tailed t-test, $p<0.05$ for the single mutants and $p<0.01$ for the double-mutant). The ratio of receptor found at the cell cortex compared to intracellularly was also significantly higher for the mutants (Figure 4-12B), which may suggest that removal of receptor from the membrane is compromised. The increased amounts of receptor found at the cell cortex is interesting as it implies that the altered pheromone-response observed in these mutants cannot be attributed to the cellular localization of receptor, but instead the functionality of the receptors is somehow altered.

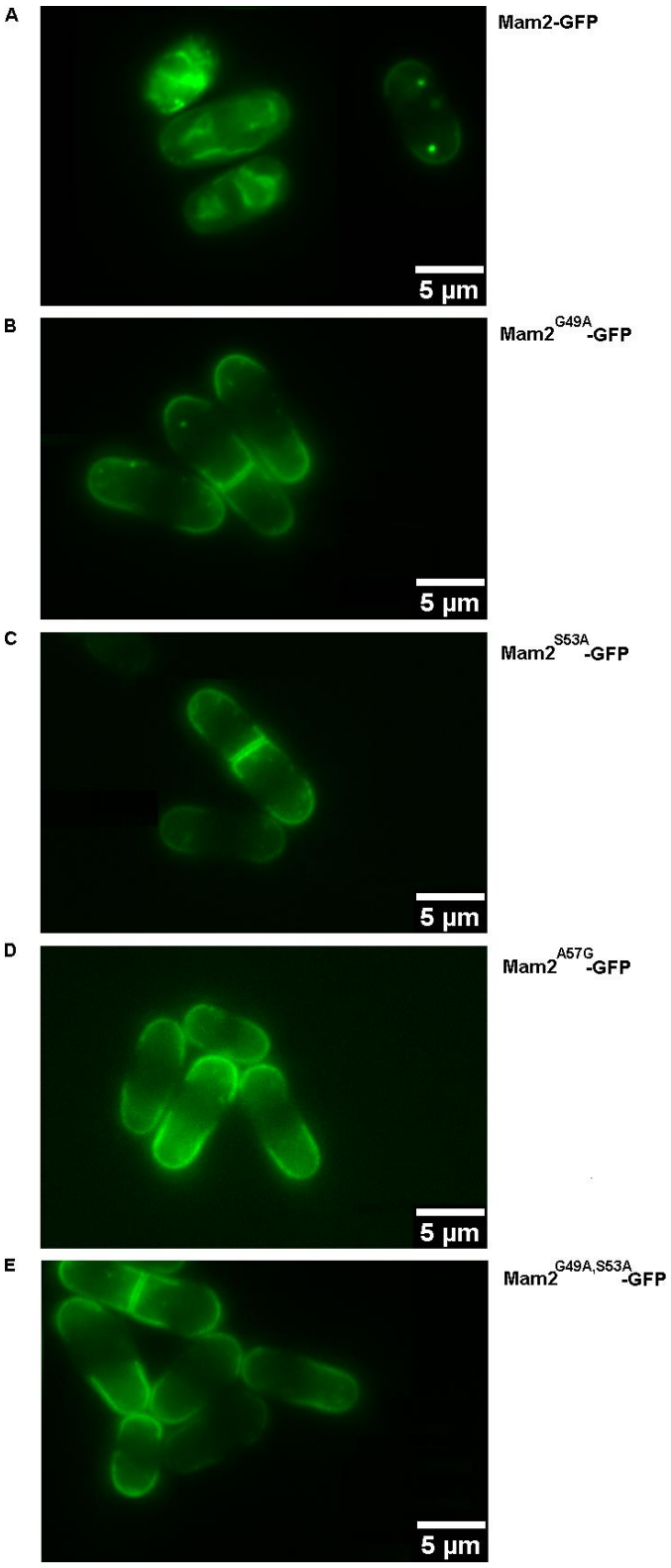

Figure 4-11: Representative images showing the localization of the conservatively mutated Mam2-GFP receptors in *Sz. pombe*

JY1169 (*sxa2>lacZ, mam2*$^{-}$) was transformed with **A:** pREP3x-Mam2-GFP, **B:** pREP3x-Mam2^{G49A}-GFP, **C:** pREP3x-Mam2^{S53A}-GFP, **D:** pREP3x-Mam2^{A57G}-GFP or **E**: pREP3x-Mam2^{G49A,S53A}-GFP. Cells were cultured in AA media lacking leucine to mid-exponential phase and examined using confocal microscopy. Images were generated using a Personal DeltaVision (Applied Precision, Inc).

A

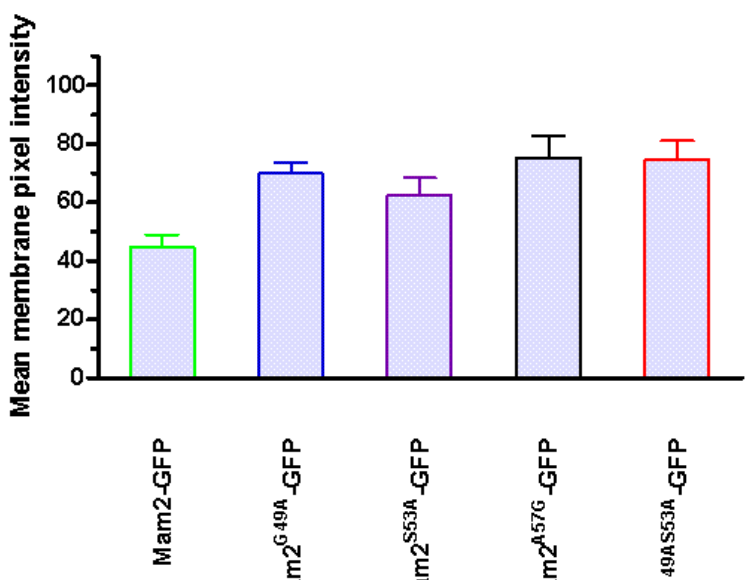

B

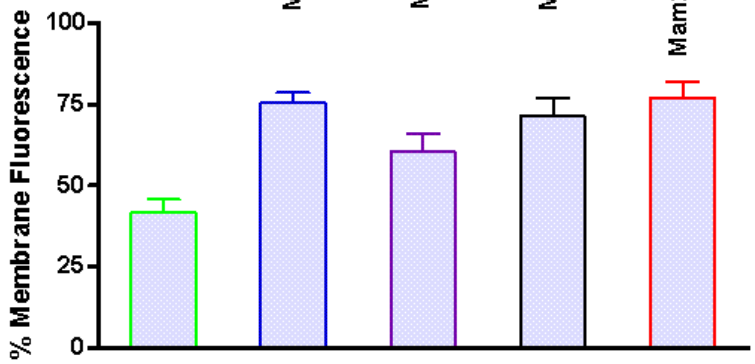

C

	PM intensity	% Membrane localization
Mam2-GFP	44.7±4.3	41.8±4.0
Mam2^{G49A}-GFP	69.8±3.7 *	75.4±3.2 ***
Mam2^{S53A}-GFP	69.8±6.8 *	60.4±5.6 *
Mam2^{A57G}-GFP	69.8±7.6 *	71.4±5.4 **
Mam2^{G56A,S60A}-GFP	69.8±6.5 **	77.0±5.0 **

Figure 4-12: Measured fluorescence intensities at the cell membrane of Mam2-GFP and the Mam2-GFP constructs containing conservative mutations

JY1169 (*sxa2>lacZ, mam2*⁻) was transformed with pREP3x-Mam2-GFP, pREP3x-Mam2^{G49A}-GFP, pREP3x-Mam2^{S53A}-GFP or pREP3x-Mam2^{G49A,S53A}-GFP. Cells were cultured in AA media lacking leucine to mid-exponential phase and examined using confocal microscopy. Images were generated using a Personal DeltaVision (Applied Precision, Inc) and the intensity of cytoplasm and membrane fluorescence was determined using the software QuimP10. Values shown are means ±SEM of 30 independent representative cells. Statistically significant differences between Mam2-GFP and mutants are denoted by asterisks. The number of asterisks reflects the p-value such that * =p<0.05, **=p<0.01 and ***=p<0.001 **A:** The mean individual pixel intensity at the membrane. **B:** The percentage membrane fluorescence of cells calculated from the total cell fluorescence. **C:** The average plasma membrane (PM) intensity and % membrane localization calculated from A and B.

4.3.8 Disfavoured Mutations in the GxxxG motif of STE2 Have a Pronounced Effect on the Pheromone-response

To investigate the effects of the non-conservative leucine mutations in the STE2 GxxxG motif, JY1169 (*sxa2>lacZ, mam2*$^-$) was transformed with pREP3x-STE2-GFP, pREP3x-STE2^{G56L}-GFP, pREP3x-STE2^{G60L}-GFP or pREP3x-STE2^{G56L,G60L}-GFP. Cells were grown to mid log-phase and incubated with 0-10^{-5} M α-factor pheromone for 16 h. Figure 4-13A show the transcriptional pheromone-response and Figure 4-13B the shmoo response of the different transformants. Figure 4-13C shows the change in cell volume calculated as the increase above the median cell volume of unstimulated cells. The pEC_{50} and maximal signalling values calculated from the dose-response in A and C are shown in Figure 4-13D.

Mutating the GxxxG motif in the first transmembrane domain of STE2 to leucine had a much more pronounced effect than mutating residues to alanine (compare Figure 4-7). A dose-response curve could not be calculated for either of the mutants, although it appears as though there is a slight increase in signalling response towards the higher concentrations of pheromone for the STE2^{G56L}-GFP mutant. This implies that the receptor binds pheromone with lower affinity, that coupling to downstream signalling effectors is affected, or that receptors are not efficiently localized to the plasma membrane, although the pheromone response assay cannot distinguish the cause.

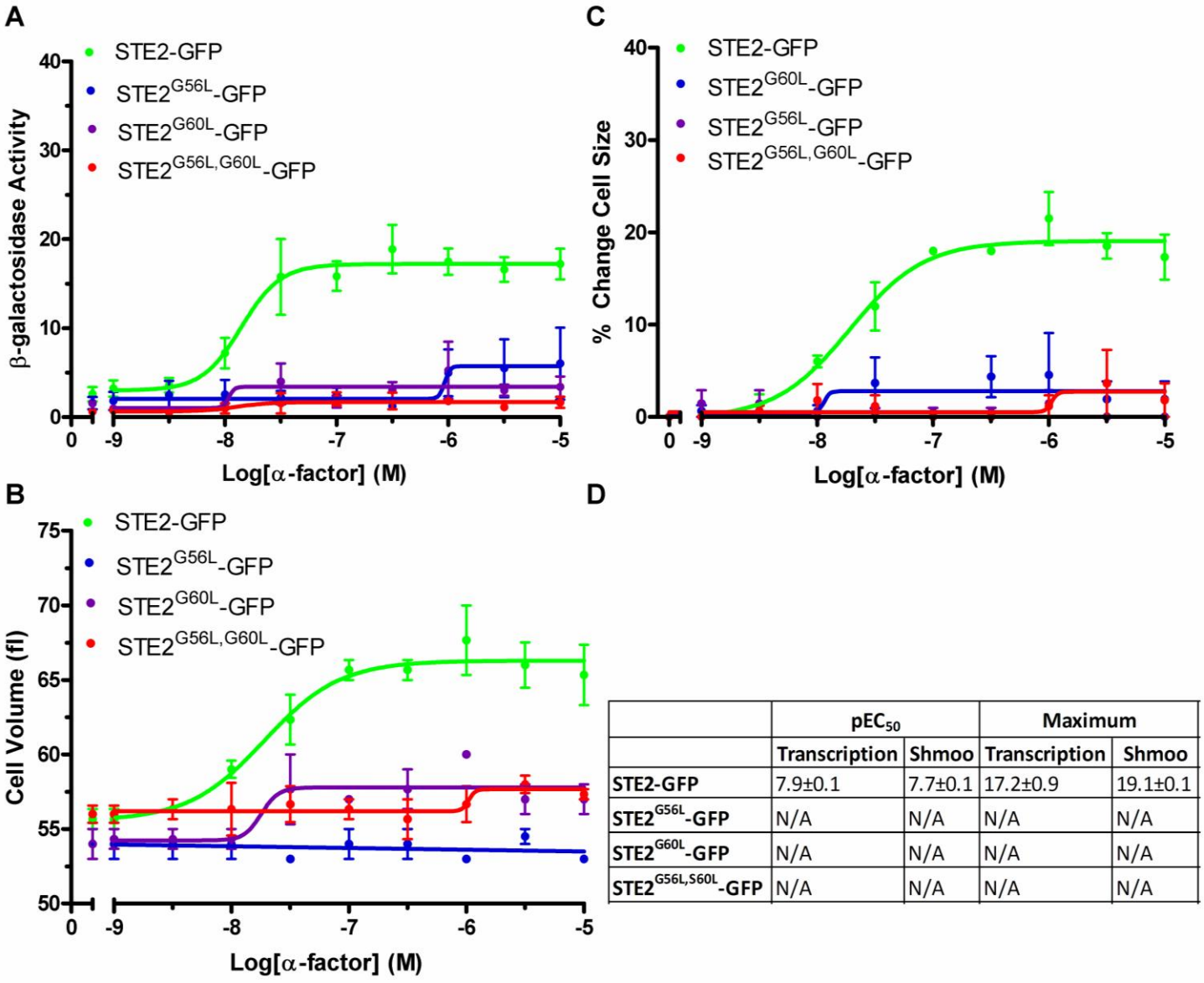

	pEC50		Maximum	
	Transcription	Shmoo	Transcription	Shmoo
STE2-GFP	7.9±0.1	7.7±0.1	17.2±0.9	19.1±0.1
STE2^{G56L}-GFP	N/A	N/A	N/A	N/A
STE2^{G60L}-GFP	N/A	N/A	N/A	N/A
STE2^{G56L,S60L}-GFP	N/A	N/A	N/A	N/A

Figure 4-13: Effect of disfavored mutations in STE2 on the pheromone-response

JY1169 (*sxa2>lacZ, mam2⁻*) was transformed with pREP3x–STE2-GFP, pREP3x-STE2^{G56L}-GFP, pREP3x-STE2^{G60L}-GFP or pREP3x-STE2^{G56L,G60L}-GFP. Cells were cultured in AA media to a density of ~5x10^6 cells/mL and incubated with 0-10^{-5} M α-factor. Results shown are means of triplicate independent determinations ±SE. **A:** The β-galactosidase activity (OD_{420}/10^6 cells) of transformants to measure the transcriptional response. **B:** Median cell volumes of transformants to quantify the morphological response. **C:** Change in cell volume calculated as the increase above the median cell volume of unstimulated cells. **D:** pEC_{50} and maximal signalling values calculated from the dose-response curves in A and C.

4.3.9 Effects of Disfavoured Mutations in STE2-GFP on Receptor Localization

Confocal imaging was performed to determine whether the absence of a pheromone-response in the STE2-GFP GxxxG leucine mutants was due to reduced expression of receptor at the plasma membrane, or may be attributable to another cause. JY1169 (*sxa2>lacZ, mam2*) was transformed with pREP3x-STE2-GFP, pREP3x-STE2^{G56L}-GFP, pREP3x-STE2^{G60L}-GFP or pREP3x- STE2^{G56L,G60L}-GFP. Cells were cultured in AA media lacking leucine to mid-exponential phase and examined using confocal microscopy. Figure 4-14 shows images of representative cells expressing each construct. An ImageJ/QuimP10 analysis was performed to quantify the amount of receptor on the membrane, as well as the ratio of receptor on the membrane to the interior of the cell Figure 4-15A and B respectively). The average pixel intensity at the plasma membrane and the average percentage of fluorescence found at the plasma membrane compared to the interior of the cell is displayed in Figure 4-15C.

The ImageJ/QuimP10 analysis of these images showed that the quantity of the leucine mutant receptors found at the cell cortex is reduced approximately three-fold compared to wild-type receptor (Figure 4-15A), a difference which is statistically significant (calculated using an unpaired two-tailed t-test, $p<0.01$). The ratio of receptor found at the cell membrane compared to the interior of the cell also differed between wild-type receptor and mutant receptor, with mutant receptors having increased amounts of internalized receptor. These appear to localize to vacuoles within the cells, highlighted by a V in Figure 4-15C. This difference was also found to be statistically significant (calculated using an unpaired two-tailed t-test $p<0.05$ for the G56L mutation and $p<0.01$ for the G60L and G56L,G60L mutations). A previous study have shown that these leucine mutants cannot bind agonist (Overton, Chinault et al. 2003) which suggests that the receptor may be misfolded and consequently is internalized before reaching the plasma membrane. Studies on misfolded mutants of STE2 have shown that, in *Sc. cerevisiae,* errors in folding in the ER lead to transport of the receptor from the ER to vacuolar structures without the receptor reaching the plasma membrane (Jenness, Li et al. 1997) which could explain this phenomenon. Furthermore, the GFP derivative used is highly stable (Ladds, Davis et al. 2005), which may explain its accumulation in the vacuoles.

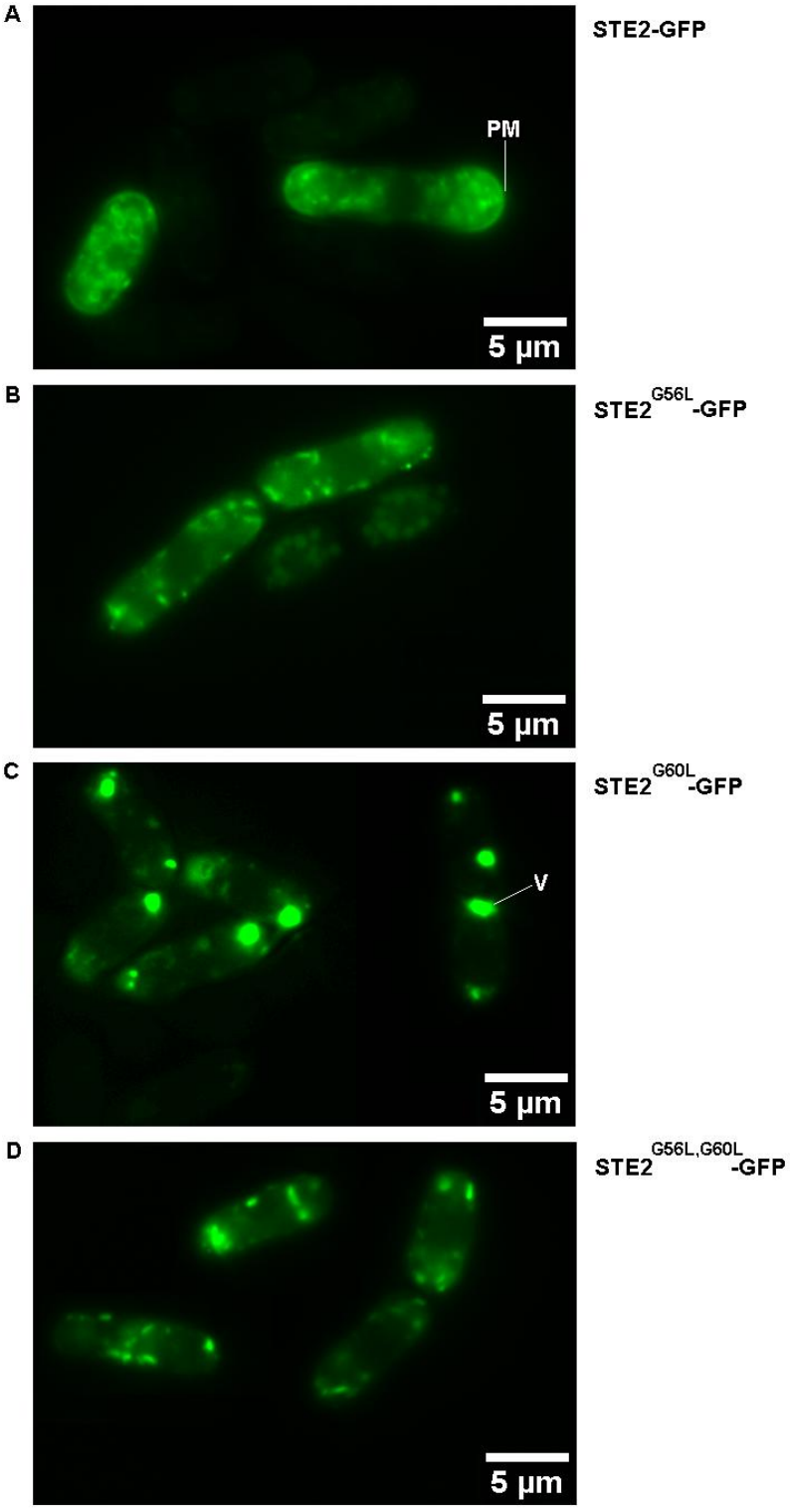

Figure 4-14: Representative images showing the localization of the STE2-GFP receptors containing the disfavored mutations in *Sz. pombe*

JY1169 (*sxa2>lacZ, mam2*) was transformed **A:** pREP3x-STE2-GFP **B:** pREP3x-STE2^{G56L}-GFP **C:** pREP3x-STE2^{G60L}-GFP or **D:** pREP3x-STE2^{G56L,G60L}-GFP. Cells were cultured in AA media lacking leucine to mid-exponential phase and examined using confocal microscopy. Images were generated using a Personal DeltaVision (Applied Precision, Inc). Plasma membrane (PM) and vacuoles (V) are highlighted.

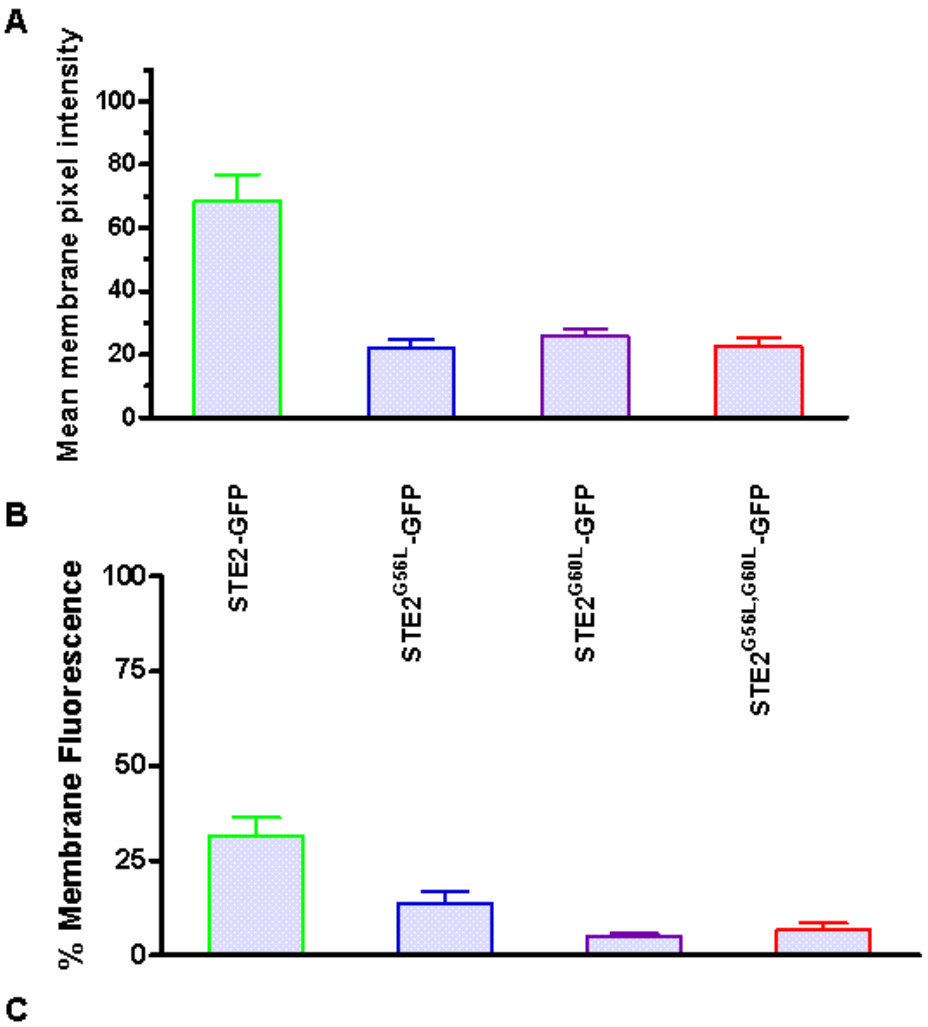

C

	PM intensity	% Membrane localization
STE2-GFP	68.4±8.5	31.6±4.9
$STE2^{G56L}$-GFP	22.0±2.8 **	13.7±3.3 *
$STE2^{G60L}$-GFP	25.6±2.7 **	5.1±0.7 **
$STE2^{G56L,S60L}$-GFP	22.6±2.8 **	6.9±1.7 **

Figure 4-15: Measured fluorescence intensities at the cell membrane of STE2-GFP and the STE2-GFP constructs containing the disfavored mutations

JY1169 (*sxa2>lacZ, mam2*) was transformed with pREP3x-STE2-GFP, pREP3x-$STE2^{G56L}$-GFP, pREP3x-$STE2^{G60L}$-GFP or pREP3x-$STE2^{G56L,G60L}$-GFP. Cells were cultured in AA media lacking leucine to mid-exponential phase and examined using confocal microscopy. Images were generated using a Personal DeltaVision (Applied Precision, Inc) and the intensity of cytoplasm and membrane fluorescence was determined using the software QuimP10. Values shown are means ±SEM of 30 independent representative cells. Statistically significant differences between STE2-GFP and mutants are denoted by asterisks. The number of asterisks reflects the p-value such that * =$p<0.05$ and **=$p<0.01$ **A:** The mean individual pixel intensity at the membrane. **B:** The percentage membrane fluorescence of cells calculated from the total cell fluorescence. **C:** The average plasma membrane (PM) intensity and % membrane localization calculated from A and B.

4.3.10 Effects of Disfavoured Mutations in Mam2-GFP on Pheromone Signalling

Mutations of the GxxxG motif in STE2 to leucine had a dramatic effect on *Sz. pombe* pheromone signalling and localization of receptor intracellularly. It was therefore of interest to investigate whether similar trends would be observed in leucine mutants of Mam2. To investigate the effects of the non-conservative leucine mutations in the smallxxxsmall motif found in the first transmembrane domain of Mam2, JY1169 (*sxa2>lacZ, mam2*$^{-}$) was transformed with pREP3x-Mam2-GFP, pREP3x-Mam2^{G59L}-GFP, pREP3x-Mam2^{S53L}-GFP, pREP3x-Mam2^{A57L}-GFP or pREP3x-Mam2^{G49L,S53L}-GFP. Cells were grown to mid log-phase and incubated with 0-10^{-5} M P-factor pheromone for 16 h. Figure 4-16A show the transcriptional pheromone-response and Figure 4-16B the shmoo response of the different transformants. Figure 4-16C shows the change in cell volume calculated as the increase above the median cell volume of unstimulated cells. The pEC_{50} and maximal signalling values calculated from the dose-response in A and C are shown in Figure 4-16D.

When mutating the smallxxxsmall motif in Mam2 to leucine, cellular signalling was much more severely affected compared to when the motif was mutated to a small residue. This is similar to what was observed for the STE2 leucine mutants; however the Mam2 leucine mutations did not appear to be as detrimental to cellular signalling as the STE2 leucine mutations. The only mutation where both the morphological and transcriptional response was completely absent was for cells transformed with the Mam2^{G49L,S53L}-GFP double mutant. All leucine mutants however were less sensitive to pheromone compared to wild-type receptor, and also exhibited lower maximal signalling. This difference was statistically significant, as calculated by an unpaired, two-tailed t-test ($p<0.05$-$p<0.001$) for all mutants.

Cells transformed with the Mam2^{G59L}-GFP construct were slightly more sensitive to pheromone compared to the other single residue mutants, and also had a slightly higher maximal signalling. If the face of the helix that these mutations map to is involved in receptor oligomerization, and if oligomerization is important for signalling, then this could imply that the S53 and A57 residues are more important than the G49 residue for close interactions of two receptors.

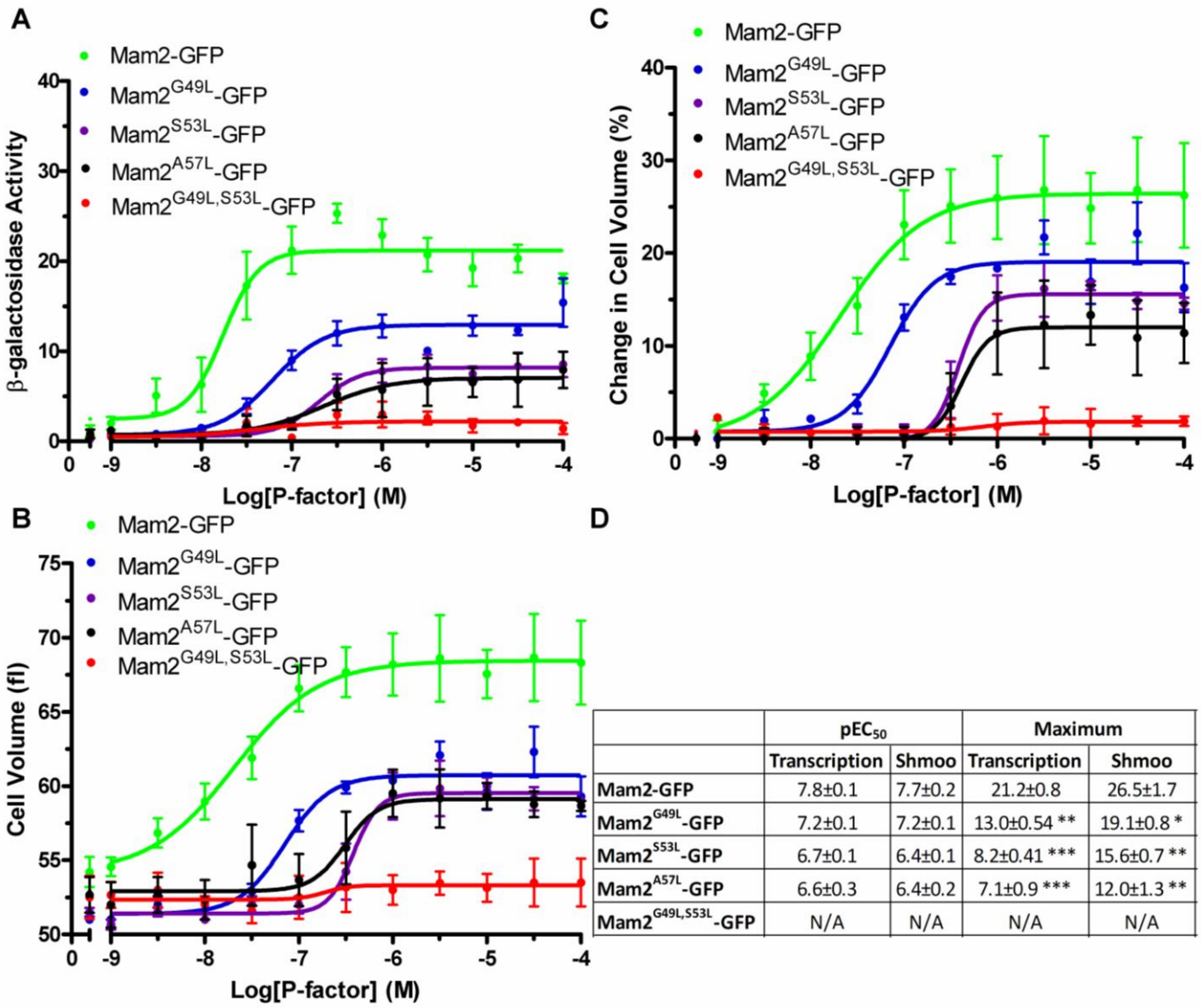

	pEC$_{50}$		Maximum	
	Transcription	Shmoo	Transcription	Shmoo
Mam2-GFP	7.8±0.1	7.7±0.2	21.2±0.8	26.5±1.7
Mam2^{G49L}-GFP	7.2±0.1	7.2±0.1	13.0±0.54 **	19.1±0.8 *
Mam2^{S53L}-GFP	6.7±0.1	6.4±0.1	8.2±0.41 ***	15.6±0.7 **
Mam2^{A57L}-GFP	6.6±0.3	6.4±0.2	7.1±0.9 ***	12.0±1.3 **
Mam2^{G49L,S53L}-GFP	N/A	N/A	N/A	N/A

Figure 4-16: Effect of disfavored mutations in Mam2 on the pheromone-response

JY1169 (*sxa2>lacZ, mam2⁻)* was transformed with pREP3x-Mam2-GFP, pREP3x-Mam2^{G49L}-GFP, pREP3x-Mam2^{S53L}-GFP or pREP3x-Mam2^{G49L,S53L}-GFP. Cells were cultured in AA media to a density of ~5x10^6 cells/mL and incubated 0 to 10^{-4} M P-factor. Results shown are means of triplicate independent determinations ±SE. **A:** The β-galactosidase activity (OD_{420}/10^6 cells) of transformants to measure the transcriptional response. **B:** Median cell volumes of transformants to quantify the morphological response. **C:** Change in cell volume calculated as the increase above the median cell volume of unstimulated cells. **D:** pEC$_{50}$ and maximal signalling values calculated from the dose-response curves in A and C. Statistically significant differences between Mam2-GFP and mutants are denoted by asterisks. The number of asterisks reflects the p-value such that * =p<0.05, **=p<0.01, ***=p<0.001.

4.3.11 The Mam2 Leucine Mutants are internalized to a Greater Extent than Wild-type Receptor

To determine whether the altered signalling behaviour observed in the Mam2 leucine mutants was due to receptor mislocalization, cells were examined using confocal microscopy. JY1169 (*sxa2>lacZ, mam2*⁻) was transformed with pREP3x-Mam2-GFP, pREP3x-Mam2^{G49L}-GFP, pREP3x-Mam2^{S53L}-GFP, pREP3x-Mam2^{A57L}-GFP or pREP3x-Mam2^{G49L,S53L}-GFP. Cells were cultured in AA media lacking leucine to mid-exponential phase and examined using confocal microscopy. Figure 4-17 shows images of representative cells expressing each construct. An ImageJ/QuimP10 analysis was performed to quantify the amount of receptor on the membrane, as well as the ratio of receptor on the membrane to the interior of the cell (Figure 4-17A and B respectively). The average pixel intensity at the plasma membrane and the average percentage of fluorescence found at the plasma membrane compared to the interior of the cell is displayed in Figure 4-17C.

In contrast to the single alanine mutants that had remarkably clear plasma membrane localization; the leucine mutants appeared to predominantly localize intracellularly. Figure 4-17A shows that the single leucine mutants had comparable levels of receptor at the plasma membrane to wild-type receptor, implying that the ER to plasma membrane transport was unaffected. When looking at the ratio of receptor found at the membrane compared to the interior of the cell however (Figure 4-17B), it is apparent that greater amounts of mutant receptors are internalized compared to wild-type receptor. For cells transformed with the pREP3x-Mam2^{S53L}-GFP and pREP3x-Mam2^{A57L}-GFP constructs this difference was statistically significant (calculated using an unpaired two-tailed t-test, $p<0.05$). The Mam2^{A57L} mutant displayed both clear plasma membrane localization as well as a high degree of accumulation in vacuoles as highlighted in Figure 4-17D. Since these mutant receptors had comparable levels of receptor found at the cell surface compared to Mam2, but displayed reduced cellular signalling; receptor trafficking and degradation as well as localization may be affected by the mutations.

In contrast, the Mam2^{G49L,S53L} double-mutant localized almost exclusively to the interior of the cell, suggesting that the double-mutation had a stronger effect on localization. This is in accordance with the pheromone-response assay where this mutant displayed the most reduced response to pheromone, and this reduction is highly likely to be caused by an absence of receptor at the cell membrane.

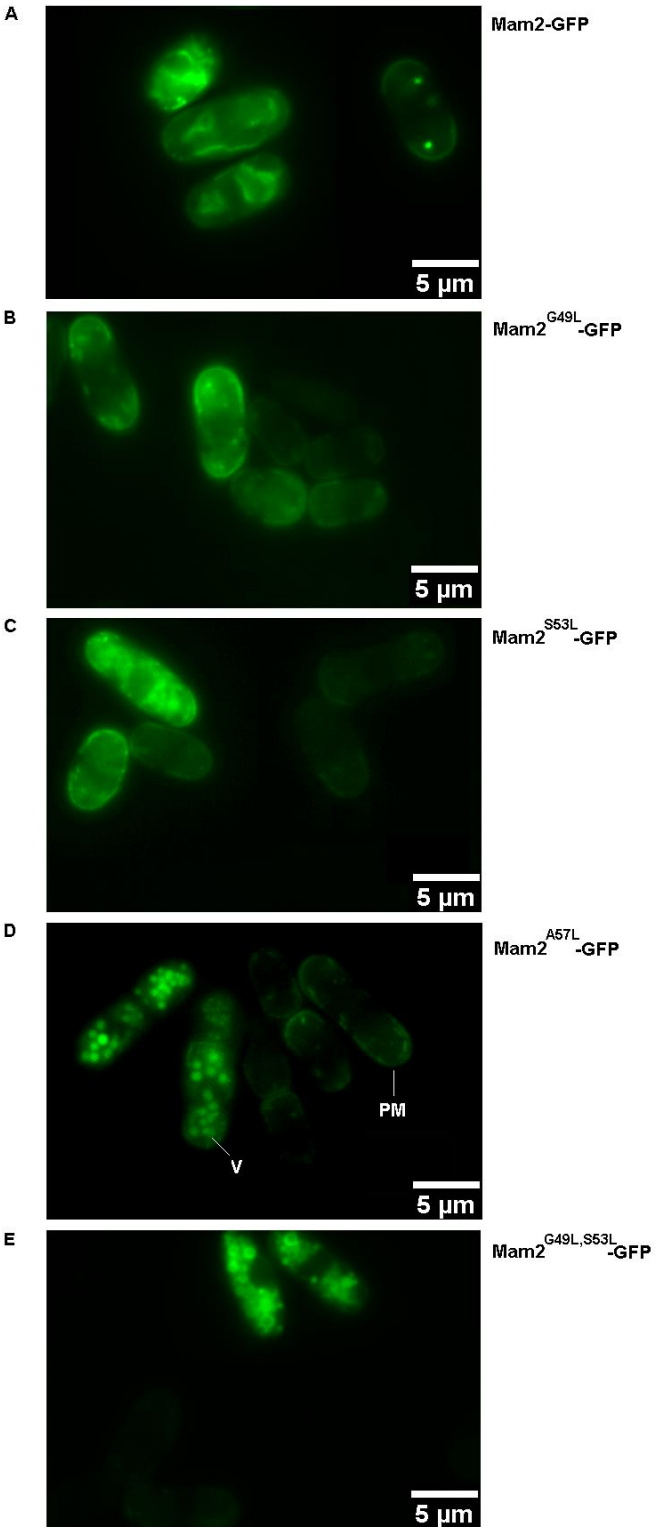

Figure 4-17: Representative images showing the localization of the Mam2-GFP receptors containing the disfavored mutations in *Sz. pombe*

JY1169 (*sxa2>lacZ, mam2*$^-$) was transformed with **A:** Mam2-GFP or the disfavored Mam2 mutants B**:** Mam2^{G49L}-GFP **C:** Mam2^{S53L}-GFP **D:** Mam2^{A57L}-GFP or **E:** Mam2^{G49L,S53L}-GFP. Cells were cultured in AA media lacking leucine to mid-exponential phase and examined using confocal microscopy. Images were generated using a Personal DeltaVision (Applied Precision, Inc). Plasma membrane (PM) and vacuoles (V) are highlighted.

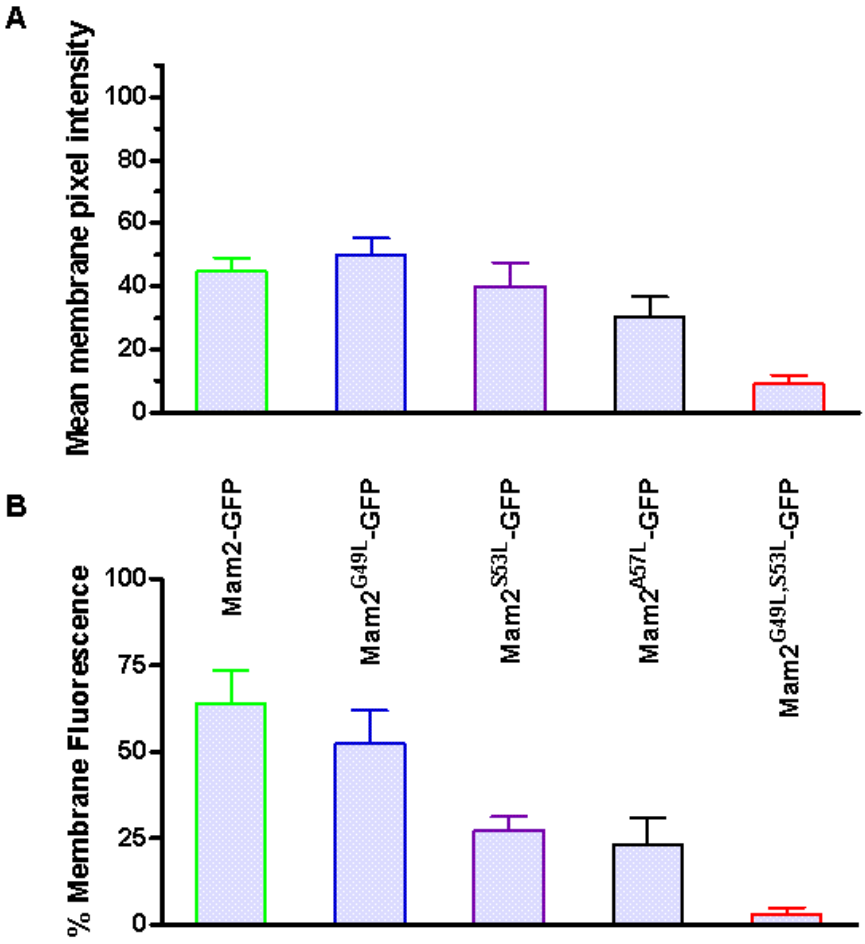

C

	PM intensity	% Membrane localization
Mam2-GFP	44.7±4.3	64.1±9.6
Mam2^{G49L}-GFP	49.7±5.5	52.4±9.6
Mam2^{S53L}-GFP	40.0±7.5	27.4±3.9 *
Mam2^{A57L}-GFP	30.5±6.1	23.3±7.6 *
Mam2^{G56L,S60L}-GFP	9.1±2.8 ***	3.1±1.9 ***

Figure 4-18: Measured fluorescence intensities at the cell membrane of Mam2-GFP and the Mam2-GFP constructs containing the disfavored mutations

JY1169 (*sxa2>lacZ, mam2*$^{-}$) was transformed with pREP3x-Mam2-GFP, pREP3x- Mam2^{G49L}-GFP, pREP3x- Mam 2^{S53L}-GFP or pREP3x- Mam2^{G49L,S53L}-GFP. Cells were cultured in AA media lacking leucine to mid-exponential phase and examined using confocal microscopy. Images were generated using a Personal DeltaVision (Applied Precision, Inc) and the intensity of cytoplasm and membrane fluorescence was determined using the software QuimP10. Values shown are means ±SEM of 30 independent representative cells. Statistically significant differences between Mam2-GFP and mutants are denoted by asterisks. The number of asterisks reflects the p-value such that * =$p<0.05$ and ***=$p<0.001$. **A:** The mean individual pixel intensity at the membrane. **B:** The percentage membrane fluorescence of cells calculated from the total cell fluorescence. **C:** The average plasma membrane (PM) intensity and % membrane localization calculated from A and B.

4.4 High Concentrations of Pheromone is Toxic to *Schizosaccharomyces pombe*

In the previous section, the transcriptional and morphological pheromone dose-response was observed to decrease towards the higher ends of the pheromone concentrations. This however did not seem as apparent for the signalling mutants displaying strong phenotypes. There are two possible reasons for the observed decrease in response. It could either reflect receptor desensitization to ligand, or toxicity of high concentrations of pheromone, or both. To test whether high concentrations of pheromone is toxic to *Sz. pombe,* cells were exposed to increasing concentrations of pheromone and assayed using a cell viability assay and flow cytometry.

Sz. pombe was cultured to a density of $1x10^6$ cells per mL and 1 mL of culture was incubated with 0, 10^{-7} M or 10^{-4} M P-factor for 16 h. Propidium iodide, which stain cells with damaged membranes and show in the PE-A channel, and SYTO9, which stain all cells and show in the FITC-A channel, were added to samples. SYTO9 fluoresce green whereas FRET between the two dyes result in red fluorescence; thus live cells can be distinguished from dead cells by the emission spectra. Flow cytometry was performed using an LSR II flow cytometer (BD Biosciences, Oxford, UK). Excitation of both dyes was achieved using a 488 nm blue laser, and emission was detected using a 550 nm long pass filter with a 575/26 nm band pass filter for propidium iodide and a 505 nm long pass filter with a 530/30 nm band pass filter for SYTO® 9. Figure 4-19 shows the output from analysis of 100.000 cells in the PE-A channel (y-axis, propidium iodide) and FIT-C (x-axis, CYTO9) for cells treated with 0 M pheromone (A), 10^{-7} M pheromone (B) and 10^{-4} M pheromone (C). As shown in Figure 4-19D, the number of dead cells in the populations is positively correlated with the amount of pheromone administered.

The same phenomenon has previously been observed in *Sc. cerevisiae* where cell death in response to pheromone has been linked to the effector kinase STE20 and apoptosis; shmooing cells are committed to either mating or programmed cell death (Madeo, Fröhlich et al. 1997; Severin and Hyman 2002; Skulachev 2002). A homologous effector kinase to STE20 has however so far not been identified in *Sz. pombe*, although apoptosis has been observed. It is believed that the vacuoles, where internalized receptor is targeted, also play a role in apoptosis (Thompson and Parker 2009) although it is unclear what the link is. The occurrence of programmed cell death in unicellular organism is believed to improve the gene pool through the removal of infertile and damaged individuals and releasing nutrients back to the population (Severin and Hyman 2002).

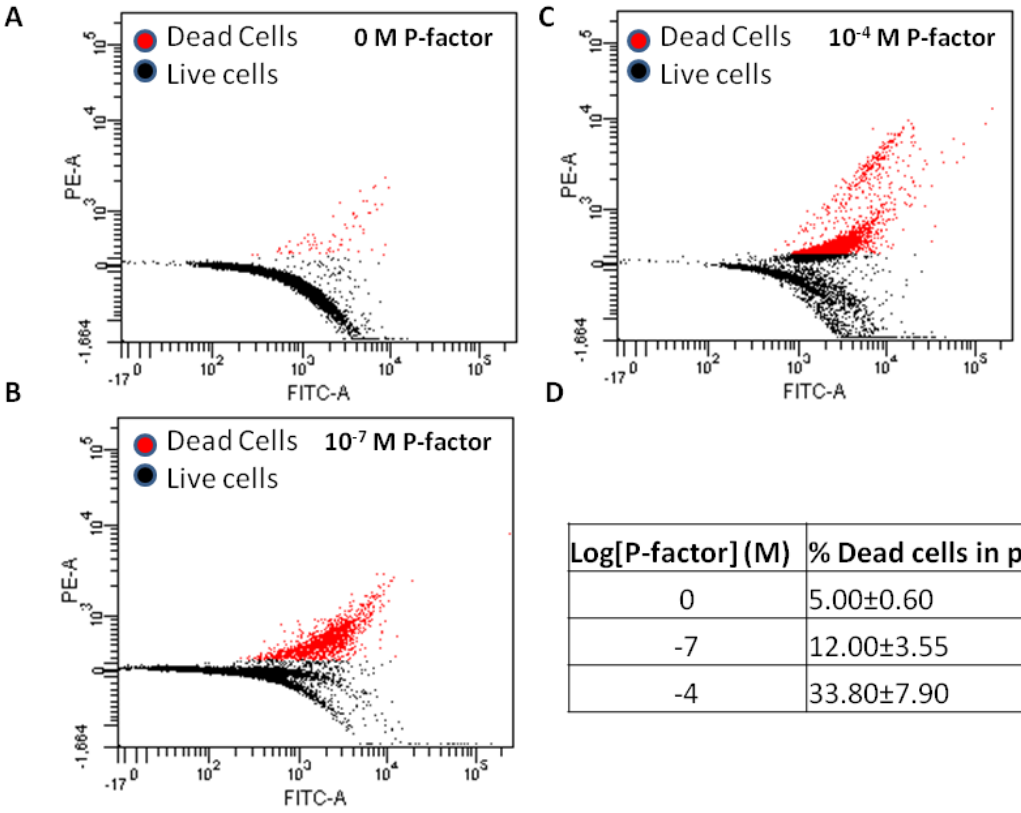

Log[P-factor] (M)	% Dead cells in population
0	5.00±0.60
-7	12.00±3.55
-4	33.80±7.90

Figure 4-19: *C*ell viability in response to pheromone

JY1169 (*sxa2>lacZ, mam2*) expressing pREP3x-Mam2-GFP was cultured in AA media lacking leucine to mid-exponential phase and exposed to 0, 10^{-7} M or 10^{-4} M P-factor and incubated on a rotating wheel for 16 h. Cells were then washed with PBS and stained with CYTO9 and propidium iodide before FACS analysis was performed. Propidium iodide exclusively stains cells with damaged membranes whereas SYTO9 stains all cells. SYTO9 fluoresce green whereas FRET between the two dyes result in emission in the red. Viable cells can therefore be distinguished from dead cells through the emission spectra. Flow cytometry was performed using an LSR II flow cytometer (BD Biosciences, Oxford, UK). Excitation of both dyes was achieved using a 488 nm blue laser, and emission was detected using a 550 nm long pass filter with a 575/26 nm band pass filter for propidium iodide and a 505 nm long pass filter with a 530/30 nm band pass filter for SYTO® 9. 100.000 cells were analysed per sample **A:** shows the results from cells incubated with no P-factor **B:** shows the results from cells incubated with 10^{-7} M P-factor **C:** shows the results from cells incubated with 10^{-4} M P-factor and **D:** results shown are means of triplicate determinations of three independent isolates ±SEM.

4.5 Developing a Bioluminescence Resonance Energy Transfer Assay to Measure Oligomerization

Mutating the smallxxxsmall motif in both Mam2 and STE2 altered cell localization as well as functionality of receptors. To see whether this is a possible effect of altering the oligomerization of receptors, in addition to cell localization, fusions of receptors to the *Renilla reniformis* luciferase Rluc were generated for live cell real-time BRET assays in *Sz. pombe*. To date, there are no publications discussing the use of BRET in *Sz. pombe* receptor oligomerization studies. In *Sc. cerevisiae* however energy transfer assays have successfully been utilized to monitor STE2 oligomerization including FRET (Overton, Chinault et al. 2003) or BRET in lysed cells (Gehret, Bajaj et al. 2006).

The main disadvantage of using FRET for investigating energy transfer between G protein-coupled receptors is that the tail of the receptor is too large to allow successful coupling between fluorophores. The tail must therefore be removed, which also removes the internalization signal in the receptor with an accumulation of receptor at the plasma membrane as a result. This has three possible outcomes on the result of assays. Firstly, aggregates of receptor on the membrane could result in false positive results. Secondly because receptor is not removed from the cell surface in response to pheromone, then any effects that the down-regulation of the pheromone-response may have on oligomerization cannot be monitored. Thirdly, in *Sz. pombe* removal of the C-terminal domain has a dramatic effect on receptor activity, because it contains the Rgs1 binding-site (McCann 2010). The use of a bioluminescent chromophore however removes this problem because it allows a longer distance between donor and acceptor for successful energy transfer.

4.5.1 The Effect of Rluc-Receptor Fusions on Cellular Signalling

To perform BRET assays, Mam2-Rluc and STE2-Rluc receptor fusions were constructed to act as the donor in the assay. These constructs were assayed for reporter activity in response to pheromone in order to determine whether labelling receptors with Rluc has any adverse effects on cellular signalling.

4.5.1.1 A STE2-Rluc Fusion Has No Effect on Pheromone Signalling

To determine whether an Rluc label has an effect on cellular signalling via STE2, the pheromone dose-response of JY1169 (*sxa2>lacZ, mam2*$^-$) transformed with pREP3x-STE2-Rluc was compared the pheromone dose-response of JY1169 transformed with pREP3x-STE2 and pREP3x-STE2-GFP. Cells were grown to mid log-phase and incubated with 0-10^{-4} M α-factor pheromone for 16 h. Figure 4-20A show the transcriptional pheromone-response and Figure 4-20B the shmoo response of the different transformants. Figure 4-20C shows the change in cell volume calculated as the increase above the median cell volume of unstimulated cells. The pEC_{50} and maximal signalling values calculated from the dose-response in A and C are shown in Figure 4-20D.

The signalling activity of cells transformed with the STE2-Rluc was statistically comparable to those transformed with STE2-GFP and STE2, calculated by an unpaired two-tailed t-test. This suggests that the Rluc label has no effect on signalling via STE2. The decrease in signalling response due to cell death in cells expressing STE2-GFP exposed to higher concentrations of pheromone was also observed in cells expressing the STE2-Rluc fusions.

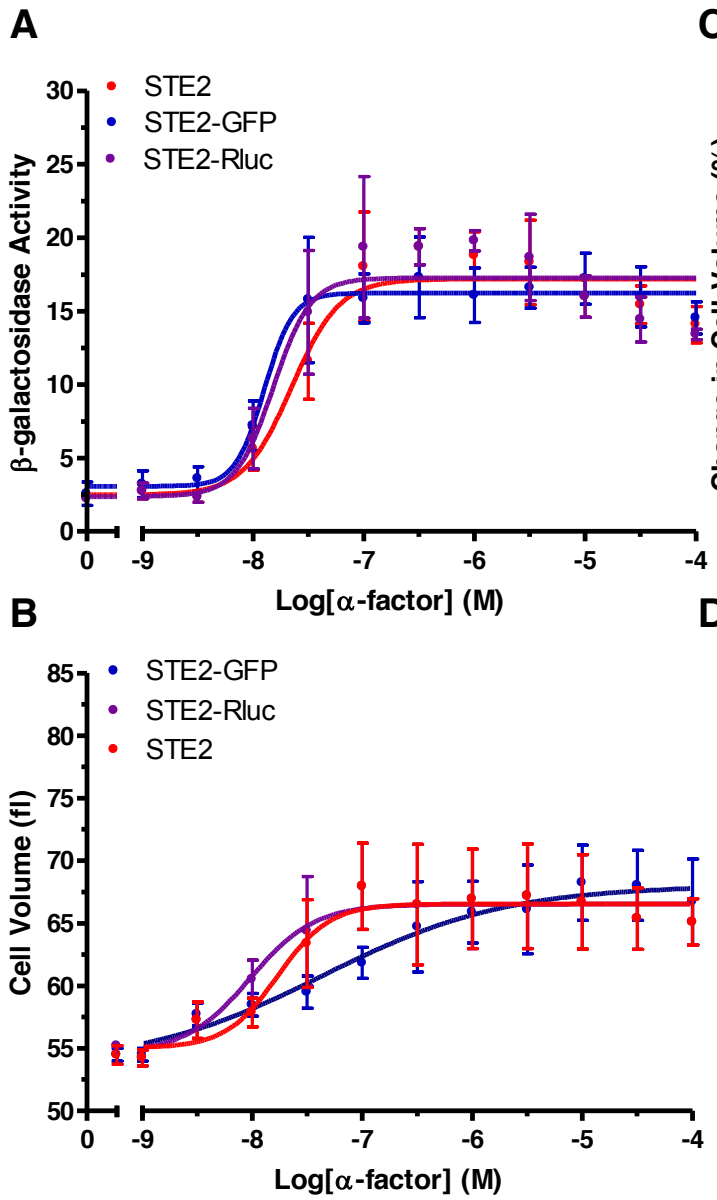

	pEC_{50}		Maximum	
	Transcription	Shmoo	Transcription	Shmoo
STE2	7.65±0.12	7.88±0.59	17.08±0.73	22.32±2.47
STE2-GFP	7.88±0.11	7.38±0.27	16.59±0.72	21.72±1.72
STE2-Rluc	7.81±0.13	7.66±0.21	17.26±0.87	25.53±1.57

Figure 4-20: Effect of Rluc and GFP tags on the activity of STE2

JY1169 (*sxa2>lacZ, mam2*$^-$) was transformed with pREP3x-STE2-GFP and pREP3x-STE2-Rluc and cells were cultured in AA media to a density of ~5x10^6 cells/mL and incubated with concentrations of α-factor ranging from 0 to 10^{-4} M. Results shown are means of triplicate independent determinations ±SE. **A:** The β-galactosidase activity ($OD_{420}/10^6$ cells) of transformants to measure the transcriptional response. **B:** Median cell volumes of transformants to quantify the morphological response. **C:** Change in cell volume calculated as the increase above the median cell volume of unstimulated cells. **D:** pEC_{50} and maximal signalling values calculated from the dose-response curves in A and C.

4.5.1.2 A Mam2-Rluc Fusion Has No Effect on Pheromone Signalling

To determine whether labelling receptors with Rluc has an effect on cellular signalling via Mam2, the pheromone dose-response of JY1169 (*sxa2>lacZ, mam2*$^{-}$) transformed with pREP3x-Mam2-Rluc was compared the pheromone dose-response of JY1169 transformed with pREP3x-Mam2-GFP. Cells were grown to mid log-phase and incubated with 0-10^{-4} M P-factor pheromone for 16 h. Figure 4-21A show the transcriptional pheromone-response and Figure 4-21B the shmoo response of the different transformants. Figure 4-21C shows the change in cell volume calculated as the increase above the median cell volume of unstimulated cells. The pEC_{50} and maximal signalling values calculated from the dose-response in A and C are shown in Figure 4-21D.

The signalling activity of cells transformed with the pREP3x-Mam2-Rluc was comparable to those transformed with pREP3x-Mam2-GFP, although cells expressing the Rluc tag appeared slightly more sensitive to pheromone. The Rluc tag does not appear to affect signalling via Mam2 significantly however.

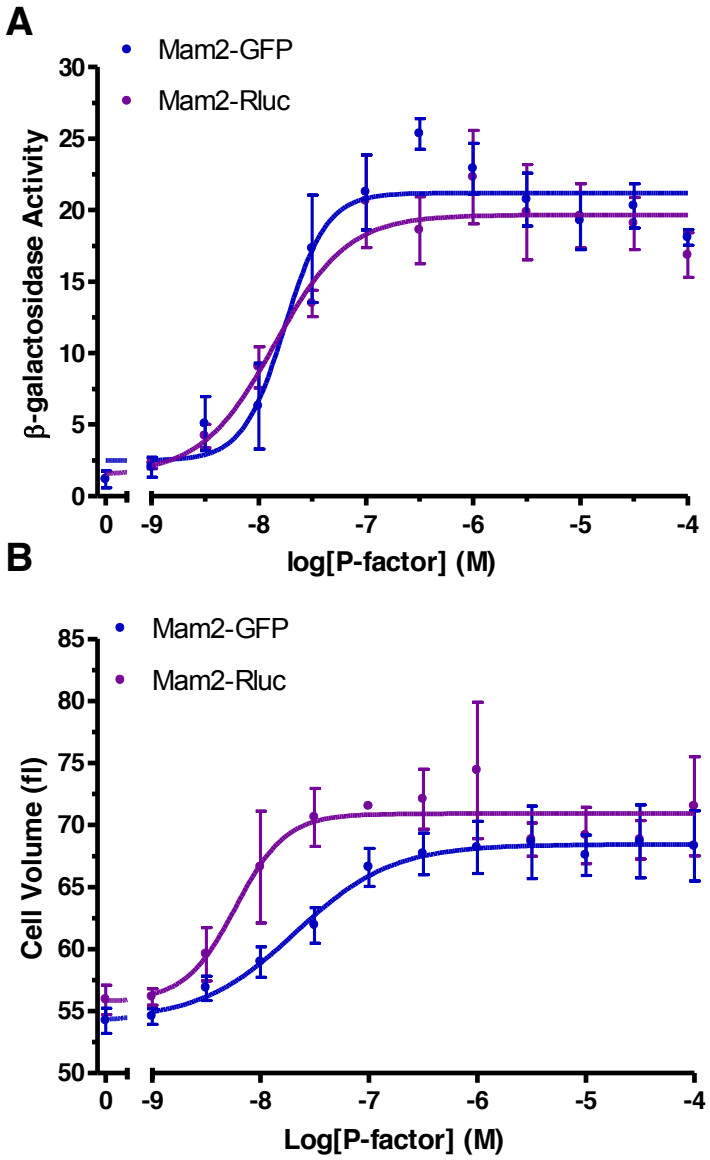

	pEC_{50}		Maximum	
	Transcription	Shmoo	Transcription	Shmoo
Mam2-GFP	7.76±0.10	7.66±0.21	21.19±0.83	26.45±1.74
Mam2-Rluc	7.85±0.15	7.99±0.49	19.65±0.85	25.62±1.58

Figure 4-21: Effect of Rluc and GFP tags on the activity of Mam2

JY1169 (*sxa2>lacZ, mam2*⁻) was transformed with pREP3x-Mam2-GFP and pREP3x-Mam2-Rluc and cells were cultured in AA media to a density of ~$5x10^6$ cells/mL and incubated with concentrations of P-factor ranging from 0 to 10^{-5} M. Results shown are means of triplicate independent determinations ±SE. **A:** The β-galactosidase activity ($OD_{420}/10^6$ cells) of transformants to measure the transcriptional response. **B:** Median cell volumes of transformants to quantify the morphological response. **C:** Change in cell volume calculated as the increase above the median cell volume of unstimulated cells. **D:** pEC_{50} and maximal signalling values calculated from the dose-response curves in A and C.

4.5.2 Receptor-Rluc Fusions Luminesce in Live cells

To determine whether a luminescence signal could be detected from receptor-Rluc fusions *Sz. pombe* JY1169 (*sxa2>lacZ, mam2*⁻) was transformed with pREP3x-STE2-Rluc or pREP3x-Mam2-Rluc. Cultures were grown to $1x10^7$ cells per mL and diluted to $1x10^6$ cells per mL or concentrated to $1x10^8$ cells per mL with the addition of 60 µM of the Rluc substrate EnduRen. Samples were incubated on a rotating wheel for 2 h before assaying in a Berthold Mithras LB940 BRET multimode microplate reader. The luminescence output from the cells transformed with the receptor-Rluc fusions was measured and results are shown in Figure 4-22. The luminescence intensity shows a linear increase with population size and is detectable for all population sizes. Further characterization of expressing Rluc in *Sz. pombe* is discussed in Chapter 7.

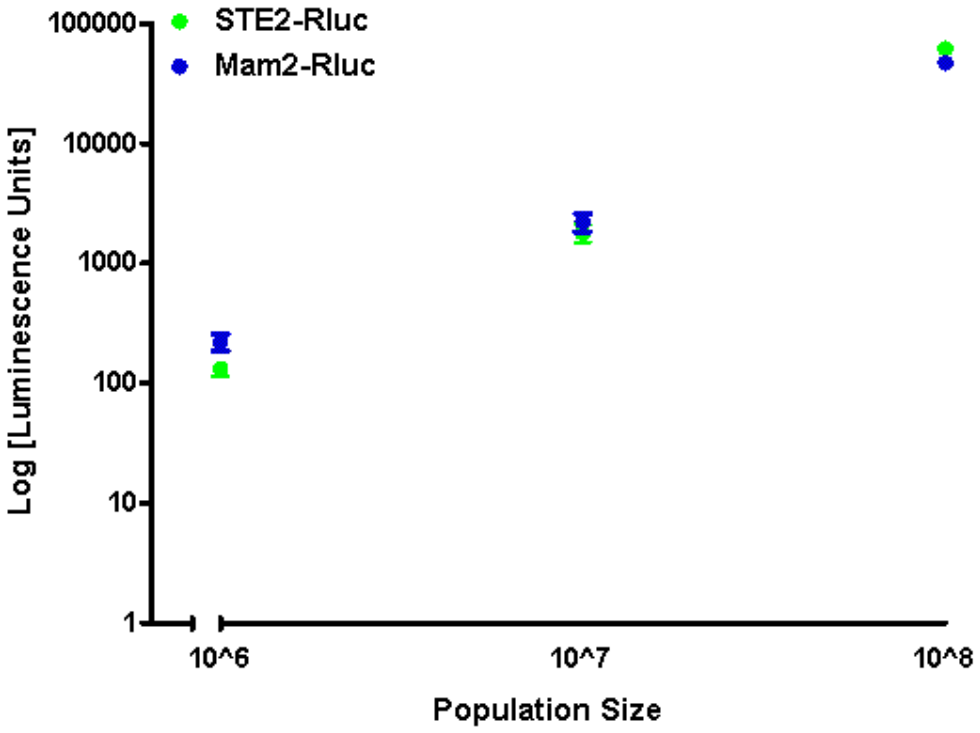

Figure 4-22: Luminescence intensity of cells expressing STE2-Rluc and Mam2-Rluc

JY1169 (*sxa2>lacZ, mam2*⁻) was transformed with pREP3x-STE2-Rluc or pREP3x-Mam2-Rluc. Cultures were grown to 10^7 cells and diluted to concentrations of $1x10^6$, $1x10^7$ or $1x10^8$ cells per sample. 60 µM EnduRen was added to samples followed by 2 h incubation on a rotating wheel. Cells were then assayed for luminescence in a Berthold Mithras LB940 BRET multimode microplate reader (Berthold Technologies, UK). Values shown are the means ±SEM of triplicate repeats and have been corrected for background signal.

4.5.3 Energetic Coupling between Receptor-Rluc and Receptor-GFP Fusions cannot be Detected

As outlined in the background, both STE2 and Mam2 have previously been shown to form receptor oligomers (Ladds, Davis et al. 2005), and in STE2 mutations to the GxxxG motif in transmembrane domain 1 reduce oligomerization. Experiments performed in this chapter demonstrated that mutations to the smallxxxsmall motif in the first transmembrane domain of Mam2 resulted in a reduction in the pheromone response, possibly caused by receptor mislocalization, similar to what was observed for the STE2 mutants. BRET technology was therefore utilized to investigate whether this is an effect of hindering receptor oligomerization.

An Rluc-GFP fusion expressed from the pREP3x vector acted as a positive control and the STE2, Mam2, Mam2^{G49A}, Mam2^{G49S,S53A} and Mam2^{G49L,S53L} receptors labelled with GFP and Rluc were chosen for initial analysis. STE2 acted as an additional positive control as BRET assays using this receptor has previously been performed successfully in *Sc. cerevisiae*. The mutants were chosen for their signalling and localization phenotypes. Mam2^{G49A} signalled comparable to wild-type receptor, but was found at higher concentrations at the plasma membrane. Mam2^{G49S,S53A} displayed reduced signalling activity but was not mislocalized and Mam2^{G49L,S53L} did not signal because it did not localize to the plasma membrane. The mutant receptors were fused to Rluc in the pREP3x vector. The receptors were also fused to GFP in the pREP4x vector. The pREP4x vector contains the selectable *ura4* marker from *Sz. pombe* and will be maintained in the JY1169 strain as this strain has a nutritional requirement for the gene product when grown in the absence of uracil. Rluc and GFP expressed without fused receptors were included as a negative control. The BRET donor and acceptor pairs that were used listed in Table 4-1.

BRET Donor	**BRET Acceptor**
pREP3x-Rluc-GFP	pREP3x-Rluc-GFP
pREP3-Rluc	pREP4x- GFP
pREP3x-STE2-Rluc	pREP4x-STE2-GFP
pREP3x-Mam2-Rluc	pREP4x-Mam2-GFP
pREP3x-Mam2^{G49A}-Rluc	pREP4x-Mam2^{G49A}-GFP
pREP3x-Mam2^{G49S,S53A}-Rluc	pREP4x-Mam2^{G49S,S53A}-GFP
pREP3x-Mam2^{G49L,S53L}-Rluc	pREP4x-Mam2^{G49L,S53L}-GFP

Table 4-1: BRET donor and acceptor pairs

Showing the BRET donor and acceptor pairs co-expressed in JY1169 (*sxa2>lacZ, mam2*¯). The left column lists the donors expressed from the pREP3x vector. The right column lists the acceptors

which were expressed from the pREP4x vector, with the exception of the pREP3x-Rluc-GFP fusion which acted as a positive control.

The BRET donor and acceptor pairs were co-expressed in JY1169 (*sxa2>lacZ*, *mam2*$^{-}$). $1x10^6$, $1x10^7$ or $1x10^8$ cells were used per sample and incubated for 2 h together with 60 µM of the Rluc substrate EnduRen prior to assaying in a micro-plate reader (see Chapter 7 for a discussion of optimization of Rluc detection). No energy transfer could be detected between any of the constructs (data not shown). This could be due to a number of reasons. The donor and acceptor may be too far apart for coupling. This seems unlikely however because resonance energy transfer has previously been reported for STE2 BRET donor and acceptor fusions (Gehret, Bajaj et al. 2006). In case the signal is too low to be detected using 10^8 cells the using more cells could lead to the detection of signal. It would be challenging however to increase the amount of cells in the sample. Lastly, GFP from *Aequorea victoria* was used, and this version may not excite at the wavelength emitted from Rluc whereby using other versions of the fluorescent protein might lead to coupling, alternative versions of Rluc also exist.

4.6 Summary

The *Sc. cerevisiae* and *Sz. pombe* pheromone receptors STE2 and Mam2 were expressed in *Sz. pombe* and assessed for their ability to activate the pheromone-response. Signalling activity of Mam2 from the pREP3x plasmid was not significantly different from signalling activity of endogenously expressed Mam2. Likewise, adding a GFP tag to either Mam2 or STE2 did not hinder signalling activity. The sensitivity of the pheromone dose-response of cells transformed with STE2 was similar to cells transformed with Mam2, but maximal signalling was reduced. This could possibly be attributable to an inability of STE2 to correctly couple to the *Sz. pombe* cellular machinery, for instance the inability to bind Rgs1. A novel method of quantifying cellular protein localization was employed, which indicated that STE2 might not be processed as efficiently as Mam2 in the *Sz. pombe* protein degradation pathways. This may again be due to an inability of STE2 to efficiently couple to *Sz. pombe* processes.

Mutations mapping to a motif of two small residues in the first transmembrane domain of the receptors influenced both the sensitivity and maximal response to pheromone in cells. In some cases, such as the G60A mutation in STE2, pheromone signalling was unaffected despite reduced expression at the plasma membrane. For STE2 mutants where pheromone signalling was affected however, this seemed to correlate with reduced plasma membrane expression. In Mam2, mutations to another small residue at residues S53 and A57 seemed to have a greater effect than when mutating residue G49, suggesting that these residues are pivotal to the correct functioning of the receptor.

The response in the morphological pathway often, but not always, correlated with the response in the transcriptional pathway. For instance the $Mam2^{G49A}$ mutant displayed a transcriptional pheromone-response comparable to wild-type Mam2 but the morphological response was halved. In most cases a reduction in signalling activity correlated with reduced expression of the receptor at the plasma membrane. This was not always the case however, for instance the $Mam2^{A57G}$ mutant was expressed at the cell cortex in higher amounts than wild-type Mam2, but had reduced signalling activity. When mutating the residues to the structurally much larger residue leucine signalling activity was decreased for all constructs. For the STE2 leucine mutants the pheromone-response was completely abolished. For the Mam2 leucine mutants there was a two-fold reduction in the pheromone-response for each single leucine mutant, and an absence of response in the double-mutant.

C-terminal fusions of Rluc to receptor were made and these successfully activated the pheromone-response in *Sz. pombe*. Luminescence intensity was shown to increase linearly

with increasing population size. Bioluminescence resonance energy transfer assays of cells co-transformed with receptor-Rluc and receptor-GFP fusions, or an Rluc-GFP construct failed to detect an energy transfer between Rluc and GFP however, suggesting that the two isoforms are not compatible donor and acceptor pairs.

5 CHARACTERIZING THE SELF-ASSOCIATION OF INDIVIDUAL TRANSMEMBRANE DOMAINS IN STE2 AND MAM2

5.1.1 Background

It might be possible to study the oligomerization of polytopic proteins through the study of their individual TM domains, utilizing the notion that separate TM domains first form individual stable units before inter-molecular contacts are formed. The aim of this chapter was to explore this possibility. To do this the TOXCAT assay was used which measure the self-association of TM domains in an *in vivo* environment. In addition to the TOXCAT assay, molecular modelling using the software suite CHI was also performed to predict specific TM-TM interactions. Sections 5.1.2 and 5.1.3 demonstrate the assays employed on the well-characterized dimerizing protein GpA and its dimerization impaired mutant G83I as proof of concept of the methods, before characterizing the oligomerization of the STE2 and Mam2 TM domains.

5.1.2 The TOXCAT Assay and Controls

The TOXCAT assay (detailed in section 2.2.9) was used to measure the propensity of individual TM domains to oligomerize. This assay measures the strength of TM-TM interactions by means of the reporter protein CAT. The TM domain of GpA, which is known to strongly dimerize, and its dimerization-impaired mutant (G83I), were used as positive and negative controls respectively, and their sequences are shown in Figure 5-1A. A Western blot was performed in order to quantify the expression level of each construct (Figure 5-1B), because the expression level of the chimera is linearly related to reporter activity. Through adjusting the TOXCAT signal to the expression level the relative strength of oligomerization of the TM domains under investigation can be normalized to GpA.

The TM domains of the two controls were expressed as MBP-TM-ToxR fusion chimera and the red arrow in the Western blot shown in Figure 5-1 points to the full-length ~66 kDa chimera. The chimera may get proteolytically cleaved however, as indicated by the presence of a second lower molecular weight band, marked with a red star at ~43 kDa and corresponds to the mass of MBP.

MBP-TM-ToxR chimeras were expressed in the *E. coli* NT326 strain, which is a *malE* deficient mutant. The *malE* gene encodes endogenous maltose binding protein, which is

needed for transport of maltose to the cytoplasm. The correct insertion and orientation of chimera can therefore be checked by the *malE* complementation assay where cells are grown on media where maltose is the sole carbon source. Only cells containing the correctly inserted and oriented MBP-TM-ToxR chimera will grow and form colonies (Figure 5-1C, left) because the expression of *malE* in the chimera compensates for the lack of *MalE* in the genome. In some instances, chimera fail to grow on the maltose plates, and the spheroplast assay can be performed instead (Figure 5-1C right). In the spheroplast assay, cell cultures are separated into fractions containing periplasm (PF), spheroplasts (SF) and spheroplasts treated with proteinase K (SPF). Since MBP is bound to the membrane it should not be detectable in the PF but appear in the membrane-containing SF (highlighted with a blue arrow). In the SPF this band disappears because MBP is liberated from the TM-ToxR domains, and is instead detectable as a lower molecular weight band, marked with a blue star. This lower molecular weight band correlates with the proteolytically cleaved chimera. If the 66 kDa band is not present in the spheroplast fraction this indicates that the chimera is not inserted into the membrane.

In the TOXCAT assay (Figure 5-1D), levels of CAT activity are normalized to the expression level relative to GpA, meaning that strengths of interactions are all relative to the strength of the GpA dimer. CAT activity of the dimerization-impaired GpA G83I mutant is ~10% of GpA and other TM domains may display interactions stronger than GpA, weaker than G83I, or in between the two (Jenei, Borthwick et al. 2009; Lawrie, Sulistijo et al. 2010). The assay cannot discriminate between different oligomeric states however, meaning that CAT activity detected could be due to dimer formation, or formation of higher order oligomers.

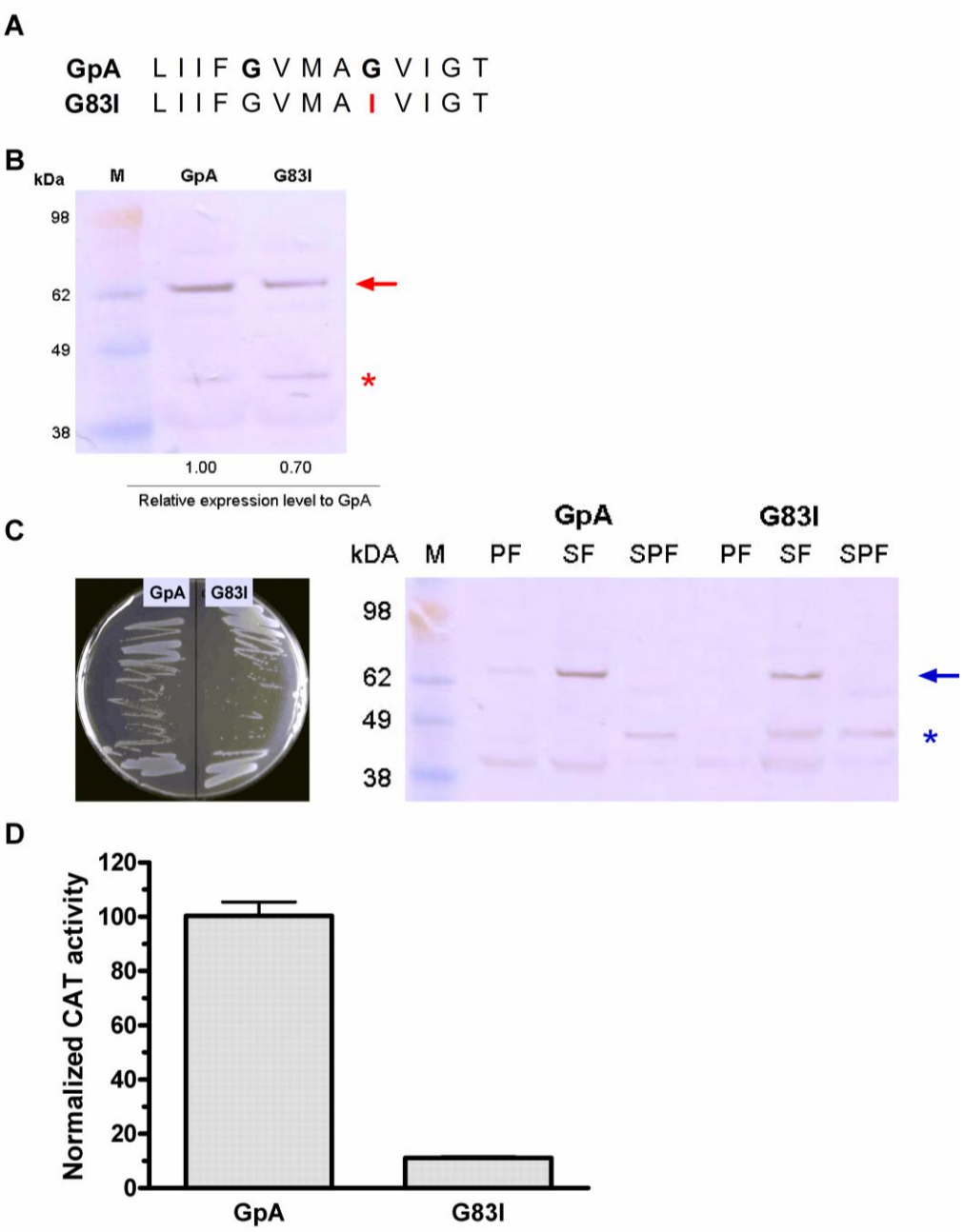

Figure 5-1: Expression, insertion and orientation checks for the TOXCAT controls

All assays were performed in the *E. coli* NT326 strain (*malE*$^-$) **A:** Showing the transmembrane domain sequence of the positive control GpA and its dimerization deficient G83I mutant, which acted as the negative control. The bold residues highlight the GxxxG motif, and the red residue marks the mutation rendering the TM domain dimerization deficient. These were inserted into the pccKan vector in order to express MBP-TM-ToxR chimera. **B:** Expression check of the positive and negative control shown on the left. The arrow indicates the full MBP-TM-ToxR chimera. The star indicates MBP proteolytically separated from the TM-ToxR chimera. **C:** *MalE* complementation assay of the positive and negative control (left) and spheroplast assay of the positive and negative control to further test its insertion and orientation in the membrane (right). **E:** CAT activity of the positive and negative control determined by the TOXCAT assay to measure the degree of homo-oligomerization. Results shown are means of triplicate determinations of three independent isolates ±S.E.M.

5.1.2.1 Molecular Modelling of GpA Dimerization

Molecular models of the dimerization of GpA were built using the CHI (CNS (Crystallography and NMR Searching) of Helix Interactions) suite described in detail in Section 2.2.13.2. Briefly, CHI builds two α-helices from the primary sequence of the TM domain of interest. The helices are then iteratively rotated about their long axis relative to each other. Each rotation is followed by simulated annealing and energy minimization in which the rotational angle phi and crossing angle omega is free to vary. Four trials are carried out in each search, each using varying starting velocities in the simulated annealing process meaning that each CHI run generate different structures. The backbone root-mean-square deviation (RMSD) is then calculated and compared between structures, and structures where the backbone RMSD differs by 1.0 Å or less are placed into a cluster. A minimum of 10 structures of similar geometry were set as a cut-off point to form a cluster, and within each cluster the structure was averaged. For each structure modelled, five rounds of CHI searches were run and compared. Results were plotted on an (x,y) coordinate graph with the frequency domain on the z-axis. The x and y axes correspond to the phi angles, i.e. the relative rotation of helix1 (phi1) to helix2 (phi2) in each cluster. Dimers containing symmetrical interaction interfaces are located on a diagonal line running between (0,0) and (360,360).

Figure 5-2A shows the clusters of structures generated via the CHI searches of GpA. Only right-handed helices are shown for all models because GpA is known to form right-handed dimers (MacKenzie, Prestegard et al. 1997), however the program does find both left and right handed solutions. The phi angles plotted on the x and y-axes represent the rotation of the helices relative to each other, and consequently clusters of structures coinciding with the red line drawn between vertices (0,360) are symmetrical structures. When modelling homo-dimers, symmetrical structures are often assumed, however the formation of higher order oligomers may involve interactions that are not symmetrical. The z-axis represents the number of clusters found in each search for each relative rotation, and clusters found in individual repeats are represented by separate colours (red, green, black, purple and blue). The data shows that in three of the repeats, a symmetrical structure is found coinciding with a rotation of the helices from the starting structure of ~70° (encircled in black). This structure has an average crossing angle (Ω) of ~45° and slight shift along the long helical axes relative to each other, which would be assumed in a symmetrical dimer. In this model the centre of the helices are separated by a minimum of ~6.3 Å. The structure of the symmetrical GpA dimer found in the CHI searches is shown in Figure 5-2A. The close association of the glycine residues (shown in blue) allows close packing of the helices of the

dimer, and optimal packing of the β-branched 'ridge' residues (represented by spheres). The GxxxG motif is often found adjacent to the large aliphatic residues isoleucine, valine, and to a lesser extent leucine (Russ and Engelman 2000; Senes, Gerstein et al. 2000). Isoleucine and valine are both β-branched residues, meaning that they have two carbons attached to their β-carbon as opposed to one, which is the case in most other amino acids. As a consequence there is a lot of bulkiness near the protein backbone in the α-helical conformation restricting the possible conformations of the protein. It is believed that the restricted side-chain motion of these residues minimize the loss of entropy upon dimerization via GxxxG motifs (Liu, Crocker et al. 2003). The NMR structure of glycophorin A reveal that the groove formed by the GxxxG motif, and the ridge of the neighbouring valine residues (GVxxGV) form a large ridges-into-grooves contact surface for dimer formation (MacKenzie, Prestegard et al. 1997).

When mutating G83 to isoleucine, the symmetrical structure involving close packing of the GxxxG motif, found at phi angle 70°, disappear as indicated by the blue arrow in Figure 5-2B. Instead a new symmetrical structure appears which is formed by packing of I77, M81 and I85 at the interface. This helix however contained a large shift, 3.7 Å, along the long helical axes of the helices relative to each other and the distance between helices increased to 8.8 Å. This is much further than the 6.3 Å observed in the wild-type dimer.

This indicates that CHI can, with interpretation and in conjunction with experimental data, be used to predict the formation of TM helix dimer formation. Since data from different searches cannot easily be assembled and because CHI exports data in a format compatible with the UNIX platform, a script was written to extract data from multiple CHI searches and to make the data windows compatible.

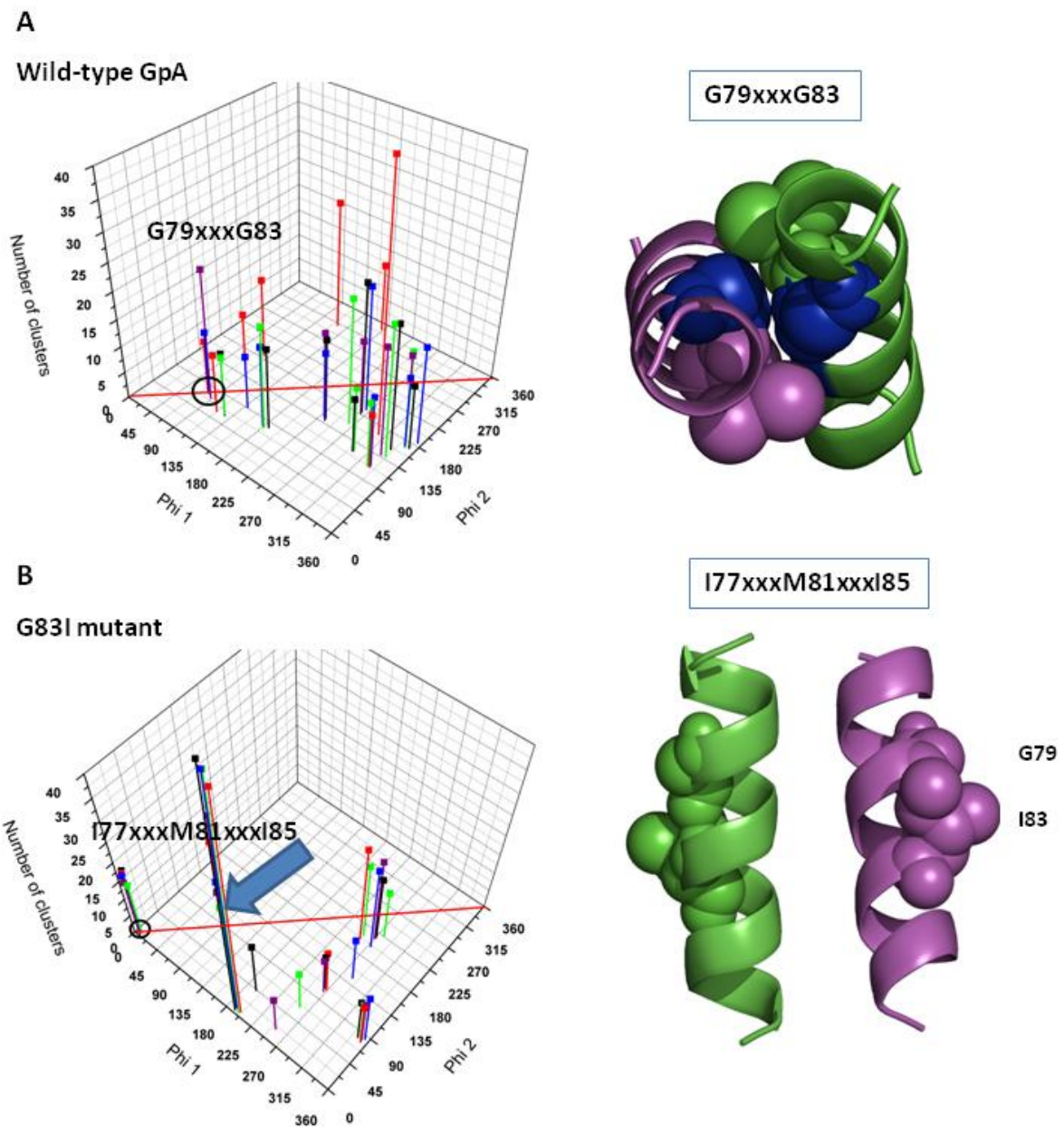

Figure 5-2: Structure of the GpA dimer

The phi plots on the left show the distribution of clusters from global searches as a function of their orientation, represented by the angle phi. Four MD repeats using random starting velocities were performed in each run and five separate searches were performed. When >10 separate structures with Cα RMSD values within <1 Å were found, their structure was averaged to generate a "cluster". Different colors of clusters indicate solutions found in separate repeats and symmetrical structures found in several repeats are encircled in black. Structural models of such clusters are shown on the right. **A:** The clusters of structural solutions found for the GpA dimer **B:** The clusters of structural solutions found for the dimerization deficient G83I mutant. The arrow indicates the absence of the cluster comprising of dimers associating via the GxxxG motif.

5.2 Homo-Oligomerization of the STE2 Transmembrane Domains

5.2.1 Oligomerization of Transmembrane Domains 1-7 from STE2

An initial screen of all seven transmembrane domains in STE2 was performed to test the propensity of each domain to self-associate in the TOXCAT assay. Seven different MBP-TM-ToxR chimeras were cloned into the pccKan vector containing sequences corresponding to the predicted TM domains 1-7 in STE2. The intracellular TM boundaries have been characterized (Choi and Konopka 2006) and the extracellular boundaries were predicted using the TM prediction software TMHMM (Krogh, Larsson et al. 2001). The sequences of each transmembrane insert are shown in Figure 5-3A. An expression check was performed because concentration differences affect the relative CAT activities found in the TOXCAT assay, and thus the strength of oligomerization. Figure 5-3B shows the western blot of whole cells to check the expression of each transmembrane insert. Two bands are present in the blot; a heavier band at ~66 kDa corresponding to the full MBP-TM-ToxR chimeras (red arrow) and a higher mobility band at ~43 kDa (red star). The presence of the lower molecular weight band, as previously discussed, has been reported in literature and corresponds to proteolytically cleaved MBP (Russ and Engelman 1999). The expression level of each transmembrane insert relative to GpA was calculated using ImageJ (Abramoff, Magalhaes et al. 2004) to allow normalization of oligomerization data, shown underneath the blot.

The *malE* complementation assay (Figure 5-3C) showed that all transmembrane domains with the exception of TM3 grow on maltose, indicating correct insertion and orientation of these chimeras. The spheroplast assay was performed on TM3 (Figure 5-3C) to further analyse its insertion into the membrane. The PF did not contain MBP as expected. The SF in contrast contained a band corresponding to the MBP-TM-ToxR chimera (blue arrow). When treated with proteinase K this band disappeared as shown in the SPF and only the band corresponding to proteolytically cleaved MBP remained (blue star). These checks confirm that all the individual TM domains from STE2 are expressed at comparable levels to GpA and insert into the membrane with the correct topology.

The propensity of TM domains 1-7 from STE2 to self-associate was measured using the quantitative CAT assay, described in detail in section 2.2.9, and results were normalized to expression levels relative to GpA. Surprisingly, despite BRET and FRET data indicating that STE2 homo-oligomerizes via a GxxxG motif in its first TM domain (Overton, Chinault et al. 2003; Gehret, Bajaj et al. 2006) and the implications of this motif for cell localization and function of STE2, presented in chapter 4, TM1 did not self-associate in the TOXCAT assay

(Figure 5-3D). Similarly, the TM3 insert did not oligomerize and resulted in the lowest CAT activity; yielding only 1% of the GpA CAT activity.

Interestingly, TM2 self-associated with measured reporter CAT activity close to the positive control; ~87% of GpA. Previously published FRET experiments using receptor fragments have shown that TM1 alone cannot self-associate, however TM1-TM2 receptor fragments self-associate with near wild-type affinity (Overton and Blumer 2002). The FRET experiments did not investigate oligomerization of TM2 alone however, and the high TOXCAT signal observed for TM2 is therefore of interest.

TM5 also exhibited high reporter activity with a mean CAT activity of 81% of GpA. In the FRET experiments on receptor fragments this domain also self-associated when expressed with TM6 and TM7, however these interactions were believed to be due to aggregation because fragments did not interact with wild-type receptor (Overton and Blumer 2002).

Expressing the TM4 and TM7 inserts resulted in only 14% and 12% CAT activity respectively, compared to GpA. This was unexpected, as TM4 has been implicated in a second oligomerization interface. This interface is believed to be separate from the TM1 motif and serve to allow the formation of higher order oligomers (Wang and Konopka 2009). TM7 has also been implied in the oligomerization of STE2 in the absence of ligand, together with TM1 (Kim, Lee et al. 2009). Expressing TM6 inserts in contrast resulted in slightly higher CAT activity; 45% of GpA.

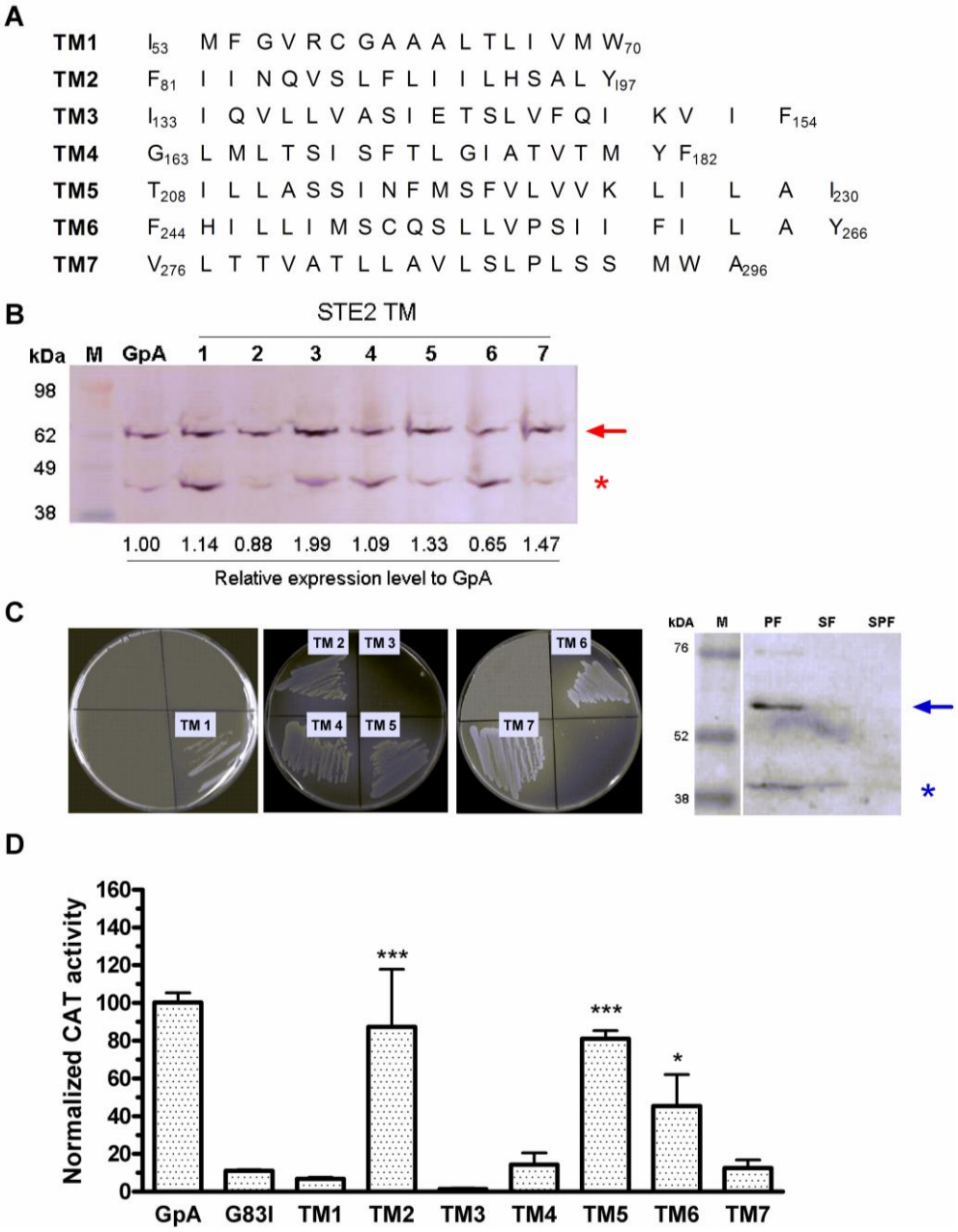

Figure 5-3: Expression, insertion, orientation and oligomerization of the STE2 TM domains 1-7 TOXCAT Chimeras

All assays were performed in the *E. coli* NT326 strain (*malE*) **A:** Showing the sequence of the seven different transmembrane inserts corresponding to STE2 transmembrane domain 1-7. These were inserted into the pccKan vector in order to express MBP-TM-ToxR chimera. **B:** Expression check of the constructs used in this study. The arrow indicates the full MBP-TM-ToxR chimera. The star indicates MBP proteolytically separated from the TM-ToxR chimera. **C:** *MalE* complementation assay of the constructs used in this study (left). The construct incorporating TM3 did not grow on maltose and therefore the spheroplast assay was performed on this construct (right) **D:** CAT activity of the TM chimeras determined by the TOXCAT assay to measure the degree of homo-oligomerization. The asterisks denote ranges of mean CAT activity normalized to GpA where *=26-50%, **=51%-75%, ***=76%-100%, ****=101%-125% and *****=>126%. Results shown are means of triplicate determinations of three independent isolates ±S.E.M.

5.2.2 Further Characterization of the Homo-oligomerization of Transmembrane Domain 1 from STE2

5.2.2.1 Length Optimization of Transmembrane Domain 1 in STE2

Due to previous reports suggesting that the *Sc. cerevisiae* GPCR STE2 oligomerizes via a GxxxG motif in its first TM domain (Overton, Chinault et al. 2003; Gehret, Bajaj et al. 2006) it was surprising that the domain did not self-associate in the TOXCAT assay. Studies have shown that the strength of reporter activity in the TOXCAT assay is dependent on the positioning of the ToxR domains relative to each other, which is influenced by the length of the TM insert (Langosch, Brosig et al. 1996; Li, Gorelik et al. 2004; Jenei, Borthwick et al. 2009). It has also been shown that the positioning of the GxxxG motif in the membrane influences the signal (Johnson, Rath et al. 2006). Since reporter activity is influenced by the insert, and because of the number of studies suggesting that STE2 self-associates via TM1-TM1 interactions, different lengths and frames of the predicted TM1 domain were inserted into the TOXCAT chimera to see if CAT activity could be improved.

Figure 5-4A shows the seven different sequences of TM1 inserted into the TOXCAT MBP-TM-ToxR chimera. Both the length and the frame of the TM domain was considerably varied in order to determine whether the absence of CAT activity was an artefact due to the length and frame of the construct assayed initially. The expression check (Figure 5-4B) shows that the 19 and 20 amino acid long TM domains were not expressed at very high levels - only 8-9% of the level of GpA expression respectively, meaning that their TOXCAT signals would need to be increased ~12.5 fold during the normalization procedure. The other constructs were expressed at levels comparable to GpA. All constructs, with the exception of the 16 amino acid-long insert, grew on maltose and it was therefore concluded that these chimeras were correctly inserted and orientated across the inner membrane (Figure 5-4C, left). The 16 amino acid-long construct was further investigated using the spheroplast assay, and it was found that the construct was correctly inserted and oriented across the membrane as indicated by the 66 kDa band present in the spheroplast fraction (Figure 5-4C, right).

All constructs had very low TOXCAT signals prior to normalization to GpA. After normalization however, the signal from the 19 amino acid long construct increased dramatically. A noticeable increase was also seen in the 20 amino acid long construct and the signal from the 25 amino acid long construct was also somewhat increased. All these constructs, however, had a much lower relative expression when compared to GpA meaning that the TOXCAT signal from the 19 amino acid long construct was increased ~12.5 fold, that of the 20 amino acid long construct increased ~11-fold, and the signal from the 25

amino acid long construct more than doubled. Due to the heavy cleavage of these constructs however, the results cannot be reliably interpreted and are likely to be artefacts of the normalization procedure. These results therefore indicate that STE2 TM1 when expressed in isolation, does not self-associate.

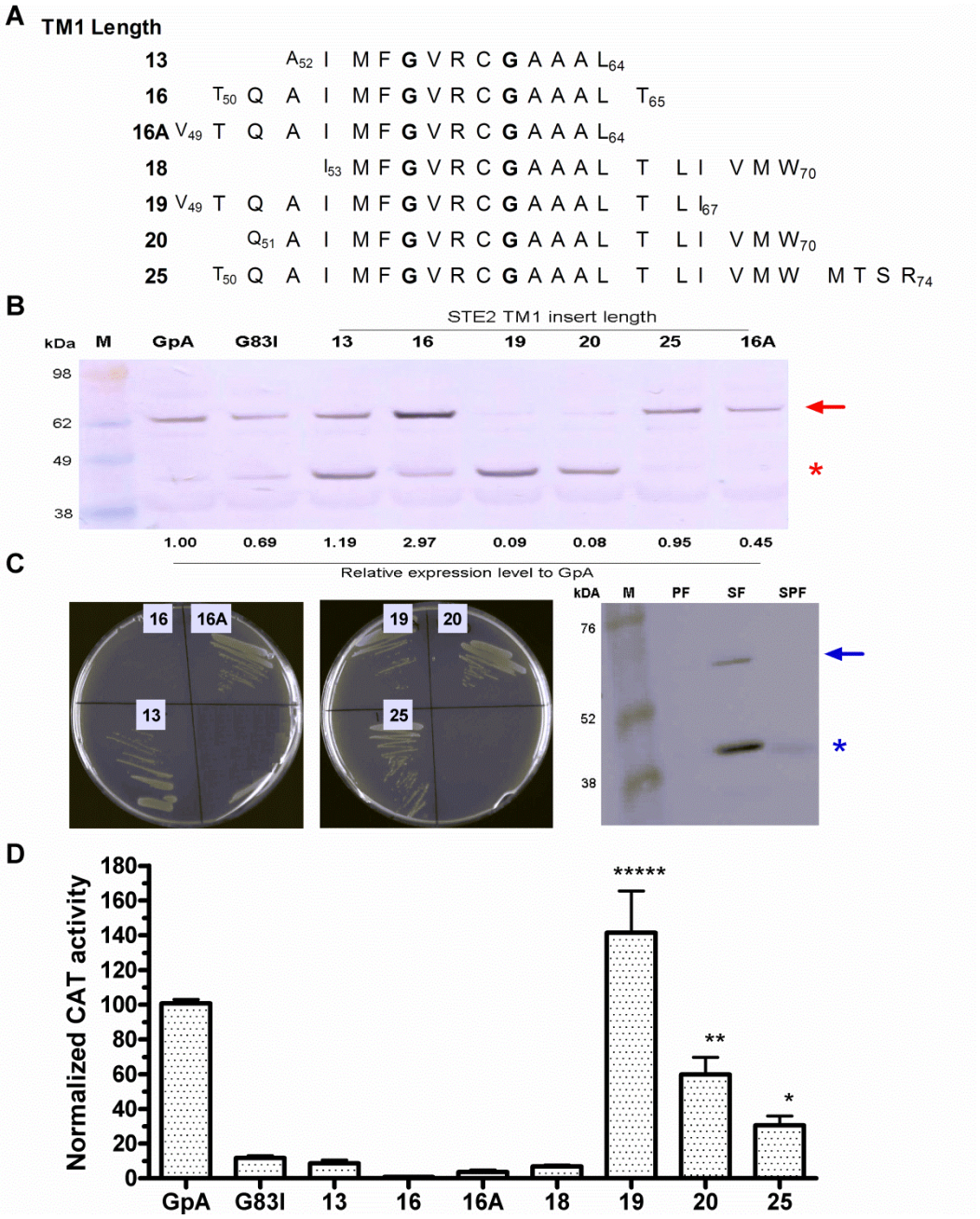

Figure 5-4: Length optimization of transmembrane domain 1 from STE2

All assays were performed in the *E. coli* NT326 strain (*malE*$^-$) **A:** Showing the sequence of the different lengths and frames of TM domain 1 from STE2 inserted into the pccKan vector to test if the TOXCAT signal could be improved. **B:** Expression check of the constructs used in this study. The arrow indicates the full MBP-TM-ToxR chimera. The star indicates MBP proteolytically separated from the TM-ToxR chimera. **C:** *MalE* complementation assay of the constructs used in this study (left). The construct incorporating the 16 amino acid long construct did not grow on maltose and therefore the spheroplast assay was performed on this construct (right) **D:** CAT activity of the TM chimeras determined by the TOXCAT assay to measure the degree of homo-oligomerization. The asterisks denote ranges of mean CAT activity normalized to GpA where *=26-50%, **=51%-75%, ***=76%-100%, ****=101%-125% and *****=>126%. Results shown are means of triplicate determinations of three independent isolates ±S.E.M.

5.2.2.2 Molecular Modelling of STE2 Transmembrane Domain 1 Dimerization

Although TM1 from STE2 did not appear to oligomerize in the TOXCAT assay, because of the effects of mutating this motif to leucine in the full-length protein (discussed in Chapter 4), the structure of a dimer was modelled. CHI modelling of the 19 amino acid long TM1 construct revealed two symmetrical right-handed structures that were present in three independent repeats respectively (Figure 5-5A) and one symmetrical left-handed dimer (Figure 5-5B) none of which involved close-packing via the GxxxG motif. In the right-handed dimer found at a relative phi angle of 100°, the centre of the helices were packed relatively close with a minimum distance of 6.9 Å between the helical axes. The close packing of the helices was achieved via interactions between opposite A52 and G56 residues (blue spheres), thereby unexpectedly implying a different smallxxxsmall motif from the previously reported G56xxxG60 motif (Overton, Chinault et al. 2003). The left-handed solution shown in Figure 5-5B was very similar structurally, and residues G60 were not involved in dimer formation as illustrated in the structure. In these two models, C59 (shown as spheres coloured by elements in Figure 5-5A) achieved close packing in the dimer interface through packing against the G60 residues of the opposite helix. This seems improbable in the full-length protein because C59 is involved in ligand binding and faces the TM bundle (Tantry, Ding et al. 2010). R58, in contrast, which is also involved in ligand binding, was pointing away from the dimer interface, as would be expected. Taken together, this structural model is not supported by experimental evidence, as both glycines 56 and 60 are implicated in oligomerization, and because of the positioning of the cysteine residue.

A second right-handed symmetrical dimer was found at a relative rotational angle of 227° (Figure 5-5A, left panel). In this model, the distance between the helical axes was much larger than found in the first model (8.9 Å) and the helices appeared to pack via the C59 and R58 residues introducing a bend in the TM domain. Bends do occur in TM helices, and have been observed in GPCRs, however not in the case of STE2 TM1 and this model therefore appears unlikely (Yeagle, Bennett et al. 2007).

In conclusion, the TOXCAT data and the structural modelling do not predict that STE2 TM1 oligomerizes via the GxxxG motif. These data therefore support the finding in the FRET studies on TM receptor fragments that STE2 TM1 cannot oligomerize on its own (Overton and Blumer 2002).

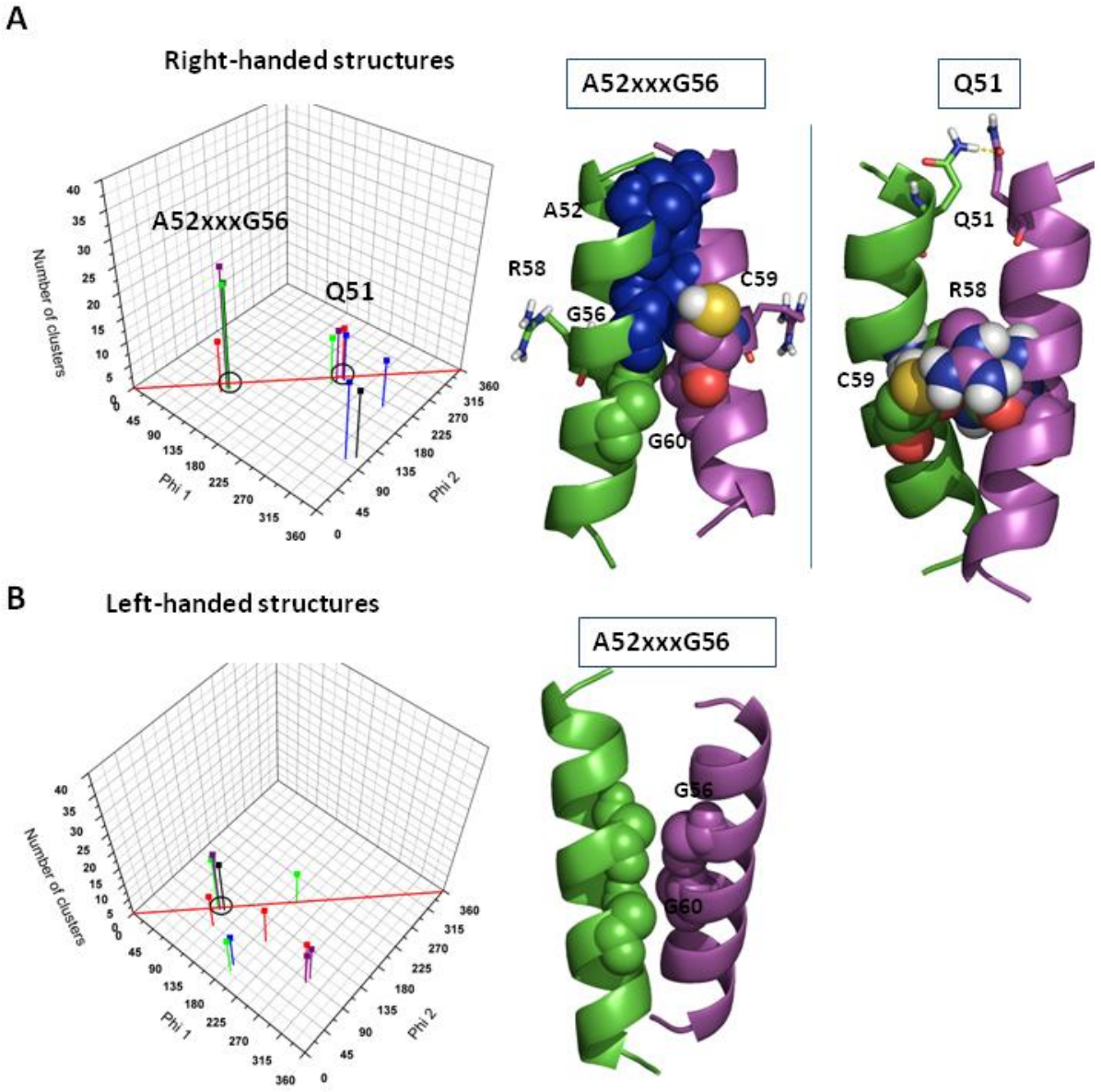

Figure 5-5: Molecular modeling of STE2 TM domain 1 dimers

The phi plot on the left show the distribution of clusters from global searches of the STE2 TM1 dimers as a function of helix orientation represented by the angle phi. Four MD repeats using random starting velocities were performed in each run and five separate searches were performed. When >10 separate structures with Cα RMSD values within <1 Å were found their structure was averaged to generate a "cluster". Different colors of clusters indicate solutions found in separate repeats and symmetrical structures found in several repeats are encircled in black. **A:** Right-handed solutions. **B:** Left-handed solutions.

5.2.3 Characterization of the Homo-oligomerization of Transmembrane Domain 2 from STE2

5.2.3.1 Transmembrane Domain 2 Contains Several Polar Residues

The TOXCAT data presented here as well as the published FRET study on receptor TM fragments (Overton and Blumer 2002) show that TM1 cannot self-associate on its own; and the FRET study suggested that TM2 is required in order to stabilize interactions. The initial TOXCAT study of the seven transmembrane domains in STE2 further implicated that TM2 self-associate strongly. Due to the functional effects of mutating the GxxxG motif in TM1 (as discussed in chapter 4) but its inability to form dimers in the TOXCAT assay and modelling, it might be possible that STE2 dimers interact via contacts formed between the TM2 domains to the other receptor, and close proximity of receptors may be achieved via close packing of TM1 domains.

TM2 contains several polar residues, including asparagine, glutamine, serine and histidine which, when plotted on a helical wheel diagram, appear to be distributed over approximately two-thirds of the helix (Figure 5-6A). Slightly polar amino acids such as serine, threonine and tyrosine have been shown to have a moderate effect on oligomerization of transmembrane domains (Gratkowski, Lear et al. 2001; Zhou, Merianos et al. 2001). More strongly polar amino acids however, have been shown to have a much greater effect on transmembrane domain oligomerization. These include, among others, asparagine and histidine (Choma, Gratkowski et al. 2000; Zhou, Cocco et al. 2000; Zhou, Merianos et al. 2001) which are present in the STE2 TM2 domain. The sequence context of the polar amino acids is, however, important. For example, the membrane protein BNIP3 dimerizes strongly via hydrogen bonding of histidine residues on separate helices, however BNIP3 also contains a GxxxG motif on the same face as the histidine residue. Mutations of the GxxxG motif disrupts dimerization by not allowing the two monomers to come into close enough proximity for histidine to hydrogen bond (Sulistijo, Jaszewski et al. 2003; Lawrie, Sulistijo et al. 2010).

The abundance of polar residues in the TM2 domain may suggest that the GxxxG motif in TM1 merely allow two TM2 domains to come into close proximity, thus allowing hydrogen bond formation between polar residues in two separate TM2 domains. This would probably involve an asymmetric interaction, either between the TM1 and TM4 domains or between the TM2 and TM7 domains. The TM7 domain has previously been implicated in oligomerization of STE2 (Kim, Lee et al. 2009) and this domain also contains a smallxxxsmall motif of two alanine residues. The TM4 domain has also been implicated in a second oligomerization motif although it is not know what interactions mediate oligomer formation. This motif does

contain a smallxxxsmall motif; TxxxA, which aligns to the same motif in rhodopsin in the homology models presented later in Chapter 6. This motif is however found packing against the TM3 domain meaning that it is unlikely to be involved in oligomer formation.

5.2.3.2 Structural Models of the Positioning of Polar Residues in Transmembrane Domain 2

Figure 5-6B shows a homology model of STE2 (discussed in detail in Chapter 6) and polar residues found in TM2 are highlighted. The asparagine residue N84 (shown in blue) is located on the lipid-facing side of TM2 and would be accessible for interactions with another receptor. The other polar residues present in TM2 appear less accessible, with H94 (shown in purple) facing the TM bundle and hydrogen bonding with Y98, which in turn also hydrogen bond to R58 in TM1. In this model both glycines from the GxxxG motif in TM1 are accessible on the lipid facing side of the protein (red spheres), which is likely if they mediate receptor-receptor interactions, together with N84 in TM2.

There is an NMR structure available in the protein databank of STE2 TM1-TM2 (PDB ID 2K9P), shown in Figure 5-6C (Neumoin, Cohen et al. 2009). In this model however, N84 projects in a direction where it would possibly pack against TM3 and/or TM4. The GxxxG motif is also inaccessible and packs together with A63 against the large hydrophobic residues in TM2; V86, L90 and L93. H94 is not H-bonding to Y98, but both residues are instead pointing into the lipid moiety in the direction that the TM3 and TM4 domains would be expected to reside.

The positioning and interactions of H94, Y98 and R58 are relevant because it is known that R58 interacts with the α-factor peptide through cation-π interactions (Tantry, Ding et al. 2010) and a Y98H mutation results in constitutive activity of the receptor (Parrish, Eilers et al. 2002). Moreover, these residues are highly conserved in the yeast receptors (Eilers, Hornak et al. 2005). A close-up view of the hydrogen bonding network in the homology model of STE2 is shown in Figure 5-6D. From this model, it seems possible that Y98 could interact with R58 to keep the receptor in its inactive state, an interaction stabilized by H94. Upon ligand binding, R58 might instead interact with the ligand, thus breaking the bond to Y98, which would relax TM1-TM2 interactions and may lead to other conformational changes in the protein. The Y98H mutant is likely to be unable to form this hydrogen bonding network, because if it is charged it may not be able to interact with the positively charged arginine residue and the histidine residue. This could explain the constitutive activity of the Y98H mutant.

The homology model thus predicts a very different structure from the NMR structure. In the former, N84 should be accessible for homo-dimer formation whereas in the latter H94 would be accessible for homo-dimer formation in the full-length protein. Both models however have their draw-backs. Membrane protein homology modelling is not at a stage where it is

considered highly accurate, due to a lack of protein structures on which to base predictions. This is further hindered by low sequence similarity between the yeast and class A GPCRs. Similarly; the NMR structure was determined using detergent micelles, which do not provide an environment in which protein structure prediction is considered highly accurate. Detergent micelles can destabilize helix-helix interactions, via competing interactions between amino acids and the polar head-groups of the detergent, thereby allowing increased side-chain flexibility in the amino acid chain or disrupting inter-helical bonds (Langosch, Brosig et al. 1996; MacKenzie 2006). To see if either structural model agrees with the TOXCAT data, the N84 and H94 residues were both mutated to alanine, to see if the mutations would disrupt oligomerization.

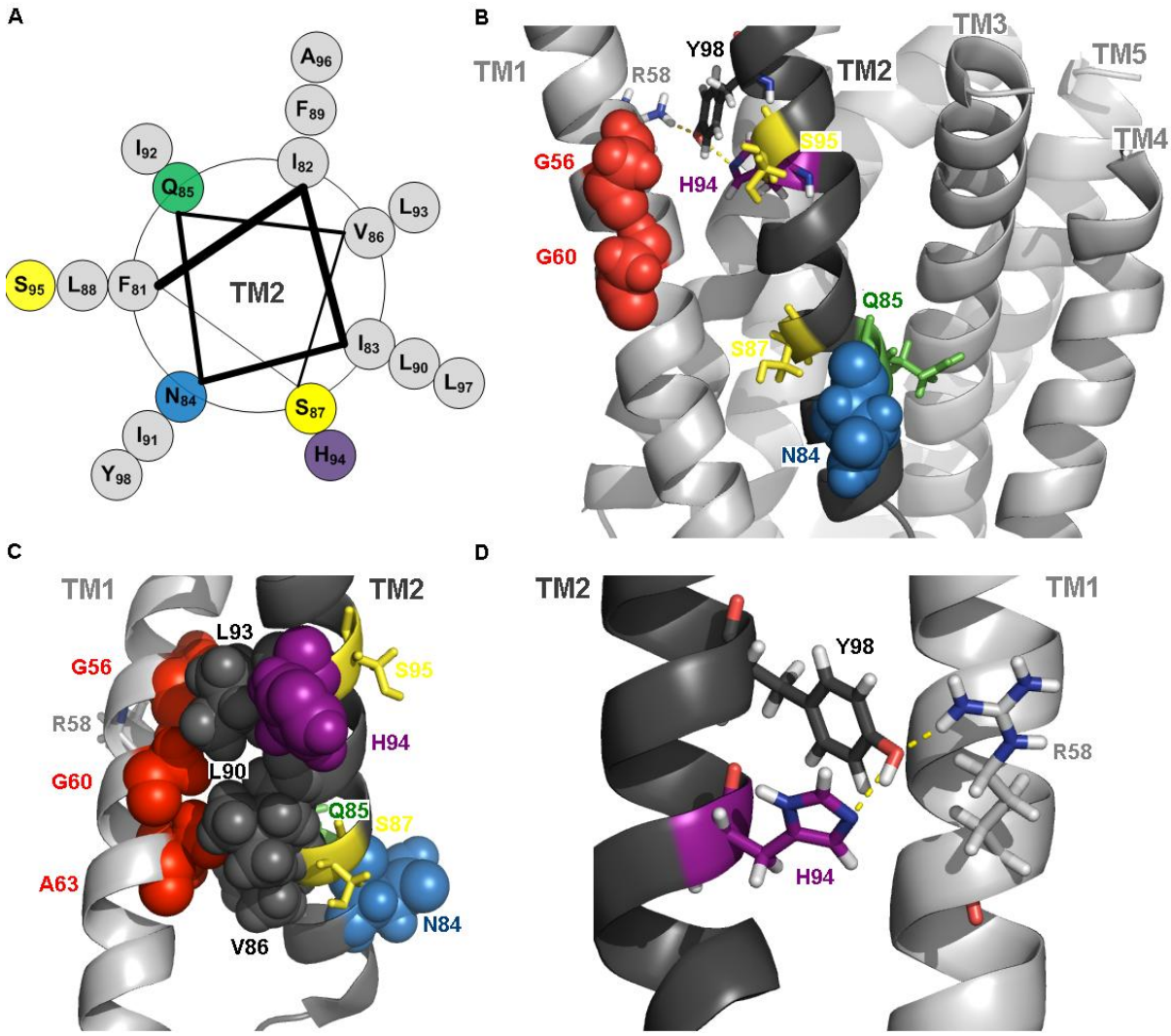

Figure 5-6: STE2 TM domain 2 in the context of the full-length protein

A: A helical wheel of STE2 TM domain 2. The colour coding corresponds to colours used in B-D. **B:** Homology model of the positioning of polar residues in STE2 TM domain 2. The GxxxG motif and R58 in TM domain 1 are also highlighted. A detailed description of the homology models can be found in Chapter 6. **C:** NMR structure of TM domain 1 and 2 resolved in micelles (Neumoin, Cohen et al. 2009), PDB ID 2K9P. **D:** Interactions between TM1 and TM2 as predicted by homology modelling.

5.2.3.3 Molecular Modelling of STE2 Transmembrane Domain 2 Dimerization

CHI modelling of the STE2 TM2 domain revealed two sets of symmetrical right-handed dimers shown in the left panel of Figure 5-7A and encircled in black, and two sets of left-handed dimers shown in the left panel of Figure 5-7B. Of the right handed dimers, one was found in four separate searches and all contained hydrogen bonds between the side-chain amide of N84 and hydroxyl group of S87 on opposite helices, as well as a hydrogen bond between the hydroxyl group of the S95 residues, as shown in the left-most structural model in Figure 5-7A. In the second symmetrical right-handed dimer, the side chain of H94 was found to hydrogen bond to a backbone carbonyl of the opposite helix, and there was also a hydrogen bond between the hydroxyl groups of opposite S87 residues (Figure 5-7A, right-most model). In this model, N84 is found pointing away from the interface. The left-handed models also implied residues N84, S87 or H94 in dimer formation. In the first dimer (middle panel, Figure 5-7B) the side chain amide of N84 H-bonds to the side-chain carbonyl of the opposite N84 residue, as well as to the protein backbone. There is also an H-bond between the hydroxyl group on the side-chain of S87 and the Q85 side-chain amide. The second symmetrical left-handed dimer contains an H-bond between the side-chain imidazoles of the H94 residues (Figure 5-7A, right-most panel).

Due to the biological importance of H94, suggesting that it is likely to face the TM bundle in the full-length protein, and the putative positioning of N84 on the opposite side of the helix, as well as their individual involvement in each of the two symmetrical dimers modelled, it was of interest to model dimer formation when these residues were mutated.

When changing N84 to alanine, three right-handed symmetrical dimers were found (Figure 5-8A). The dimer found at 43° was stabilized by a hydrogen bond between the imidazole ring of H94 and the hydroxyl group on S95, as shown in the middle panel. The structures found at 235° involved a polar contact between the two helices formed by Q85 hydrogen bonding to the main chain of the opposite helix via its side-chain amide (right-most structural model in Figure 5-8A). The third dimer involved interactions between the free N-termini of the peptides, which is an artefact due to the method of modelling free peptide termini and not physiologically relevant and therefore won't be discussed further. No H-bonds were found between the two left-handed dimers (Figure 5-7B) but interactions appeared to be stabilized by other forces. In one dimer residues V86, F89 and L93 were found at the interface and in the other S87 and H94 were found at the interface.

When H94 was changed to alanine, a right-handed dimer similar to that observed for wild-type TM2 was observed (Figure 5-9A, middle panel). This dimer was stabilized by a H-bond between the hydroxyl groups of S95, and additional H-bonding between the side-chain N84 amide with the hydroxyl group of S87 on the opposite helix (stabilized by interactions between N84 and S87 and S95-S95) was present at 25° (Figure 5-9A). There are also a number of dimers present at 10° that contained the interactions between residues N84 and S87, but not S95. The second right-handed symmetrical dimer identified in this search resembled the second symmetrical dimer found in the wild-type search, and is stabilized by a hydrogen bond between the hydroxyl groups of S87, but obviously without the H-bond formed by H94 in the wild-type dimer (shown in Figure 5-9A, right panel). Only one left-handed symmetrical dimer was identified, shown in Figure 5-9B. This dimer formed a hydrogen bonding network between the N84 side-chain amide to the Q85 side-chain carbonyl and the N84 side-chain amide to the opposite N84 side-chain carbonyl. It also contained a hydrogen bond between the hydroxyl groups on the side-chain of S95.

It is not straight-forward to draw any conclusions from this data. It appears as though a N84A mutation will disrupt oligomerization resulting from either N84A-N84A interactions or H94/S87-S87 interactions in the left-handed models, but only N84A-N84A interactions in the right-handed models. In contrast, a H94A mutation does not disrupt oligomerization resulting from N84-N84 interactions in either the left-handed or right-handed models.

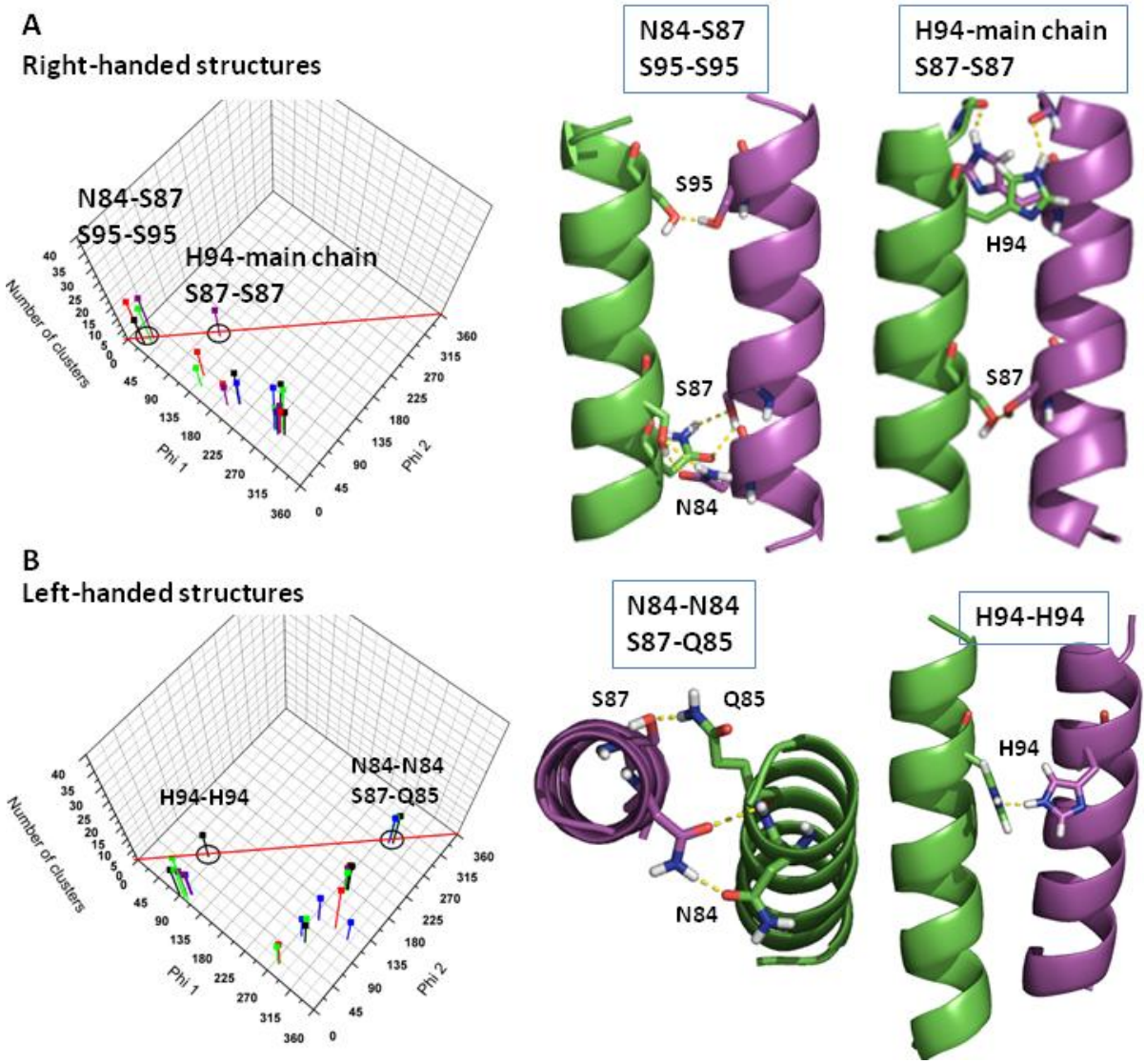

Figure 5-7: Structural models of wild-type STE2 TM domain 2 dimers

The phi plots on the left show the distribution of clusters from global searches as a function of their orientation, represented by the angle phi. Four MD repeats using random starting velocities were performed in each run and five separate searches were performed. When >10 separate structures with Cα RMSD values within <1 Å were found their structure was averaged to generate a "cluster". Different colors of clusters indicate solutions found in separate repeats and symmetrical structures found in several repeats are encircled in black. Structural models of such clusters are shown on the right. Yellow dashed lines indicate a predicted H-bond **A:** The clusters of right-handed structural solutions **B:** The clusters of left-handed structural solutions.

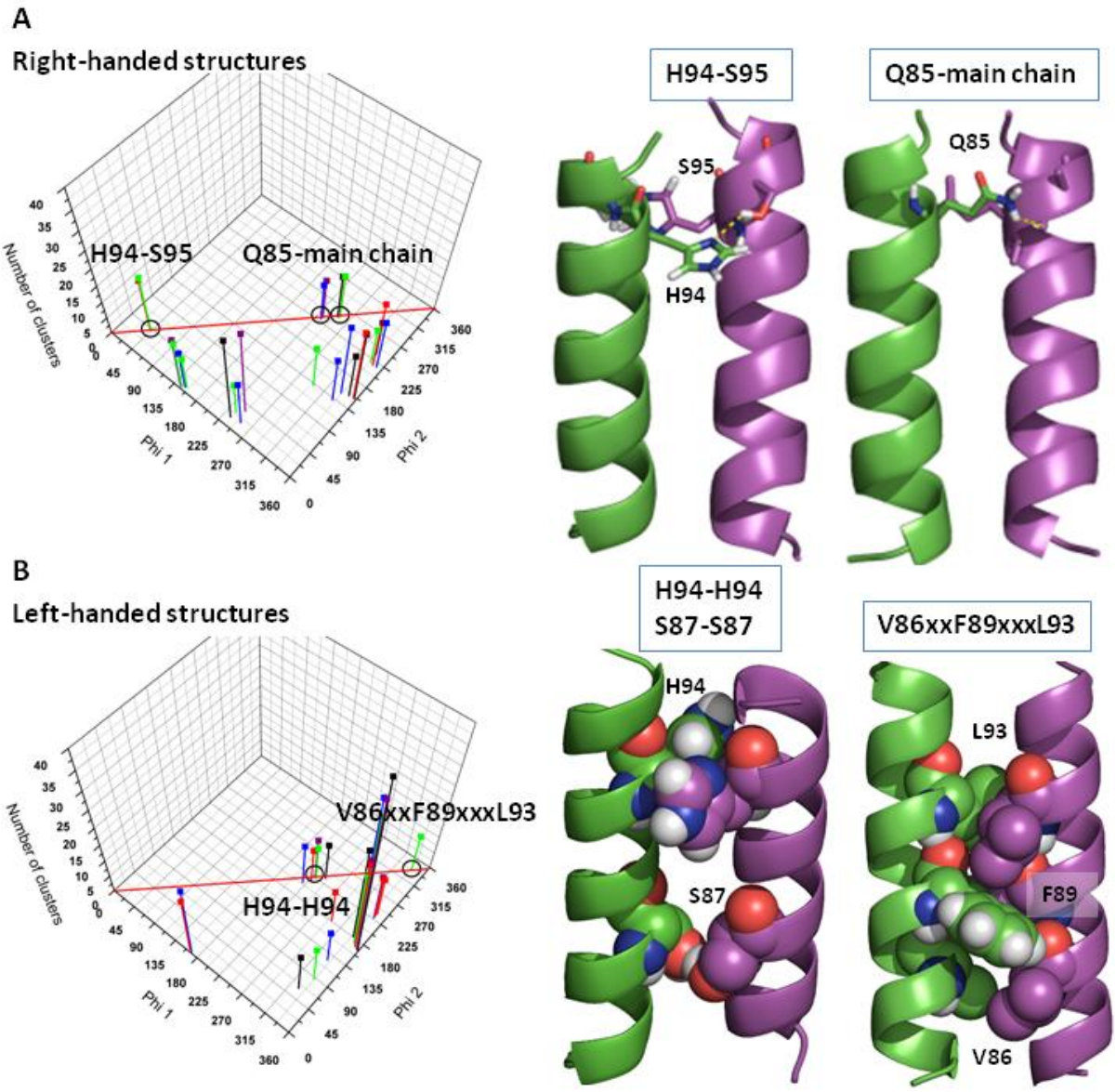

Figure 5-8: Structural dimeric models of STE2 TM domain 2 N84A mutants

The phi plots on the left show the distribution of clusters from global searches as a function of their orientation, represented by the angle phi. Four MD repeats using random starting velocities were performed in each run and five separate searches were performed. When >10 separate structures with Cα RMSD values within <1 Å were found their structure was averaged to generate a "cluster". Different colors of clusters indicate solutions found in separate repeats and symmetrical structures found in several repeats are encircled in black. Structural models of such clusters are shown on the right. Yellow dashed lines indicate a predicted H-bond **A:** The clusters of right-handed structural solutions **B:** The clusters of left-handed structural solutions.

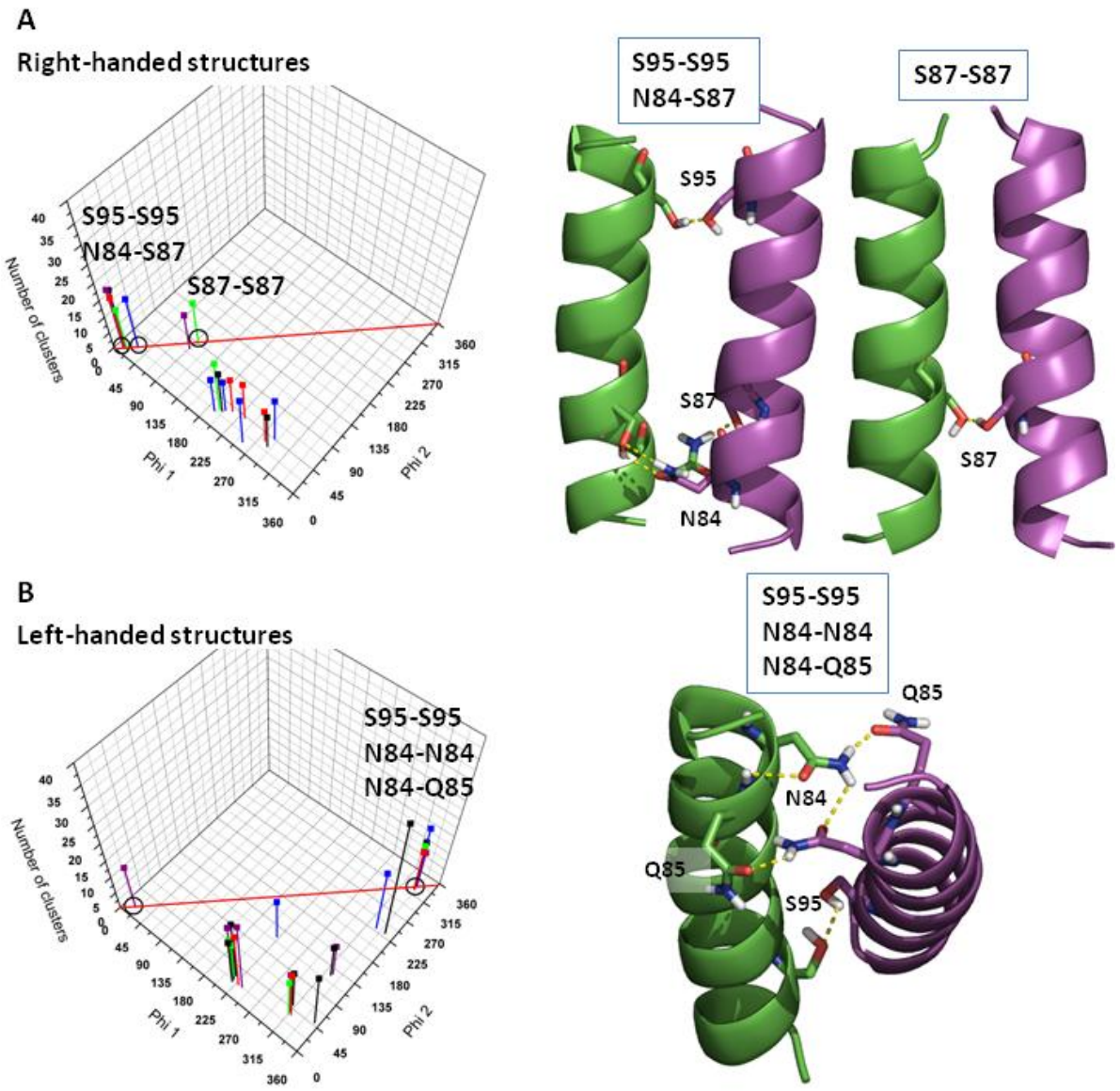

Figure 5-9: Structural dimeric models of STE2 TM domain 2 H94A mutants

The phi plots on the left show the distribution of clusters from global searches as a function of their orientation, represented by the angle phi. Four MD repeats using random starting velocities were performed in each run and five separate searches were performed. When >10 separate structures with Cα RMSD values within <1 Å were found their structure was averaged to generate a "cluster". Different colors of clusters indicate solutions found in separate repeats and symmetrical structures found in several repeats are encircled in black. Structural models of such clusters are shown on the right. Yellow dashed lines indicate a predicted H-bond **A:** The clusters of right-handed structural solutions **B:** The clusters of left-handed structural solutions.

5.2.3.4 Mutations of N84 and H94 Affect the *In Vivo* Oligomerization of Transmembrane Domain 2

To test if either N84 or H94 is involved in the self-association of STE2 TM2, each residue was mutated to alanine and inserted into the TOXCAT MBP-TM-ToxR expression vector. The sequences are shown in Figure 5-10A with the relevant amino acids shown in bold. Both chimeras containing mutated TM2 domains had a ~2-fold increased expression level compared to GpA (Figure 5-10B) and little proteolytically cleaved chimera was found, as indicated by the much larger ratio of the 66 kDa band compared to the 43 kDa band. Both chimeras were inserted and oriented correctly across the *E. coli* plasma membrane as indicated by the *MalE* complementation assay (Figure 5-10C).

Figure 5-10D shows the CAT activities for the TM2 domains containing the N84A and H94A mutations, normalized to expression levels, with wild-type TM2 shown for comparison. Both mutations reduced self-association of the domain. The N84A mutation greatly reduced the ability of TM2 to self-associate, yielding a 20-fold decrease in CAT activity compared to wild-type TM2 levels. The H94A mutation also reduced reporter activity, but to a lesser degree than the N84A mutation, yielding a ~5-fold decrease in CAT activity. Assuming a symmetrical interaction between TM domains, from the predictions made by the structural modelling of these dimers, this may implicate that STE2 TM2 oligomerization involved residues H94 and S87.

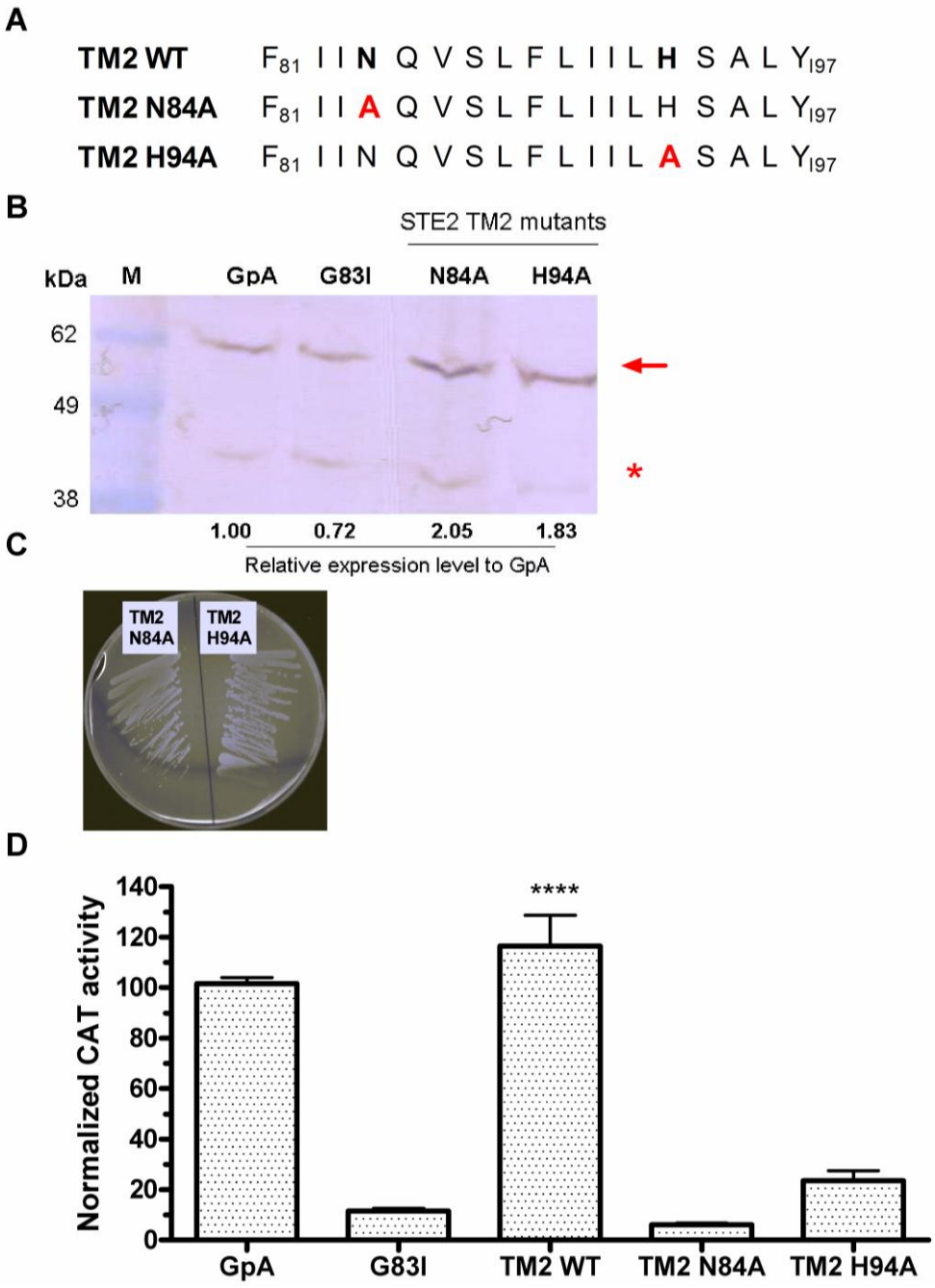

Figure 5-10: Mutations affecting STE2 TM domain 2 dimerization

All assays were performed in the *E. coli* NT326 strain (*malE*$^-$) **A:** Showing the sequence of STE2 TM2 and highlighting in black the two mutations tested for their affects on TM2 dimerization; N84A and H94A (sequences shown underneath and highlighted in red), that were investigated in the TOXCAT assay **B:** Expression check of the constructs used in this study. The arrow indicates the full MBP-TM-ToxR chimera. The star indicates MBP proteolytically separated from the TM-ToxR chimera. **C:** *MalE* complementation assay of the constructs used in this study **D:** CAT activity of the TM chimeras determined by the TOXCAT assay to measure the degree of homo-oligomerization. The asterisks denote ranges of mean CAT activity normalized to GpA where *=26-50%, **=51%-75%, ***=76%-100%, ****=101%-125% and *****=>126%. Results shown are means of triplicate determinations of three independent isolates ±S.E.M.

5.3 Homo-oligomerization of the Mam2 Transmembrane Domains

5.3.1 Oligomerization of Transmembrane Domains 1-7 from Mam2

An initial screen of all seven transmembrane domains in Mam2 was performed to investigate the propensity of each domain to self-associate and to identify similarities and differences between Mam2 and STE2. Seven different MBP-TM-ToxR chimeras were cloned into the pccKan vector containing sequences corresponding to TM 1-7 in Mam2. The sequences of each transmembrane insert are shown in Figure 5-11A. An expression check was performed to measure the relative levels of chimera expression and allow normalization to GpA expression levels, shown in Figure 5-11B. The blot shows both bands described previously; the heavier band at ~66 kDa corresponding to the full MBP-TM-ToxR chimeras (red arrow) and the higher mobility band at ~43 kDa (red star) corresponding to proteolytically cleaved chimeras. The expression level of each TM insert relative to GpA is shown underneath the blot.

The *malE* complementation assay (Figure 5-11C) showed that all TM domains with the exception of TM5 grew on maltose, indicating correct insertion and orientation of these chimeras. The spheroplast assay was performed on TM5 (Figure 5-11C) to further analyse its insertion into the membrane. The PF did not contain MBP as was expected. The SF in contrast contained a band corresponding to the MBP-TM5-ToxR chimera (blue arrow). When treated with proteinase K this band disappeared as shown in the SPF and only the band corresponding to proteolytically cleaved MBP remained (blue star). These checks confirm that the individual transmembrane domains from Mam2 are expressed at comparable levels to GpA and insert into the membrane with the correct topology.

Figure 5-11D shows the TOXCAT data for Mam2 TM domains 1-7 normalized to expression levels relative to GpA. Interestingly, TM1 in Mam2 displayed relatively high levels of self-association, in contrast to what was observed for STE2 TM1. The mean CAT activity for Mam2 TM1 was 60% of GpA compared to 7% for the STE2 TM1 domain. Similar to STE2 however, the Mam2 TM2 domain was observed to self-associate strongly. The interaction between Mam2 TM2 domains (112% CAT activity of GpA) was stronger than that observed for STE2 TM2 (87% CAT activity of GpA).

TM5 from Mam2 also self-associated, although the reporter activity observed for Mam2 was somewhat lower than for the corresponding domain in STE2; 59% of GpA compared to 81%. Like STE2, Mam2 TM3 and TM4 did not strongly self-associate and TM6 and TM7 self-associated moderately stronger than the oligomerization deficient GpA G83I mutant.

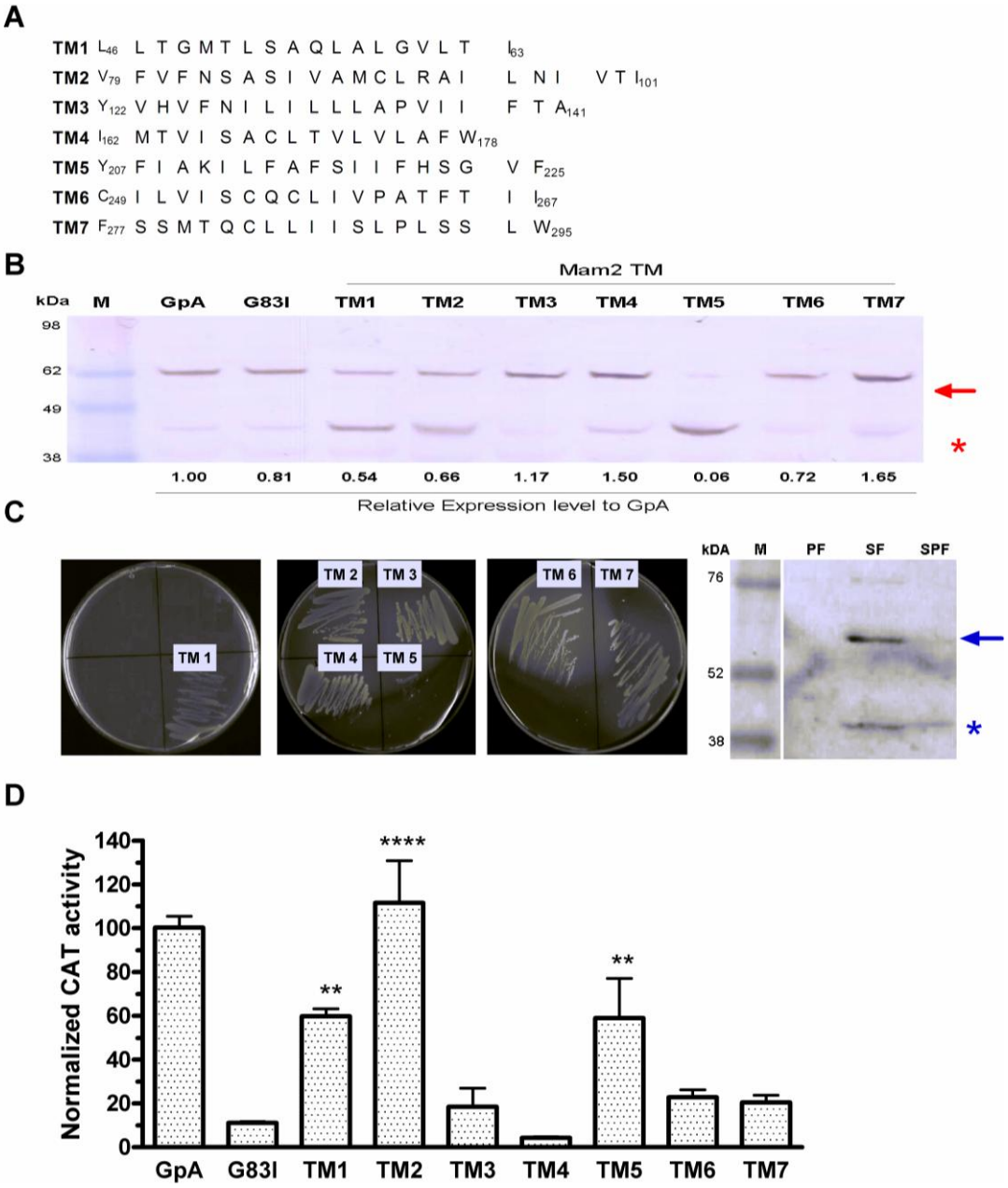

Figure 5-11: Expression, insertion, orientation and oligomerization of the Mam2 TM domains 1-7 TOXCAT Chimeras

All assays were performed in the *E. coli* NT326 strain (*malE*) **A:** Showing the sequence of the seven different transmembrane inserts corresponding to Mam2 transmembrane domain 1-7. These were inserted into the pccKan vector in order to express MBP-TM-ToxR chimera. **B:** Expression check of the constructs used in this study. The arrow indicates the full MBP-TM-ToxR chimera. The star indicates MBP proteolytically separated from the TM-ToxR chimera. **C:** *MalE* complementation assay of the constructs used in this study (left). The construct incorporating TM5 did not grow on maltose and therefore the spheroplast assay was performed on this construct (right) **D:** CAT activity of the TM chimeras determined by the TOXCAT assay to measure the degree of homo-oligomerization. The asterisks denote ranges of mean CAT activity normalized to GpA where *=26-50%, **=51%-75%, ***=76%-100%, ****=101%-125% and *****=>126%. Results shown are means of triplicate determinations of three independent isolates ±S.E.M.

5.3.2 Further Characterization of the Homo-Oligomerization of Transmembrane Domain 1 from Mam2

5.3.2.1 Length-Optimization of Transmembrane Domain 1

Length optimization of the Mam2 TM1 domain was performed to investigate whether CAT activity could be further increased. It was also of interest to centre the two different putative smallxxxsmall motifs discussed in Chapter 4; G49xxxS53 and S53xxxA57 to explore whether centralizing either motif within the TM domain of the chimera would result in higher reporter activity.

Figure 5-12A shows the five different frames and lengths of the predicted Mam2 TM1 inserted into the TOXCAT chimera. All constructs were expressed at levels comparable to GpA (Figure 5-12B) and the western blot displays both bands characteristic of expression of TOXCAT constructs; the full-length chimera and the proteolytically cleaved chimera. All constructs grew on maltose in the *malE* complementation assay, indicating correct orientation and insertion of chimera (Figure 5-12C). The 18 amino acid-long construct was investigated in the initial screen and therefore the expression and insertion of this construct is not shown in this section however its CAT activity is shown in Figure 5-12D for comparison.

The 13 amino acid-long constructs “13” and “13A” centre the S53xxxA57 and G49xxxS53 motifs respectively (Figure 5-12A). As discussed in Chapter 4, when mutating the S53 and A57 residues to glycine in the full-length protein, the β-galactosidase reporter activity is reduced ~2-fold. In contrast, when G49 is mutated to alanine, reporter activity is indistinguishable from wild-type Mam2. If this decrease in signalling is due to a reduction in oligomeric state, then it seems likely that the construct centering the SxxxA motif would oligomerize more strongly in the TOXCAT assay than the construct centring GxxxS. Indeed, construct “13”, centring the S53xxxA57 motif, displayed a significantly stronger degree of self-association compared to construct “13A” that centred the G49xxxS53 motif. (Figure 5-12D). The reporter activity for the construct centring the SxxxA motif was 42% of GpA and that of the construct centring the GxxxS motif was 10%. This may indicate that oligomerization of Mam2 is achieved via packing of the S53xxxA57 motif in TM1.

The highest degree of self-association was observed for the 16 amino acid-long construct, with 75% CAT activity compared to GpA. This construct also centred the SxxxA motif in the TM domain, but was slightly longer than the 13 amino acid-long construct. The longer length

of this construct might allow the domain to traverse the membrane in a more relaxed configuration, which may lead to the stronger interaction observed.

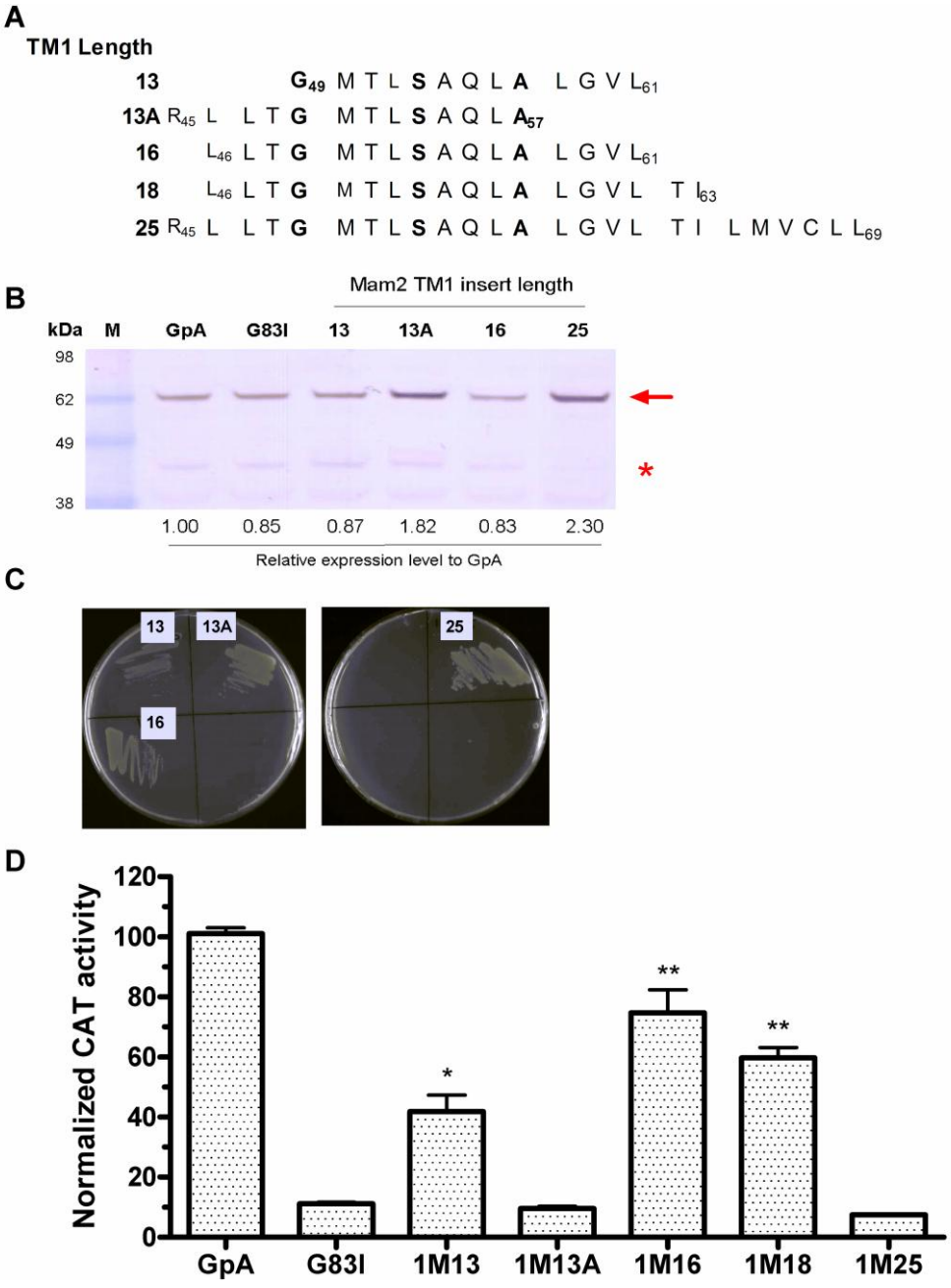

Figure 5-12: Length optimization of transmembrane domain 1 from Mam2

All assays were performed in the *E. coli* NT326 strain (*malE*) **A:** The sequence of the different lengths and frames of TM domain 1 from Mam2 inserted into the pccKan vector to test if the TOXCAT signal could be improved. Note that the two 13 amino acid long constructs each centre a different putative smallxxxsmall motif; SxxxA and GxxxS **B:** Expression check of the constructs used in this study. The arrow indicates the full MBP-TM-ToxR chimera, the star indicates MBP proteolytically separated from the TM-ToxR chimera. **C:** *MalE* complementation assay of the constructs used in this study, all constructs grew on maltose indicating correct insertion and orientation of chimera. **D:** CAT activity of the TM chimeras determined by the TOXCAT assay to measure the degree of homo-oligomerization. The asterisks denote ranges of mean CAT activity normalized to GpA where *=26-50%, **=51%-75%, ***=76%-100%, ****=101%-125% and *****=>126%. Results shown are means of triplicate determinations of three independent isolates ±S.E.M.

5.3.2.2 Molecular Modelling of Mam2 Transmembrane Domain 1 Dimerization suggests that Interactions are mediated by the S53xxxA57 motif

CHI modelling of the 16 amino acid-long Mam2 TM1 construct revealed two symmetrical right-handed structures that were present in three and five independent repeats respectively, shown in Figure 5-13A. The first symmetrical structure was found at a relative rotational angle of 90° and involved hydrogen bonding between the side-chain amide of Q55 to a backbone carbonyl on the opposite helix (either Q55 or L52) as shown in the middle panel of Figure 5-13A. Interestingly, the second symmetrical structure, which was found in all five independent runs and at a relative rotational angle of 290°, involved interactions between the S53xxxA57 motifs. In this model dimer formation occurred via close packing of the motif and hydrophobic interactions rather than hydrogen bonding. This model is shown on the right in Figure 5-13A. The helices in this model were separated by a shorter interhelical distance than observed in the Q55 model on the left, with the centre of the helices separated by ~7.8 Å compared to ~8.6 Å in the Q55 model. One symmetrical left-handed dimer was predicted, shown in Figure 5-13B. This dimer was only found in three repeats and the clusters only contained 10 structures each. This dimer associated through packing via a L52xxxL56 motif resulting in a relatively large inter-helical distance of ~9 Å.

The most abundantly found model for a Mam2 TM1 dimer interacted via an SxxxA motif. As discussed in Chapter 4, mutations of these two residues in the full-length protein resulted in strong signalling-defective phenotypes *in vivo*. These single mutants expressed comparable amounts of receptor at the cell membrane, suggesting that the functionality of the receptor was affected, rather than its localization. Models were therefore built to investigate whether mutations of this motif to the structurally larger residue leucine would remove interactions between this face of the helices. Only right-handed models were considered since the motif was not involved in dimerization of the left-handed dimers. As shown in Figure 5-14B, leucine mutations to this motif completely abolish dimer formation at the S53xxxA57 interface (indicated by the arrow).

Dimerization via Q55 was also implicated in the right-handed structures. Q55 is located on the opposite face of the helix compared to the S53xxxA57motif. This residue was also mutated to leucine to see what effects this would have on dimer formation in the models. Interestingly, in the right-handed models, a Q55L mutation resulted in the loss of dimerization via S53xxxA57, shown in Figure 5-14C.

The structural models of these mutants therefore predict that if Q55 is involved in the oligomerization of Mam2 TM1, then a Q55L mutation would disrupt this interaction. Mutating the S53xxxA57 motif to leucine in contrast will most likely not have an effect on oligomerization because Q55 can still hydrogen bond to the opposite helix.

If instead the S53xxxA57motif is responsible for the interactions between TM1 helices, then mutating this motif to leucine will disrupt oligomerization. A Q55L mutation is however also likely to disrupt oligomerization via the S53xxxA57motif, because interactions via the S53xxxA57motif disappeared when mutating Q55L in the models.

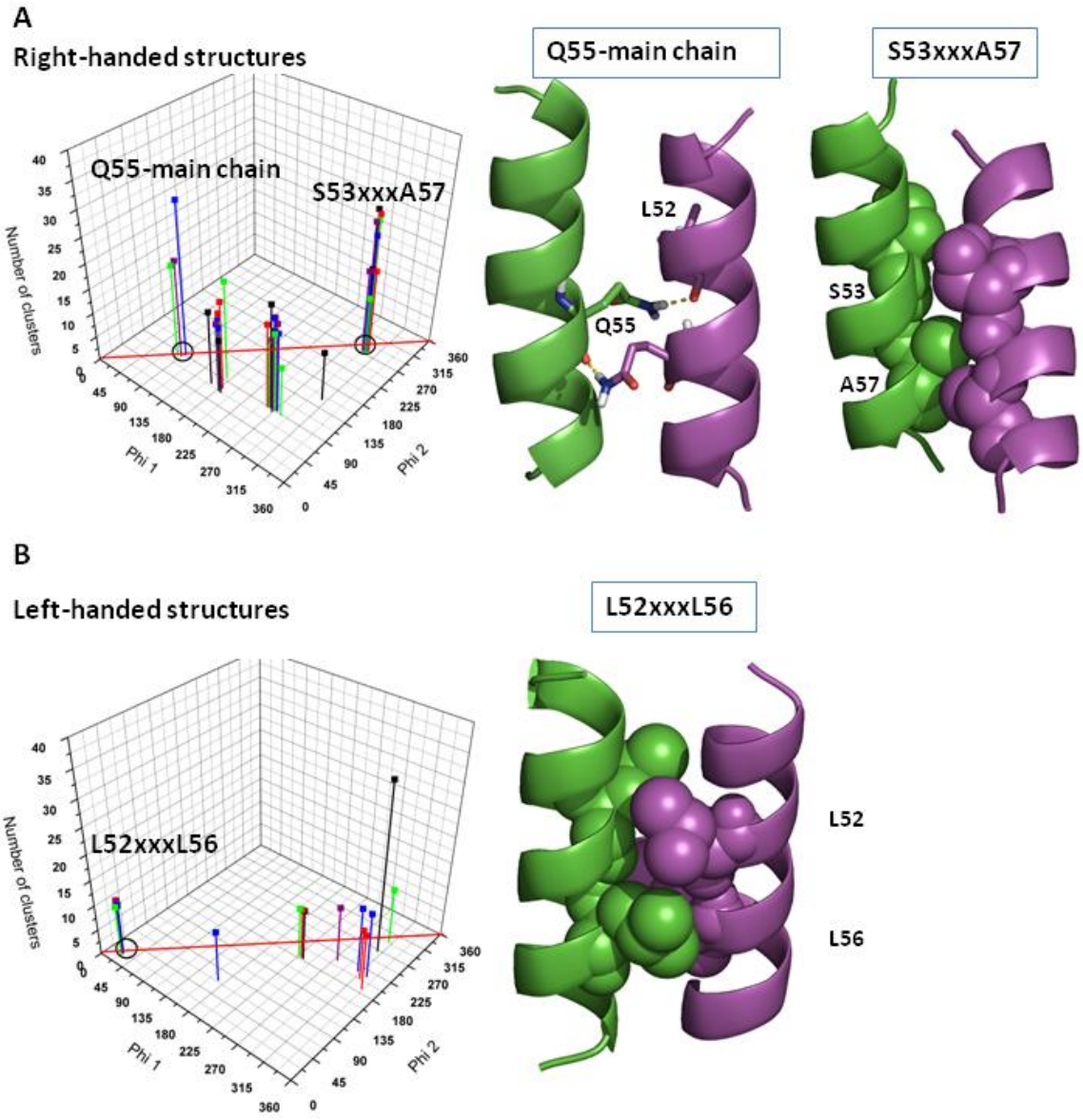

Figure 5-13: Structural models of Mam2 TM domain 1 dimers

The phi plots on the left show the distribution of clusters from global searches as a function of their orientation, represented by the angle phi. Four MD repeats using random starting velocities were performed in each run and five separate searches were performed. When >10 separate structures with Cα RMSD values within <1 Å were found their structure was averaged to generate a "cluster". Different colors of clusters indicate solutions found in separate repeats and symmetrical structures found in several repeats are encircled in black. Structural models of such clusters are shown on the right. **A:** Right-handed solutions **B:** Left-handed solutions.

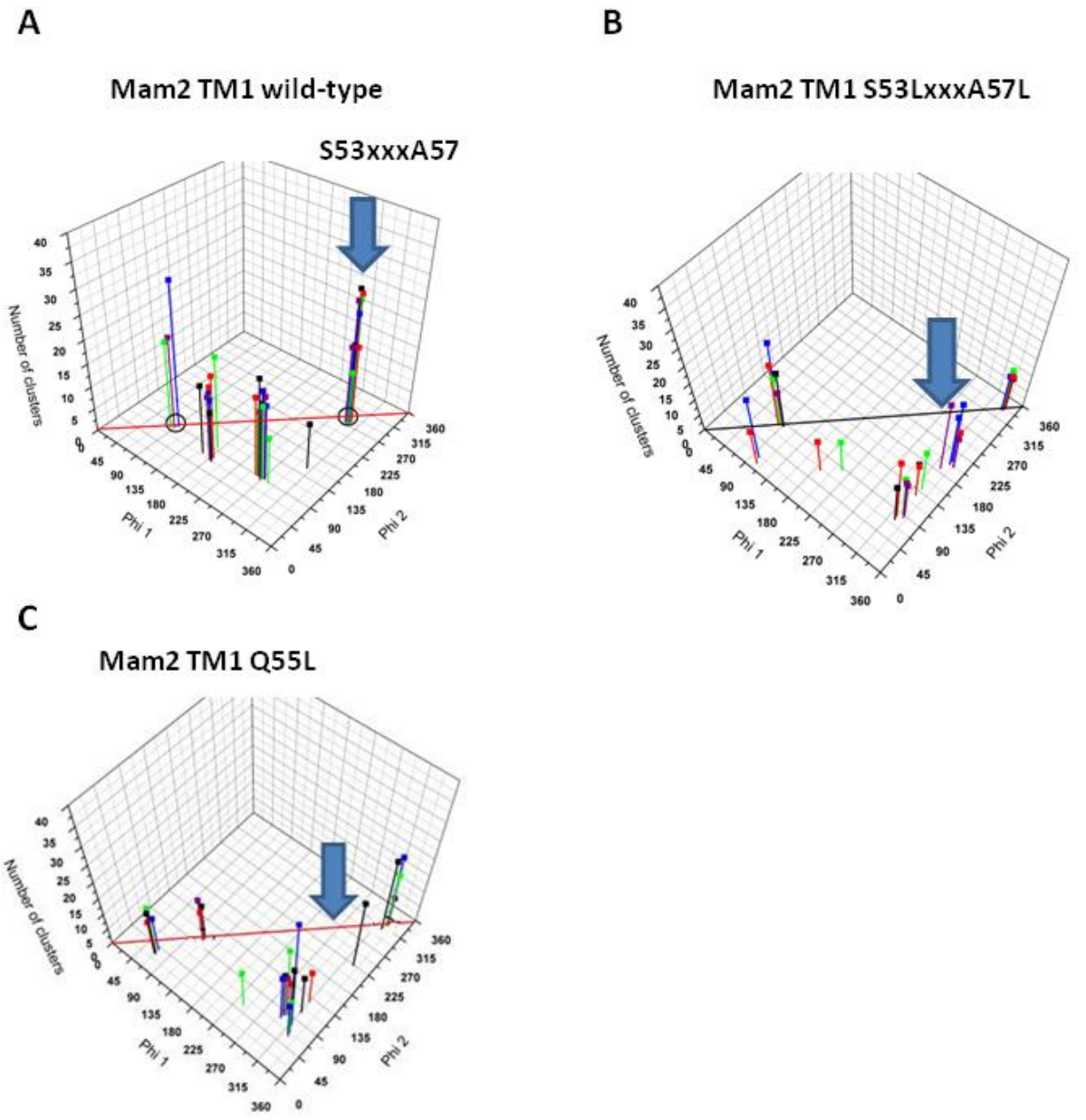

Figure 5-14: Mutations affecting wild-type Mam2 TM domain 1 dimer formation

A: The SxxxA motif is implied in the dimerization of wild-type TM1 when modeling helix interactions using CHI, dimers associating via this motif are marked with a blue arrow in the phi plot. **B:** When mutating the SxxxA motif to leucine, interactions via this face of the helix is diminished, as marked by the blue star. Compare to A. **C:** When mutating Q55 to leucine, interactions via SxxxA are also diminished.

5.3.2.3 Mutations Affecting the Oligomerization of Mam2 Transmembrane Domain 1

The structural models presented in the previous section predicted that symmetrical dimers of Mam2 TM domain 1 are formed either by hydrogen bonding of the side-chain amide in Q55 the main chain L52 or Q55 on the opposite helix or by close packing of the S53xxxA57 motif. Mutations to the S53 and A57 residues furthermore had a strong effect on pheromone signalling. It was therefore of interest to mutate these residues in the TOXCAT chimera to see if either of these mutations would reduce the strength of oligomerization. The 16 amino acid long construct was used because this chimera displayed the highest CAT activity in the TOXCAT length optimization assay.

The sequence of the 16 amino acid long Mam2 TM1 construct is shown in Figure 5-15A. The two mutants tested (S53L, A57L and Q55L) are shown underneath with the respective mutations highlighted. Figure 5-15B shows the expression check of these two mutants; the constructs containing each mutant TM domain were expressed at levels comparable to GpA. The *MalE* complementation assay shown in Figure 5-15C indicate that both constructs are inserted and orientated correctly across the plasma membrane, meaning that any reduction in CAT activity is due to a reduction in oligomerization of the TM domain.

Interestingly, both mutations reduced oligomerization of Mam2 TM 1, shown in Figure 5-15D. Wild-type TM1 reporter activity is shown for comparison. Reporter activity was slightly higher for the S53L,A57L double mutant compared to the Q55L mutant, with mean activity of 21% compared to 9% of GpA. The structural models predicted that the S53L,A57L double mutant would not affect oligomerization via Q55 but the Q55L mutation could reduce oligomerization via the S53xxxA57 motif. Since oligomerization was reduced in both mutants in the TOXCAT assay, it is therefore plausible that Mam2 TM1 dimerizes via the S53xxxA57 motif, if a symmetrical interaction between helices is assumed.

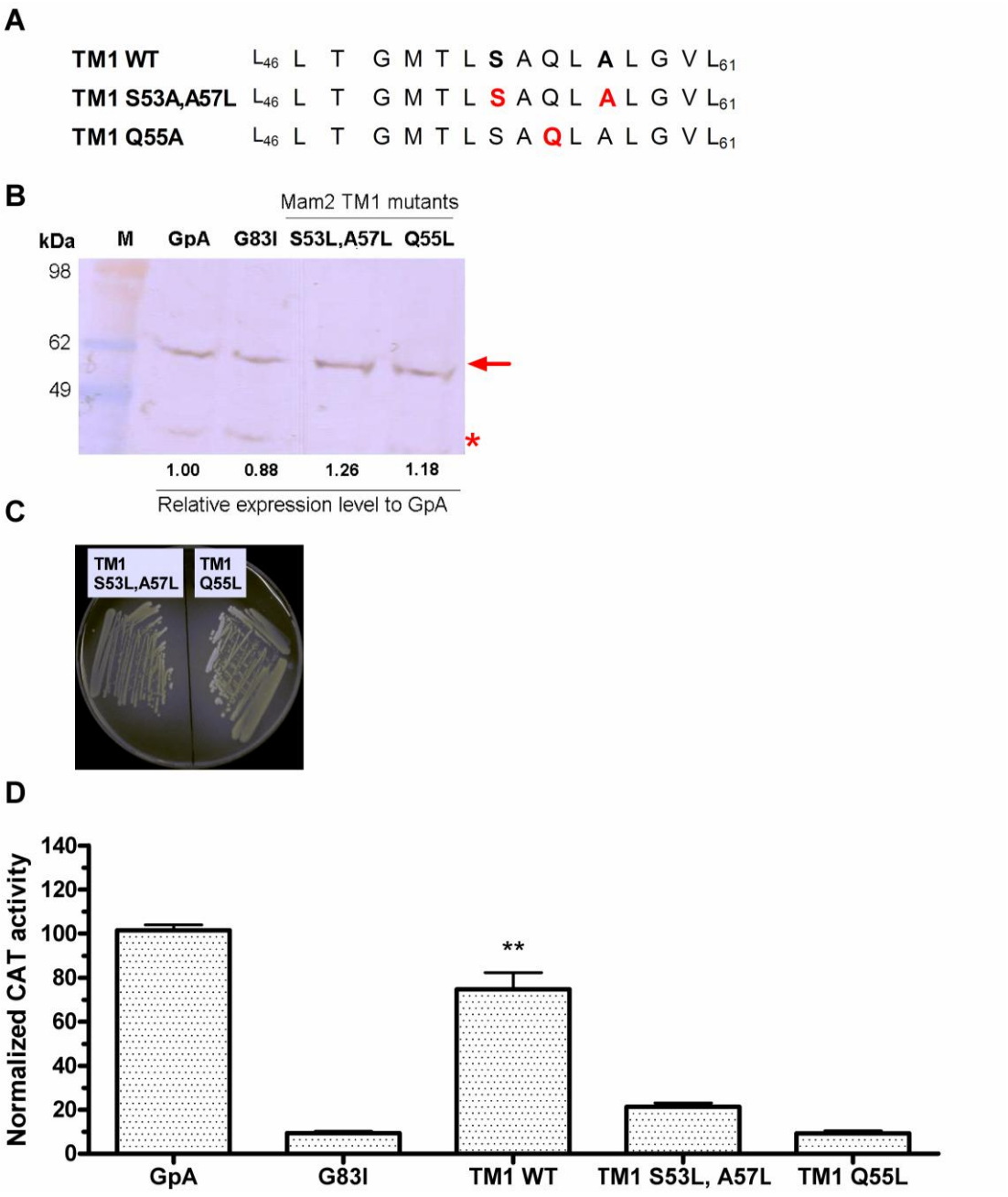

Figure 5-15: Mutations affecting Mam2 TM domain 1 dimerization

All assays were performed in the *E. coli* NT326 strain (*malE*⁻) **A:** Showing the sequence of Mam2 TM1 with the predicted smallxxxsmall motif highlighted in black. The sequence of the two TM1 mutants assayed; S53L,A57L and Q55L, are shown underneath with their respective mutations highlighted in red. **B:** Expression check of the constructs used in this study. The arrow indicates the full MBP-TM-ToxR chimera. The star indicates MBP proteolytically separated from the TM-ToxR chimera. **C:** *MalE* complementation assay of the constructs used in this study, all constructs grew on maltose indicating correct insertion and orientation of chimera. **D:** CAT activity of the TM chimeras determined by the TOXCAT assay to measure the degree of homo-oligomerization. The asterisks denote ranges of mean CAT activity normalized to GpA where *=26-50%, **=51%-75%, ***=76%-100%, ****=101%-125% and *****=>126%. Results shown are means of triplicate determinations of three independent isolates ±S.E.M.

5.3.3 Further Characterization of the Homo-Oligomerization of Transmembrane Domain 2 from Mam2

5.3.3.1 Mam2 Transmembrane Domain 2 Contains Polar Residues at Similar Positions to STE2 Transmembrane Domain 2

The N84A and H94A mutations each reduced oligomerization of the STE2 TM2 domain. A sequence alignment of TM2 in Mam2 and STE2 predicts that N84 and H94 in STE2 align to N83 and R93 in Mam2, as shown in Table 5-1. It is interesting that H94 aligns to an arginine residue in Mam2 because, as previously discussed, H94 may be involved in keeping the receptor in its inactive state in the absence of ligand through interactions with Y98 and R58. Upon ligand binding, R58 could instead interact with the α-factor peptide (Tantry, Ding et al. 2010) and the loss of these contacts may relax TM1-TM2 interactions and lead to structural changes in the protein required for activation. In Mam2, Q58 in TM1 aligns to R58 (see Figure 4-6), and in TM2 N97 align to Y98. The similarity of these residues to the aligned residues in STE2 indicates the possibility that TM1-TM2 interactions and P-factor binding in Mam2 are mediated by interactions between R93 and N97 and Q58 respectively. Although the distribution of polar residues in the two TM domains appears very similar, there are differences; Mam2 does not contain a polar residue aligning to S95 in STE2 but does contain a polar residue at position 91, which is non-existent in STE2.

STE2	81-98	F I I **N** Q V S L F L I I L **H** S A L Y
Mam2	79-101	V F V F **N** S A S I V A M C L **R** A I L N I V T I

Table 5-1: Sequence alignment of STE2 and Mam2 TM2

Sequence alignment between TM2 of the *Sc. cerevisiae* receptor STE2 and TM2 of the *Sz. pombe* pheromone receptor Mam2. The two residues that reduced oligomerization of STE2 TM2 when mutated to alanine are highlighted in black. The corresponding residues in Mam2 are also highlighted.

5.3.3.2 Effects of Mutations in Mam2 Transmembrane Domain 2

Since an N84A and a H94A mutation in STE2 TM2 each reduced oligomerization of this domain in the TOXCAT assay, and because of the sequence similarity between Mam2 and STE2, it was of interest to mutate the corresponding residues N83 and R93 in Mam2 TM2 to see if the same effects would be observed for this domain. Residue N83 is furthermore of interest because mutations at this position have been linked to constitutive activity of the receptor (Goddard, Ladds et al. 2005).

Figure 5-16A shows the sequence of Mam2 TM2 with each mutation tested highlighted in bold. All chimeras were expressed at levels similar to expression of the GpA control (Figure 5-16B) and the full-length 66 kDa chimera was the predominant species present (only low levels of the 43 kDa proteolytically cleaved chimera were observed). The *malE* complementation assay indicated that all chimeras were correctly inserted and oriented across the *E. coli* inner membrane (Figure 5-16C).

The results from the TOXCAT assay (Figure 5-16D) of the N83A and R93A mutants were surprising. When mutating the residues that align to N83 and R93 in STE2, oligomerization was reduced, and the same was expected for Mam2. In Mam2 however, each mutation slightly increased reporter activity relative to GpA, indicating that interactions are stronger than for wild-type TM domain 2. In the N83A mutant, mean reporter activity was 131% of GpA and for the H93A mutant CAT activity was 133% of GpA, compared to the 112% CAT activity observed for wild type TM2.

Since the N83A and R93A mutations did not reduce CAT activity, C91; a residue which is positioned on the opposite face of the helix (shown in the helical wheel projection in Figure 5-16E), was mutated to alanine to investigate whether this would have an effect on CAT activity. In this mutant, CAT activity was reduced to 68% of GpA, indicating that the oligomerization interface may involve this face of the helix.

A second possibility is that the TM domain aggregate, and that aggregation mediated by the N83 and R93 residues does not result in ToxR dimerization, whereas dimerization through another face of the helices does. Consequently when changing the N83 and R93 residues to alanine, the TOXCAT signal is increased, although overall oligomerization may not be increased.

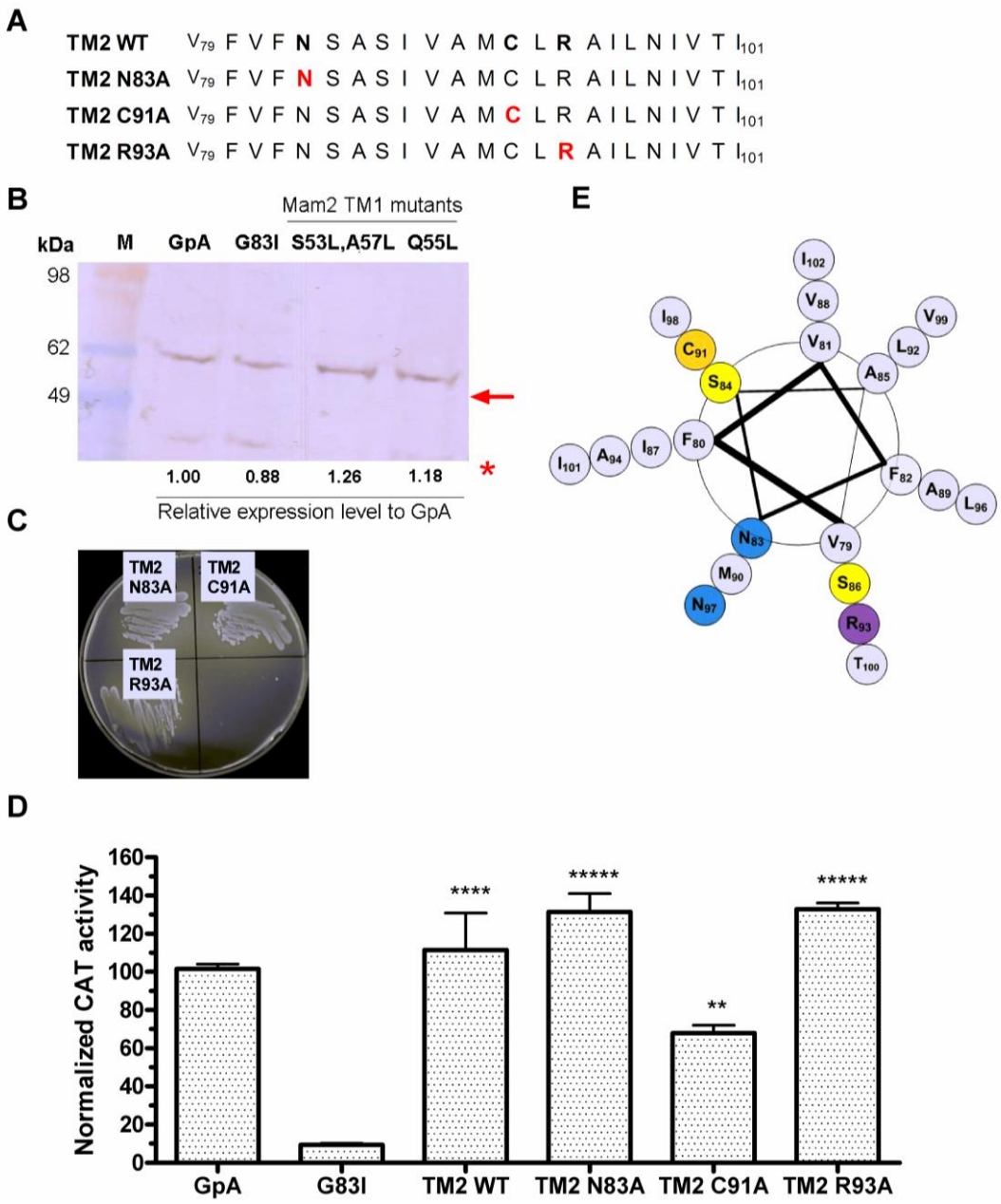

Figure 5-16: TOXCAT assay and controls for Mam2 TM domain 2 mutants

All assays were performed in the *E. coli* NT326 strain (*malE*⁻) **A:** Showing the sequence of Mam2 TM domain 2 and three mutations tested for their effect on dimerization; N83A, C91A and R93A, that were investigated in the TOXCAT assay. Residues mutated are highlighted in black in the wild-type sequence and respective mutations are shown in red in each mutant. **B:** Expression check of the constructs used in this study. The arrow indicates the full MBP-TM-ToxR chimera. The star indicates MBP proteolytically separated from the TM-ToxR chimera. **C:** *MalE* complementation assay of the constructs used in this study, all constructs grew on maltose indicating correct insertion and orientation of chimera. **D:** CAT activity of the TM chimeras determined by the TOXCAT assay to measure the degree of homo-oligomerization. The asterisks denote ranges of mean CAT activity normalized to GpA where *=26-50%, **=51%-75%, ***=76%-100%, ****=101%-125% and *****=>126%. Results shown are means of triplicate determinations of three independent isolates ±S.E.M. **E:** Helical wheel projection of Mam2 TM2 with polar residues highlighted.

5.3.3.3 Molecular Modelling of Mam2 Transmembrane Domain 2 Dimerization

CHI modelling of the Mam2 TM 2 domain revealed a cluster of right-handed symmetrical dimers in Figure 5-17A found at 100°. This structure contained H-bonds between the side-chain hydroxyl groups of opposite S84 residues as well as a hydrogen bond between the side-chain hydroxyl group of S83 on one helix and the side-chain hydroxyl group of N84 on the other helix, as shown in the structural model, and was found in four of five independent CHI searches. One symmetrical left-handed interaction was found V88, L92, I95 and V99, shown in Figure 5-17B.

The residues that aligned to STE2 N98 and H94 in Mam2, N83 and R93, were then changed to alanine in Mam2. When changing N83 to alanine, the cluster at phi = 100° disappeared and instead a structure at 335° appeared. This was found in two of the five CHI searches as shown in Figure 5-18B. The modelling of the wild-type TM2 domain suggests that N83 is involved in dimer formation. If this is the case then another contact must compensate when N83 is mutated to alanine, because the N83A mutant interacted strongly in the TOXCAT assay. The structure found in the search of the N83A mutant contained hydrogen bonds between the side chain amine of R93 to the side-chain carbonyl of N97 and between the side-chain hydroxyl group of S86 to the side-chain amine of R93 on each respective helix, which could act as the compensating contacts as shown in the structural model in Figure 5-18.

When mutating R93 to alanine, again only one symmetrical right-handed dimer was found in the CHI searches, shown in the phi plot in Figure 5-19A. This dimer contained a hydrogen bond between the side-chain hydroxyl groups of adjacent S95 residues as shown in the structural model in the right panel of Figure 5-19A. Two symmetrical left-handed dimers were found. One appeared similar in structure to the left-handed dimer found for the N83A mutant and interacted via a L92xxL95 motif (Figure 5-19B, middle panel). The second dimer interacted via interactions between the side-chain carbonyl of N84 and the hydroxyl group on the S85 side-chain (Figure 5-19B, right panel).

In the predicted wild-type dimer, C91 does not appear to be involved in any direct polar or non-polar interactions. It is therefore surprising that the C91 mutant was the only mutant shown to reduce oligomerization. Structural modelling of the C91A mutant revealed four symmetrical right-handed clusters. These all interacted via N83 and S84, however due to the variability in their relative rotation the nature of these interactions varied. No symmetrical left-handed dimer was generated during the CHI searches of the C91A mutant.

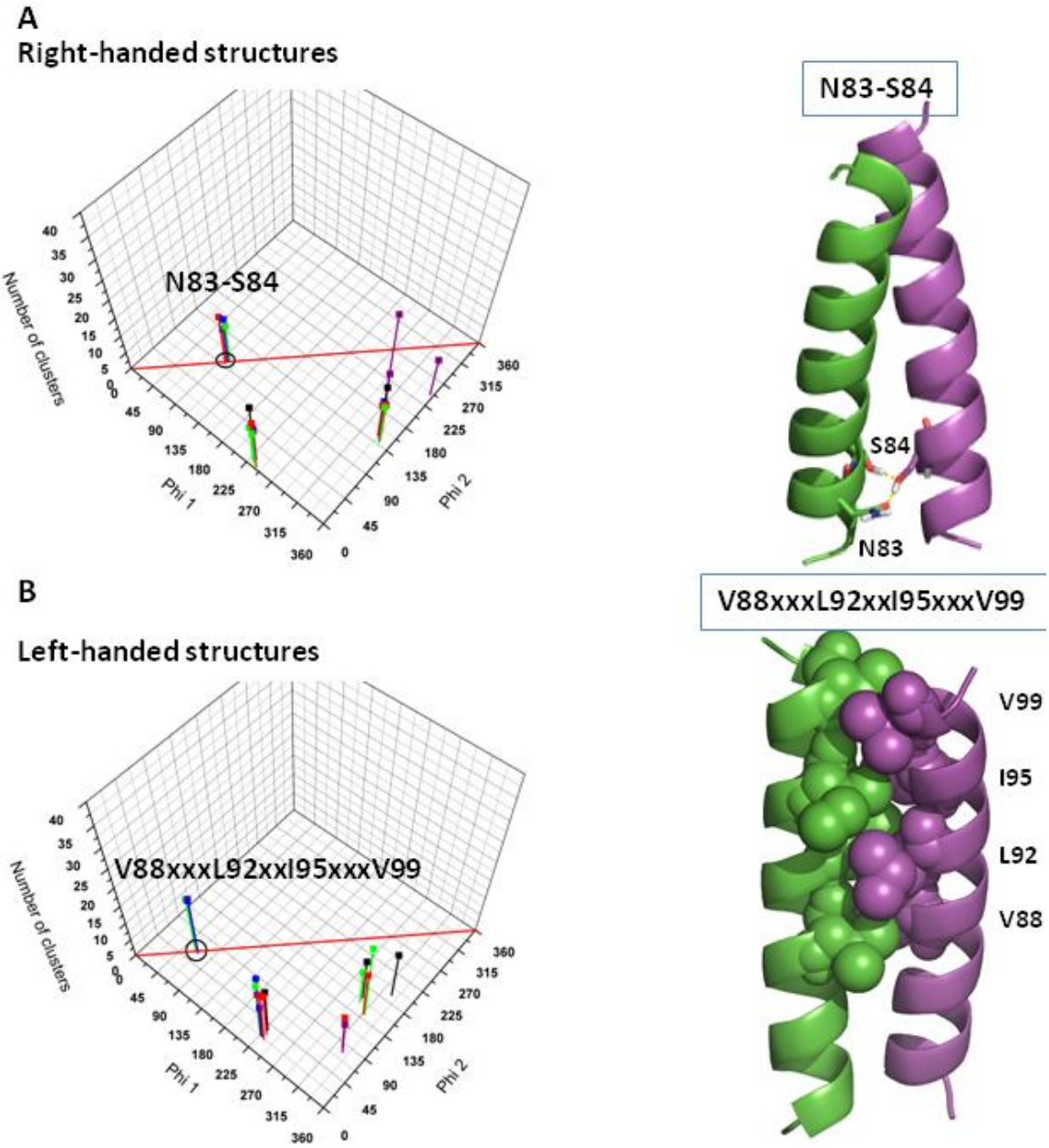

Figure 5-17: Structural models of Mam2 TM domain 2

The phi plots on the left show the distribution of clusters from global searches as a function of their orientation, represented by the angle phi. Four MD repeats using random starting velocities were performed in each run and five separate searches were performed. When >10 separate structures with Cα RMSD values within <1 Å were found their structure was averaged to generate a "cluster". Different colors of clusters indicate solutions found in separate repeats and symmetrical structures found in several repeats are encircled in black. Structural models of such clusters are shown on the right. **A:** Right-handed solutions **B:** Left-handed solutions.

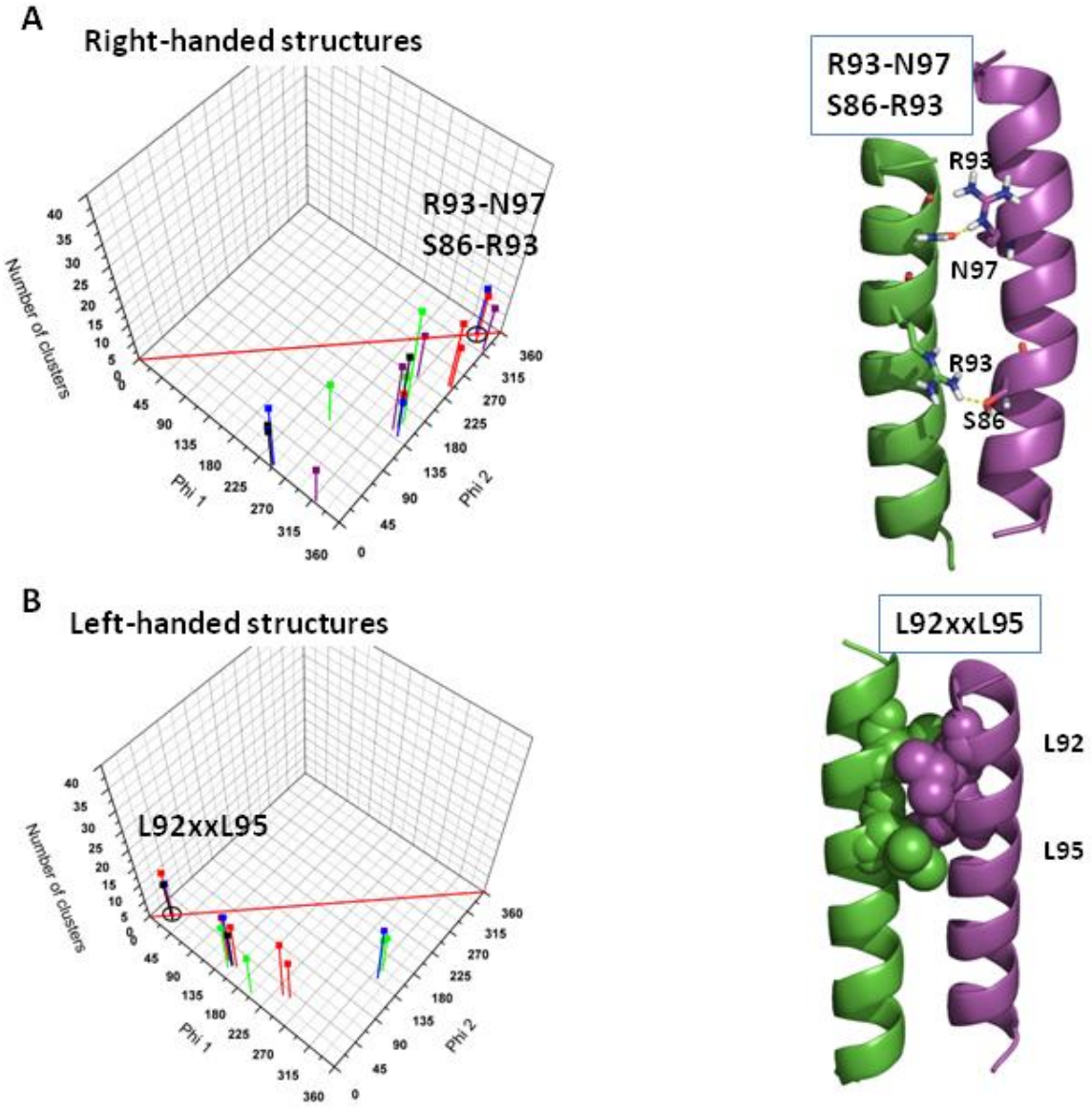

Figure 5-18: Structural dimeric models of Mam2 TM domain 2 incorporating a N83A mutation

The phi plots on the left show the distribution of clusters from global searches as a function of their orientation, represented by the angle phi. Four MD repeats using random starting velocities were performed in each run and five separate searches were performed. When >10 separate structures with Cα RMSD values within <1 Å were found their structure was averaged to generate a "cluster". Different colors of clusters indicate solutions found in separate repeats and symmetrical structures found in several repeats are encircled in black. Structural models of such clusters are shown on the right. Yellow dashed lines indicate a predicted H-bond **A:** The clusters of right-handed structural solutions **B:** The clusters of left-handed structural solutions.

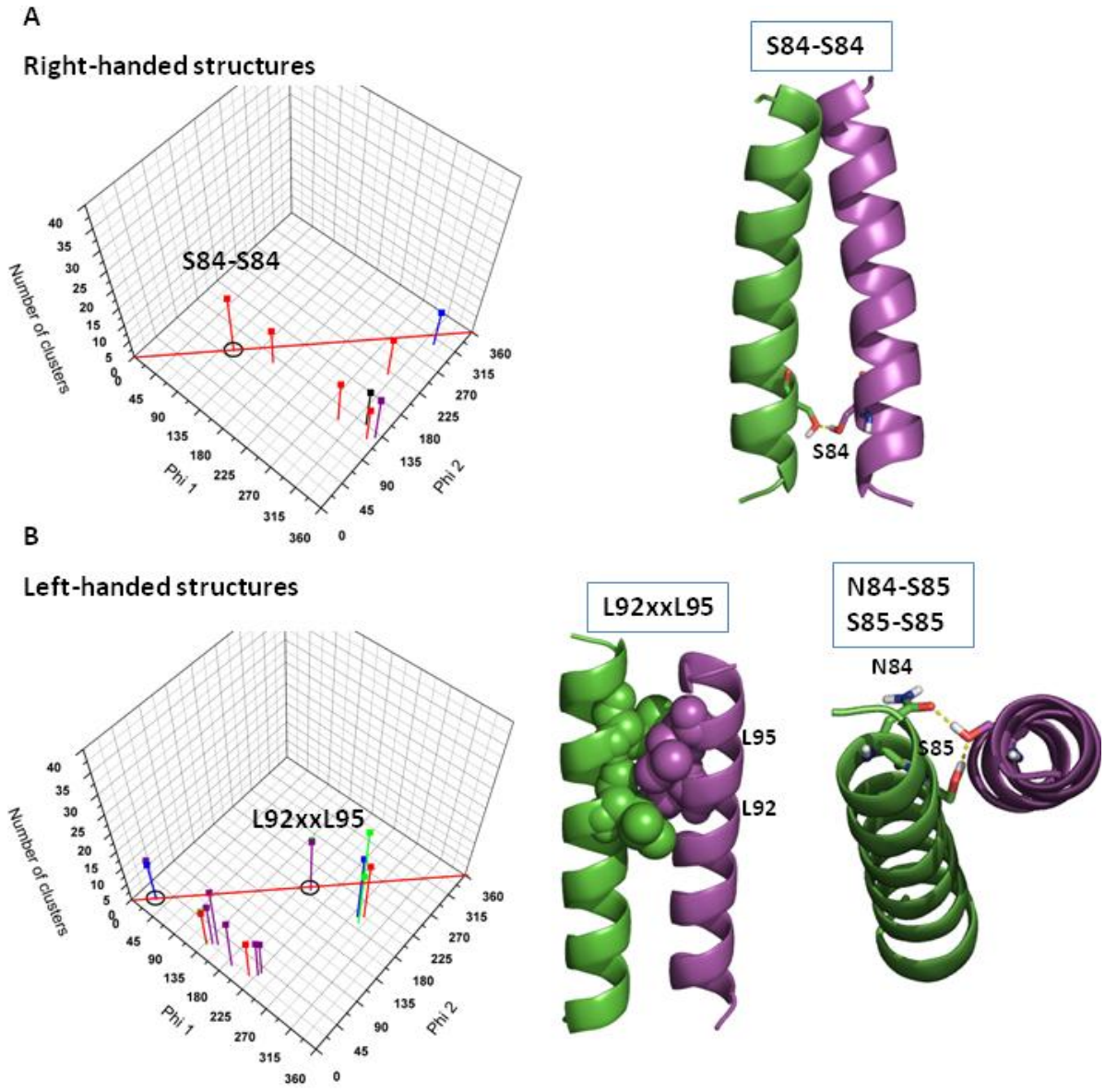

Figure 5-19: Structural dimeric models of Mam2 TM domain 2 incorporating a R93A mutation

The phi plots on the left show the distribution of clusters from global searches as a function of their orientation, represented by the angle phi. Four MD repeats using random starting velocities were performed in each run and five separate searches were performed. When >10 separate structures with Cα RMSD values within <1 Å were found their structure was averaged to generate a "cluster". Different colors of clusters indicate solutions found in separate repeats and symmetrical structures found in several repeats are encircled in black. Structural models of such clusters are shown on the right. Yellow dashed lines indicate a predicted H-bond **A:** The clusters of right-handed structural solutions **B:** The clusters of left-handed structural solutions.

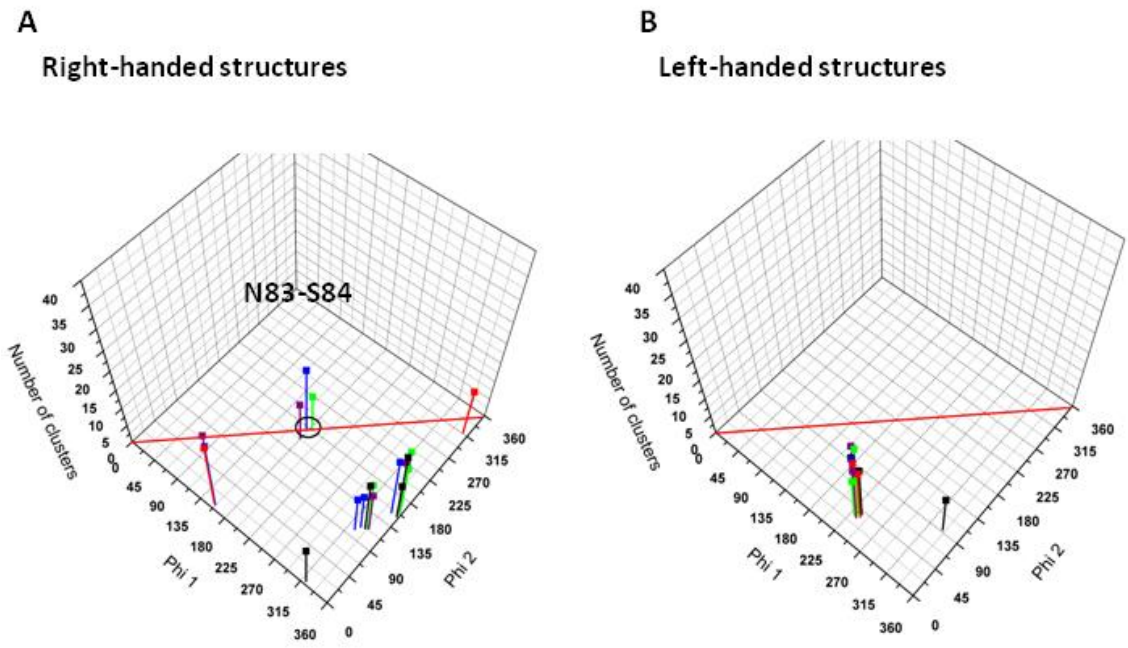

Figure 5-20: Structural modeling of Mam2 TM domain 2 incorporating a C91A mutation

The phi plots on the left show the distribution of clusters from global searches as a function of their orientation, represented by the angle phi. Four MD repeats using random starting velocities were performed in each run and five separate searches were performed. When >10 separate structures with Cα RMSD values within <1 Å were found their structure was averaged to generate a "cluster". Different colors of clusters indicate solutions found in separate repeats and symmetrical structures found in several repeats are encircled in black. **A:** The clusters of right-handed structural solutions **B:** The clusters of left-handed structural solutions.

5.4 Summary

The oligomerization of the individual transmembrane domains from the STE2 and Mam2 receptors was investigated using the TOXCAT assay and CHI searches. It was found that TM1 from STE2 did not oligomerize in the TOXCAT assay, and structural modelling did not predict dimerization via the GxxxG motif, which has previously been implied in oligomerization of the receptor (Overton, Chinault et al. 2003). This was however in agreement with studies suggesting that STE2 TM1 requires the presence of additional domains in order to oligomerize (Overton and Blumer 2002). In contrast, TM1 from the Mam2 receptor was found to self-associate strongly in the TOXCAT assay and modelling predicted that oligomerization was driven by a SxxxA motif present in the domain. Experimental data where residues S53 and A57 were mutated to leucine confirmed that this motif is involved in the self-association of this domain. This is interesting because, as discussed in Chapter 4, even seemingly conservative mutations of these residues affect pheromone signalling activity in *Sz. pombe*, and larger mutations such as the leucine mutation further affects the receptor localization.

TM2 was found to oligomerize strongly in both receptors. In STE2, a N84A and a H94A mutation were found to reduce oligomerization. Molecular dynamics simulations suggested that interactions might occur via the histidine residue, because when changing both N84 and H94 to alanine this interaction was weakened. In contrast, mutating the residues N83 and R93 in Mam2, which align to N84 and H94 in STE2 TM2, resulted in increased oligomerization of TM domains. Homology modelling of STE2 to rhodopsin suggests that the H94 residue faces the TM bundle and oligomerization via this residue implies that separate TM domains from polytopic proteins may not be stable individually, particularly not the more polar TM domains. This was further suggested by the sheer amount of structures of dissimilar conformations found for the Mam2 R93A mutant in the CHI searches.

TM5 from both receptors was also found to self-associate strongly. Fragments of this domain from STE2 have previously been shown to non-specifically aggregate (Overton and Blumer 2002) and it was therefore not pursued further. In the light of recent models of the CXCR4 receptor this is however interesting, as high-resolution crystal structures have demonstrated homo-dimerization of CXCR4 via TM5 (Wu, Chien et al. 2010). In contrast, TM3 from both receptors exhibited the lowest level of oligomerization measured for all TM domains. Low to medium CAT activity was measured from TM6, a domain that was additionally shown to be involved in CXCR4 dimerization (Wu, Chien et al. 2010). TM4 and TM7 also did not appear to self-associate in the TOXCAT assay. This was somewhat unexpected because both these

domains have previously been implied in the oligomerization of the STE2 receptor (Kim, Lee et al. 2009; Wang and Konopka 2009). It cannot be ruled out however that reporter activity would not have improved for TM domains exhibiting low CAT activity if length optimization had been performed.

6 MOLECULAR MODELS OF THE STE2 AND MAM2 G PROTEIN-COUPLED RECEPTORS

6.1 Homology Models of STE2

Homology modelling is the process by which a protein sequence of interest (the query) is aligned to a protein sequence of known structure (the template), and the structure of the query is predicted on the basis of the template. Protein structure tends to be more highly conserved than protein sequence; however mutations, deletions and insertions in the sequence all result in changes in the 3D structure of the protein. Therefore higher sequence similarity between query and template produce better models. To date there are no experimentally solved structures of the class D fungal mating pheromone receptors, and predictions must therefore be made based on alignments to the class A receptors. The low sequence similarities between the classes are likely to make models less reliable, however the overall functional and structural similarity between receptors of different classes makes modelling efforts worthwhile nevertheless. For instance, human Gα subunits have been shown to couple to both STE2 (Crowe, Perry et al. 2000) and Mam2 (Ladds, Davis et al. 2003) and yeast GPCRs are activated and desensitised similarly to the class A receptors (Chen, Lin et al. 2002; Lin, Duell et al. 2004) suggesting some degree of structural similarity between the receptors.

This chapter presents structural homology models of STE2 based on the structure of bovine rhodopsin and the human β2-adrenergic receptor. These models were compared to a previously published structural model of the STE2 receptor (Eilers, Hornak et al. 2005). To evaluate the quality of the models produced the positioning of residues important to the functioning of rhodopsin and the β2-adrenergic receptors were compared to aligned residues in STE2. These models were then used to predict whether the GxxxG motif in the first transmembrane domain of STE2 is accessible as an oligomerization interface. This chapter also continued the work presented in Chapter 5 of modelling separate transmembrane domains as individual stable units. Individual TM domains from rhodopsin and the β2-adrenergic receptor were modelled to see whether intra-protein TM domain interactions could be predicted using CHI. Individual TM domains from STE2 were also modelled to see whether the interactions found in the homology models could be reproduced. STE2 was modelled rather than Mam2 due to the low sequence similarity of Mam2 to template receptors; 20% similarity is regarded as a minimum standard (Clothia and Lesk 1986) and

even for STE2 similarity to class A receptors is only ~10%-14% for the TM spanning domains.

6.1.1 Alignment of a Previously Published Model of STE2 to Two Class A Receptors

A homology model of STE2 based on the class A receptors has previously been published, its alignment to rhodopsin and the β2-adrenergic receptors shown in Figure 6-1 (Eilers, Hornak et al. 2005). In the alignment it is notable that the TM domains in STE2 all are predicted to be shorter than the TM domains in rhodopsin and the β2-adrenergic receptor. A comparison of the number of amino acids in each helix is shown in Table 6-1. To date there appear to be no reports suggesting that the thickness of the yeast plasma membrane is different to mammalian plasma membranes however considering that on average the STE2 transmembrane domains are 5.71 residues shorter than the class A receptor's and that each residue result in a 0.15 nm rise of the helix, assuming that the tilt angles of the helices are similar then the yeast plasma membrane could possibly be ~0.86 nm thinner than mammalian plasma membrane. Moreover, the hydrophobic core of a typical cell membrane is estimated to 0.2-0.3 nm making it likely that TM helices are ~15-20 amino acids long (Beevers and Dixon 2010).

The tilt angles of the rhodopsin transmembrane domains have been estimated to be 28.4° for TM1, 27.2° for TM2, 29.6° for TM3, 3.8° for TM4, 22.7° for TM5, 7.4° for TM6 and 13.4° for TM7 (Unger, Hargrave et al. 1997). Of the least tilted domains; TM4, TM6 and TM7, TM4 and TM7 have the shortest amino sequences of all transmembrane domains. If the length of the transmembrane domain relate to its tilt then this would be expected as these domains do not need to span the same distance across the membrane as the more tilted domains. TM6 in contrast is longer which could be to accommodate the outward tilt of the helix during activation as opsin is tilted 6-7 Å outwards compared to dark state rhodopsin (Scheerer, Park et al. 2008). However, considering at the lengths of the STE2 transmembrane domains it is unlikely that the length of the domains relate clearly to their tilt angles, as the same trends are not as prominent for STE2. In STE2, although TM4 and TM7 are among the shortest domains, TM6 is the shortest. STE2 TM6 contain the characteristic proline present in 90% of GPCRs believed to enable movement of the helix upon activation (Elling, Frimurer et al. 2005) and when mutated incur constitutive activity of the yeast receptors (Konopka, Margarit et al. 1996; Ladds, Davis et al. 2005). Surprisingly in the alignment presented by Eilish and co-workers, the proline present in TM6 of STE2 does not align to the proline in TM6 of rhodopsin or the β2-adrenergic receptor.

TM domain	Rhodopsin	B2-adrenergic	STE2
1	30	30	23
2	29	29	20
3	29	29	24
4	25	25	21
5	26	26	24
6	28	28	19
7	24	24	20

Table 6-1: Comparison of TM domain lengths

Showing a comparison of the number of residues found in TM domains 1-7 from bovine rhodopsin, human β2-adrenergic receptor and STE2.

Figure 6-1: Sequence alignment of the rhodopsin, β2-adrenergic and STE2 receptors (Eilers, Hornak et al. 2005)

Alignment based on previously published models of STE2 (Eilers, Hornak et al. 2005). Row 1 shows the sequence of rhodopsin, row 2 the β2-adrenergic receptor and row 3 the STE2 receptor. Red arrows denote cuts in the sequence (i.e. the N-termini, extracellular loop 1 and 2 and the C-termini). TM1 is shown in light blue, TM2 in orange, TM3 in green, TM4 in purple, TM5 in dark blue, TM6 in red and TM7 in grey. Sequences displayed in black represent extra-membrane sequences and the residue number of rhodopsin in shown above the sequences. Gaps are represented by dots

6.1.2 Sequence Alignments Demonstrate Low Sequence Similarity between STE2 and Class A Receptors

Despite being aligned to similar criteria, the alignment presented in this chapter is considerably different to the model proposed by Eilers and co-workers (Eilers, Hornak et al. 2005) which may reflect the sequence divergence of the query and templates, and the resulting challenge in making predictions. Despite the alignments being different, the transmembrane boundaries are identical and are both in agreement with previously described experimentally defined intracellular boundaries (Choi and Konopka 2006) and very similar to predictions calculated with the TMHMM (TransMembrane prediction using Hidden Markov Models) algorithm (Krogh, Larsson et al. 2001). A comparison of the predicted TM spanning boundaries is shown in Table 6-2.

The alignment and models presented here were produced in collaboration with Dr. Stefano Costanzi from the National Institute of Diabetes & Digestive & Kidney Diseases (NIDDK) at the National Institutes of Health (NIH). Two models were built; one based on the structure of the human β2-adrenergic receptor PDB ID 2RH1 (Cherezov, Rosenbaum et al. 2007) and one based on the structure of bovine rhodopsin PDB ID 1GZM (Li, Edwards et al. 2004). The alignment is shown in Figure 6-2. Due to low sequence similarity between the template and STE2 query; 10% for rhodopsin and 14% for the β2-adrenergic receptor, the N-termini and C-termini and the extracellular loop 1 and 2 were excluded in order to produce more meaningful alignments. Furthermore, multiple alignments were built with evolutionary related receptors. Transmembrane boundaries were defined by maximising the distribution of charged residues to serve as anchors to the polar heads of the lipid bilayer.

In comparison to the previously published alignment (Eilers, Hornak et al. 2005), TM1 of STE2 is shifted four residues towards the N-termini of rhodopsin and the β2-adrenergic receptor. There are 3.6 residues per turn of a helix, and therefore this shift will result in an upward translation of the helix, rather than dramatically changing the side of the helix interacting with other helices. TM2 in the previously published alignment of STE2 is shifted 5 residues, TM3 is shifted 2 residues and TM4 is shifted 1 residue closer to the N-termini of rhodopsin and the β2-adrenergic receptor. The biggest difference is seen in TM5 where the alignment proposed by Eilers and co-workers push the helix 7 residues along the length of TM5 in rhodopsin and the β2-adrenergic receptor. In TM6 however, the previously published alignment positions the start of the helix two residues upstream from the new alignment. In TM7 there is a shift of 3 residues towards the C-terminus of the previously published alignment compared to the new alignment.

Helix	TMHMM	New alignment	Eilers *et al's* alignment	Experimentally defined intracellular boundary
1	51-73	51-73	51-73	73
2	80-102	83-102	83-102	83
3	133-155	133-156	133-156	156
4	162-184	164-184	164-184	164
5	209-231	209-232	209-232	232
6	244-266	248-266	248-266	248
7	276-298	276-295	276-295	295

Table 6-2: Comparison of STE2 TM boundaries

A comparison between the TM boundaries of STE2 defined by TMHMM (TransMembrane prediction using Hidden Markov Models), criteria set to produce the new alignment, the previously published model (Eilers, Hornak et al. 2005) and experimental data defining the intracellular boundaries (Choi and Konopka 2006). The TMHMM algorithm was accessed via the TMHMM server (http://www.cbs.dtu.dk/services/TMHMM/).

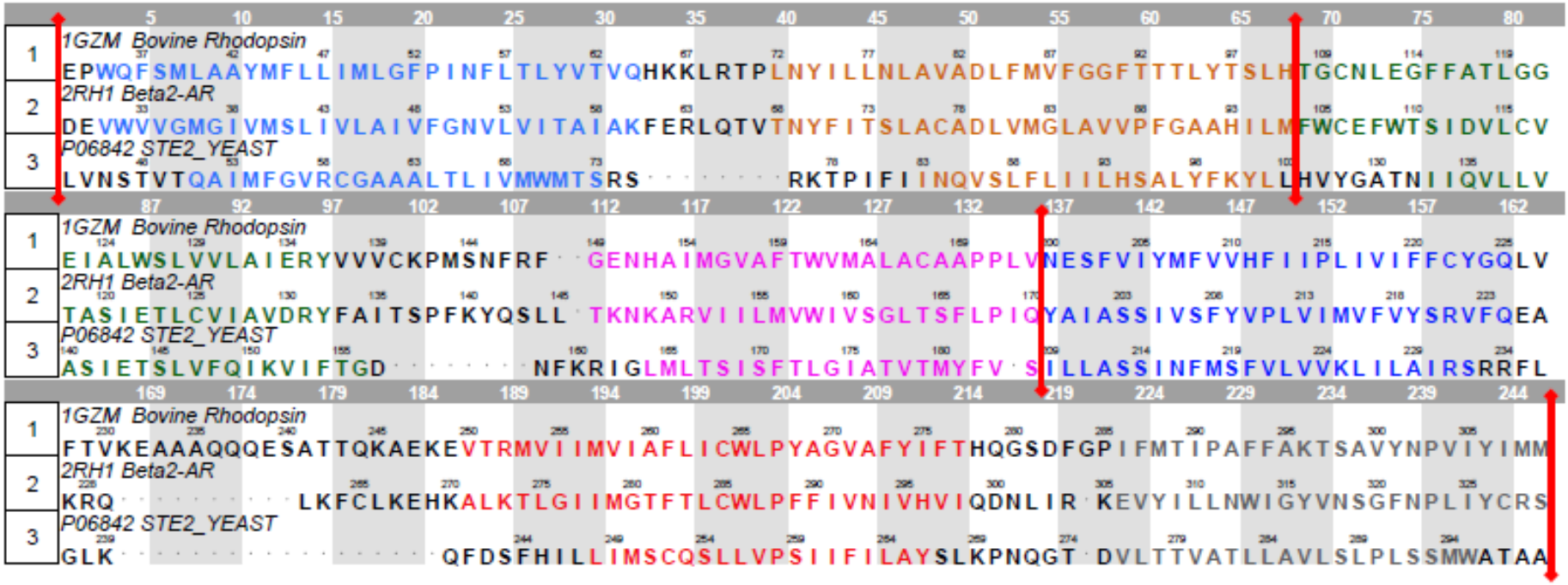

Figure 6-2: Sequence alignment of the rhodopsin, β2-adrenergic and STE2 receptors

Row 1 shows the sequence of rhodopsin, row 2 the β2-adrenergic receptor and row 3 the STE2 receptor. Red arrows denote where cuts have been made in the sequence in order to increase the percent similarity i.e. the N-termini, extracellular loop 1 and 2 and the C-termini. TM1 is shown in light blue, TM2 in orange, TM3 in green, TM4 in purple, TM5 in dark blue, TM6 in red and TM7 in grey. Sequences displayed in black represent extra-membrane sequences and the residue number of rhodopsin in shown above the sequences. Gaps are represented by dots. The alignment was made in collaboration with Dr. Stefano Costanzi from the National Institute of Diabetes & Digestive & Kidney Diseases (NIDDK) at the National Institutes of Health (NIH).

6.1.3 The Differences in Alignments Result in Different Models

The homology models of STE2 based on the previously published sequence alignment and the new alignment appear quite different from the structures of rhodopsin and the β2-adrenergic receptor, which they were modelled on. To demonstrate differences and similarities, the homology models were compared to conserved features in the class A receptors.

6.1.3.1 Close Packing of Transmembrane Domains 1 and 7

Residue G51 in TM1 of rhodopsin is important for close packing to V300 in TM7, and substitution of G51 for the structurally larger residue leucine results in misfolding of the protein and retinitis pigmentosa - an eye condition ultimately leading to blindness (Sung, Davenport et al. 1993; Hwa, Garriga et al. 1997). Close packing between helix 1 and 7 is crucial as it facilitates an H-bond between the side-chain amide of N55 to the backbone carbonyl of A299 (Figure 6-3A). In the new alignment rhodopsin G51 aligns to STE2 A62; both of which are small residues. The Cα distance between the residues in the STE2 model compared to rhodopsin are similar, with 5.1 Å in STE2 and 5.2 Å in rhodopsin. In STE2 a hydrogen bond forms between the side-chain of R58 and the backbone carbonyl of L283 (Figure 6-3B) although the bond forms on the side near the extracellular side of the membrane rather than the side near the intracellular end of the membrane as in rhodopsin. In the previously published alignment (Eilers, Hornak et al. 2005) G51 is aligned to C49, a residue which has a considerably larger side-chain than both alanine and glycine. The aligned residue in TM7 is also large – L287, and as a result of two residues with bulky side-chains the two helices are spaced much further apart with a Cα distance of 6.0 Å between residues, and there are no polar contacts between helices (Figure 6-3C). It also appears as though helix 7 is a lot straighter compared to rhodopsin TM7, which is not apparent in the new homology model of STE2 based on rhodopsin.

The β2-adrenergic receptor also contains a small residue packing against a larger residue, although for this receptor TM7 contains the small residue (G320) and TM1 contains the larger residue (I47) as shown in Figure 6-3D. This brings the two TM domains tightly together with a resulting Cα distance of 4.3 Å between the two residues and allows an H-bond to form between the side-chain amide of N51 and the backbone carbonyl of S319 (Figure 6-3D). Both homology models of STE2 based on the β2-adrenergic receptor have a Cα distance of 4.6 Å between the residues aligning to I47 and G320 which is slightly more distal compared to the template receptor (Figure 6-3E&F for the model proposed in this thesis compared to the model proposed by Eilers and co-workers respectively). Neither of

the homology models based on the β2-adrenergic receptor facilitates a polar contact between TM1 and TM7 in contrast to what is observed in the β2-adrenergic receptor.

Neither of the homology models exposes residues T278, A285 and L285 in TM7 to the lipid bilayer. These residues have previously been implicated in oligomerization of STE2 (Kim, Lee et al. 2009) suggesting that they might face the lipid bilayer.

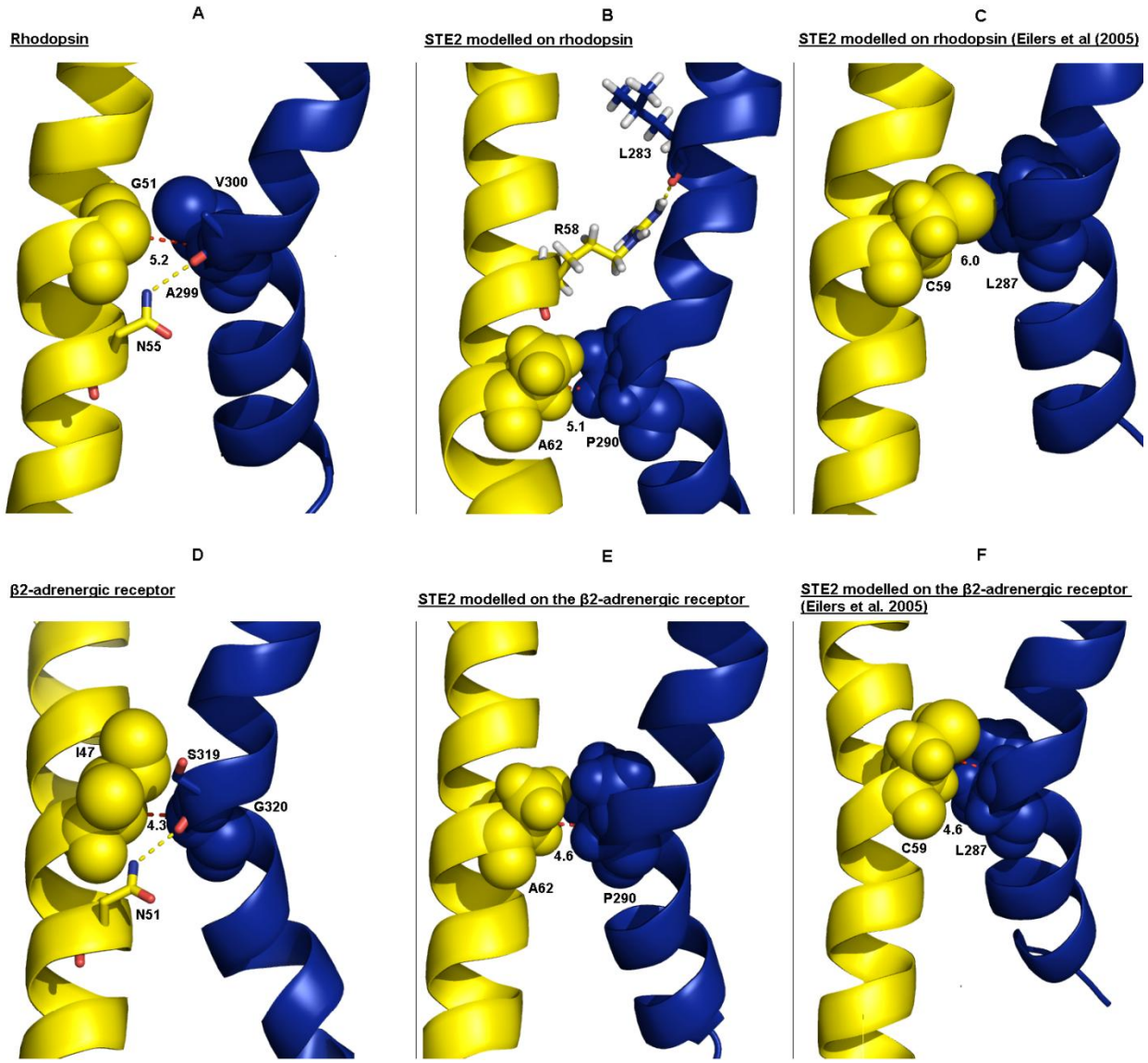

Figure 6-3: Homology models of STE2 TM1 and TM7 on bovine rhodopsin and the human β2-adrenergic receptor

Homology models of STE2 TM1 and TM7 based on bovine rhodopsin and the human β2-adrenergic receptor. TM1 and TM7 are shown in yellow and blue respectively. Spheres mark the residues important for close packing of TM1 and TM7 in the two class A receptors. The corresponding residues in STE2 are shown as spheres. The distance between the Cα atoms in these residues is shown by the red dotted line. The yellow dotted line shows the hydrogen bonds between helices and interacting residues are represented as stick models. All models were built using the full alignments but TM2, TM3, TM4, TM5 and TM6 are not shown for clarity. **A:** Structure of bovine rhodopsin (Li, Edwards et al. 2004). **B:** Homology model of STE2 to bovine rhodopsin based on the new alignment. **C:** Homology model of STE2 to rhodopsin based on the previously published alignment (Eilers, Hornak et al. 2005). **D:** Structure of the human β2-adrenergic receptor (Cherezov, Rosenbaum et al. 2007). **E:** Homology model of STE2 to the β2-adrenergic receptor based on the new alignment. **F:** Homology model of STE2 to the β2-adrenergic receptor based on the alignment made by Eilers and co-workers.

6.1.3.2 Interactions between Transmembrane Domains 2, 3 and 4

In the new alignment, TM2 does not span the portion of rhodopsin TM2 containing the highly conserved residue N78 whose side-chain hydrogen bonds to the indole nitrogen of W161, conserved in 97% of class A receptors, shown in Figure 6-4A (Li, Edwards et al. 2004). In rhodopsin, W161 spans the gap between TM4 and TM2 and is responsible for effectively locking TM3 in place. In the new alignment this residue is replaced by L173, however in STE2 the side-chain appears to point into the lipid bilayer rather than providing a 'lock' effect, as shown in Figure 6-4B. In the alignment proposed by Eilers and co-workers (2005) W161 aligns to G174, a much smaller residue. The model based on this alignment also contains an extensive hydrogen bonding network between TM2, TM3 and TM4 (Figure 6-4C) like in rhodopsin, although they appear dissimilar.

TM2, TM3 and TM4 in the β2-adrenergic receptor also contain a network of polar contacts (shown in Figure 6-4D) (Rasmussen, Choi et al. 2007). This appears to have a similar effect to the network found in bovine rhodopsin in that TM3 is locked into position by a tryptophan in TM4; residue W158 for the β2-adrenergic receptor, which H-bond to the side-chain hydroxyl group on S74 in TM2. Neither model of STE2 based on the β2-adrenergic receptor contains this interaction between TM2 and TM4 as shown in Figure 6-4E and F for the model presented here and Eilers and co-worker's (2005) model respectively.

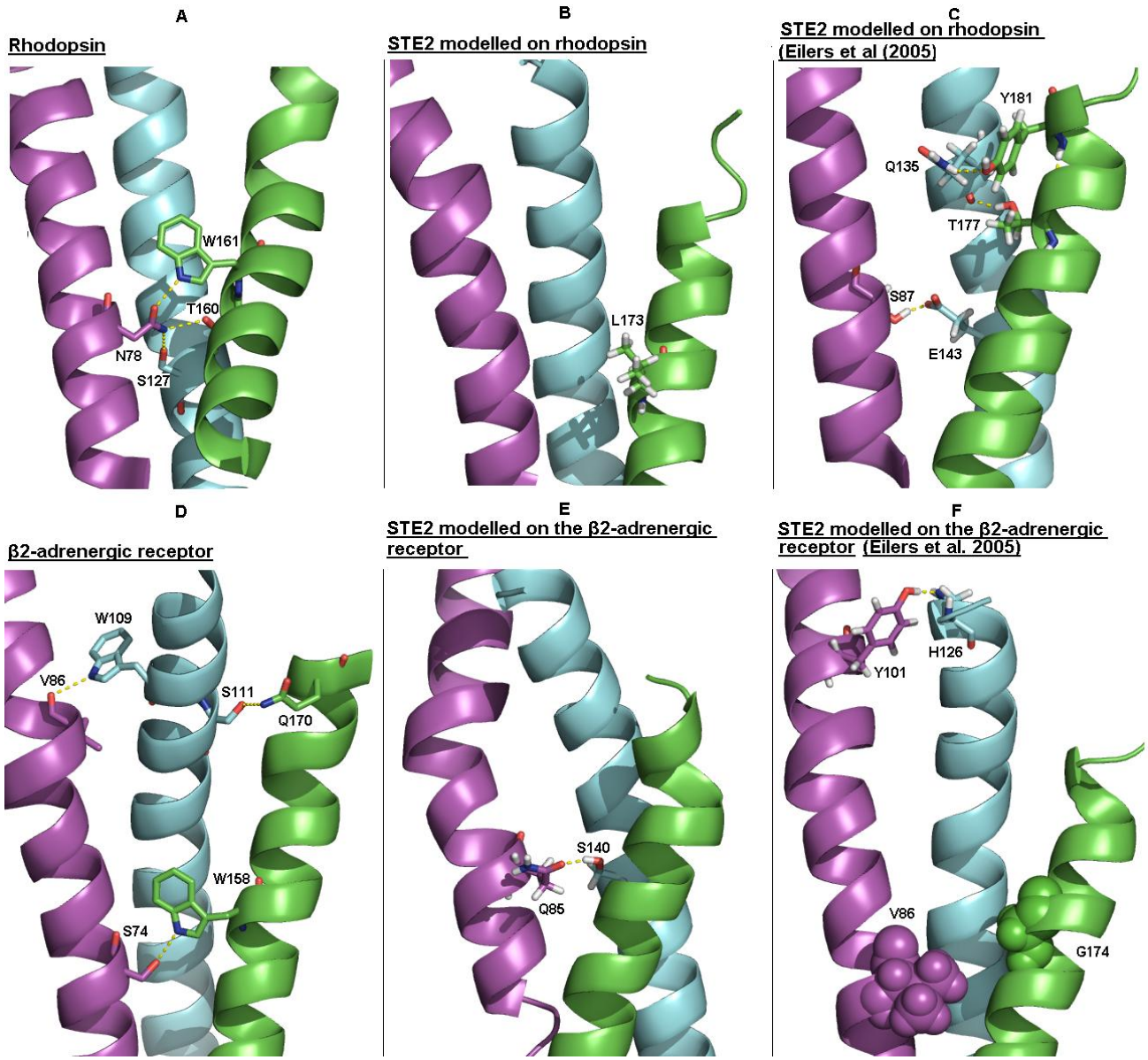

Figure 6-4: Homology models of STE2 TM2, TM3 and TM4 on rhodopsin and β2-adrenergic receptor

Homology models of STE2 TM2, TM3 and TM4 based on bovine rhodopsin and human β2-adrenergic receptor. TM2 is shown in purple, TM3 in cyan and TM4 in green. Hydrogen bonds between helices are shown by the yellow dotted line and interacting residues are represented as stick models. All models were built using the full alignments but TM1, TM5, TM6 and TM7 are not shown for clarity. **A:** Structure of bovine rhodopsin (Li, Edwards et al. 2004). **B:** Homology model of STE2 to bovine rhodopsin based on the new alignment. **C:** Homology model of STE2 to bovine rhodopsin based on the previously published alignment (Eilers, Hornak et al. 2005). **D:** Structure of human β2-adrenergic receptor (Cherezov, Rosenbaum et al. 2007). **E:** Homology model of STE2 to the β2-adrenergic receptor based on the new alignment.

6.1.3.3 Presence of the Ionic Lock in the Homology Models

Class A GPCRs in the inactive state are believed to contain an 'Ionic lock' formed between a highly conserved E/DRY motif located on the intracellular side of TM3 and acidic residues in TM6. The presence of an ionic lock has been demonstrated in inactive bovine rhodopsin (Li, Edwards et al. 2004) and human dopamine D3 receptor (Chien, Liu et al. 2010). In the crystal structure of the β2-adrenergic receptor the ionic lock was absent, however it was argued that the presence of T4 lysozyme may have disrupted the interaction (Rasmussen, Choi et al. 2007; Rosenbaum, Rasmussen et al. 2009) and its presence is important to stabilize the inactive conformation as its disruption results in constitutive activity of the receptor (Ballesteros, Jensen et al. 2001). In the crystal structure of activated rhodopsin the ionic lock is disrupted (Scheerer, Park et al. 2008) and these residues are also observed to move apart in the crystal structure of activated adenosine A_{2A} receptor (Xu, Wu et al. 2011).

In rhodopsin the ionic lock is formed via a hydrogen bond between the side-chain guanidium group of R135 in TM3 and the side-chain carboxylate group of E247 in TM6 (shown in Figure 6-5A) (Li, Edwards et al. 2004). The fungal GPCRs in contrast do not contain an E/DRY motif in TM3. In the alignment of STE2 to bovine rhodopsin and human β2-adrenergic receptor the E/DRY motif align to residues V_{152}IF in the alignment presented in this thesis (see Figure 6-2) and I_{150}KV in the previously published alignment (Eilers, Hornak et al. 2005) (see Figure 6-1). In TM6, E247 in rhodopsin align to L238 in the alignment presented in this thesis and Q240 in the previously published alignment (Eilers, Hornak et al. 2005).

In the homology model of STE2 based on the previously published alignment (Eilers, Hornak et al. 2005) to rhodopsin and the β2-adrenergic receptor there was no hydrogen bond formed between TM3 and TM6. In contrast, both homology models presented in this thesis based on the alignment to rhodopsin and the β2-adrenergic receptor contained a hydrogen bond between Q149 in TM3 and H245 in TM6 (shown in Figure 6-5B and Figure 6-5C respectively). The models of STE2 presented in this thesis therefore contain a putative ionic lock in contrast to the previously published homology model of STE2.

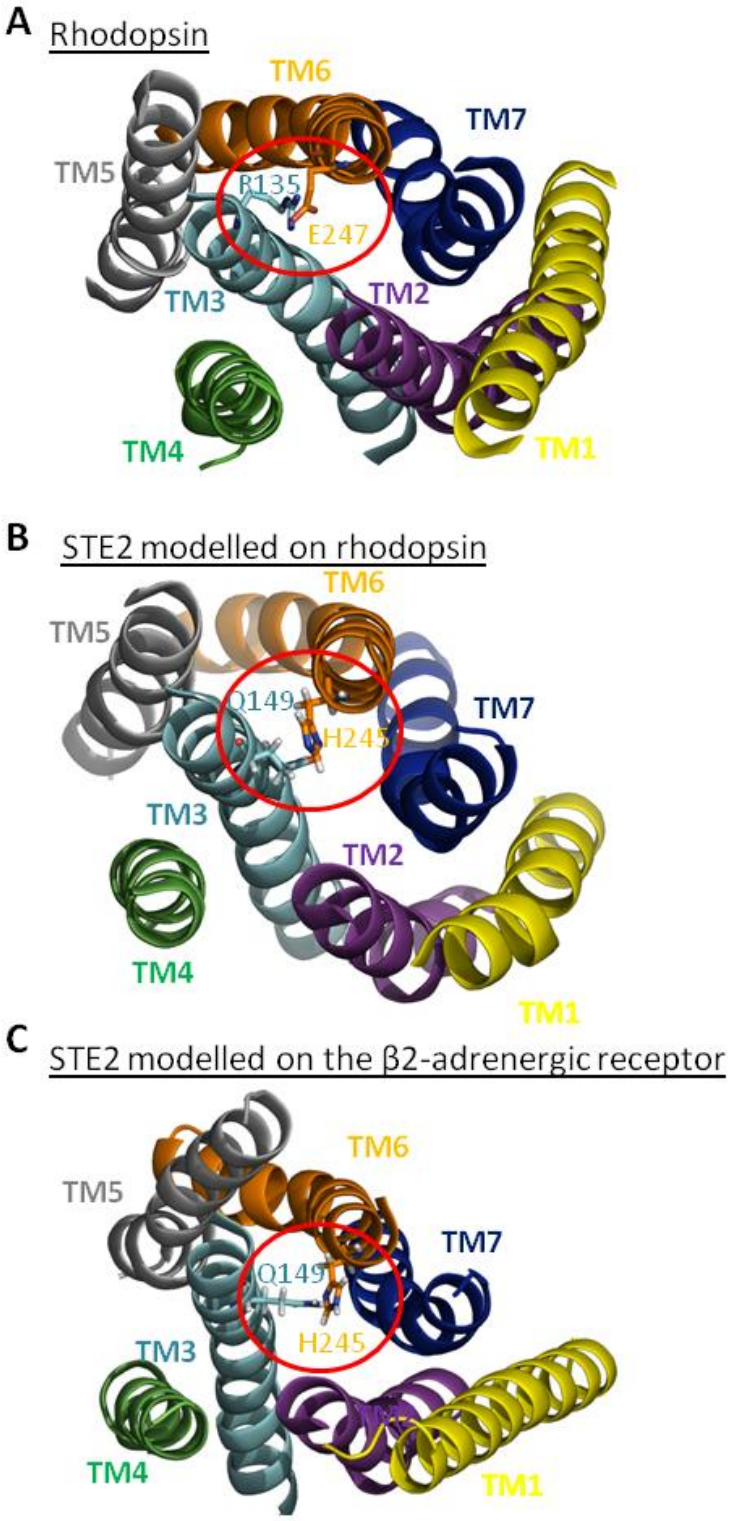

Figure 6-5: Presence of a putative ionic lock in the homology models of STE2

Intracellular view of the ionic lock present in **A:** Rhodopsin PDB ID: 1GZM (Li, Edwards et al. 2004). **B:** STE2 based on the structure of bovine rhodopsin (PDB ID: 1GZM (Li, Edwards et al. 2004)) and the alignment presented in this thesis. **C:** STE2 based on the structure of human β2-adrenergic receptor (PDB ID: 2RH1 (Cherezov, Rosenbaum et al. 2007)) and the alignment presented in this thesis. The ionic lock is circled in red and interacting residues are shown as stick models.

6.1.3.4 Presence of Proline Residues in the Receptors

Proline is unique among the amino acids because its amino nitrogen is cyclised with the terminal carbon of the propyl side-chain. Proline therefore cannot occupy many main-chain conformations easily occupied by other amino acids and consequently proline distorts secondary structures by introducing a kink in α-helices or melting β-sheets (Nilsson and von Heijne 1998). Proline residues are consequently most commonly found at the start of α-helices and β-sheets, or within loops, turns or unordered structures of proteins (Reiersen and Rees 2001) with the notable exception of transmembrane helices where proline residues are often found in the middle of the helix (Barlow and Thornton 1988). Figure 6-6A shows hydrogen bonding within the main-chain of a canonical α-helix containing no proline residues. As illustrated by the yellow dotted lines, the backbone N-H group of residue *i* hydrogen bonds the backbone C=O group of the residue found four residues preceding *i*.

Proline residues introduce kinks in helices because its cyclic side-chain prevents hydrogen bonding of the backbone amine *i* to the *i-4* backbone carbonyl causing a steric clash and bending of the helix as a consequence. This bend further prevents hydrogen bonding of the *i+1* backbone amine to the *i-3* carbonyl. Remarkably, proline residues are present at 60% of transmembrane helix deformation sites and it's been proposed that in cases where proline is not present, the proline could have been lost with time as the kink got stabilized by other molecular forces (Yohannan, Faham et al. 2003). Mutations of transmembrane proline residues have been shown to have an effect on both ligand binding and activation of GPCRs (Ladds, Davis et al. 2005; Reis, Santos et al. 2007; Mazna, Grycova et al. 2008) demonstrating their importance. With the exception of TM6 and TM7, proline is absent from the TM domains in STE2 (see Figure 6-2). This is in contrast to bovine rhodopsin and human β2-adrenergic receptor that contain prolines in all TM domains except TM3. The proline containing TM domains TM6 and TM7 are highly conserved between Mam2 and STE2 as illustrated in the alignment shown in Table 6-3. The proline present in TM6 (Table 6-3A) is conserved in both the class A receptors and the fungal receptors and plays a pivotal role in GPCR activation (Ladds, Davis et al. 2005; Schwartz, Frimurer et al. 2006). Prolines are believed to reduce the stability and rigidity of TM helices due to the loss of the NH···O=C bond thereby allowing a "global toggle switch" upon activation through motion flexibility (Elling, Frimurer et al. 2005; Schwartz, Frimurer et al. 2006).

As illustrated in the left panel of Figure 6-6B and C, the conserved proline residue (shown in green) in TM6 introduce a kink in the TM domain of both bovine rhodopsin and human β2-adrenergic receptor. Consequently there is an absence of two hydrogen bonds between the N-H group of P267 and the C=O group of I263 (red dots) and the N-H group of Y268 and

C=O group of C264 (black dots) in rhodopsin (Figure 6-6B left panel). H-bonds present within the main-chain are illustrated by yellow dots. Similarly for the β2-adrenergic receptor (Figure 6-6C left panel) there is an absence of a hydrogen bond between the N-H group of P288 and the C=O group of L284 (red dots) and the N-H group of F289 and the C=O group of C285 (black dots).

The models presented in this thesis align the STE2 TM6 proline with the homologous residues in rhodopsin and the β2-adrenergic receptor and as a result the main-chain of the homology models of STE2 look very similar to the class A receptors (shown in Figure 6-6B and C, middle panel, for the model based on rhodopsin and the β2-adrenergic receptor respectively). Hydrogen bonds present within the main-chain are illustrated by yellow dots. The models contain no hydrogen bond between the N-H group of P258 and the C=O group of S254 (red dots) and the N-H group of S259 and the C=O group of L255 (black dots) in STE2, denoting a loss of the *i-4* to *i* and *i+1* to *i-3* hydrogen bonds.

Interestingly in contrast, the previously published model of STE2 (Eilers, Hornak et al. 2005) did not align to the proline residue in TM6 of STE2 to the proline residue in TM6 of the class A GPCRs (see Figure 6-1). Consequently the main-chain of the STE2 homology model is structurally considerable different to the main-chain of the class A GPCRs and contain an additional helix deformation site. The model of STE2 based on rhodopsin is shown in the right panel of Figure 6-6B. This model lacks the *proline* to *proline-4* hydrogen bond (cyan dots in the right panel of Figure 6-6B) as expected (the H-bond between the N-H group of P258 to the C=O group of S254). It does not however lack the *proline+1* to *proline-3* hydrogen bond (and as it is present this bond is represented by yellow dots). The break in the helix imposed by structural alignment to rhodopsin are represented by red and black dots and occur between the N-H groups of I260 and I261 to the C=O groups of L256 and V258 respectively. In this model there is also a loss of an additional H-bond between the N-H group of L264 and the C=O group of S259 (represented by purple dots in the right panel of Figure 6-6B). The model of STE2 to the β2-adrenergic receptor based on the alignment by Eilers and co-workers (2005) does contain a H-bond between the N-H group of L264 and the C=O group of S259 (therefore shown as yellow dots) but besides this bond there is an absence of the same H-bonds as the model based on the crystal structure of rhodopsin (Figure 6-6C, right panel).

The alignment presented in this thesis therefore appear to produce models that more closely resemble the class A GPCRs on which they are modelled compared to the previously published model (Eilers, Hornak et al. 2005). This may suggest that the alignment presented

in this thesis is based on more relevant criteria and consequently may have produced more accurate models.

A																
TM6																
Rhodopsin	M	V	I	A	F	L	I	C	W	L	**P**	Y	A	G	V	A	F
β2-adrenergic receptor	I	M	G	T	F	T	L	C	W	L	**P**	F	F	I	V	N	I
STE2	L	I	M	S	C	Q	S	L	L	V	**P**	S	I	I	F	I	L
Mam2	L	V	I	S	C	Q	C	L	I	V	**P**	A	T	F	T	I	I

B																			
TM7																			
Rhodopsin	I	F	M	T	I	**P**	A	F	F	A	K	T	S	A	V	Y	N	**P**	V	I
β2-adrenergic receptor	E	V	Y	I	L	L	N	W	I	G	Y	V	N	S	G	F	N	**P**	L	I
STE2	V	L	T	T	V	A	T	L	L	A	V	L	S	L	**P**	L	S	S	M	W
Mam2	G	F	S	S	M	T	Q	C	L	L	I	I	S	L	**P**	L	S	S	L	W

Table 6-3: Alignment of core residues in TM6 and TM7 of rhodopsin, β2-adrenergic receptor, STE2 and Mam2

Showing the alignment of core TM residues in TM6 and TM7 of the budding yeast STE2 GPCR and fission yeast Mam2 GPCR and aligned residues in bovine rhodopsin and human β2-adrenergic receptor. Proline residues in the two TM domains are highlighted in red. **A:** Aligned residues in TM6 spanning M257-F273 in rhodopsin, I278-I294 in the β2-adrenergic receptor, L248-L264 in STE2 and L251-I267 in Mam2. **B:** Aligned residues in TM7 spanning I286-I305 in rhodopsin, E306-I325 in the β2-adrenergic receptor, V276-W295 in STE2 and G276-W295 in Mam2.

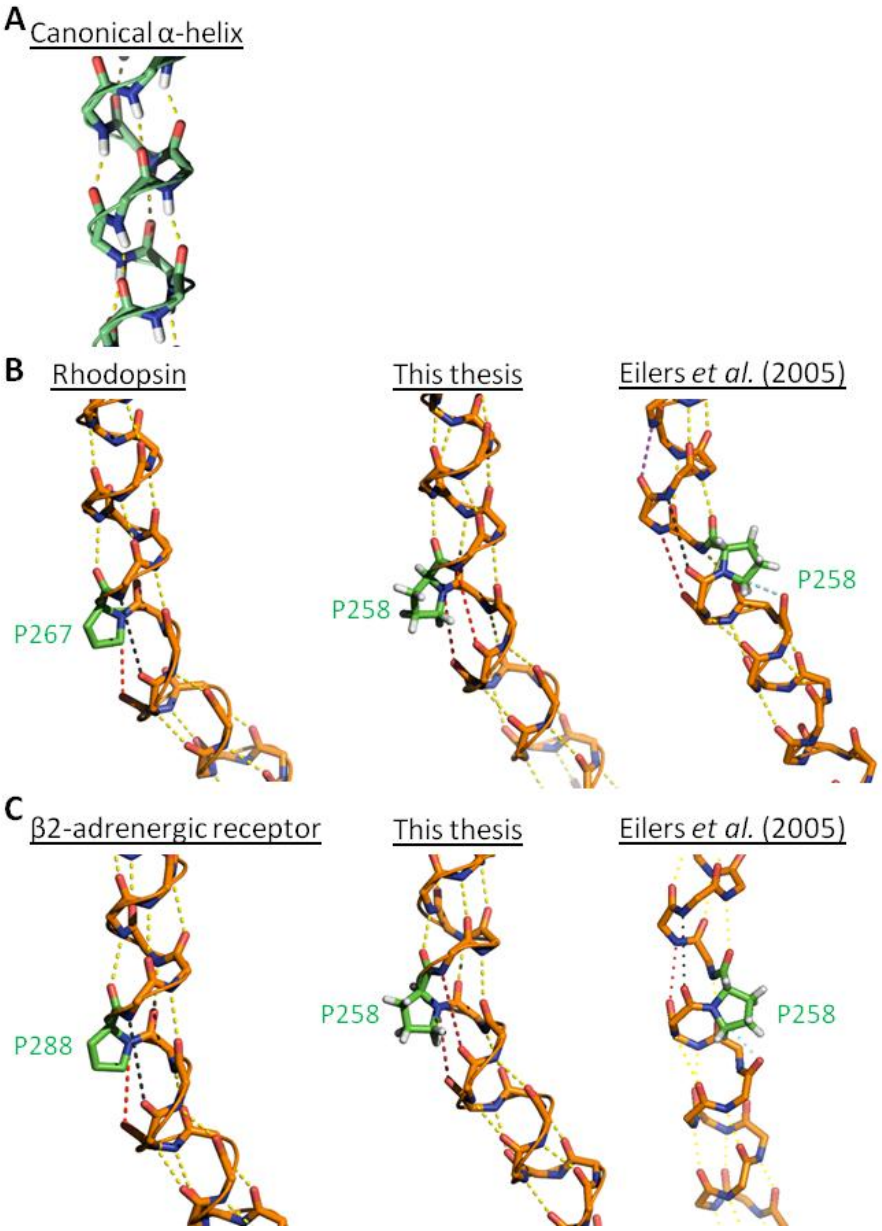

Figure 6-6: Effect of a conserved proline residue on hydrogen-bonding in the main-chain of TM6 of GPCRs

Illustrating the disruptive effects of a proline residue on intra-main-chain hydrogen-bonding in TM6 of GPCRs. All GPCR models (B-C) were produced by modeling the full-length protein but only TM6 is shown for clarity. Yellow dots represent existing hydrogen-bonds within the models. Bonds represented by other colors denote the absence of a bond that would be present in a canonical α-helix. **A:** Side-view of the main-chain of a canonical α-helix. Note that the N-H group of residue *i* hydrogen bonds to the C=O group of the *i-4* residue. **B:** Crystal structure of rhodopsin PDB ID: 1GZM (Li, Edwards et al. 2004) (left panel), model of STE2 based on 1GZM and the alignment presented in this thesis (middle panel), model of STE2 based on 1GZM and the previously published alignment (Eilers, Hornak et al. 2005) (right panel). **C:** Crystal structure of the β2-adrenergic receptor PDB ID: 2RH1 (Cherezov, Rosenbaum et al. 2007) (left panel), model of STE2 based on 1GZM and the alignment presented in this thesis (middle panel), model of STE2 based on 1GZM and the previously published alignment (Eilers, Hornak et al. 2005) (right panel).

6.1.4 The New Models of STE2 Renders the GxxxG Motif Accessible for Interactions unlike the Previously Published Model

Several studies have suggested that the GxxxG motif in the first TM domain of STE2 is pivotal to oligomerization of the receptor (Overton and Blumer 2002; Overton, Chinault et al. 2003; Gehret, Bajaj et al. 2006). Work presented in Chapter 4 of this thesis showed that mutations to the GxxxG motif cause mis-localization of the receptor, and decreased cellular signalling in response to pheromone, although the work presented in Chapter 5 implied that TM1 is not sufficient alone to induce oligomerization.

If the GxxxG motif is involved in directly mediating receptor-receptor interactions then the motif would be expected to be available at the lipid interface, as opposed to being buried in the TM bundle. In both models of STE2 presented in this thesis the GxxxG motif is located at the lipid interface (shown in Figure 6-7A for the model based on the structure of bovine rhodopsin and Figure 6-7C for the model based on the structure of the human β2-adrenergic receptor). This is in contrast to the previously published model of STE2 (Eilers, Hornak et al. 2005) where the GxxxG motif is not readily accessible at the protein-lipid interface (shown in Figure 6-7B for the model based on the structure of bovine rhodopsin and Figure 6-7D for the model based on the structure of the human β2-adrenergic receptor). This further suggests that the models presented in this thesis represent more meaningful structures than the previously published models.

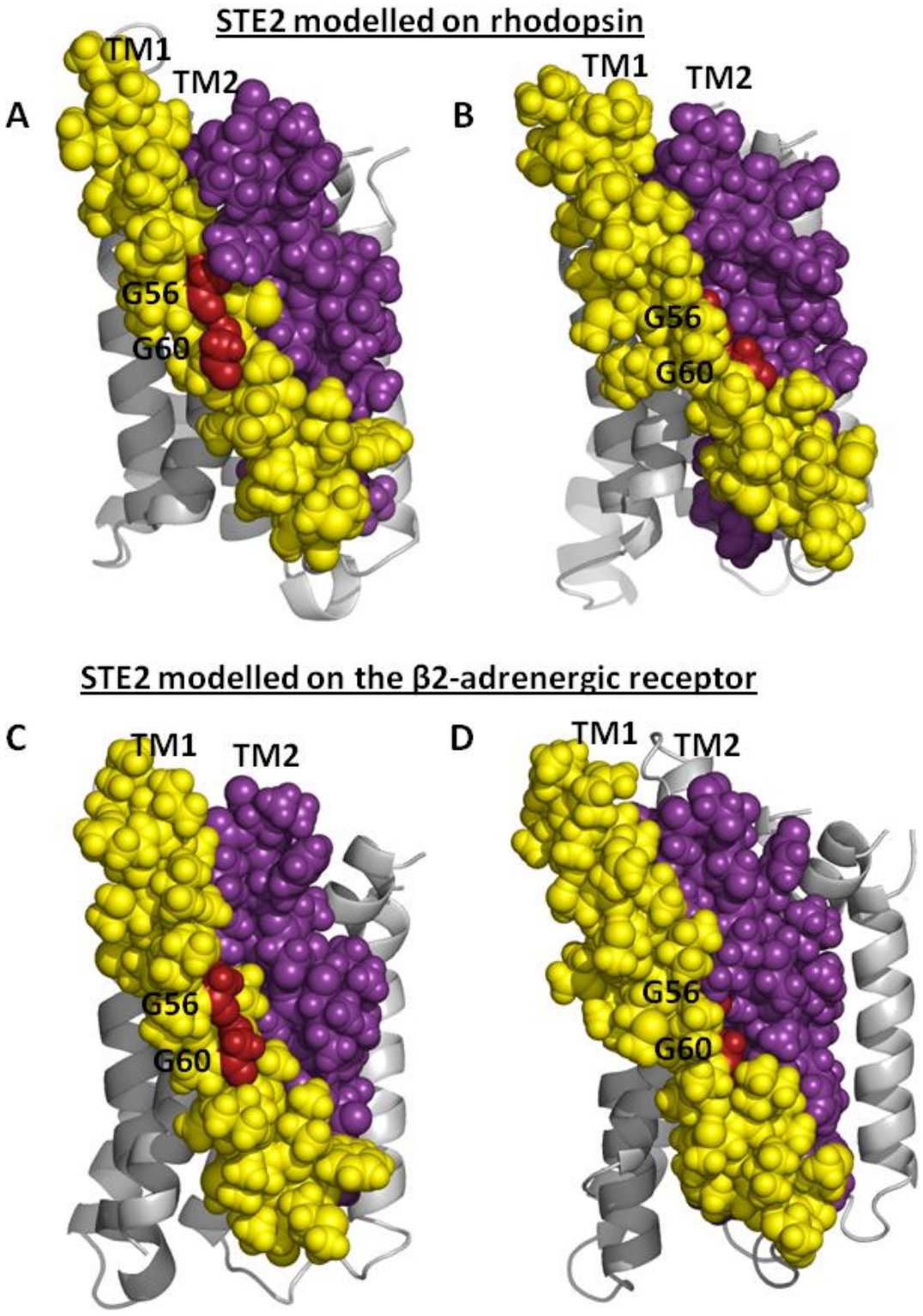

Figure 6-7: The GxxxG motif is accessible for interactions in the new models

Showing the homology models of STE2. TM1 is shown in yellow, TM2 in purple and the GxxxG motif in TM is shown in red. **A:** Modeled on rhodopsin based on the new alignment **B:** Modeled on rhodopsin based on the alignment by Eilers and coworkers (Eilers, Hornak et al. 2005). **C:** Modeled on the β2-adrenergic receptor based on the new alignment **D:** Modeled on the β2-adrenergic receptor based on the alignment by Eilers and coworkers (Eilers, Hornak et al. 2005).

6.2 Molecular Modelling of Interactions in Individual Transmembrane Domains

The software suite CHI has previously been used to successfully predict oligomerization of several TM-spanning proteins (Adams, Arkin et al. 1995; Brunger, Adams et al. 1998; Jenei, Borthwick et al. 2009; Pang, Savva et al. 2009; King, Oates et al. 2011) but not interactions within TM domains of large polytopic proteins such as GPCRs. As discussed in the introduction, the two-stage model of membrane protein folding postulates that individual TM domains in polytopic proteins can be regarded as individual stable domains (Popot and Engelman 1990; Engelman, Chen et al. 2003). To further explore this possibility, oligomerization of TM1 and TM2 from bovine rhodopsin was modelled using CHI and compared to the crystal structure of the receptor (Li, Edwards et al. 2004). TM1 and TM2 were chosen because they do not appear to undergo extensive rotation upon activation (Scheerer, Park et al. 2008) and do not contain inter-helical hydrogen-bonds, a property which was considered desirable due to the modelling of non-polar TM1-TM1 interactions in Chapter 5 of this thesis. Since data from different searches cannot easily be assembled and because CHI exports data in a format compatible with the UNIX platform, a script was written to extract data from multiple CHI searches and to make the data windows compatible. This script was similar to the one written for Chapter 5 but handles data from hetero-oligomers.

Figure 6-8A shows TM1 (yellow) and TM2 (purple) from the crystal structure of bovine rhodopsin (Li, Edwards et al. 2004). Residues I48 in TM1 and V87 in TM2 are located at the interface of the two TM domains and are shown as van der Waals spheres. These two residues were highlighted in the CHI models to identify models containing a similar geometry to the crystal structure. Figure 6-8B shows the right-handed solutions to CHI modelling of oligomerization of bovine rhodopsin TM1 and TM2. None of the structures appearing in more than one CHI search display similar packing to the crystal structure. Figure 6-8C shows the left-handed solutions. Like when modelling homo-oligomerization of GPCR TM domains (see Chapter 5), fewer left-handed solutions were found compared to right-handed solutions. Again, structures appearing in more than one run did not resemble the crystal structure. These results suggest that TM domains in complex polytopic proteins cannot be modelled as individual domains and therefore this was not explored further.

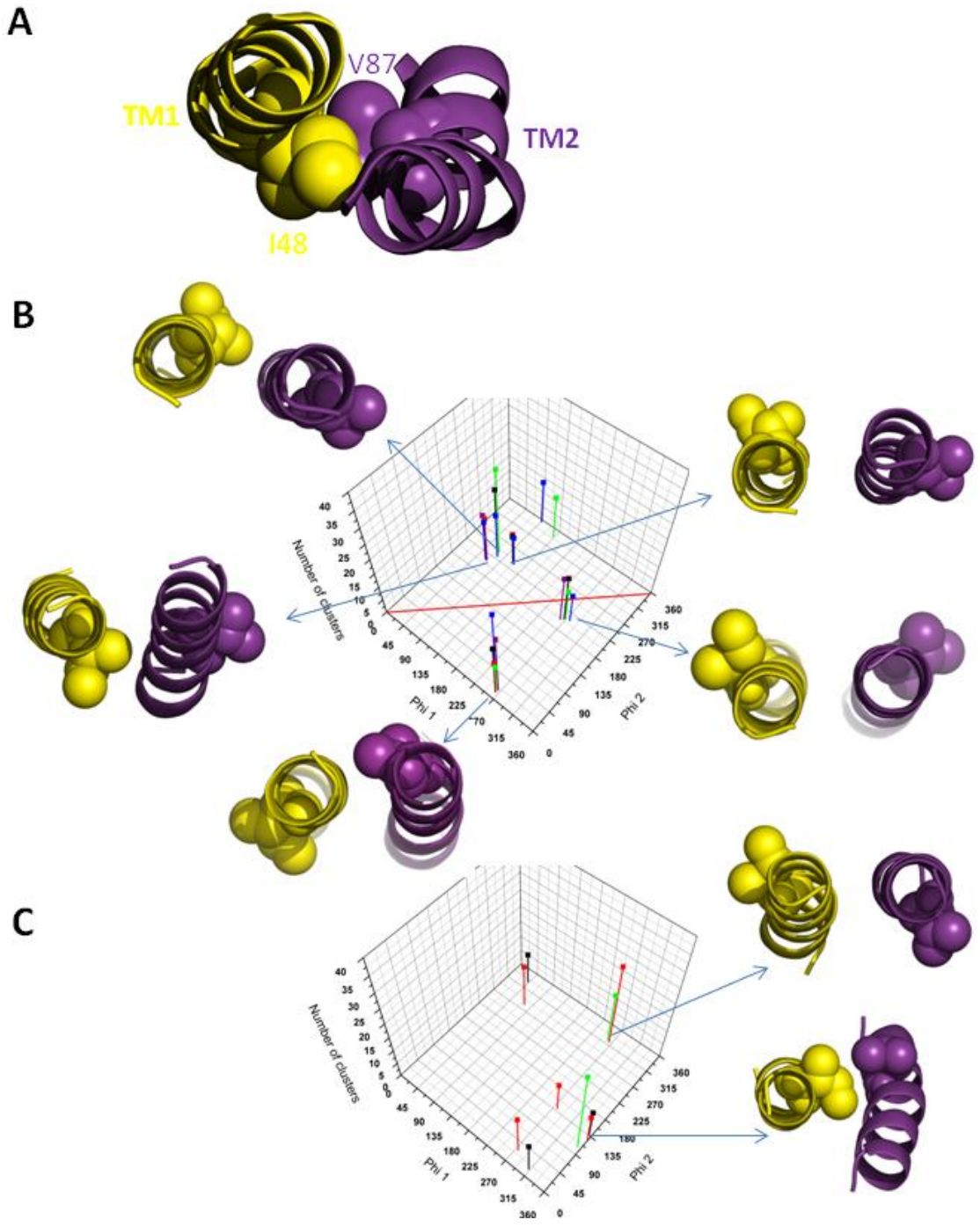

Figure 6-8: CHI models of interactions between TM1 and TM2 in bovine rhodopsin

Using CHI modeling to predict the interactions between bovine rhodopsin TM1 and TM2. Four MD repeats using random starting velocities were performed in five separate searches. When >10 separate structures with Cα RMSD values within <1 Å were found their structure was averaged to generate a "cluster", indicated by different colours in the phi plots. Structural models of clusters found in >1 search are indicated by the arrows projecting from the phi plots. **A:** Showing the relative orientation of TM1 (yellow) and TM2 (purple) of bovine rhodopsin as determined by X-ray crystallography (Li, Edwards et al. 2004). Residues I48 and V87 are located at the helix-helix interface and are highlighted as van der Waals spheres. **B:** Right-handed solutions from the CHI modeling. **C:** Left-handed solutions from the CHI modeling.

6.3 Summary

This chapter compared and contrasted new homology models of the fungal STE2 GPCR to a previously published model of the receptor (Eilers, Hornak et al. 2005). These models were based on alignments to solved structures of the class A GPCRs bovine rhodopsin (Li, Edwards et al. 2004) and the human β2-adrenergic receptor (Rasmussen, Choi et al. 2007). Alignments of these receptors are challenging to produce due to the low sequence similarity between the fungal GPCRs and class A GPCRs and therefore structural features were compared and contrasted between the homology models and the template receptors.

The homology models presented in this thesis appear to represent more relevant and accurate structural models than the model proposed by Eilers and co-workers (2005) for several reasons. Firstly, the GxxxG motif implied as an oligomerization motif of the receptor is located at the protein-lipid interface in the models presented in this thesis. Secondly, the conserved proline in TM6 is located at the helix deformation site and thirdly, TM3 and TM6 interact via a hydrogen bond which may represent an ionic lock important for stabilizing the inactive state of class A receptors. In contrast, in the previously published model of STE2 the GxxxG motif is buried into the TM bundle, the conserved proline in TM6 forms a second helix deformation site and there is no hydrogen bond between TM3 and TM6.

This chapter also sought to validate the methods used in Chapter 5 where oligomerization of the receptor was modelled based on interactions between single TM domains. This was done by modelling the interactions between TM1 and TM2 in bovine rhodopsin to see if the crystal structure of this portion of the GPCR could be reproduced. This was unsuccessful however through using CHI modelling. This raises questions as to how useful CHI modelling is to predict TM-TM interactions and also how physiologically relevant it is to study interactions in polytopic proteins via single TM domains.

7 THE DEVELOPMENT OF A LUMINESCENT REPORTER SYSTEM FOR THE *SCHIZOSACCHAROMYCES POMBE* PHEROMONE-RESPONSE PATHWAY

7.1 Background

7.1.1 Reporter Systems

It is often desirable to study changes in genetic activity in signalling pathways. Traditionally used techniques to study gene expression, such as northern blots, are however often time-consuming and therefore costly. Instead, gene reporter systems are today commonly used to quantify the transcription of genes under the control of a promoter of interest. The reporter should be easily quantified and ideally have sufficiently low mRNA stability and protein half-life to accurately reflect changes in transcriptional activity. The use of bacterial reporters to probe eukaryotic gene regulation was commenced in the 1980's using the genes *cat* (Gorman, Moffat et al. 1982) and *lacZ (Sambrook, Fritsch et al. 1989)*. The bacterial protein CAT catalyzes the transfer of acetyl groups from acetyl CoA to chloramphenicol, which detoxifies the antibiotic. The acetylation reaction of CAT was traditionally measured using radiolabels although nowadays there are fluorescent alternatives available. The *lacZ* gene encodes β-galactosidase which has traditionally been a popular reporter because it can be monitored both quantitatively and qualitatively (Serebriiskii and Golemis 2000). β-galactosidase hydrolyzes a range of substrates including the synthetic substrate o-nitrophenol β-D-galactopyranosidase to form a yellow product. This product can readily be quantified using a spectrophotometer; however assays tends to be time-consuming, low-throughput, performed in lysed cells and it is also possible to measure endogenous cellular activity.

The development of luminescent reporters marked a key advance in using reporter assays to monitor changes in transcriptional events. Luminescent reporters are proteins that catalyze a reaction to produce light, which can be quantified. The development of assays involving the expression of the bioluminescent protein luciferase in heterologous systems, derived from organisms such as click beetle luciferase and firefly luciferase, resulted in highly sensitive assays. Click beetle luciferase however require the use of cofactors which are typically not available *in vivo* in sufficiently high amounts, and firefly luciferase require an

exogenously added substrate for luminescence which is not membrane permeable, meaning that cells must be lysed (Naylor 1999). The development of the GFP reporter removed the requirement for an exogenously added substrate and quantification could be done *in vivo* rather than on cell lysate (Kain, Adams et al. 1995). Both fluorescence and bioluminescence produce photons upon transition from excited state molecular orbitals to lower energy orbitals. Fluorescence and bioluminescence differ however in how the excited states are achieved; fluorescent molecules are excited by light whereas bioluminescent molecules catalyze chemical reactions producing photons. Bioluminescence has the advantage over fluorescence in that no influx of light is required, thereby reducing background noise. The GFP reporter however allows automated assays using intact cells, resulting in high-throughput data. The development of the *Renilla reniformis* luciferase Rluc as a reporter removed the requirement of using cell lysate in luciferase assays because its substrate coelenterazine can cross cell membranes. Assays can therefore be performed *in vivo* similar to the GFP reporter but without the high background noise. The half-life of coelenterazine is short, ~17 minutes, and result in a high degree of auto-luminescence in cells (Promega 2009). The development of the stable coelenterazine derivative EnduRen (Promega Corporation, Southampton, UK) instead allow stable luminescence measurements over long periods of time with low auto-luminescence making the reporter suitable for high-throughput experiments over time.

7.1.2 Existing *Schizosaccharomyces pombe* Reporter Systems

Several methods currently exist for the quantification of the *Sz. pombe* pheromone response including the β-galactosidase and GFP-based reporter assays. As outlined in section 1.4.3 however, these reporter assays may be insensitive, low-throughput, or rely on lysed cells and it is therefore desirable to develop and characterize alternative reporter assays. The luminescent reporter Rluc is regarded as a more sensitive reporter than GFP because of low background noise in assays. The enzyme also does not require any post-translational modifications unlike β-galactosidase or GFP thereby reducing maturation time, and it has a short half-life of only 0.5-1 h (Loening, Fenn et al. 2006). The Rluc reporter may therefore provide a more sensitive reporter able to detect the pheromone-response earlier than GFP-based assays, whilst maintaining the advantage of allowing continuous high-throughput assays to be performed. The work presented in section 4.5 demonstrated that Rluc, when expressed as a receptor fusion under the control of the *nmt1* promoter, functioned in *Sz. pombe* but did not couple energetically to GFP. It was therefore of interest to optimize the conditions under which the activity of Rluc is assayed. This chapter discusses the

development and characterization of a bioluminescence based reporter system for the *Sz. pombe* pheromone-response pathway using the *Renilla reniformis* luciferase Rluc.

7.1.3 The GFP and β-Galactosidase Reporters Do Not Appear To Accurately Reflect the Transcription of the Pheromone-response Genes

Reporter assays measure the total accumulated reporter protein within the cell population to determine rate of transcription. The accumulation of reporter is therefore a problem because a build-up of transcriptional activity is measured rather than the transcriptional rate at a specific point in time. Accumulation is influenced by the stability of the reporter protein and its mRNA. Certain versions of β-galactosidase and GFP are not ideal reporters of cell signalling for this reason because the half-lives of these reporters can be up to 48 h (Park and Oh 2010). The β-galactosidase and GFP reporters also continue to signal in samples after the point of cell death (Miller 1972; Guthrie and Fink 2002) further adding to accumulation of reporter.

The GFP reporter system and the β-galactosidase reporter both appear to accumulate when used as quantifiers of the transcriptional pheromone-response in *Sz. pombe.* Measurements of the activity of a GFP reporter over time is shown in Figure 7-1A (Smith 2009). In this graph, the pheromone-response appears to increase almost linearly with time with no indication of down-regulation of the pheromone-response. This is not an accurate depiction of pheromone signalling as the pheromone-response is down-regulated via several mechanisms. These include among others; degradation of extracellular pheromone via Sxa2, although down-regulation will occur in the presence of pheromone (Imai and Yamamoto 1992; Ladds, Rasmussen et al. 1996; Ladds and Davey 2000), regulation of signalling via RGS proteins (Pereira and Jones 2001; Smith, Hill et al. 2009), dephosphorylation of the MAP kinase (Didmon, Davis et al. 2002) and down-regulation of receptor (Hicke and Riezman 1996; Hicke, Sanolari et al. 1998). The stable increase in fluorescence may be caused by an accumulation of reporter, due to protein and/or mRNA stability, or reflect other problems with the assay.

The use of the β-galactosidase reporter provides a better indication of the down-regulation of the pheromone-response over time, shown in Figure 7-1B. Briefly, JY544 cells (*sxa2>lacZ*) were cultured in AA media to a density of ~$5x10^6$ cells/mL. Cells were incubated with concentrations of pheromone ranging from 0 to 10^{-4} M for 0-16 h and the β-galactosidase activity was measured at 2 h intervals. An increase in β-galactosidase production is observed after 2-4 h and a plateau is reached after 12-14 h in cells incubated with 10^{-7} M or

higher concentrations of pheromone. At lower concentrations of pheromone only a slight increase of β-galactosidase production is observed. After 14 h, there is a decrease in β-galactosidase production indicative of down-regulation of the pheromone-response. It is however unlikely that there is a 2-4 h lag before the pheromone-response is initiated. The observed lag is likely to be due to the sensitivity of the assay i.e. the minimum amounts of β-galactosidase that can be detected by the instrumentation and background noise. The rate of protein folding and maturation may also have an impact on the lag phase. The rate of formation of functional units of β-galactosidase is limited by protein quantity and it has been observed that a two-fold increase in protein concentration lead to a two-fold increase in correctly folded β-galactosidase units (Nichtl, Buchner et al. 1998).

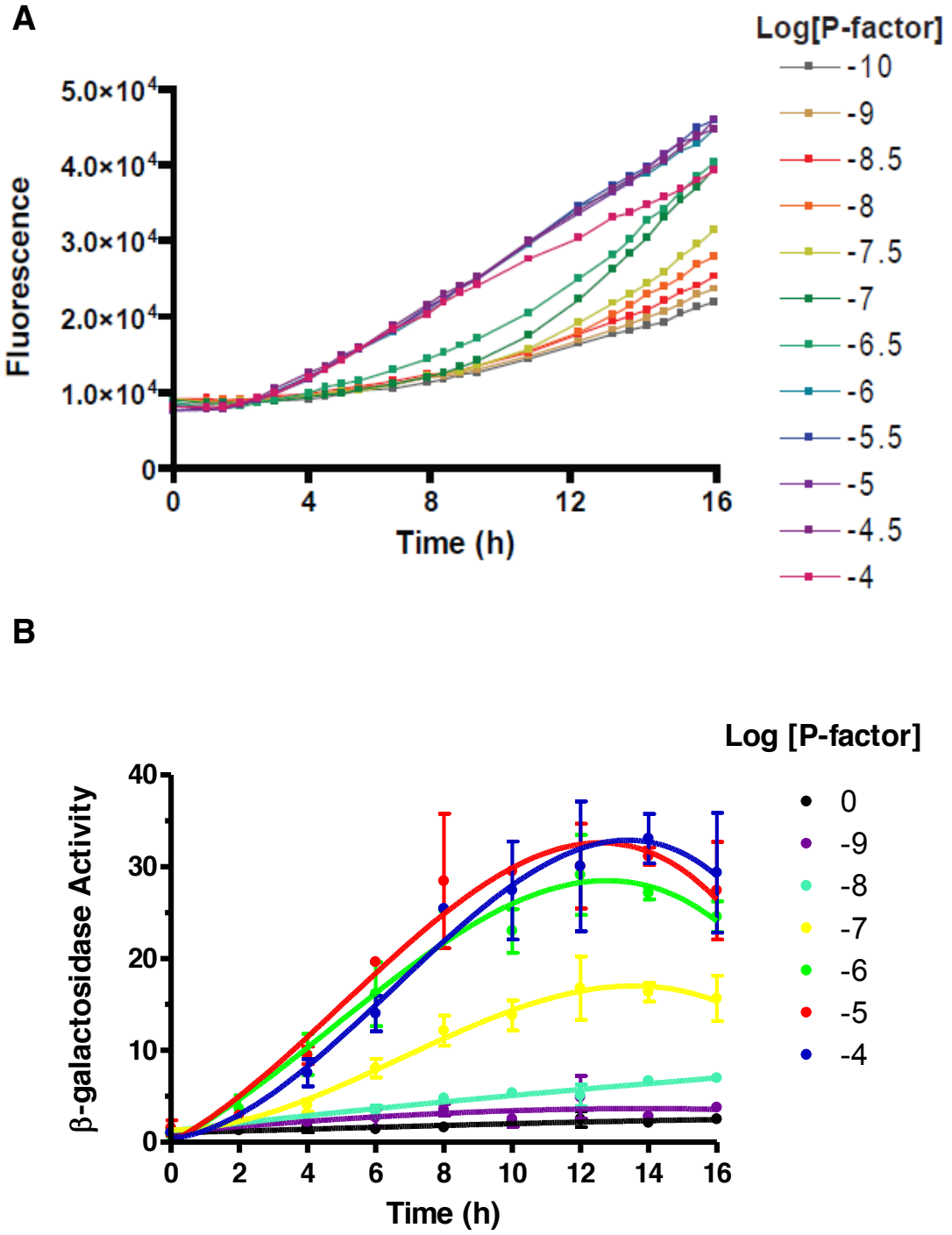

Figure 7-1: Activity of the GFP and β-galactosidase reporters

A: Fluorescence intensity over time in a sxa2>GFP *Sz. pombe* reporter strain subjected to varying concentrations of pheromone. Adapted from (Smith 2009). **B:** β-galactosidase activity ($OD_{420}/10^6$ cells) over time in the JY544 (*sxa2>lacZ*) reporter strain. Cells were cultured in DMM to a density of ~$5x10^6$ cells/mL. Cells were incubated with concentrations of pheromone ranging from 0 to 10^{-4} M for 0-16 h on a rotating wheel and the β-galactosidase activity was measured at 2 h intervals.

7.2 Development of a Luminescent *Schizosaccharomyces pombe* Reporter Strain

Two luminescent reporter strains for the *Sz. pombe* pheromone-response pathway were developed to test whether a more sensitive assay could be produced utilizing luminescence. One strain incorporated the *Renilla reniformis* luciferase *Rluc* (modified to remove an internal *Bam*HI site) and the other incorporated *Rluc8* which is a mutated version of *Rluc* containing eight mutations in the protein sequence (A55T, C124A, S130A, K136R, A143M, M185V, M253L and S287L) (Loening, Fenn et al. 2006). Rluc8 when expressed in mammalian cell lines provide brighter luminescence readings compared to Rluc making it easier to detect. Rluc8 is however also reported to be a more stable derivative, meaning that the dynamics of gene activation and suppression may be more difficult to infer when using the protein as a reporter of transcription. Both *Rluc* and *Rluc8* were therefore tested to assess their suitability as reporters of the *Sz. pombe* pheromone-response.

The JD3649 and JD3647 constructs (created as detailed in section 3.4) were digested with *Spe*I and *Bam*HI and transformed into a yeast strain containing the 5' and 3' UTR of *sxa2* with the ORF (open reading frame) disrupted by the *ura4* cassette (JY522; *Mat1-M, Δmat2/3::LEU2-, leu1-, ade6*-M216, *ura4*-D18*, cyr1*-D51*, sxa2::ura4+)* a strategy described previously (Didmon, Davis et al. 2002) and illustrated in Figure 7-2. Potentially successful transformants, those which had replaced *sxa2*::*ura4* with *sxa2*::*Rluc* or *sxa2*::*Rluc8*, were plated onto 5-fluoro-orotic-acid (FOA) plates. Orotidine 5'-monophosphate decarboxylase, encoded by *ura4*, converts FOA to a toxic compound (fluoro-uracil), and therefore only cells lacking the cassette are expected to grow on FOA plates (Grimm, Kohli et al. 1988). These colonies were picked and grown to mid-log phase in AA growth media.

Having selected for cells no longer containing the *ura4* cassette, flanked by the *sxa2* 5'- and 3'-UTRs, it remained to select those which had successfully integrated *sxa2>Rluc* and *sxa2>Rluc8* in place of *ura4*. To do this, genomic DNA from resultant colonies were prepared and subjected to PCR screening using primers JO2681 and JO2628 for *Rluc* and JO2690 and JO2691 for *Rluc8* (sequences specified above). This amplified the reporters to demonstrate their genome integration, and strains that had successfully integrated the reporters yielded bands ~1 kb in size, as shown in Figure 7-3A for strains that had incorporated *Rluc* and Figure 7-3B for strains that had incorporated *Rluc8* (top gel in each image). A second PCR screen was performed to demonstrate that the reporters had integrated into the correct chromosomal site using the forward primers JO2681 for *Rluc* and JO2691 for *Rluc8* together with JO1934 (TAGCCAACGCTAAGGAAC). JO1934 binds the 3'

UTR of *sxa2* (position 2222-2205 relative to the *sxa2* ATG) and this screen therefore yields a larger DNA fragment ~1600 bp in size.

The absence of amplified PCR product indicates that the reporter has not integrated into the genome (illustrated by the green arrows in Figure 7-3). If only the PCR using the reporter specific primers yields a band, then the reporter has incorporated at the wrong locus in the chromosome (illustrated by the blue arrows in Figure 7-3). If both screens yield an amplified PCR product then the reporter has incorporated into the chromosome at the correct locus (illustrated by the purple arrows in Figure 7-3). For strains transformed with *Rluc* colonies 3-11 and 13-16 appeared to have incorporated *Rluc* successfully and for *Rluc8* colonies 5 and 7-10 appeared to have incorporated the reporter successfully (Figure 7-3A and B respectively, bottom gel). The strain created incorporating *sxa2*::*Rluc* was named JY1552 and the strain created incorporating *sxa2*::*Rluc8* was named JY1553.

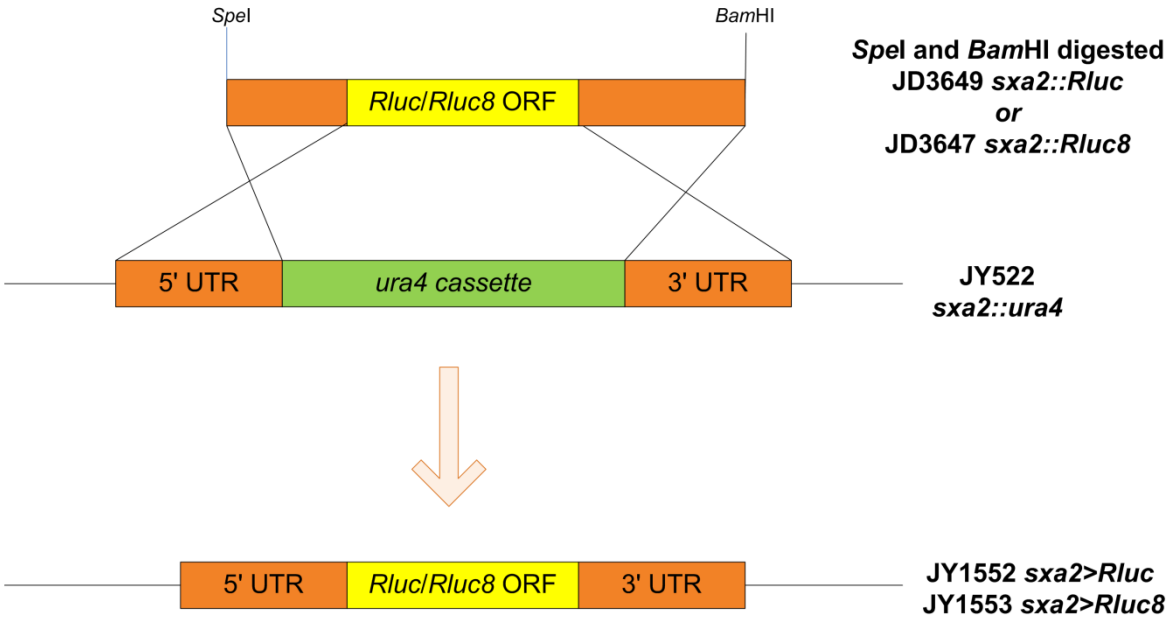

Figure 7-2: Creation of the *sxa2*::*Rluc* and *sxa2*::*Rluc8* strains

The *Spe*I/*Bam*HI fragments from JD3649 (*sxa2>Rluc*) and JD3647 (*sxa2>Rluc8*) were used to transform JY522 (*sxa2::ura4+*) and strains were selected by growth in the presence of FOA. Growth in the presence of FOA indicates loss of the *ura4* cassette as the *ura4* product Orotidine 5'-monophosphate decarboxylase converts FOA into the toxic compound fluoro-uracil.

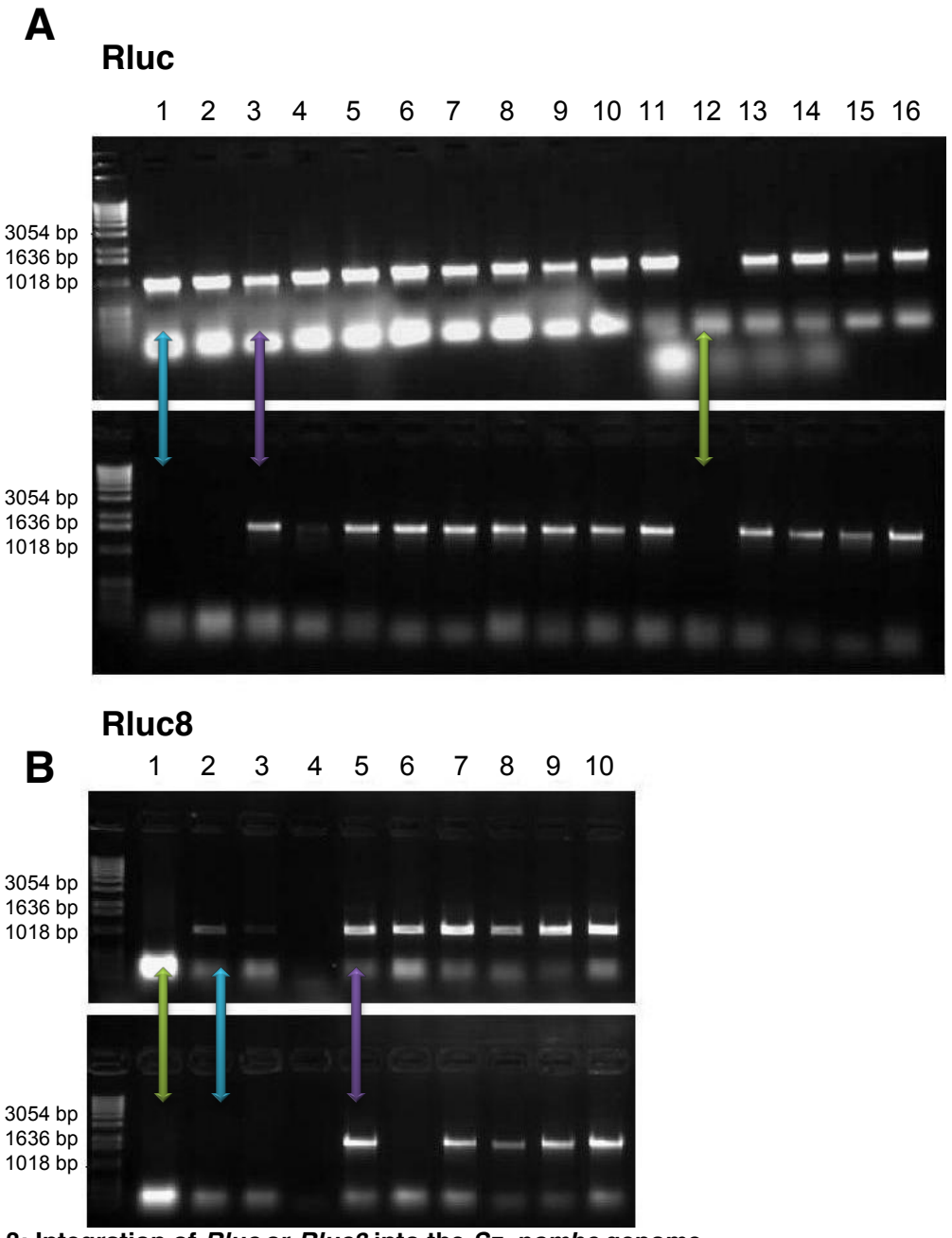

Figure 7-3: Integration of *Rluc* or *Rluc8* into the *Sz. pombe* genome

Homologous recombination between the 5' and 3' UTRs contained in JD3649 or JD3647 and in JY522 replaced the *ura4* cassette with either *Rluc* (A) or *Rluc8* (B). PCR reactions of genomic extracts from potential integrants were performed to show that the reporters had integrated into the genome (top gels in both A and B) using primers JO2681/JO2628 for *Rluc* and JO2690/JO2691 for *Rluc8*. A second PCR reaction was performed to show that the reporters were incorporated at the correct loci (bottom gels in both A and B) using primers JO2681/JO1934 for *Rluc* and JO2691/JO1934 for *Rluc8*. Bands present in both the top and bottom gels represent strains that have successfully integrated the reporter gene (3-11 and 13-16 for *Rluc* and 5 and 7-10 for *Rluc8*) as illustrated by the purple arrows. The green arrows indicate that homologous recombination was not successful. The blue arrow indicates that the reporters had integrated into the genome at the wrong locus. Agarose gel was documented with G:Box gel documentation system. This created the strains JY1552 (*sxa2*::*Rluc*) and JY1326 (*sxa2*::*Rluc8*).

7.3 Signal:Noise Optimization

7.3.1 Intrinsic Noise Levels to the System

Initial luminescence measurements on cells expressing the Rluc and the brighter Rluc8 reporters revealed large amounts of noise generated from the micro-plates (Figure 7-4A). Subsequent investigations revealed that due to a manufacturing error the Berthold Mithras LB940 BRET multimode microplate reader (Berthold Technologies, UK) lacked an infrared filter to block out autoluminescence due to excitation of the plates in the far red, a previously unknown issue with these instruments. After the installation of an infrared filter the signal to noise ratio improved (Figure 7-4B), note the difference in scales between the two graphs. Excitation of the plate could still be detected up to two min after commencing measurements. A 2 min delay was therefore incorporated before luminescence readings were taken, unless otherwise stated.

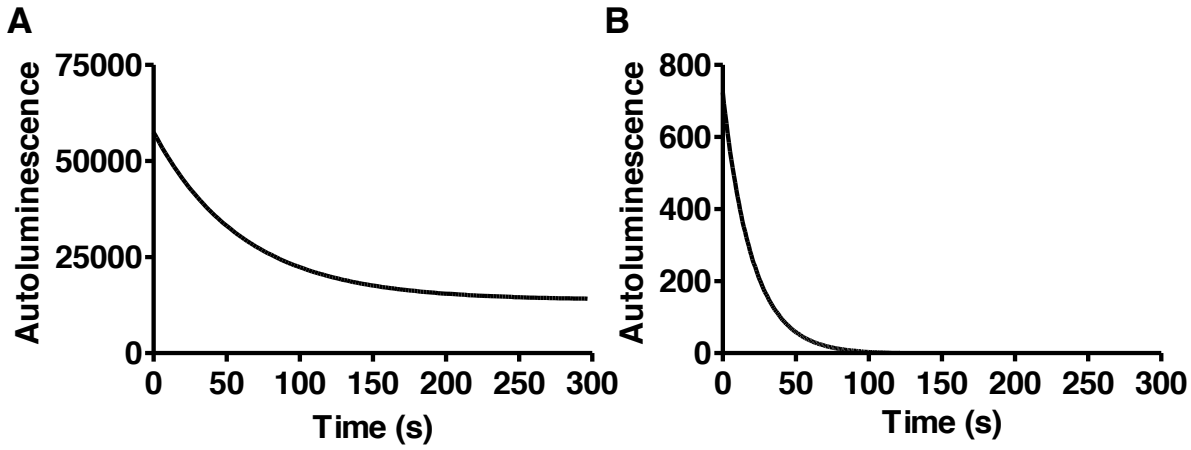

Figure 7-4: Time-dependent decay of luminescence

Measurements were taken on a single well containing AA media using a Berthold Mithras LB940 BRET multimode microplate reader (Berthold Technologies, UK). **A:** Time-dependent auto-luminescence decay before the infrared filter was installed. **B:** Time-dependent auto-luminescence decay after the infrared filter was installed. Note the difference in scales.

7.3.2 Noise Levels Vary With the Type of Micro-Well Plate Used

When measuring reporter activity a high signal to noise ratio is desirable in order to obtain accurate readings. Therefore a trial of five different 96 micro-well plates was performed to identify the plate with the lowest background noise levels. White plates are believed to provide better luminescence readings because they reflect light and thereby amplify the signal. Using a plate with a clear bottom however has the advantage of enabling cell density measurements via OD_{600} readings. Black plates are often used in fluorescence assays where white plates often lead to cross-talk and high background levels (Promega 2011). Figure 7-5 shows the different micro-well plates that were tested. They were A: white plate with grey wells B: white plate with white wells C: black plate with white wells D: black plate with clear bottomed wells and E: black plate with black wells. All plates were manufactured by Berthold (Berthold Technologies, UK).

Figure 7-6A shows the pheromone-response of 10^6 JY1552 (*sxa2>Rluc*) cells incubated with 0-10^{-4} M concentrations of pheromone for 16 h on a rotating wheel with 60 µM EnduRen added 2 h prior to measurements. A 5 min delay was incorporated before luminescence readings in the plate-reader due to the signal decay time-frame (Figure 7-6C). Luminescence could not be measured from the black plates, however other experiments have shown that a luminescent signal can be measured from these plates when using in the excess of 10^7 cells in the assay. A luminescent signal was detected from the three plates containing white wells. The plate shown in Figure 7-5C exhibited the highest noise levels, which is likely to be due to high intrinsic noise levels on this plate even after a 5 minute delay (Figure 7-6C). The dose-response for the plates shown in Figure 7-5A and C appear very similar. When comparing their best-fit values however for the dose-response curve (Figure 7-6B) it appears as though the plate shown in Figure 7-5C give more consistent readings, because the standard error of the mean is much smaller across all values describing the curve. These results indicate that the plate shown in Figure 7-5C provide the most reproducible results, and that a delay of at least 100 seconds need to be incorporated in the assays prior to luminescence readings.

Figure 7-5: The different micro-well plates tested

Five different plates (Berthold Technologies, UK), were compared for their relative luminescence intensities. **A:** white plate with grey wells **B:** white plate **C:** black plate with white wells **D:** black plate with clear bottom **E:** black plate with black backdrop.

A

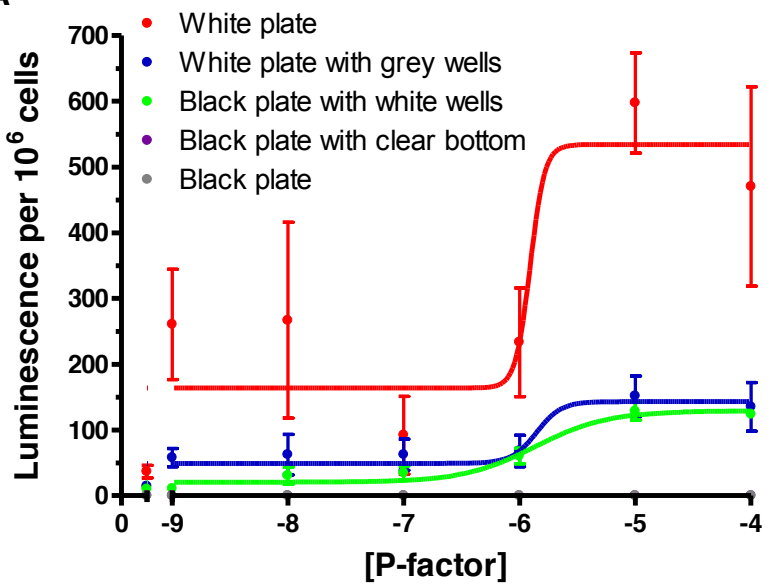

B

	pEC_{50}	Maximum
White plate	5.9±3144.00	534.10±104.5
White plate with grey wells	5.9±15.2	143.2±35.4
Black plate with white wells	5.9±0.2	129±10.3
Black plate with a clear bottom	N/A	N/A
Black plate	N/A	N/A

C

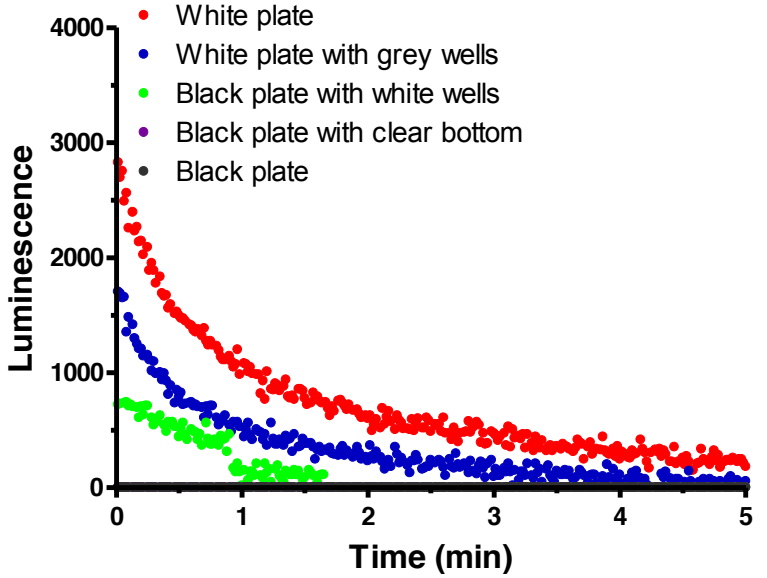

Figure 7-6: The effects of using different micro-well plates on the luminescent signal

A: JY1552 (*sxa2>Rluc*) was cultured to a density of 10^6 cells per mL and pheromone was added to cells at concentrations ranging from 0 to 10^{-4}. Cells were incubated for 14 h on a rotating wheel and 60 µM EnduRen was added followed by further two h incubation. Luminescence from the different samples was then measured using the different plates in succession using a Berthold Mithras LB940 BRET multimode microplate reader (Berthold Technologies, UK). A five minute delay was incorporated prior to readings. Results shown are means of at least triplicate repeats ±S.E.M **B:** The best-fit alues of the dose-response curve shown in A. **C:** Time-dependent decay of auto-luminescence of the different plates.

7.4 Characterization of the Rluc and Rluc8 Reporters

7.4.1 Cells Expressing Rluc8 Provide Higher Luminescent Readings in Response to Pheromone Compared to Cells Expressing Rluc

The dynamics of Rluc and Rluc8 reporter activity were measured and compared to assess which reporter provides a better approximation of the *Sz. pombe* transcriptional pheromone-response. JY1552 (*sxa2>Rluc*) and JY1553 (*sxa2>Rluc8*) were grown to a density of 10^6 cells and exposed to 0 to10^{-4} M pheromone for 16 h on a rotating wheel. Luminescence measurements were then taken using a Berthold Mithras LB940 BRET multimode microplate reader (Berthold Technologies, UK).

Figure 7-7A shows the pheromone dose-response of *Sz. pombe* incorporating the reporter genes *Rluc* or *Rluc8* in its genome. A ~2 fold increase in maximal signalling is observed when expressing the Rluc8 reporter compared to the Rluc reporter. The pEC_{50} value is slightly lower for Rluc8 than for Rluc, which might reflect the increased brightness of the mutated version of Rluc so that it is detected at lower levels (Figure 7-7B). In contrast, the morphological response of the two strains was very similar (Figure 7-7C) indicating that the differences seen in the measured transcriptional activity is due to differential dynamics of the two reporters rather than any other cellular events. Interestingly, the pheromone-response decrease in the morphological response at the highest concentration of pheromone in accordance with what was observed when using β-galactosidase as a reporter (see chapter 3.4) but not the transcriptional response.

A

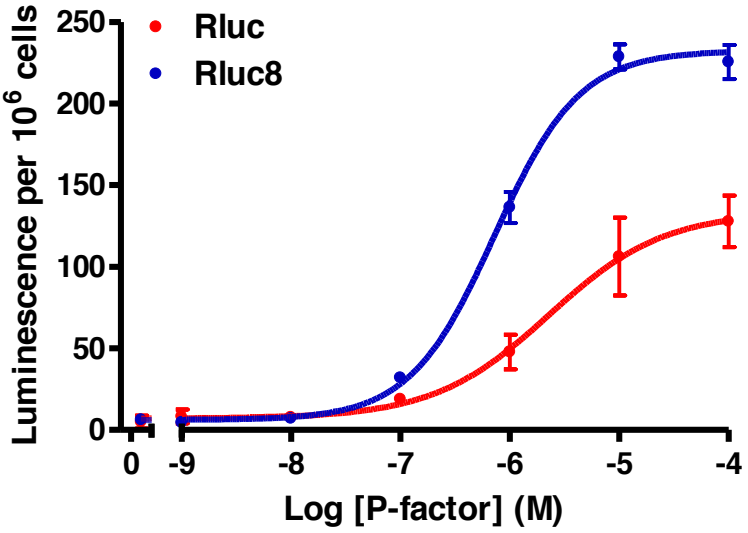

B

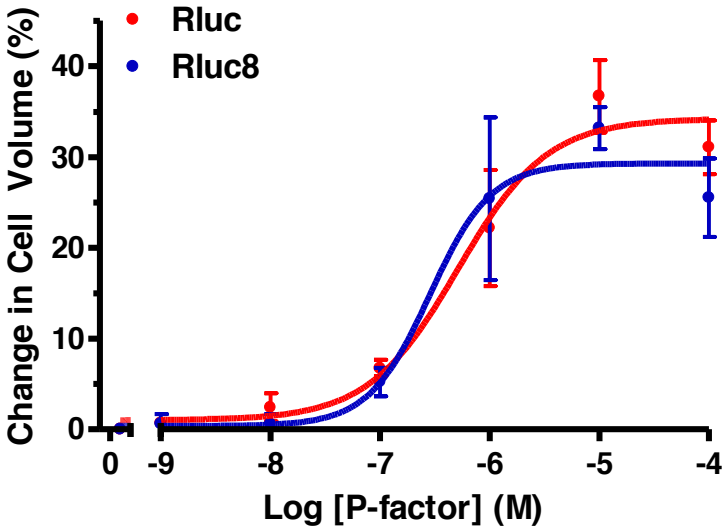

C

	pEC_{50}		Maximum	
	Transcription	Shmoo	Transcription	Shmoo
Rluc	6.0±0.3	7.4±0.2	133.8±9.9	31.2±2.7
Rluc8	6.2±0.1	7.5±0.3	232.4±5.5	28.3±2.8

Figure 7-7: A comparison of the Rluc and Rluc8 Reporters

JY1552 (*sxa2>Rluc*) and JY1553 (*sxa2>Rluc8*) were cultured in AA media to a density of 10^6 cells. Cells were exposed to pheromone and placed on a rotating wheel for 16 h. 60 µM EnduRen was added 2 h prior to measuring the luminescence signal and cell density. Cells were assayed for luminescence intensity using a Berthold Mithras LB940 BRET multimode microplate reader (Berthold Technologies, UK). Results shown are means of triplicate results ±S.E.M and normalized to 10^6 cells. **A:** The luminescence intensity per 10^6 cells of the two reporters. **B:** The morphological response of cells expressing the two different reporters **C:** The pEC_{50} values of the transcriptional and morphological response in cells expressing the two different reporters.

7.4.2 Only Viable Cells Signal

Both the transcriptional response and the morphological response measured in strains expressing the β-galactosidase reporter decrease at the higher concentrations of pheromone (~10^{-5} M and 10^{-4} M) compared to the medium concentrations (~10^{-7} M and 10^{-6} M). It was demonstrated (see chapter 4) that exposing cells to high concentrations of pheromone increase the amount of inviable cells in samples compared to treating cells to no or medium concentrations of pheromone, in addition to cells arresting in G_1 (Davey and Nielsen 1994). In contrast, when using Rluc and Rluc8 as a reporter, the transcriptional response was not observed to decrease at the higher pheromone concentrations although the morphological response did (see section 7.4.1). The toxicity of high concentrations of pheromone, coupled to the long half-life of the enzyme β-galactosidase and assaying cell lysate may bias measurements of the pheromone-response when using the β-galactosidase assay. The Rluc enzyme catalyzes the oxygenation of the substrate coelenterazine to produce luminescence. The EnduRen substrate has protective groups added to the site of oxygenation to make the substrate more stable in aqueous environments. This protective group must be removed by esterases found in live cells before Rluc can oxygenate the substrate and produce light (Promega 2009). Therefore, the addition of EnduRen to dead cells should not result in luminescence. Since the transcriptional response does not appear to decrease in cells expressing Rluc and Rluc8, it was of interest to investigate whether these strains also have increased cell death at increasing concentrations of pheromone and to see whether a pheromone-response could be measured from dead cells.

Flow cytometry was used to quantify the amount of dead cells in strains JY1552 (*sxa2>Rluc*) and JY1553 (*sxa2>Rluc8*) exposed to low, medium and high concentrations of pheromone (Figure 7-8A). Cell viability decreased in response to pheromone when expressing the *Rluc* reporter, demonstrating that this phenomenon is not confined to cells expressing the *lacZ* reporter. To test whether these dead cells contribute to luminescence readings cells were exposed to pheromone and incubated on a rotating wheel for 16 h. At 16 h cells were lysed and 60 μM EnduRen was added to the samples. After a 2 h incubation period luminescence was measured. In the unlysed control EnduRen was added at the 14 h time-point rather than the 16 h time-point. Figure 7-8B shows that although the live cells signal normally, no signal is detected from the lysed cells. This suggests that dead cells are unlikely to contribute to the luminescence readings and the absence of a decrease in pheromone-response in cells exposed to high concentrations of pheromone may be due to accumulation of reporter. Due to the toxic effects of high concentrations of pheromone it was further decided to exclude the high concentrations of pheromone from further experiments.

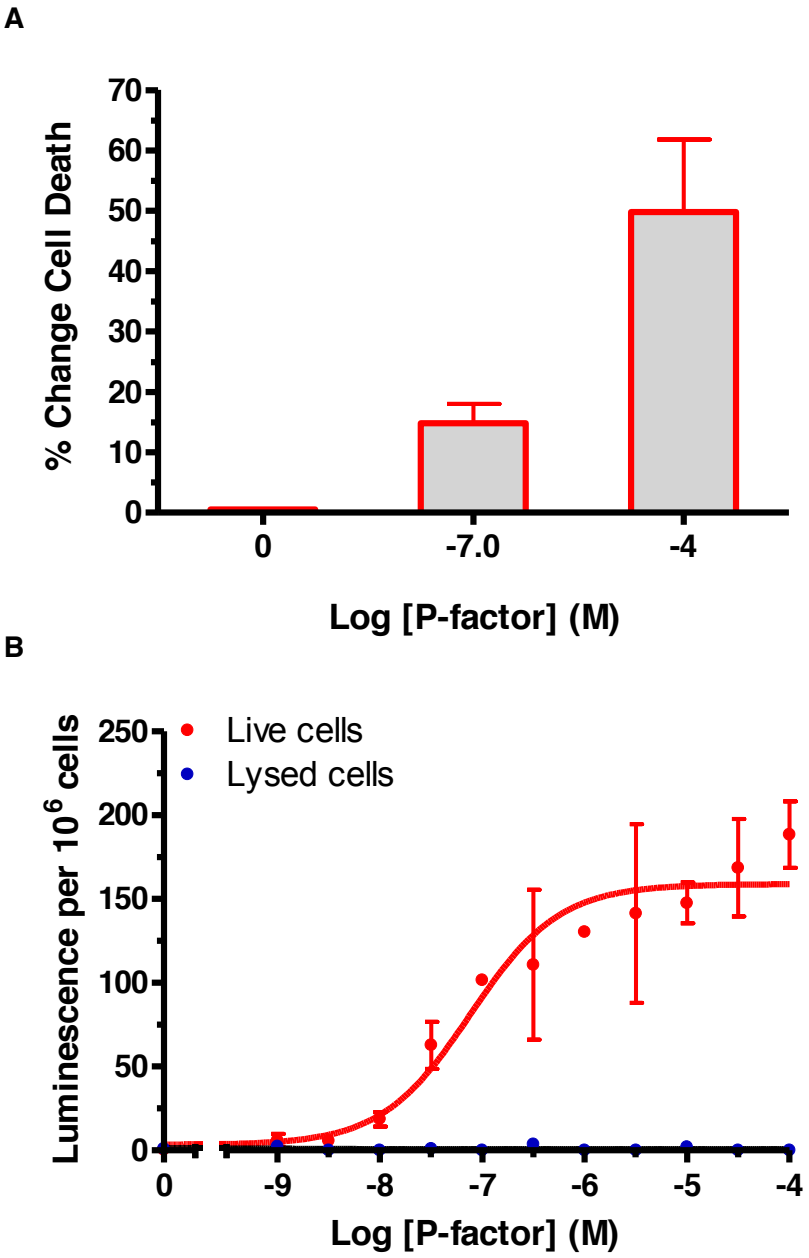

Figure 7-8: The number of dead cells increases in response to pheromone but do not signal

A: Flow cytometry to determine the amount of dead JY1552 (*sxa2>Rluc*) cells in the sample following incubation on a rotating wheel for 16 h with 0, 10^{-7} M and 10^{-4} M pheromone. Cells were then washed with PBS and stained with cyto-9 and propidium iodine before FACS analysis was performed. Results shown are means of triplicate determinations of three independent isolates ±SEM. Results are normalized to the number of dead cells in the population of cells not exposed to pheromone. **B:** The transcriptional pheromone-response of live or lysed cells. JY1552 (*sxa2>Rluc*) was cultured in AA media to a density of 10^6 cells per mL, exposed to pheromone concentrations ranging from 0-10^{-4} M and incubated on a rotating wheel for 16 h. At 16 h cells were lysed and 60 µM EnduRen was added to the samples and after a two h incubation period luminescence was measured. In the unlysed control EnduRen was added at the 14 h time-point rather than the 16 h time-point and luminescence was measured at 16 h.

7.4.3 The Use of Different Media Does Not Appear To Influence Luminescence Output Significantly

The stability of Rluc and Rluc8 is affected by the type of media that the reporters are expressed in, with Rluc8 being more stable (Loening, Fenn et al. 2006). To see if a difference could be measured using different media typically used when studying the *Sz. pombe* pheromone-response, cells were cultured in two different media; DMM minimal media and the richer media AA. The strains JY1552 and JY1553 (*sxa2>Rluc* and *sxa2>Rluc8*) were cultured to a density of $1x10^6$ cells per mL and treated with pheromone concentrations ranging from 0 to 10^{-4} and incubated on a rotating wheel for 16 h in either DMM or AA media. 60 µM EnduRen was added at 14 h. Luminescence intensity was then measured from the samples, results shown in Figure 7-9A, with pEC_{50} values shown in Figure 7-9B. Although there is some variability between measurements the results indicate that the stability of Rluc or Rluc8 expressed in either DMM or AA media is very similar.

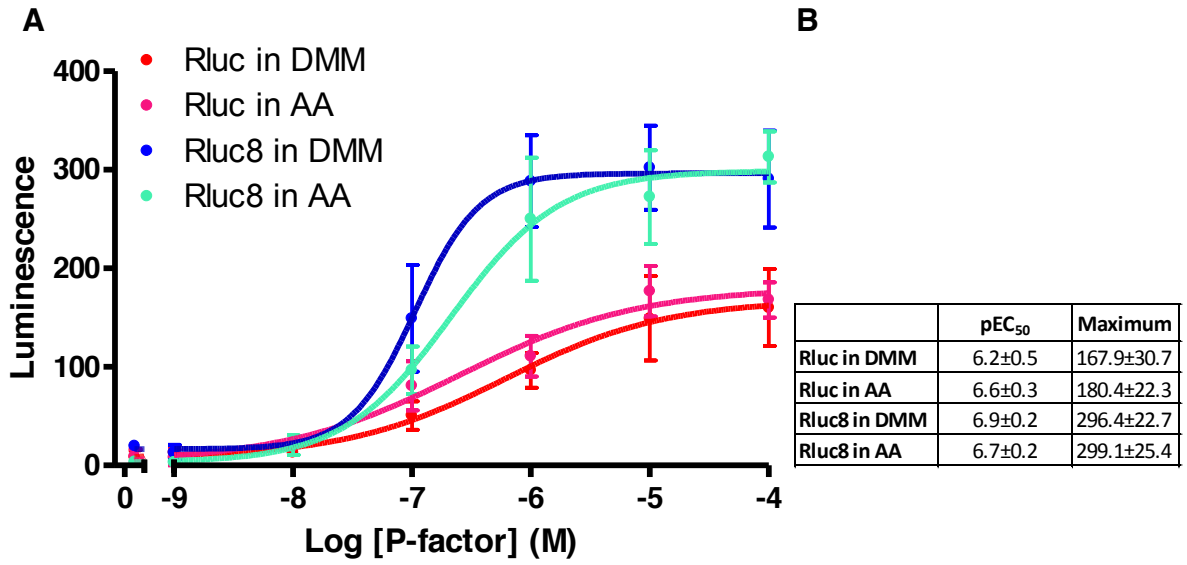

	pEC_{50}	Maximum
Rluc in DMM	6.2±0.5	167.9±30.7
Rluc in AA	6.6±0.3	180.4±22.3
Rluc8 in DMM	6.9±0.2	296.4±22.7
Rluc8 in AA	6.7±0.2	299.1±25.4

Figure 7-9: Comparison of the effects of different media on the luminescent reporters Rluc and Rluc8

The Rluc8 reporter strain JY1552 and JY1553 (*sxa2>Rluc and sxa2>Rluc8*) were cultured to a density of 10^6 cells and incubated with varying concentrations of pheromone (0-10^{-4} M) in either AA media or DMM media on a rotating wheel for 16 h. 60 µM EnduRen was added at 14 h Cells were assayed for luminescence intensity using a Berthold Mithras LB940 BRET multimode microplate reader (Berthold Technologies, UK) and results shown are normalized to 10^6 cells and are means of triplicate repeats ±S.E.M. **A:** The pheromone dose-response **B:** The pEC_{50} values of the dose-response of samples.

7.4.4 Rluc Appears More Abundant in Cells than Rluc8 in Response to Pheromone

To compare the relative amounts of Rluc and Rluc8 in the cells in response to pheromone, SDS-PAGE and western blotting was performed. JY1552 (*sxa2>Rluc*) and JY1553 (*sxa2>Rluc8*) were grown to a high density (~$5x10^7$ cells/ mL) and incubated with concentrations of pheromone ranging from 0 to 10^{-6} M. Whole cell extracts were prepared and protein concentrations were determined using the Bradford assay (Bradford 1976). Equal amounts of sample were then subjected to SDS-PAGE and western blotting. Figure 7-10 shows the western blots of the expression of Rluc and Rluc8 in these strains. For strain JY1552 expression of Rluc appear to correlate with increasing concentrations of pheromone and there is a 16-fold increase in Rluc for cells treated with 10^{-6} M pheromone compared to no pheromone. For JY1553 there is a 2-fold increase in quantified Rluc at 10^{-6} M pheromone compared to no pheromone. For this strain however, there is an additional smaller band present (marked by the star). This band is not likely to represent non-specific binding because it is not present in the strain expressing Rluc, but may represent break-down product of Rluc8. This band has previously been identified in the literature (Venisnik, Olafsen et al. 2006). It is not known whether this breakdown product is catalytically functional or not.

It is interesting that despite being present in much lower abundance than Rluc, Rluc8 is much more readily detected in terms of luminescence. It is also interesting that the dynamics of the reporters in response to pheromone is so similar for the two reporters despite their relative abundance (see section 7.4.1). Since the abundance of Rluc appeared to correlate more strongly with the administered pheromone dose, this reporter strain was chosen for further characterization.

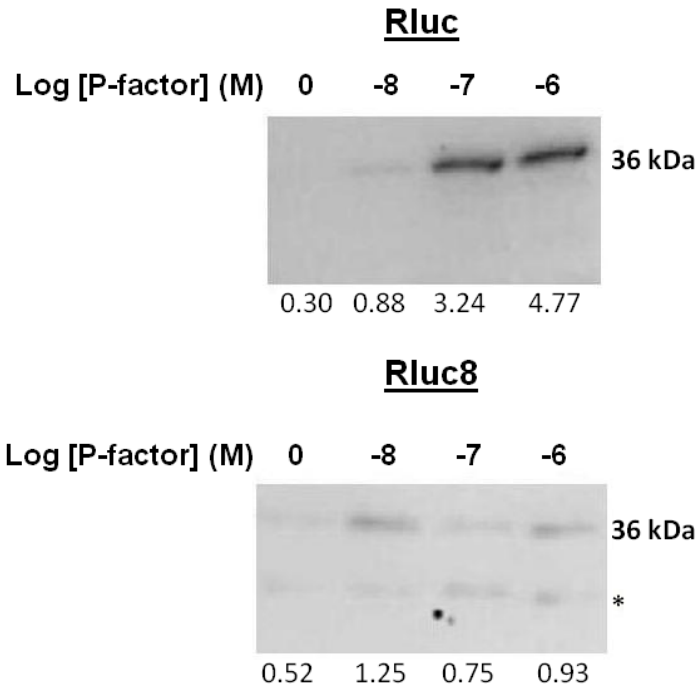

Figure 7-10: Rluc and Rluc8 expression levels

JY1552 (*sxa2>Rluc*) and JY1553 (*sxa2>Rluc8*) were grown to a density of ~5x10^7 cells per mL. Cells were then exposed to varying concentrations of pheromone and placed in a shaking incubator for 16 h. Yeast whole extracts were prepared and the Bradford assay was used to determine protein concentration. Equal amounts of sample were loaded onto each gel. Western blots using the Rluc antibody were performed on the samples (Medical & Biological Laboratories Ltd, Nagoya Japan) shown at the top of the figure. The chemi-luminescence intensities detected on the western blots were normalized to the 38 kDa marker run on each gel to allow comparison across gels. The star marks what appears to be Rluc8 break-down product.

7.5 Discrete Time-Courses

7.5.1 Rluc Reporter Activity Plateau Earlier Than GFP or β-Galactosidase Reporter Activity

Due to the potential issues with reporter accumulation it is desirable to use reporters with shorter half-life and reduced mRNA stability. Rluc has a half-life of just 0.5-1 h (Loening, Fenn et al. 2006) and the time-dependent dynamics of Rluc reporter activity was therefore measured to contrast it to the time-dependent dynamics of GFP reporter activity and β-galactosidase reporter activity. The integrated *sxa2>Rluc* reporter construct (JY1552) was cultured to a density of 10^6 cells per mL. Cells were then treated with pheromone and incubated on a rotating wheel for 0-14 h. The Rluc substrate EnduRen was added 2 h prior to luminescence intensity measurements, which were taken at 2 h intervals using a Berthold Mithras LB940 BRET multimode microplate reader (Berthold Technologies, UK). When uncorrected for cell number the luminescence output of cells exposed to 10^{-6} and 10^{-5} M pheromone was near identical (Figure 7-11A). Cells exposed to 10^{-4} pheromone initially display a similar luminescence intensity output, but at 6 h and onwards the intensity decreases in comparison to the lower concentrations of pheromone.

Figure 7-11B shows the increase in cell density as a function of time. Cell cultures display logistic growth with an initial lag phase followed by exponential growth. At 14 h following a ~5 fold increase in cell number the cells appear to enter the stationary phase. This ordinary cell growth pattern indicates that the addition of the Rluc substrate EnduRen or expression of Rluc is tolerated by cells.

Plotting the luminescence intensity per 10^6 cells highlights the importance of normalizing data to the density of cells in the sample measured (Figure 7-11C). A more pronounced reduction in transcriptional activity is observed at later time-points compared to when plotting the raw data. It appears as though the Rluc reporter may be more sensitive than the β-galactosidase reporter as a reduction in transcriptional activity is observed after 10-12 h rather than 16 h. It is also apparent from this graph that cells exposed to the higher concentrations of pheromone 10^{-4} and 10^{-5} M initially display a higher transcriptional response than the 10^{-6} M concentration. At 4 h the transcriptional response of cells exposed to 10^{-6} M pheromone surpass cells exposed to 10^{-4} M pheromone, and at 8 h it is higher than cells exposed to 10^{-5} M pheromone.

It is possible that cells treated to higher concentrations of pheromone are desensitized to pheromone sooner than cells exposed to lower concentrations of pheromone, however a plot of the morphological response suggest that desensitization occurs at the same point in time for all concentrations of pheromone tested here (Figure 7-11D). In the morphological response the cell volume is initially increased in response to pheromone at ~4 h. Cells then continue to grow in size, indicative of arrest in G_1 (Davey and Nielsen 1994) until ~10 h when they are desensitized to pheromone.

The morphological response is comparable for cells exposed to all three concentrations of pheromone, which is not the case for the transcriptional response. In the transcriptional response (Figure 7-11C) the 10^{-6} M concentration of pheromone initially displays a lower response than the two higher concentrations of pheromone, but at 8 h it elicits a higher response. The response of cells exposed to the two higher concentrations of pheromone plateau earlier than cells exposed to 10^{-6} M pheromone. This might reflect limitations in the assay design: Rluc acts on an exogenously added substrate, and this substrate might become limited in the assay. The substrate was added 2 h prior to luminescence readings, and it is possible that at high levels of Rluc transcription, there is not enough substrate in the media to accurately reflect Rluc activity.

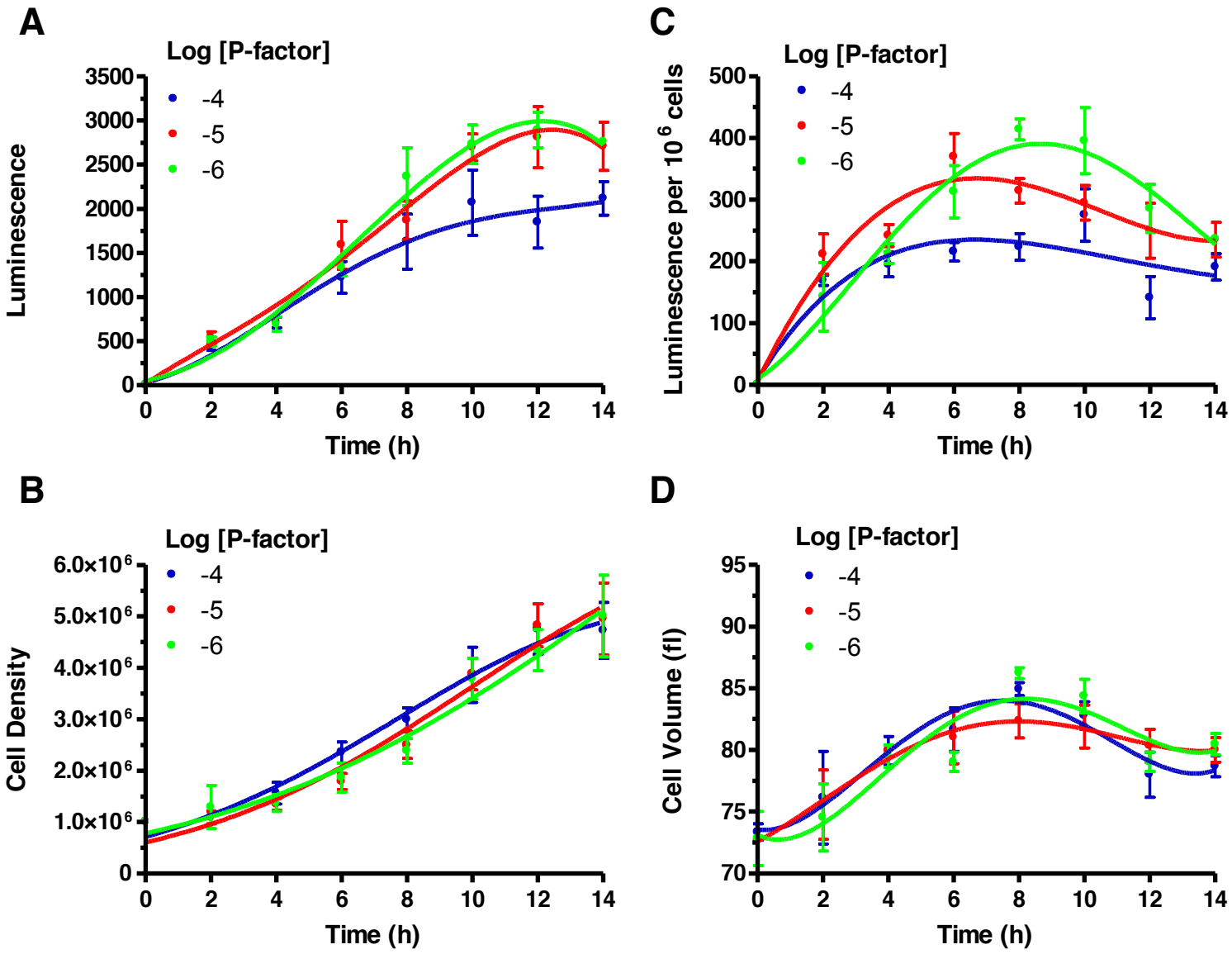

Figure 7-11: Time-course of Rluc reporter activity

JY1552 (*sxa2>Rluc*) was cultured in YE media to a density of 10^6 cells. 10^{-6}, 10^{-5} or 10^{-4} M pheromone was added to samples and placed on a rotating wheel for 0-14 h. 60 µM EnduRen was added 2 h prior to measurements which were taken every two h. Cells were assayed for luminescence intensity using a Berthold Mithras LB940 BRET multimode microplate reader (Berthold Technologies, UK). Results shown are means of triplicate results ±S.E.M. **A:** The luminescence intensity uncorrected for cell number. **B:** The change in cell number. **C:** The luminescence intensity per 10^6 cells. **D:** The change in cell volume.

7.5.2 Additions of the Rluc Substrate at the Start of the Assay Result in Lower Luminescence Measurements

As discussed in section 7.2, the reduction in Rluc activity could be due to depletion of the Rluc substrate EnduRen, rather than reflecting a reduction in transcription. To test whether EnduRen is depleted in the reporter assay a time-course was performed where EnduRen was added 2 h prior to the start of the assay rather than 2 h prior to measurements. The experiment was performed as in section 7.2 but EnduRen was added at the beginning of the experiment instead of prior to measurements. Measurements were also taken at 1 h intervals rather than every 2 h to provide better resolution of the data. Figure 7-12A shows the measured luminescence intensity over time of cells exposed to 10^{-5} and 10^{-4} pheromone. A peak in luminescence intensity was observed at ~13 h, which then decreased, similar to when pheromone was added 2 h prior to measurements (Figure 7-11A). The peak was about ~20% lower however, despite there being more cells present in the samples; ~$8x10^6$ (Figure 7-12B) compared to $4.7x10^6$ in the previous assay (Figure 7-11B).

When the luminescence intensity per 10^6 cells was plotted there was a pronounced difference when adding the EnduRen substrate at the start of the assay compared to adding the substrate 2 h prior to measurements. Figure 7-12C shows a comparison of the data where substrate was added 2 h prior to starting the assay (solid lines) compared to adding the substrate 2 h prior to measurements (dashed lines). Up to and including the 4 h time-point the data appears near identical. At 6 h and on however, the measured transcriptional activity of cells that had EnduRen added prior to starting the assay decrease steadily, whereas it does not decrease until the ~10 h time-point for cells where EnduRen was added 2 h prior to measurements.

The morphological response appeared normal in this assay (Figure 7-12D) indicating that there were no other variable that could be attributed to the change in transcriptional response other than the EnduRen substrate. It is unclear whether the substrate is destabilized or depleted. According to the manufacturer's manual, the substrate should be stable in solution for ≥24 h (Promega 2009) however, assaying conditions in *Sz. pombe* may differ from the experimental conditions in mammalian cell-lines used by the manufacturer.

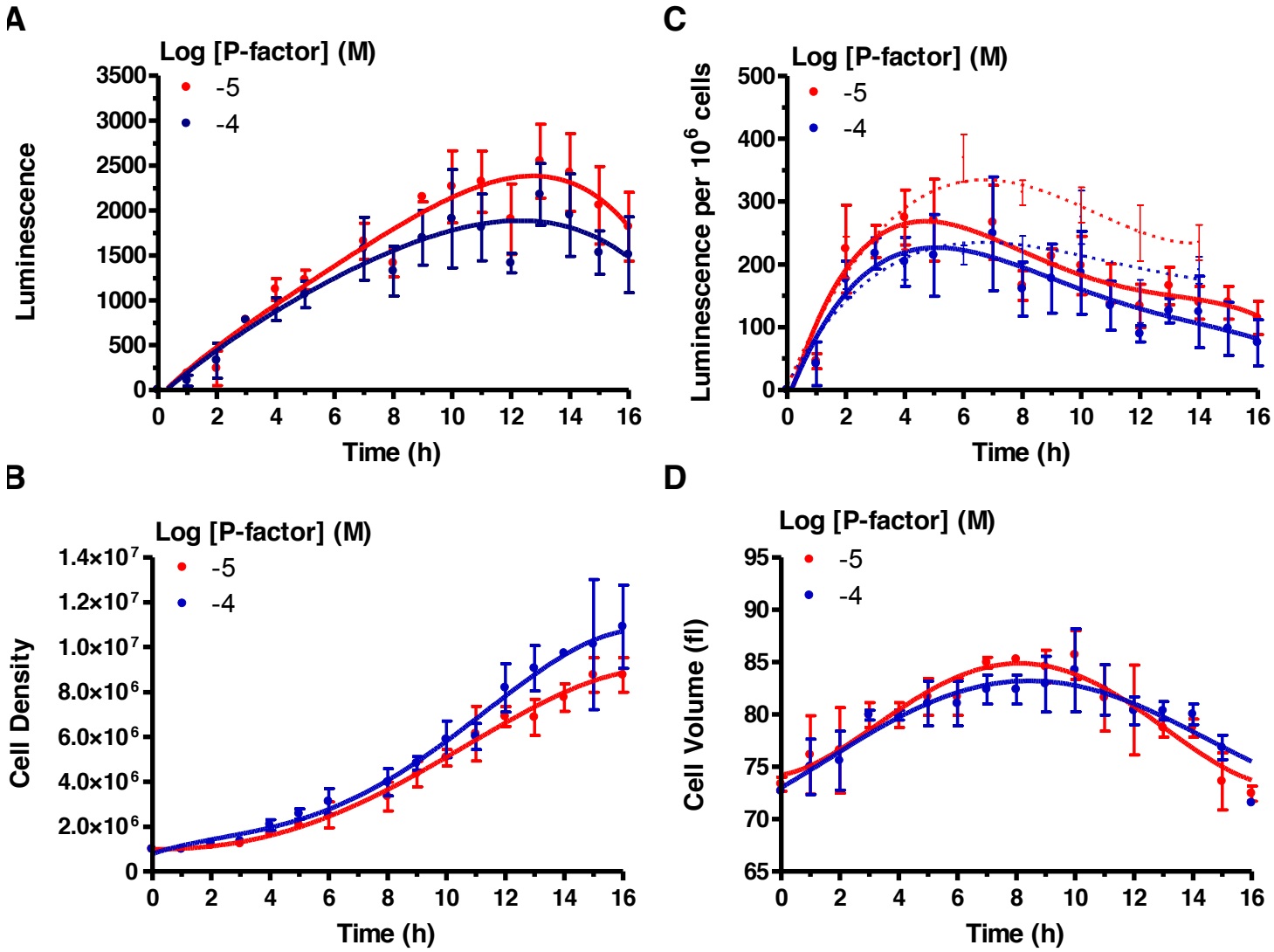

Figure 7-12: Time-course of Rluc reporter activity with substrate addition at the start of the assay

JY1552 (*sxa2>Rluc*) was cultured in YE media to a density of 10^6 cells. 10^{-5} or 10^{-4} M pheromone and 60 µM EnduRen was added to samples and placed on a rotating wheel for 0-16 h. Cells were assayed for luminescence intensity every 1 h using a Berthold Mithras LB940 BRET multimode microplate reader (Berthold Technologies, UK). Results shown are means of triplicate results ±S.E.M. **A:** The luminescence intensity uncorrected for cell number. **B:** The change in cell number. **C:** The luminescence intensity per 10^6 cells. The results from the assay where EnduRen was added 2 h prior to measurements are shown in the dotted line **D:** The change in cell volume.

7.5.3 Fewer Cells Cannot Be Used In the Assay

In the time-courses performed in this section, 10^6 JY1552 cells (*sxa2>Rluc*) were used per assay. The manufacturer recommends using cell densities below 10^4 cells to provide stable luminescence readings and to avoid overcrowding effects (Promega 2009). Adding the substrate EnduRen at the start of the assay resulted in lower luminescence readings than when adding it 2 h prior to measurements. This could either be due to a depletion of the substrate or degradation of the substrate over the time-course, however the manufacturer claims that the substrate is stable ≥24 h in solution (Promega 2009). If the substrate is depleted then using fewer cells might solve this issue. The pheromone-response of a serial dilution of *Sz. pombe* cells strain JY1552 (*sxa2>Rluc*) ($1x10^2$, $3x10^2$, $1x10^3$, $3x10^3$, $1x10^4$, $3x10^4$, $1x10^5$ and $3x10^6$) was therefore measured to see if using fewer cells would improve the luminescence readings when EnduRen was added 2 h prior to the start of the assay, compared to adding it 2 h prior to measurements. Despite the recommendations made by the manufacturer a pheromone-response could not be detected for cell densities $<10^6$ cells. This could be the result of insufficient levels of expression of Rluc but the manufacturer makes no recommendations regarding the amounts of protein needed for detection.

7.5.4 Increasing the Amount of Substrate Does Not Improve the Signal

If substrate depletion is the factor leading to lower luminescence reading when EnduRen is added at the start of the assay, then adding more substrate could resolve the issue, rather than using fewer cells. JY1552 cells (*sxa2>Rluc*) were cultured to a density of 10^6 cells and incubated with varying concentrations of pheromone on a rotating wheel for 16 h. At 0 or 14 h varying concentrations of EnduRen was added to the samples (6 µM, 60 µM, 240 µM, 480 µM or 600 µM). Figure 7-13A shows the transcriptional pheromone dose-response when EnduRen is added 2 h prior to measurements. Addition of 6 µM substrate results in a much lower signal than adding 60 µM EnduRen 2 h prior to measurements. The addition of higher concentrations of EnduRen however does not increase the measured response suggesting that the amount of EnduRen is not limiting luminescence readings. In contrast, when adding the substrate at the start of the assay (Figure 7-13B), the response is decreased for all concentrations of EnduRen. Higher concentrations of EnduRen does not result in higher luminescence suggesting that EnduRen is not depleted, but is possibly not stable in solution for the duration of the time-course.

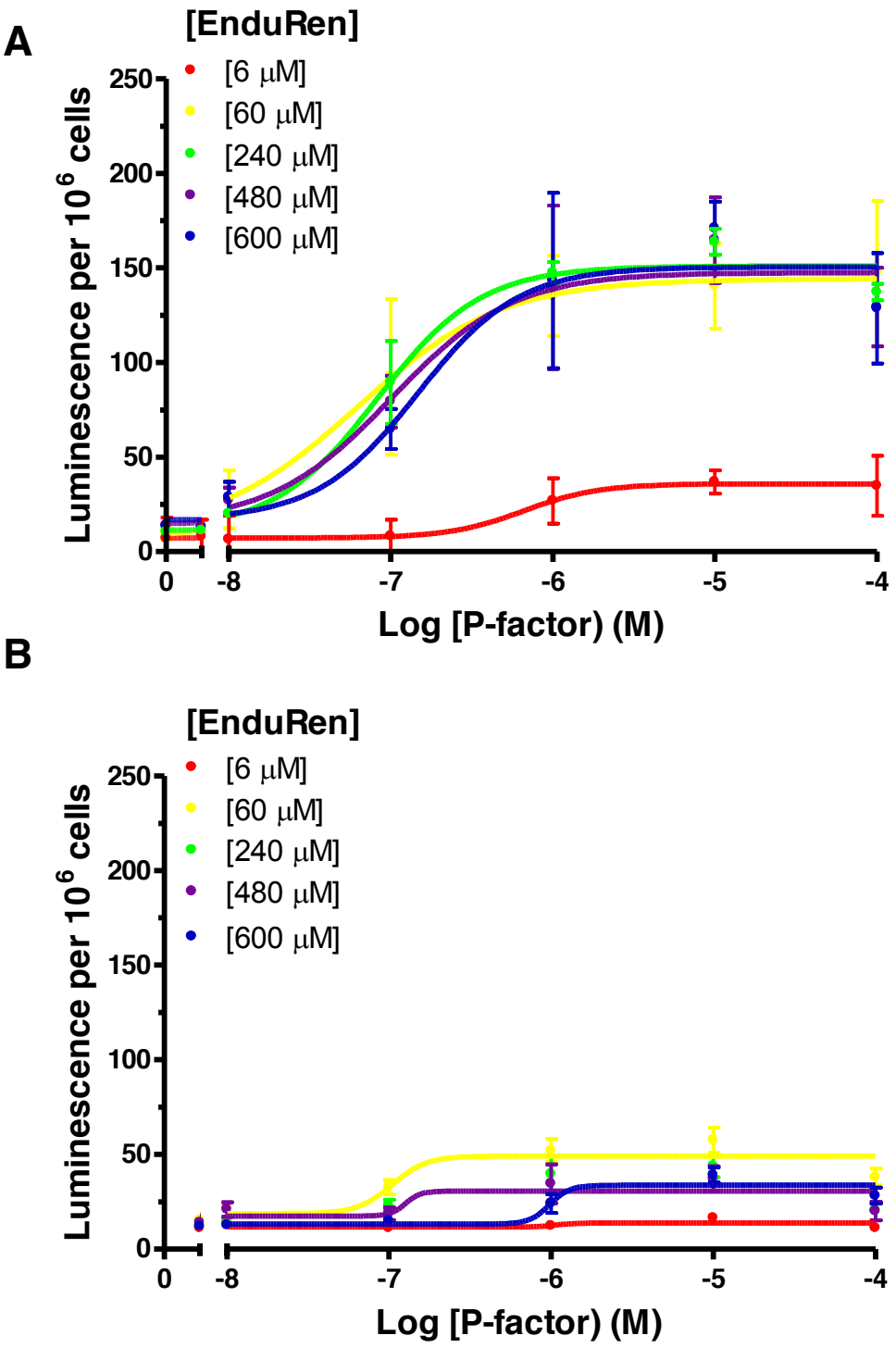

Figure 7-13: The effects of varying the concentration of EnduRen on luminescent signal

The Rluc reporter strain JY1552 (*sxa2>Rluc*) was cultured to a density of 10^6 cells and incubated with varying concentrations of pheromone (0 and 10^{-8}-10^{-4} M) on a rotating wheel for 16 h. At 0 or 14 h varying concentrations of EnduRen was added to the samples: 6 μM, 60 μM, 240 μM, 480 μM or 600 μM. Cells were assayed for luminescence intensity using a Berthold Mithras LB940 BRET multimode microplate reader (Berthold Technologies, UK) and results shown are normalized to 10^6 cells. **A:** Adding substrate 2 h prior to measurements. **B:** Adding substrate at the start of the assay. Results shown are the means of triplicate repeats ±S.E.M

7.6 Automated Time-Courses

The discrete time-course presented in 7.2 seemed to accurately reflect the transcriptional pheromone-response. Discrete time-courses are however extremely laborious to perform as cells must be assayed manually at regular intervals over long periods of time. Since time-courses provide dynamic details for modelling the pheromone-response it was of interest to develop an automated time-course. In an automated time-course, cells, substrate and pheromone are added to the microplate wells before the start of the assay, and readings are taken automatically at regular intervals. The Berthold Mithras LB940 BRET multimode microplate reader (Berthold Technologies, UK) allows temperature control for optimal growth temperature.

7.6.1 An Automated Time-Course in Suspension Is Not As Sensitive As the Discrete Time-Course

To perform an automated time-course, the strain JY1552 (*Sxa2>Rluc*) was cultured to a density of 10^6 cells per mL. 10^7 cells were spun down, re-suspended in 150 µL AA media and incubated for 1 h with 60 µM EnduRen. Samples were then added to tubes containing pheromone to final concentrations of 10^{-7} to 10^{-6} M. Cells were incubated for 0.5 h to allow mixing with pheromone. Samples were added to a micro-well plate and a plastic film lid was placed on top of the microplate to prevent evaporation. Luminescence readings were automatically recorded hourly for 24 h. The results shown in Figure 7-14 show that cells responded to pheromone in a time and dose-dependent manner. Compared to the discrete time-course presented in section 7.5.2 however, there was a lag before luminescence was detected. In the discrete assay, a response to pheromone could be detected after 1 h, whereas this automated time-course only detected an increase after 6 h. This indicates that some factor in the experimental set-up influence measurements.

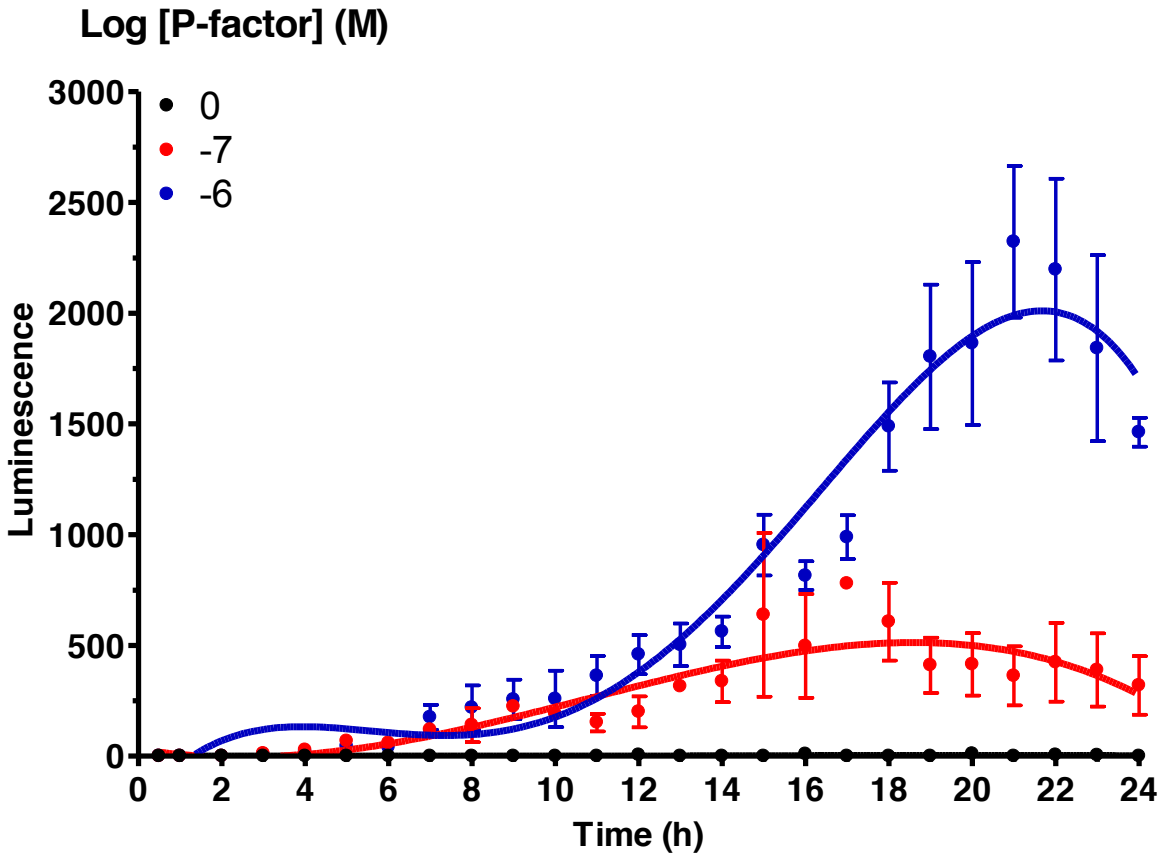

Figure 7-14: Time courses in suspension

10^6 JY1552 (*Sxa2>Rluc*) cells suspended in 150 µL AA media were incubated with 60 µM EnduRen for 1 h on a rotating wheel followed by incubation with 10^{-7} or 10^{-6} M P-factor for 0.5 h. Luminescence readings were then taken each h using a Berthold Mithras LB940 BRET multimode microplate reader (Berthold Technologies, UK) with a plastic film lid placed on top of the plate to prevent evaporation. Results shown are means of triplicate repeats ± S.E.M

7.6.2 Cell Settling Effects

The experiments performed in sections 7.5.1 and 7.6.1 show that there is a difference in luminescence readings when cells are grown in the plate-reader compared to on a rotating wheel, despite being grown at the same temperature. In the plate-reader cells were observed to respond to pheromone at >6 h whereas in the discrete time-course cells were observed to respond >2 h. The main difference between growing cells in the plate-reader compared to on a rotating wheel is that in the plate-reader cells are allowed to settle to the bottom of the wells rather than remaining in suspension. It is unclear whether the delayed measured response is an effect of growing cells in the plate-reader that cannot be reversed by re-suspending the cells, or whether re-suspension would reverse the effects meaning that cells are responding but somehow luminescence readings cannot be taken as readily from settled cells.

To determine whether a decrease in luminescence intensity is correlated with cells settling, JY1552 cells (*sxa2>Rluc*) were grown to a density of 10^6 cells and incubated with pheromone for 16 h. 60 µM EnduRen was added at 14 h. Figure 7-15A shows the luminescence measurements which were taken at 16 h (cells in suspension, represented by the yellow line) and 17 h when cells had settled to the bottom of the well (red line) and 17 h when cells had been re-suspended (blue line). When cells had been allowed to settle, the maximum of the dose-response was reduced; from 183 luminescence units per 10^6 cells to 162 luminescence units per 10^6 cells for cells exposed to 10^{-5} M pheromone. When resuspending the cells however the maximum signal measured increase to 230 luminescence units per 10^6 cells. Cells also appeared more sensitive to pheromone than was apparent when the cells were settled (compare the blue and red lines).

Cells settling clearly reduce the amount of signal measured; Figure 7-15B shows the difference over time for when 10^{-6} M pheromone is added. The dramatic increase in the pheromone-response observed when cells are resuspended is interesting because it clearly shows that cells are responding to pheromone when they are settled, but the measured luminescence intensity does not reflect this. It is unclear why the luminescence intensity from settled cells is lower than for cells in suspension. It may be due to cell crowding effects affecting the luminescence emitted from the sample. Another possible explanation is that the substrate EnduRen partitions from the media. EnduRen is initially dissolved in DMSO before addition to samples, and if the substrate precipitates in stagnant suspension, cells may not be able to absorb the substrate.

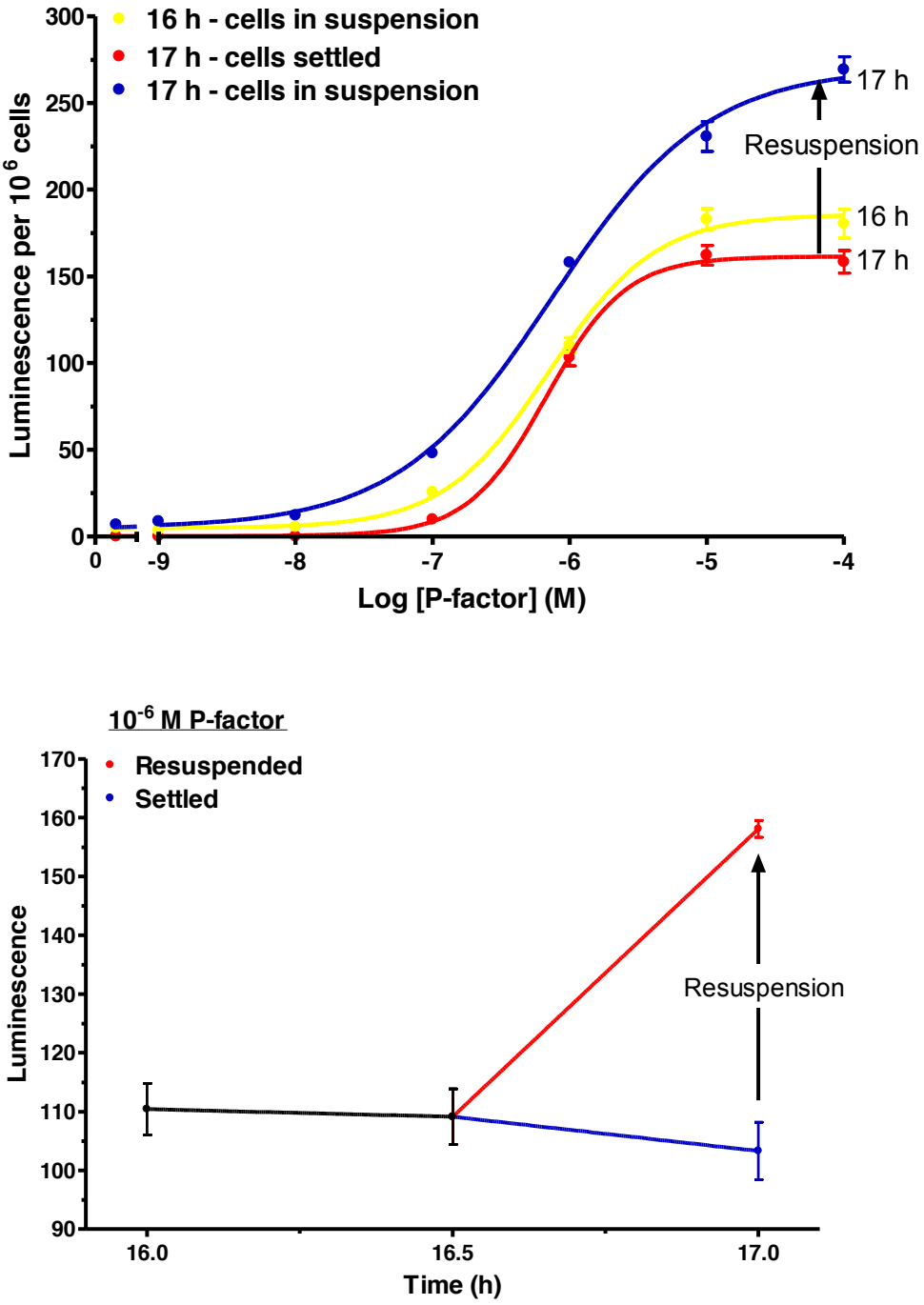

Figure 7-15: The effects of cells settling

JY1552 (*sxa2>Rluc)* was incubated on a rotating wheel with concentrations of pheromone ranging from 0 to 10^{-4} and 60 µM EnduRen. Luminescence measurements were taken using a Berthold Mithras LB940 BRET multimode microplate reader (Berthold Technologies, UK) and results shown are means of triplicate repeats ± S.E.M **A:** At 16 h the luminescence of cells was measured. Cells were then allowed to settle and further measurements were taken at 16.5 and 17 h. Cells were then resuspended by pipetting and a second measurement was taken at ~17 h. **B:** The effects of settling on cells incubated with 10^{-6} M pheromone over time.

7.6.3 Time-Courses on Agarose Plugs

As shown in sections 7.6.1 and 7.6.2, automated time-courses performed in suspension result in delayed reporter activity possibly due to cells settling in the wells. A different protocol was therefore utilized using 24-well plates where each well is used as a petri-dish containing agarose media, as opposed to growing cells in suspension. This protocol has previously been used for the GFP reporter (Smith 2009). 2.5 mL of AA media containing 1% Agarose and pheromone (concentrations of 0, 10^{-7} and 10^{-6} M) was added to each well and allowed to dry in a flow-cabinet. 100 µL of AA media containing 10^5, 10^6, 10^7, or 10^8 JY1552 (s*xa2>Rluc)* cells and 60 µM EnduRen was then uniformly "plated" onto each well and luminescence measurements were taken every 10 minutes.

Using less than 10^7 cells did not result in a detectable response as shown in Figure 7-16A (10^5 cells) and Figure 7-16B (10^6 cells). When assaying 10^7 cells luminescence was detected for cells treated with 10^{-6} M pheromone as shown in Figure 7-16C, with a maximum luminescence intensity of 726 recorded at 24 h. A time-dependent increase in luminescence intensity could not be detected for cells treated with 10^{-7} M pheromone. When 10^8 cells were assayed, luminescence was detected for samples treated with both 10^{-6} M pheromone and 10^{-7} M pheromone as shown in Figure 7-16D, note the difference in scale compared to Figure 7-16C. The maximum luminescence intensity measured from cells treated with 10^{-6} M pheromone was 19578 recorded at the end time-point 24 h, and 11076 for cells treated with 10^{-6} M.

Luminescence intensity was not observed to tail off or decrease in any of the assays regardless of cell concentration or pheromone concentration. This may reflect, or in part reflect, cell growth not accounted for over the course of the assay. The 100 µL media containing cells and EnduRen added to the wells was however found to evaporate over the duration of the time-course and cells appeared to form colonies on the plugs at the 24 h time-point, indicating cell growth. Furthermore, luminescence could only be detected after >10 h, which is later than the >6 h observed for cultures in suspension. Cells were added to the wells suspended in 100 µl media; however the pheromone was added to the agar-media. These experiments may therefore indicate that cells only sense the pheromone once the liquid media has sufficiently dried out for cells to start growing on the agar.

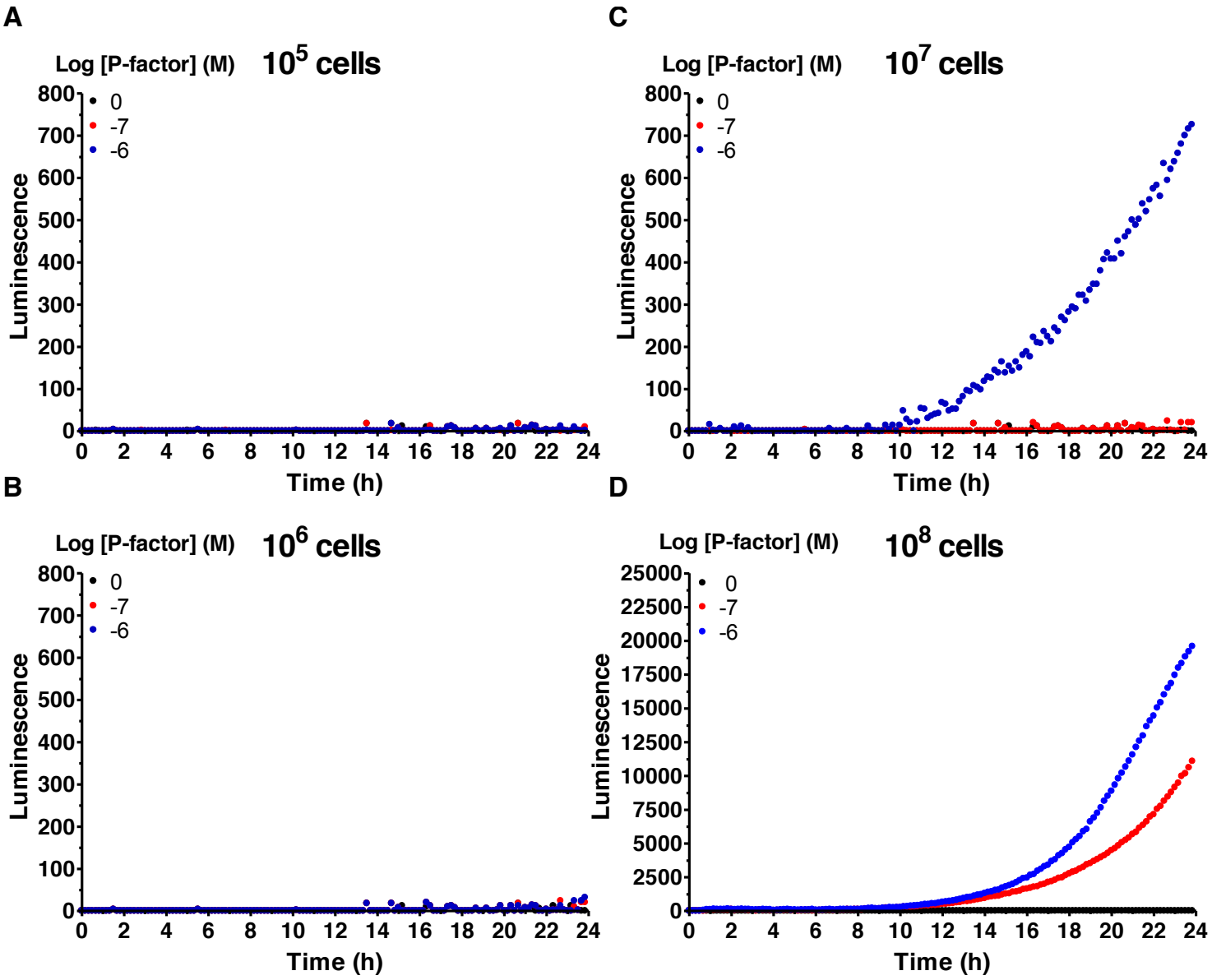

Figure 7-16: Time-course on agarose plugs

Agarose-plugs were prepared in the wells of a 24-well microplate. Plugs contained 1% agarose and 0-10^{-4} M pheromone dissolved in AA media. 10^5, 10^6, 10^7 or 10^8 cells suspended in 100 µL AA media containing 60 µM EnduRen were uniformly distributed on each plug. The Luminescence intensity from samples was then measured every 10 min for 24 h using a Berthold Mithras LB940 BRET multimode microplate reader (Berthold Technologies, UK). **A:** Luminescence intensity of 10^5 cells over time. **B:** Luminescence intensity of 10^6 cells over time. **C:** Luminescence intensity of 10^7 cells over time. **D:** Luminescence intensity of 10^8 cells over time. Note the shift in scale.

7.6.4 The Amount of Liquid Media Used on Plugs Does Not Seem to Influence Measurements

The results presented in the previous section showed that cells plated onto the micro-well agar plugs when suspended in 100 µL media only responded to pheromone after a period of ~10 h. This is significantly different from the discrete time-courses where cells appeared to respond after ~2 h and the automated time-course in suspension where cells responded after ~6 h. This may be caused by cells only starting to respond to the pheromone in the agarose-AA media once the liquid AA media has evaporated sufficiently for cells to settle on the agarose containing AA plug.

To test whether plating a smaller amount of liquid would allow cells to respond to pheromone sooner, 10^8 JY1552 cells (s*xa2>Rluc*) were resuspended in 20, 30, 40, or 50 µL liquid AA media containing 60 µM EnduRen (instead of 100 µL media used in the previous experiment). Cells were uniformly distributed on plugs in a 24-well microplate containing 1% agarose, pheromone (0, 10^{-7} or 10^{-6} M) and AA media. Measurements of the luminescence intensity from the cells were then recorded over a 22 h time-period. Figure 7-17A shows the result when plating 20 µL media, B: 30 µL media, C: 40 µL media and D: 50 µL media onto pheromone-containing agarose AA plugs. For all liquid volumes, cells responded earlier than when plating 100 µL media; 2 h as opposed to >10 h, suggesting that uptake of pheromone is indeed dependent upon cell growth on the agar. In comparison to plating 100 µL media, the response seemed to tail off towards the later time-points rather than exhibiting an exponential increase. For all volumes higher concentrations of pheromone resulted in higher luminescence intensities.

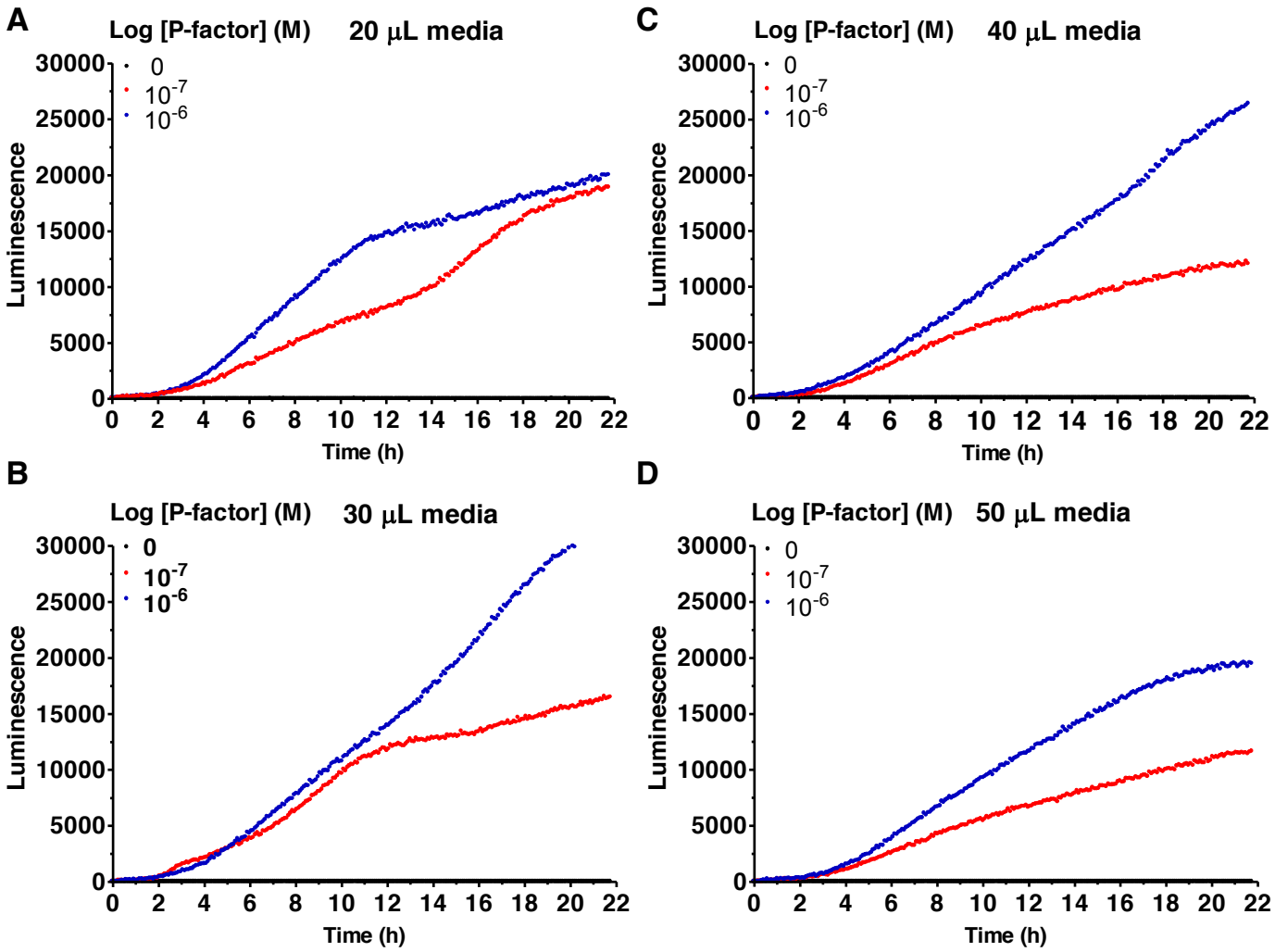

Figure 7-17: Varying the amount of media used in cell suspensions added to plugs

Agarose-AA plugs were prepared in the wells of a 24-well microplate. Plugs contained 1% agarose and 0-10^{-4} M pheromone dissolved in AA media. 10^8 JY1552 cells (*sxa2>Rluc*) suspended in 20, 30, 40 or 50 µL AA media containing 60 µM EnduRen were uniformly distributed on each plug. The Luminescence intensity from samples was then measured every 10 minutes for 24 h using a Berthold Mithras LB940 BRET multimode microplate reader (Berthold Technologies, UK) **A:** Luminescence intensity of 10^8 cells over time suspended in 20 µL AA media **B:** Luminescence intensity of 10^8 cells over time suspended in 30 µL AA media **C:** Luminescence intensity of 10^8 cells over time suspended in 40 µL AA media. **D:** Luminescence intensity of 10^8 cells over time suspended in 50 µL AA media.

7.7 Summary

Two new *Sz. pombe* reporters were successfully constructed incorporating the *Rluc* or *Rluc8* genes in place of *sxa2* in the yeast genome. A discrete assay measuring the changes in luminescence intensity produced from cells successfully depicted the pheromone-response, and luminescence was found to increase linearly with increased amounts of cells used in the assays. The Rluc reporter appeared more sensitive than the previously characterized GFP reporter and to some extent the β-galactosidase reporter because cells were found to respond earlier. Higher sensitivity was likely achieved through low background noise levels, short half-life of the Rluc enzyme and minimized signalling from dead cells within populations. The Rluc8 enzyme produced brighter luminescence readings compared to Rluc, although it was unclear if this is due to increased activity of the enzyme or other factors. Western blots showed that Rluc is more abundant in cells compared to Rluc8 in response to pheromone, possibly because of degradation of Rluc8 as indicated by the Rluc8 break-down product. The use of different media did not appear to influence signals however the choice of microplate proved important for reproducible measurements. The black plate with white wells provided the most repeatable measurements but autoluminescence of the plate meant that a delay of 2 minutes was implemented prior to measurements.

A continuous automated assay proved difficult to develop. This in part appeared to be due to destabilization of the Rluc substrate EnduRen with time, which is needed for production of photons, because increased concentrations of EnduRen did not result in higher luminescence measurements. Another factor making continuous monitoring of the pheromone-response challenging was the settling of cells to the bottom of wells and settling was shown to decrease the measured response. The pheromone-response also did not appear to tail-off, which is observed both in the discrete time-resolved assay and when using the *lacZ* reporter, but instead increased at a constant rate similar to the GFP reporter (Smith 2009). When continuous measurements were performed on agarose plugs, rather than in suspension, the amount of media used for plating was found to influence the onset of the pheromone-response, possibly because cells need to settle onto the pheromone-containing agar before pheromone can be sensed.

8 DISCUSSION

8.1 Overview

GPCRs couple extracellular ligands to intracellular signalling components, enabling cells to sense and respond to their environment. These receptors all adopt a common structural topology consisting of seven transmembrane-spanning domains and contrary to the traditional view that these domains merely act as anchors to the lipid bilayer, they appear to influence many processes such as protein function, localization, activation, structure, ligand binding and protein-protein interactions. A better understanding of GPCRs has the potential to lead to better therapeutics; however, the study of GPCR signalling in mammalian cells is complicated by the existence of multiple, overlapping signalling pathways. The model organism fission yeast *Sz. pombe* in contrast provides a simplified system in which to investigate isolated signalling pathways.

This thesis mainly focused on the first transmembrane domain of the *Sz. pombe* GPCR Mam2 and the *Sc. cerevisiae* GPCR STE2 and their roles in the pheromone-signalling response as well as putative GPCR-GPCR interactions. Both STE2 (Overton, Chinault et al. 2003) and Mam2 (Ladds, Davis et al. 2005) have previously been shown to form oligomeric complexes, although the nature and role of these oligomers are largely unknown. Therefore, this thesis focused on elucidating the effects of mutating the GxxxG motif of TM1 in STE2 to investigate the effects on subcellular localization, oligomerization, as well as its overall effects on pheromone signalling in *Sz. pombe*. This was done with the view to compare it to mutations of small residues found in the *Sz. pombe* pheromone receptor Mam2 that are potentially homologous to the GxxxG motif. A wide range of techniques was employed in order to characterize the TM domains. These included confocal microscopy to elucidate subcellular localization of the full length receptor, the β-galactosidase reporter assay to quantify pheromone signalling *in vivo*, resonance energy transfer to study oligomerization of full-length receptor, the TOXCAT reporter system as well as *in silico* modelling to investigate the dimerization of individual TM domains. Additionally, this thesis also discusses the development of a novel reporter assay to study pheromone signalling in *Sz. pombe*.

8.2 Effects of Mutating Small Residues in the First Transmembrane Domain of STE2 and Mam2

8.2.1 Positioning of the SmallxxxSmall Motif in TM1

The GxxxG motif in STE2 has been implicated in the oligomerization of the receptor in several studies (Overton and Blumer 2002; Overton, Chinault et al. 2003; Gehret, Bajaj et al. 2006). This thesis presented homology models of STE2, which in comparison to a previously published model appeared to be more accurate because key features in GPCRs appeared better conserved. The homology models suggested that the GxxxG motif is located at the protein:lipid interface, making it accessible to form a contact surface for receptor:receptor interactions. The Mam2 receptor contained two putative SmallxxxSmall motifs in TM1; one consisting of G49xxxS53 and one consisting of S53xxxA57. Sequence alignments of Mam2 to STE2 shown in Chapter 4 suggested that the S53xxxA57 motif represented the homologous residues to the GxxxG motif in STE2. This was further supported by TOXCAT and modelling data presented in Chapter 5, where S53xxxA57 was implicated in the oligomerization of TM1, but not G49xxxS53. The effect of mutations in the smallxxxsmall motif on the cellular level was explored in Chapter 4 where it was further shown that mutations to S53 and A57 had greater effects compared to mutating G49, as is discussed in the following sections.

8.2.2 Effects of Conservative Mutations

The cellular effects of conservative mutations to the GxxxG motif in STE2 and GxxxSxxxA in Mam2 are summarized in Table 8-1. From the summary it appears as though mutations in Mam2 had a greater effect than mutations in STE2. This may in part be due to the differences observed between wild-type Mam2 and STE2 i.e. wild-type STE2 had reduced plasma membrane localization compared to Mam2 and the receptor was found internalized to a greater extent.

For the conservative Mam2 mutants, a reduced transcriptional response was observed but not a reduced morphological response. Differences in activation of the morphological pathway and transcriptional pathway have previously been observed in *Sz. pombe* (Ladds, Goddard et al. 2007) although the reasons for this phenomenon are yet unknown. It is possible that Ras1 and STE6, which are the transcriptional activators, somehow interact with the receptor, either directly or via scaffolding mechanisms and these interactions may be altered in the mutants. The conservative Mam2 mutants were furthermore all localized to the plasma membrane to a greater extent than wild-type Mam2, suggesting that the functionality

of the receptor, rather than expression at the plasma membrane, was affected. In the TOXCAT assay, Mam2 TM1 was found to oligomerize strongly, an effect not observed for STE2. Mutations to the SxxxA residues were found to have a greater effect on cellular signalling as well as oligomerization of the TM domain, compared to the GxxxS residues. This data was also supported by *in silico* CHI modelling of receptor dimerization. This may suggest that the transcriptional response is amplified by receptor oligomers. In contrast, mutations to the STE2 GxxxG motif had less of an effect on the cellular signalling, but this domain was not however found to oligomerize strongly in neither the TOXCAT assay nor *in silico* CHI modelling. Other studies on STE2 have suggested that the presence of TM2 is necessary to form stable receptor oligomers (Overton and Blumer 2002) which is not contradictory to the findings here. The studies on TM2 presented in this thesis however seemed to be hampered by the presence of high amounts of polar residues in the TM domain.

	Conservative mutation	Transcriptional response	Morphological response	Plasma membrane localization	Ratio of internalized receptor
STE2	**G56A**	-	-	-	-
	G60A	-	-	-	-
	G56A,G60A	↓	↓	↓	↑
Mam2	**G49A**	-	-	↑	↑
	S53A	↓	-	↑	↑
	A57G	↓	-	↑	↑
	S53A,A57G	↓	-	↑	↑

Table 8-1: The effects of conservative mutations on STE2 and Mam2

The effects of conservative mutations made in TM1 of STE2 and Mam2 on the transcriptional pheromone-response, the morphological pheromone-response, plasma membrane localization and the ratio of internalized receptor to receptor found on the plasma membrane are summarized. A – indicates that no significant difference could be detected compared to wild-type receptor. Cells colored in orange indicate that a moderately decreased effect was observed compared to wild-type receptor. Green cells indicate that an increased effect was observed compared to wild-type receptor.

8.2.3 Effects of Non-Conservative Mutations

In comparison to the conservative mutations, the leucine mutations all had a much greater effect on the cellular responses observed, as illustrated in Table 8-2. In particular, leucine mutations to any of the STE2 GxxxG residues greatly reduced the observed responses. Because there was a decrease both in the pheromone-response as well as plasma membrane localization, it appears likely that the reduction in signaling is due to few receptors being available for signal transduction. It therefore appears likely that these mutant receptors are either not transported to the plasma membrane as effectively as wild-type receptor, or they get internalized at a greater rate. The confocal images suggest that the receptors localized to endosomes and/or vacuoles suggesting that they were not trapped in the ER. Previous studies on misfolded mutants of STE2 have shown that in *Sc. cerevisiae,* errors in folding in the ER may lead to transport of the receptor from the ER to vacuolar structures, without the receptor reaching the plasma membrane (Jenness, Li et al. 1997) which could explain this phenomenon.

Mam2 also displayed a reduction in activity when the small G49, S53 and A57 residues were mutated to leucine, although these effects were less severe than for STE2. Most notably, the mutants did not display a significant decrease in plasma membrane expression, with the exception of the GxxxS double mutant, suggesting that the functionality of the receptor was affected rather than the amounts available for signal transduction. In general, mutations to the S53 and A57 residues had a greater effect than for the G49 residue. Additionally, SxxxA was implied as an oligomerization motif in the *in silico* modelling, and mutations to this motif decreased oligomerization. It therefore appears likely that Mam2 oligomers may form via the SxxxA motif. Unfortunately, the BRET assay was not successfully implemented in the lab in time for completion of this thesis. Work is currently underway to clone different fusions of acceptors and donors, to find a suitable pair, including Rluc, Rluc8, GFP and YFP.

	Disfavored mutation	Transcriptional response	Morphological response	Plasma membrane localization	Ratio of internalized receptor
STE2	**G56L**	↓	↓	↓	↑
	G60L	↓	↓	↓	↑
	G56L,G60L	↓	↓	↓	↑
Mam2	**G49L**	↓	↓	-	-
	S53L	↓	↓	-	↑
	A57L	↓	↓	-	↑
	S53L,A57L	↓	↓	↓	↑

Table 8-2: The effects of disfavored mutations on STE2 and Mam2

The effects of disfavored mutations made in TM1 of STE2 and Mam2 on the transcriptional pheromone-response, the morphological pheromone-response, plasma membrane localization and the ratio of internalized receptor to receptor found on the plasma membrane are summarized. A – indicates that no significant difference could be detected compared to wild-type receptor. Cells colored in orange indicate that a moderately decreased effect was observed compared to wild-type receptor. Red cells indicate that a greatly decreased effect was observed compared to wild-type receptor.

8.3 Prospects of Modelling Interactions between Single Transmembrane Domains from Polytopic Transmembrane Proteins

CHI has previously been used to successfully model the dimerization or higher-order oligomerization of a range of single-spanning membrane proteins such as GpA (Adams, Engelman et al. 1996), phospholamban (Adams, Arkin et al. 1995), holin (Pang, Savva et al. 2009), granulocyte colony-stimulating factor receptor (Plo, Zhang et al. 2009) or the bovine papillomavirus E5 protein (King, Oates et al. 2011). Although CHI has been used to predict the structure of the bitopic protein Carnitine Palmitoyltransferase (Jenei, Borthwick et al. 2009), it has not traditionally been used extensively to model the oligomerization of transmembrane domains from polytopic proteins.

In the studies presented in Chapter 5, it was attempted to exploit modelling to predict interactions between wild-type and mutated TM domains and to draw parallels between the two and extrapolate the findings to full-length receptor. The results appear mixed. Modelling of the relatively hydrophobic TM1 domain of Mam2 produced structures that could be interpreted relatively readily and which agreed with experimental data. Similarly the modelling of TM1 from STE2 agreed with experimental data and indicated that this TM domain is not sufficient to drive oligomerization, similar to findings that TM2 is also needed for interactions (Overton and Blumer 2002). In comparison, the relatively long hydrophilic TM2 domains from STE2 and Mam2 produced complex and inconclusive results, which were difficult to interpret. This was probably in part due to the sheer amount of interactions that could be formed by the relatively polar domains through intra- or inter-molecular contacts. These results suggested that the stability of isolated TM domains may depend on their relative hydrophobicity.

To investigate how relevant it is to model GPCR oligomerization on the basis of isolated TM domains, the interactions between two TM domains from rhodopsin were modelled and compared to the crystal structure of the receptor. It was found that the interactions observed in the crystal structure could not be reproduced via CHI modelling. This raised questions as to whether individual domains from large polytopic proteins can be treated as individual stable units, as postulated by the two-stage model of membrane protein folding. Previous studies on the 7TM receptor bacteriorhodopsin have also shown that TM6 and TM7 are not stable in isolation of other TM domains (Hunt, Earnest et al. 1997). Furthermore, an existing NMR structure of STE2 TM1-TM2 (Neumoin, Cohen et al. 2009) did not structurally agree with the homology model of STE2, which further highlights disagreement both between

computational models and experimental data and also between full-length receptor models and models of isolated TM domains.

8.4 Foundations for a More Sensitive High-Throughput Pheromone-response Reporter Assay

The creation of the luminescent reporter strain JY1552 (*sxa2>Rluc*) allowed for the development of a discrete live-cell assay that is more sensitive than the assay measuring β-galactosidase reporter activity in lysed cells. A continuous, high-throughput assay was also developed, which appeared more sensitive than the equivalent high-throughput GFP reporter assay.

8.5 Future Directions

Despite the many studies on GPCR oligomerization there still remains much to be understood regarding how interactions between receptors are formed. The research presented in this thesis has demonstrated that although the study of isolated TM domains from GPCRs is more amenable, it may not be physiologically relevant. There is consequently a need for high resolution structures of receptors in order to gain further understanding of GPCR pharmacology. More experimental structural data would also allow the development of more accurate computer algorithms in order to produce better models. It would be interesting to test the accuracy of the homology models presented in this thesis. This could be achieved for instance through mutating the residues involved in forming the putative ionic lock in the STE2 receptor, to see whether a CAM phenotype is observed similar to in the β2-adrenergic receptor.

It would be useful to advance the work initiated on developing a BRET assay for *Sz. pombe*. Partly in order to elucidate real-time interactions between wild-type components of the pheromone-response pathway, but also to test the importance of individual residues on processes such as oligomerization. This could be achieved by testing different donor and acceptor combinations. Rluc may for instance couple more successfully to YFP, and Rluc8 may provide a better donor.

9 REFERENCES

Abramoff, M., P. Magalhaes, et al. (2004). "Image processing with ImageJ." Biophotonics International **11**: 36-42.

Achour, L., C. Labbe-Jullie, et al. (2008). "An escort for GPCRs: implicatios for regulation of receptor density at the cell surface." Trends in Pharmacological Sciences **29**: 528-535.

Adams, P., I. Arkin, et al. (1995). "Computational searching and mutagenesis suggest a structure for the pentameric transmembrane domain of phospholamban." Nature Structural Biology **2**: 154-162.

Adams, P., D. Engelman, et al. (1996). "Improved prediction for the structure of the dimeric transmembrane domain of glycophorin A obtained through global searching." Proteins **26** 257-261.

Ahmadian, M. R., P. Stege, et al. (1997). "Confirmation of the arginine-finger hypothesis for the GAP stimulated GTP hydrolysis reaction of Ras." Nature Structural Biology **4**: 686-689.

Ahuja, S. and S. O. Smith (2009). "Multiple switches in G protein-coupled receptor activation." Trends in Pharmacological Sciences **30**: 494-502.

Alberts, B., A. Johnson, et al. (2002). Molecular Biology of the Cell, 4th edition. New York, Garland Sciences.

Albizu, L., M. Cottet, et al. (2010). "Time-resolved FRET between GPCR ligands reveals oligomers in native tissues." Nature chemical biology **6**: 587-597.

Arkinstall, S., M. Edgerton, et al. (1995). "Coexpression of the neurokinin NK2 receptor and G-protein components in the fission yeast Schizosaccharomyces pombe." FEBS Letters **375**: 183-187.

Balabanian, K., B. Lagane, et al. (2005). "WHIM syndromes with different genetic anomalies are accounted for by impaired CXCR4 desensitization to CXCL12." Blood **105**: 2449-2457.

Ballesteros, J. A., A. D. Jensen, et al. (2001). "Activation of the beta 2-adrenergic receptor involves disruption of an ionic lock between the cytoplasmic ends of transmembrane segments 3 and 6." Journal of Biological Chemistry **276**: 29171-29177.

Barlow, D. J. and J. M. Thornton (1988). "Helix geometry in proteins." Journal of Molecular Biology **201**: 601-619.

Barlowe, C. (2003). "Signals for COPII-dependent export from the ER: what's the ticket out?" Trends in Cell Biology **13**: 295-300.

Beevers, A. J. and A. M. Dixon (2010). "Helical membrane peptides to modulate cell function." Chemical Society Reviews **39**: 2146-2157.

Bibi, E. and H. R. Kaback (1990). "In vivo expression of the lacY gene in two segments leads to functional lac permease." Proceedings of the National Academy of Science USA **87**: 4325-4329.

Bill, R. M., P. J. F. Henderson, et al. (2011). "Overcoming barriers to membrane protein structure determination." Nature Biotechnology **29**: 335-340.

Blumer, J. B., M. J. Cismowski, et al. (2005). "AGS proteins: receptor-independent activators of G-protein signaling." Trends in Pharmacological Sciences **26**: 470-476.

Bocharov, E. V., P. E. Volynsky, et al. (2010). "Structure elucidation of dimeric transmembrane domains of bitopic proteins." Cell Adhesion & Migration **4**: 284-298.

Bockaert, J. and J. P. Pin (1999). "Molecular tinkering of G protein-coupled receptors: an evolutionary success." The EMBO Journal **18**: 1723-1729.

Bosco, E. E., J. C. Mulloy, et al. (2009). "Rac1 GTPase: a "Rac" of all trades." Cellular and Molecular Life Sciences **66**: 370-374.

Bouschet, T., S. Martin, et al. (2005). "Receptor-activity-modifying proteins are required for forward trafficking of the calcium-sensing receptor to the plasma membrane." Journal of Cell Science **118**: 4709-4720.

Boyd, D., C. Schierle, et al. (1998). "How many membrane proteins are there?" Protein Science **7**: 201-205.

Bradford, M. M. (1976). "A rapid and sensitive method for the quantitation of microgram quantities of protein utilizing the principle of protein-dye binding." Analytical Biochemistry **72**: 248-254.

Brismar, H., M. Asghar, et al. (1998). "Dopamine-induced recruitment of dopamine D1 receptors to the plasma membrane." Proceedings of the National Academy of Science USA **95**: 5573-5578.

Brooker, R. J., E. P. Widmaier, et al. (2007). Biology, McGraw-Hill, New York.

Brunger, A. T., P. D. Adams, et al. (1998). "Crystallography & NMR system: A new software suite for macromolecular structure determination." Acta Crystallogr D Biol Cystallogr **54**: 905-921.

Canals, M., L. Jenkins, et al. (2006). "Up-regulation of the angiotensin II type 1 receptor by the MAS proto-oncogene is due to constitutive activation of Gq/G11 by MAS." The Journal of Biological Chemistry **281**: 16757-16767.

Chabre, M. and M. le Maire (2005). "Monomeric G-protein-coupled receptor as a functional unit." Biochemistry **44**: 9395-9403.

Chen, S. H., F. Lin, et al. (2002). "Mutation of a single TMVI residue, Phe(282), in the beta2-adrenergic receptor results in structurally distinct activated receptor conformations." Biochemistry **41**: 6045-6053.

Cherezov, V., D. M. Rosenbaum, et al. (2007). "High-resolution crystal structure of an engineered human beta/2 adrenergic G protein-coupled receptor." Science **318**: 1258-1265.

Chien, E. Y., W. Liu, et al. (2010). "Structure of the human dopamine D3 receptor in complex with a D2/D3 selective antagonist." Science **330**: 1091-1095.

Choe, H. W., Y. J. Kim, et al. (2011). "Crystal structure of metarhodopsin II." Nature **471**: 651-655.

Choi, Y. and J. B. Konopka (2006). "Accessibility of Cysteine Residues Substituted into the Cytoplasmic Regions of the alpha-Factor Receptor Identifies the Intracellular Residues That Are Available for G protein Interaction." Biochemistry **45**: 15310-15317.

Choma, C., H. Gratkowski, et al. (2000). "Asparagine-mediated self-association of a model transmembrane helix." Nature Structural Biology **7**: 161-166.

Ciruela, F., M. Gomez-Soler, et al. (2011). "Adenosine receptor containing oligomers: their role in the control of dopamine and glutamate neurotransmission in the brain." Biochimica et Biophysica Acta - Biomembranes **1808**: 1245-1255.

Cismowski, M. J. (2006). "Non-receptor activators of heterotrimeric G-protein signaling (AGS proteins)." Seminars in cell & developmental biology **17**: 334-344.

Cismowski, M. J., A. Takesono, et al. (1999). "Genetic screens in yeast to identify mammalian nonreceptor modulators of G-protein signaling." Nature Biotechnology **17**: 878-883.

Clothia, C. and A. M. Lesk (1986). "The relation between the divergence of sequence and structure in proteins." The EMBO Journal **5**: 823-826.

Cohen, L., B. Arshava, et al. (2008). "Expression and biophysical analysis of two double-transmembrane domain-containing fragments from a yeast G protein-coupled receptor." Biopolymers **90**: 117-130.

Costanzi, S. (2010). "Modeling G protein-coupled receptors: a concrete possibility." Chimica oggi **28**: 26-31.

Crowe, M. L., B. N. Perry, et al. (2000). "G_{olf} complements a GPA1 null mutation in *Saccharomyces cerevisiae* and functionally couples to the STE2 pheromone receptor." Journal of Receptors and Signal Transduction Research **20**: 61-73.

Curran, A. R. and D. M. Engelman (2003). "Sequence motifs, polar interactions and conformational changes in helical membrane proteins." Current Opinion in Structural Biology **13**: 412-417.

Davey, J. (1991). "Isolation and quantitation of M-factor, a diffusible mating factor from he fission yeast Schizosaccharomyces pombe." Yeast **7**: 357-366.

Davey, J. (1992). "Mating pheromones of the fission yeast Schizosaccharomyces pombe: purification and structural characterization of M-factor and isolation and analysis of two genes encoding the pheromone." The EMBO Journal **11**: 951-960.

Davey, J. (1998). "Fusion of a fission yeast." Yeast **14**: 1529-1566.

Davey, J. and O. Nielsen (1994). "Mutations in cyr1 and pat1 reveal pheromone-induced G1 arrest in the fission yeast schizosaccharomyces pombe." Current Genetics **26**: 105-112.

David, M., M. Richer, et al. (2006). "Interactions between GABA-B1 receptors and Kir3 inwardly recrifying potassium channels." Cellular Signalling **18**: 2172-2181.

Davis, K., C. Pateman, et al. (1999). "Gene disruption in *Schizosaccharomyces pombe* using a temperature-sensitive Ura4p." Yeast **15**: 1231-1236.

Decaillot, F. M., M. A. Kazmi, et al. (2011). "CXCR7/CXCR4 heterodimer constitutively recruits {beta}-arrestin to enhance cell migration." The Journal of Biological Chemistry **Epub ahead of print**.

DeFea, K. (2011). "Beta-arrestins as regulators of signal termination and transduction: How do they determine what to scaffold? ." Cellular Signalling **23**: 621-629.

Didmon, M., K. Davis, et al. (2002). "Identifying regulators of pheromone signalling in the fission yeast Schizosaccharomyces pombe. ." Current Genetics **41**: 241-253.

Doherty, G. J. and H. T. McMahon (2009). "Mechanisms of endocytosis." Annual Review of Biochemistry **78**: 857-902.

Dohlman, H. G. (2002). "G proteins and pheromone signalling." Annual Review of Physiologyy **64**: 129-152.

Dohlman, H. G., D. Apaniesk, et al. (1995). "Inhibition of G-protein signaling by dominant gain-of-function mutations in Sst2p, a pheromone desensitization factor in Saccharomyces cerevisiae." Molecular and Cellular Biology **15**: 3635-3643.

Dohlman, H. G. and J. Thorner (1997). "RGS proteins and signaling by heterotrimeric G proteins." The Journal of Biological Chemistry **272**: 3871-3874.

Dong, C., C. M. Filipeanu, et al. (2007). "Regulation of G protein-coupled receptor export trafficking." Biochimica et Biophysica Acta **1768**: 853-870.

Dormann, D., T. Libotte, et al. (2002). "Simultaneous quantification of cell motility and protein-membrane-association using active contours." Cell Motility and the Cytoskeleton **52**: 221-230.

Dougherty, D. A. (1996). "Cation-pi interactions in chemistry and biology: a new view of benzene, phe, tyr and trp." Science **271**: 163-168.

Doura, A. K., F. J. Kobus, et al. (2004). "Sequence context modulates the stability of a GxxxG mediated transmembrane helix-helix dimer." Journal of Molecular Biology **341**: 991-998.

Dowell, S. J. and A. J. Brown (2002). "Yeast assays for G protein-coupled receptors." Receptors Channels **8**: 343-352.

Edrington, T. C. t., M. Bennett, et al. (2008). "Calorimetric studies of bovine rod outer segment disk membranes support a monomeric unit for both rhodopsin and opsin." Biophys J. **95**: 2859-2866.

Eilers, M., V. Hornak, et al. (2005). "Comparison of class A and D G protein-coupled receptors: common features in structure and activation." Biochemistry **44**: 8959-8975.

Elling, C. E., T. M. Frimurer, et al. (2005). "A global toggle switch activation mechanism for 7TM receptors - dissected through metal ion site engineering." Journal of Molecular Biology.

Engelman, D., Y. Chen, et al. (2003). "Membrane protein folding: beyond the two-stage model." FEBS Letters **555** 122-125.

Escher, C., F. Cymer, et al. (2009). "Two GxxxG-like motifs facilitate promiscuous interactions of the human ErbB transmembrane domains." Journal of Molecular Biology **389**: 10-16.

Ferré, S., R. Baler, et al. (2009). "Building a new conceptual framework for receptor heteromers." Nat Chem Biol **5**: 131-134.

Ficca, A. G., L. Testa, et al. (1995). "The human β2-adrenergic receptor expressed in Schizosaccharomyces pombe retains its

pharmacological properties." The Journal of Biological Chemistry **274**: 6188-6190.

Fisher, L. E., D. M. Engelman, et al. (1999). "Detergents modulate dimerization, but not helicity, of the glycophorin A transmembrane domain." Journal of Molecular Biology **293**: 639-651.

Forfar, R. (2007). Expression and characterisation of GPCRs in *Schizosacharomyces pombe* PhD, University of Warwick.

Fredriksson, R., M. C. Lagerstrom, et al. (2003). "The G-protein-coupled receptors in the human genome form five main families. Phylogenetic analysis, paralogon groups, and fingerprints. ." Molecular Pharmacology **63**: 1256-1272.

Gabriely, G., R. Kama, et al. (2007). "Involvement of specific COPI subunits in protein sorting from the late endosome to the vacuole in yeast." Molecular and Cellular Biology **27**: 526-540.

Gachet, Y. and J. S. Hyams (2005). "Endocytosis in fission yast is spatially associated with the actin cytoskeleton during polarised cell growth and cytokinesis." Journal of Cell Science **118**: 4231-4242.

Gehret, A., A. Bajaj, et al. (2006). "Oligomerization of the yeast α-factor receptor, implications for dominant negative effects of mutant receptors." The Journal of Biological Chemistry **281** 20698-20714.

Gether, U., S. Lin, et al. (1997). "Agonists induce conformational changes in transmembrane domains III and VI of the beta2 adrenoceptor." The EMBO Journal **16**: 6737-6747.

Glynn, J. M., R. J. Lustig, et al. (2001). "Role of bud6p and tea1p in the interaction between actin and microtubules for the establishment of cell polarity in fission yeast." Current Biology **11**: 836-845.

Goddard, A., G. Ladds, et al. (2005). "Development of a semi-quantitative plate-based alpha-galactosidase gene reporter for Schizosachharomyces pombe and its use to isolate a constitutively active Mam2." Yeast Functional Analysis Report **22**: 31-41.

Goddard, A., G. Ladds, et al. (2006). "Identification of Gnr1p, a negative regulator of Gα signalling in Schizosaccharomyces pombe, and its complementation by human Gβ subunits." Fungal Genetics and Biology **43**: 840-851.

Gorman, C. M., L. F. Moffat, et al. (1982). "Recombinant genomes which express chloramphenicol acetyltransferase in mammalian cells." Molecular and Cellular Biology **2**: 1044-1051.

Gratkowski, H., J. D. Lear, et al. (2001). "Polar side chains drive the association of model transmembrane peptides." Proceedings of the National Academy of Science USA **98**: 880-885.

Grimm, C., J. Kohli, et al. (1988). "Genetic engineering of Schizosaccharomyces pombe: a system for gene disruption and replacement using the ura4 gene as a selectable marker." Molecular genetics and genomics **215**: 81-86.

Groves, J. D. and M. J. Tanner (1995). "Co-expressed complementary fragments of the human red cell anion exchanger (band 3 AE1) generate stilbene disulfonate-sensitive anion transport." The Journal of Biological Chemistry **270**: 9097-9105.

Gulbins, E., K. M. Coggeshall, et al. (1994). "Activation of Ras in vitro and in intact fibroblasts by the Vav guanine nucleotide exchange protein." Molecular and Cellular Biology **14**: 906-913.

Gurevich, V. and E. Gurevich (2008). "GPCR monomers and oligomers: it takes all kinds." Trends in Neurosciences **31**: 74-81.

Guthrie, C. and G. R. Fink (2002). "Guide to yeast genetics and molecular and cell biology Part C." 414.

Han, Y., I. S. Moreira, et al. (2009). "Allosteric communication between protomers of dopamine class A GPCR dimers modulates activation." Nature chemical biology **5**: 688-695.

Hanson, M. A. and R. C. Stevens (2009). "Discovery of New GPCR Biology: One Receptor Structure at a Time " Structure **17**: 8-14.

Hargrave, P. A., J. H. McDowell, et al. (1983). "The structure of bovine rhodopsin." Biophysics of Structure and Mechanism **9**: 235-244.

Hebert, T., S. Moffett, et al. (1996). "A peptide derived from a beta2-adrenergic receptor transmembrane domain inhibits both receptor dimerization and activation." The Journal of Biological Chemistry **271**: 16384-16392.

Hein, L., K. Ishii, et al. (1994). "Intracellular targeting and trafficking of thrombin receptors. A novel mechanism for resensitization of a G protein-coupled receptor." The Journal of Biological Chemistry **269**: 27719-27726.

Henderson, R., J. M. Baldwin, et al. (1991). "Model for the structure of Bacteriorhodopsin based on high-resolution Electron Cryo-microscopy." Journal of Molecular Biology **213**: 899-929.

Hicke, L. and H. Riezman (1996). "Ubiquitination of a yeast plasma membrane receptor signals its ligand-stimulated endocytosis." Cell **84**: 277-287.

Hicke, L., B. Sanolari, et al. (1998). "Cytoplasmic tail phosphorylation of the alpha-factor receptor is required for it ubiquitination and internalization." The Journal of Cell Biology **141**: 349-358.

Higy, M., T. Junne, et al. (2004). "Topogenesis of membrane proteins at the endoplasmic reticulum." Biochemistry **43**: 12716-12722.

Hill, C., A. Goddard, et al. (2009). "The cationic region of Rhes mediates its interactions with specific Gbeta subunits." Cellular Physiology and Biochemistry **23**: 1-8.

Hoffman, C. and F. Winston (1987). "A ten-minute DNA preparation from yeast efficiently releases autonomous plasmids for transfomration of Escherichia coli. ." Gene **57**: 267-272.

Hoffman, C. S. (2005). "Except in every detail: comparing and contrasting G-protein signaling in Saccharomyces cerevisiae and Schizosaccharomyces pombe." Eukaryotic cell **4**: 495-503.

http://pdbtm.enzim.hu/. (2011). Retrieved 2011-06-09.

Hunt, J. F., T. N. Earnest, et al. (1997). "A biophysical study of integral membrane protein folding." Biochemistry **36**: 15156-15176.

Hwa, J., P. Garriga, et al. (1997). "Structure and function of rhodopsin - packing of the helices in the transmembrane domain and folding to a tertiary structure in the intradiscal domain are coupled." Proceedings of the National Academy of Science USA **94**: 10571-10576.

Imai, Y. and M. Yamamoto (1992). "Schizosaccharomyces pombe sxa1+ and sxa2+ encode putative proteases involved in the mating response." Molecular and Cellular Biology **12**: 1827-1834.

Imai, Y. and M. Yamamoto (1994). "The fission yeast mating pheromone P-factor: its molecular structure, gene structure, and ability to induce gene expression and G1 arrest in the mating partner " Genes and Development **8**: 328-338.

Ittner, L. M., D. Koller, et al. (2005). "The N-terminal extracellular domain 23-60 of the calcitonin receptor-like receptor in chimeras with the parathyroid hormone receptor mediates association with receptor activity-modifying protein 1." Biochemistry **44**: 5749-5754.

Ivey, F. D. and C. S. Hoffman (2005). "Direct activation of fission yeast adenylate cyclase by the Gpa2 Gα of the glucose signaling pathway." Proceedings of the National Academy of Science USA **102**: 6108-6113.

Jaakola, V. P., M. T. Griffith, et al. (2008). "The 2.6 angstrom crystal structure of a human A2A adenosine receptor bound to an antagonist." Science **322**: 1211-1217.

Jalink, K. and W. H. Moolenaar (2010). "G protein-coupled receptors: the inside story." Bioessays **32**: 13-16.

Javadpour, M. M., M. Eilers, et al. (1999). "Helix packing in polytopic membrane proteins: role of glycine in transmembrane helix association." Biophysical Journal **77**: 1609-1618.

Jenei, Z. A., K. Borthwick, et al. (2009). "Self-association of transmembrane domain 2 (TM2), but not TM1, in carnitine palmitoyltransferase 1A: role of GXXXG(A) motifs." The Journal of Biological Chemistry **284**: 6988-6997.

Jenness, D. D., Y. Li, et al. (1997). "Elimination of defective alpha-factor pheromone receptors." Molecular and Cellular Biology **17**: 6236-6245.

Johnson, R., A. Rath, et al. (2006). "The position of the Gly-xxx-Gly motif in transmembrane segments modulates dimer affinity." Biochemistry and Cell Biology **84** 1006-1012.

Johnson, R. M., K. Hecht, et al. (2007). "Aromatic and cation-pi interactions enhance helix-helix association in a membrane environment." Biochemistry **46**: 9208-9214.

Johnsson, N. and A. Varshavsky (1994). "Split ubiquitin as a sensor of protein interactions in vivo." Proceedings of the National Academy of Science USA **91**: 10340-10344.

Johnston, J., M. Aburi, et al. (2011). "Making structural sense of dimerization interfaces of delta opioid receptor homodimers." Biochemistry **50**: 1682-1690.

Jones, D., W. Taylor, et al. (1994). "A mutation data matrix for transmembrane proteins." FEBS Letters **339**: 269-275.

Jordan, B. and L. Devi (1999). "G-protein-coupled receptor heterodimerization modulates receptor function." Nature **399**: 697-700.

Jordan, B. A., N. Trapaidze, et al. (2001). "Oligomerization of opioid receptors with beta 2-adrenergic receptors: a role in trafficking and mitogen activated protein kinase activation." Proceedings of the National Academy of Science USA **98**: 343-348.

Kahn, T. W. and D. M. Engelman (1992). "Bacteriorhodopsin can be refolded from two independently stable transmembrane helixes and the complementary five-helix fragment." Biochemistry **31**: 6144-6151.

Kain, S. R., M. Adams, et al. (1995). "Green fluorescent protein as a reporter of gene expression and protein localization." Biotechniques **19**: 650-655.

Kaksonen, M., Y. Sun, et al. (2003). "A pathway for association of receptors, adaptors, and actin during endocytic internalization." Cell **115**: 475-487.

Kataoka, M., T. W. Kahn, et al. (1992). "Bacteriorhodopsin reconstituted from two individual helices and the complementary five-helix fragment is photoactive." Photchemistry and photobiology **56**: 895-901.

Kenakin, T. (2002). "Efficacy at G protein-coupled receptors." Nature Reviews Drug Discovery **1**: 103-110.

Khafizov, K., G. Lattanzi, et al. (2003). "G protein inactive and active forms investigated by simulation methods." Proteins **75**: 919-930.

Kim, H., B. K. Lee, et al. (2009). "Identification of specific transmembrane residues and ligand-induced interface changes involved in homo-dimer formation of a yeast G protein-coupled receptor." Biochemistry **48**: 10976-10987.

Kim, H., P. Yang, et al. (2003). "The kelch repeat protein, Tea1, is a potential substrate target of the p21-activated protein kinase, Shk1, in the fission yeast, *Schizosaccharomyces pombe*. ." The Journal of Biological Chemistry **278**: 30074-30082.

King, G. and A. M. Dixon (2010). "Evidence for role of transmembrane helix-helix interactions in the assembly of the Class II major histocompability complex." Molecular BioSystems **6**: 1650-1661.

King, G., J. Oates, et al. (2011). "Towards a structural undersanding of the smallest known oncoprotein: Investigation of the bovine papillomavirus E5 protein using solution-state NMR." Biochimica et Biophysica Acta **1808**: 1493-1501.

Kjaerulff, S., I. Lautrup-Larsen, et al. (2005). "Constitutive activation of the fission yeast pheromone-responsive pathway induces ectopic meiosis and reveals ste11 as a mitogen-activated protein kinase target." Mol Cell Biol **25**: 2045-2059.

Klar, A. and L. Miglio (1986). "Initiation of meiotic recombination by double-strand DNA breaks in S. pombe. ." Cell **46**: 725-731.

Klco, J., T. Lassere, et al. (2003). "C5a receptor oligomerization. I. Disulfide trapping reveals oligomers and potential contact surfaces in a G protein-coupled receptor." The Journal of Biological Chemistry **278**: 35345-35353.

Konopka, J. B., S. M. Margarit, et al. (1996). "Mutation of Pro-258 in transmembrane domain 6 constitutively activates the G protein-coupled alpha-factor receptor." Proceedings of the National Academy of Science USA **93**: 6764-6769.

Kostenis, E., G. Milligan, et al. (2005). "G-protein-coupled receptor Mas is a physiological antagonist of the angiotensin II type 1 receptor." Molecular Cardiology **111**: 1806-1813.

Krebs, M. P., S. M. Noorwez, et al. (2004). "Quality control of integral membrane proteins." TRENDS in Biochemical Sciences **29**: 648-655.

Krogh, A., B. Larsson, et al. (2001). "Predicting transmembrane protein topology with a hidden Markov model: Application to complete genomes. ." Journal of Molecular Biology **305**: 567-580.

Kruse, M. S., S. Adachi, et al. (2003). "Recruitment of renal dopamine 1 receptors requires an intact microtubulin network." Pflugers Archiv: European journal of physiology **445**: 534-539.

Kuhl, I., L. Dujeancourt, et al. (2011). "A genome wide study in fission yeast reveals nine PPR proteins that regulate mitochondrial gene expression." Nucleic Acids Research **Epub ahead of print**.

Kunishima, N., Y. Shimada, et al. (2000). "Structural basis of glutamate recognition by a dimeric metabotropic gltamate receptor." Nature **407**: 971-977.

Kuwasako, K., Y. Shimekake, et al. (2000). "Visualization of the calcitonin receptor-like receptor and its receptor activity-modifying proteins during internalization and recycling." The Journal of Biological Chemistry **275**: 29602-29609.

Ladds, G. Pers comm.

Ladds, G. and J. Davey (2000). "Sxa2 is a serine carboxypeptidase that degrades extracellular P-factor in the fission yeast Schizosaccharomyces Pombe." Molecular microbiology **36**: 377-390.

Ladds, G., K. Davis, et al. (2005). "A constitutively active GPCR retains its G protein specificity and the ability to form dimers." Molecular microbiology **55** 482-497.

Ladds, G., K. Davis, et al. (2003). "Modified yeast cells to investigate the coupling of G protein-coupled receptors to specific G proteins." Molecular Microbiology **47**: 781-792.

Ladds, G., A. Goddard, et al. (2005). "Functional analysis of heterologous GPCR signalling pathways in yeast." Trends in biotechnology **23**: 367-373.

Ladds, G., A. Goddard, et al. (2007). "Differential effects of RGS proteins on Gαq and Gα11 activity." Cellular Signalling **19**: 103-113.

Ladds, G., E. Rasmussen, et al. (1996). "The sxa2-dependent inactivation of the P-factor mating pheromone in the fission yeast Schizosaccharomyces pombe." Molecular microbiology **20**: 35-42.

Laemmli, U. (1970). "Cleavage of structural proteins during the assembly of the head of bacteriophage T4." Nature **227**: 680-685.

Lagane, B., K. Y. Chow, et al. (2008). "CXCR4 dimerization and beta-arrestin-mediated signaling account for the enhanced chemotaxis to CXCL12 in WHIM syndrome." Blood **112**: 34-44.

Lambright, D. G., J. P. Noel, et al. (1994). "Structural determinants for activation of the alpha-subunit of a heterotrimeric G protein." Nature **369**: 621-628.

Langosch, D., B. Brosig, et al. (1996). "Dimerisation of the glycophorin A transmembrane segment in membranes probed with the ToxR transcription activator." Journal of Molecular Biology **263**: 525-530.

Langosch, D. and J. Heringa (1998). "Interaction of transmembrane helices by a knobs-into-holes packing characteristic of soluble coiled coils." Proteins **31**: 150-159.

Lawrie, C. M., E. S. Sulistijo, et al. (2010). "Intermonomer hydrogen bonds enhance GxxxG-driven dimerization of the BNIP3 transmembrane domain: rolse for sequence context in helix-helix association in membranes." Journal of Molecular Biology **396**: 924-936.

Lee, A. G. (2004). "How lipids affect the activities of integral membrane proteins." Biochimica et Biophysica Acta **1666**: 62-87.

Lemmon, M. A., J. M. Flanagan, et al. (1992). "Glycophorin A dimerization is driven by specifc interactions between transmembrane alpha-helices." The Journal of Biological Chemistry **267**: 7683-7689.

Leon, S. and R. Haguenauer-Tsapis (2008). "Ubiquitin ligase adaptors: regulators of ubiquitylation and endocytosis of plasma membrane proteins." Experimental Cell Research **315**: 1574-1583.

Lewis, B. A. and D. M. Engelman (1983). "Lipid bilayer thickness varies linearly with acyl chain length in fluid phosphatidylcholine vesicles." Journal of Molecular Biology **166**: 211-217.

Li, J., P. Edwards, et al. (2004). "Structure of bovine rhodopsin in a trigonal crystal form." Journal of Molecular Biology **343**: 1409-1438.

Li, R., R. Gorelik, et al. (2004). "Dimerization of the transmembrane domain of integrin alphaIIb subunit in cell membranes." The Journal of Biological Chemistry **279** 26666-26673.

Liang, Y., D. Fotiadis, et al. (2003). "Organization of the G protein-coupled receptors rhodopsin and opsin in native membranes." The Journal of Biological Chemistry **278**: 21655-21662.

Lin, J. C., K. Duell, et al. (2004). "A microdomain formed by the extracellular ends of the transmembrane domains promotes activation of the G protein-coupled alpha-factor receptor." Mol Cell Biol **24**: 2041-2051.

Lindner, R. and H. Y. Naim (2009). "Domains in biological membranes." Experimental Cell Research **315**: 2871-2878.

Liu, W., E. Crocker, et al. (2003). "Role of side-chain conformational entropy in transmembrane helix dimerization of Glycophorin A." Biophysical Journal **84**: 1263-1271.

Lodish, H., A. Berk, et al. (2000). Molecular Cell Biology, 4th edition. New York, W. H. Freeman.

Loening, A. M., T. D. Fenn, et al. (2006). "Consensus guided mutagenesis of Renilla luciferase yields enhanced stability and light output." Protein Engineering, Design & Selection **19**: 391-400.

Luneberg, J., M. Widmann, et al. (1998). "Secondary structure of bacteriorhodopsin fragments. External sequence constraints specify the conformation of transmembrane helices." The Journal of Biological Chemistry **273**: 28822-28830.

Luo, W., Y. Wang, et al. (2007). "p24A, a type I transmembrane protein, controls ARF-1-dependent resensitization of protease-activated receptor-2 by influence on receptor trafficking." The Journal of Biological Chemistry **282**: 30246-30255.

MacKenzie, K. R. (2006). "Folding and stability of a-helical integral membrane proteins." Chemical Reviews **106**: 1931-1977.

MacKenzie, K. R. and D. M. Engelman (1998). "Structure-based prediction of the stability of transmembrane helix-helix interactions: the sequence dependence of glycophorin A dimerization." Proceedings of the National Academy of Science USA **95**: 3583-3590.

MacKenzie, K. R., J. H. Prestegard, et al. (1997). "A transmembrane helix dimer: structure and implications." Science **276**: 131-133.

Madeo, F., E. Fröhlich, et al. (1997). "A yeast mutant showing diagnostic early markers of early and late apoptosis." The Journal of Cell Biology **139**: 729-734.

Maeda, T., N. Mochizuki, et al. (1990). "Adenylyl cyclase is dispensable for vegetative cell growth in the fission yeast Schizosaccharomyces pombe." Proceedings of the National Academy of Science USA **87**: 7814-7818.

Marti, T. (1998). "Refolding of bacteriorhodopsin from expressed polypeptide fragments." The Journal of Biological Chemistry **273**: 9312-9322.

Martin, N. P., L. M. Leavitt, et al. (1999). "Assembly of G protein-coupled receptors from fragments: identification of functional receptors with discontinuities in each of the loops connecting transmembrane segments." Biochemistry **38**: 682-695.

Martinez-Gil, L., A. Sauri, et al. (2011). "Membrane protein integration into the endoplasmic reticulum." The FEBS journal **Epub ahead of print**

Matia, A. M., J. Sotelo, et al. (2011). The RNA binding protein Csx1 regulates sexual differentiation in fission yeast. The Sixth International Fission Yeast Meeting. Boston, MA.

Maundrell, K. (1993). "Thiamine-respressible expression vectors pREP and pRIP for fission yeast." Gene **123**: 127-130.

Maurice, P., M. Kamal, et al. (2011). "Asymmetry of GPCR oligomers supports their functional relevance." Trends in Pharmacological Sciences **Epub ahead of print**.

Mayor, S. and R. E. Pagano (2007). "Pathways of clathrin-independent endocytosis." Nature Reviews Molecular Cell Biology **8**: 2007.

Mazna, P., L. Grycova, et al. (2008). "The role of proline residues in the structure and function of human MT2 melatonin receptor." Journal of Pineal Research **45**: 361-372.

McCann, E. C. (2010). Investigating the role of the Mam2 C-terminal tail in the pheromone-signalling pathway of Schizosaccharomyces pombe. PhD, University of Warwick.

McClain, M. S., H. Iwamoto, et al. (2003). "Essential role of a GXXXG motif for membrane channel formation by Heliobacter pylori vacuolating toxin." The Journal of Biological Chemistry **278**: 12101-12108.

McLatchie, L. M., N. J. Fraser, et al. (1998). "RAMPs regulate the transport and ligand specificity of the calcitonin-receptor-like receptor." Nature **393**: 333-339.

Miller, E. A., T. H. Beilharz, et al. (2003). "Multiple cargo binding sites on the COPII subunit Sec24p ensure capture of diverse membrane proteins into transport vesicles." Cell **114**: 497-509.

Miller, J. H. (1972). Experiments in molecular genetics, Cold Spring Harbor Laboratory Press.

Milligan, G. and M. Bouvier (2005). "Methods to monitor the quaternary structure of G protein-coupled receptors." The FEBS journal **272**: 2914-2925.

Milligan, G., D. Ramsay, et al. (2003). "GPCR dimerisation." Life Sciences **74**: 181-188.

Moreno, S., A. Klar, et al. (1991). "Molecular genetic analysis of fission yeast Schizosaccharomyces pombe." Methods in enzymology **194**: 795-823.

Moser, B., M. Wolf, et al. (2004). "Chemokines: multiple levels of leukocyte migration control." Trends in immunology **25**: 75-84.

Mothes, W., S. U. Heinrich, et al. (1997). "Molecular mechanisms of membrane protein integration into the endoplasmic reticulum." Cell **89**: 523-533.

Mousavi, S. A., L. Malerod, et al. (2004). "Clathrin-dependent endocytosis." The Biochemical Journal **377**: 1-16.

Murakami, M. and T. Kouyama (2008). "Crystal structure of squid rhodopsin." Nature **453**: 363-367.

Naylor, L. H. (1999). "Reporter gene technology: the future looks bright." Biochemical Pharmacology **58**: 749-757.

Neumoin, A., B. Arshava, et al. (2007). "NMR studies in dodecylphosphocholine of a fragment containing the seventh transmembrane helix of a G-protein-coupled receptor from Saccharomyces cerevisiae." Biophysical Journal **93**: 467-482.

Neumoin, A., L. S. Cohen, et al. (2009). "Structure of a double transmembrane fragment of a G-protein-coupled receptor in micelles." Biophysical Journal **96**: 3187-3196.

Neves, S. R., P. T. Rarn, et al. (2002). "G protein pathways." Science **296**: 1636-1639.

Niccoli, T., M. Arellano, et al. (2003). "Role of Tea1p, Tea3p and Pom1p in the determination of cell ends in Schizosaccharomyces pombe." Yeast **16**: 1349-1358.

Nichtl, A., J. Buchner, et al. (1998). "Folding and association of beta-galactosidase." Journal of Molecular Biology **282**: 1083-1091.

Nielsen, O. (2004). Mating type control and differentiation. The Molecular Biology of Schizosaccharomyces pombe. R. Egel, Springer**:** 281-296.

Nilsson, I. M. and G. von Heijne (1998). "Breaking the camel's back: proline-induced turns in a model transmembrane helix." Journal of Molecular Biology **284**: 1185-1189.

Nishimura, N., H. Plutner, et al. (2002). "The delta subunit of AP-3 is required for efficient transport of VSV-G from the trans-Golgi network to the cell-surface." Proceedings of the National Academy of Science USA **99**: 6755-6760.

Oakley, R. H., S. A. Laporte, et al. (1999). "Association of beta-arrestin with G protein-coupled receptors during clathrin-mediated endocytosis dictates the profile of receptor resensitization." The Journal of Biological Chemistry **274**: 32248-322457.

Obara, T., M. Nakafuku, et al. (1991). "Isolation and characterization of a gene encoding a G-protein α subunit from

Schizosaccharomyces pombe: Involvement in mating and sporulation pathwa." Proceedings of the National Academy of Science USA **88**: 5879-5881.

Okazaki, K., N. Okazaki, et al. (1990). "High-frequency transformation method and library transducing vectors for cloning mammalian cDNAs by trans-complementation of Schizosaccharomyces pombe." Nucleic Acids Research **18**: 6485-6489.

Overington, J. P., B. Al-Lazikani, et al. (2006). "How many drug targets are there?" Nature Reviews Drug Discovery **5**: 993-996.

Overton, M. C. and K. J. Blumer (2000). "G-protein-coupled receptors function as oligomers in vivo." Current Biology **10** 341-344.

Overton, M. C. and K. J. Blumer (2002). "The extracellular N-terminal domain and transmembrane domains 1 and 2 mediate oligomerization of a yeast G protein-coupled receptor." The Journal of Biological Chemistry **277** 41463-41472.

Overton, M. C., S. L. Chinault, et al. (2003). "Oligomerization, biogenesis, and signaling is promoted by a glycophorin A-like dimerisation motif in transmembrane domain 1 of a yeast G-protein coupled receptor." The Journal of Biological Chemistry **278** 49369-49377.

Padte, N. N., S. G. Martin, et al. (2006). "The cell-end factor pom1p inhibits mid1p in specification of the cell division plane in fission yeast." Current Biology **16**: 2480-2487.

Palczewski, K., T. Kumasaka, et al. (2000). "Crystal structure of rhodopsin: A G protein-coupled receptor." Science **289** 739-745.

Pan, K. Z., T. E. Saunders, et al. (2011). Construction of a dynamic, robust pom1p kinase gradient in fission yeast cells. The 6th international fission yeast meeting. Boston, MA.

Pang, T., C. G. Savva, et al. (2009). "Structure of the lethal phage pinhole." Proceedings of the National Academy of Science USA **106**: 18966-18971.

Papadaki, P., V. pizon, et al. (2002). "Two Ras pathways in fission yeast are differentially regulated by two ras guanine nucleotide exchange factors " Mol Cell Biol **22**: 4598-4606.

Parameswara, V. K. and W. S. Spielman (2006). "RAMPs: the past, present and future " Trends in Biochemical Sciences **31**: 631-638.

Park, A. R. and D. K. Oh (2010). "Galacto-oligosaccharide production using microbial beta-galactosidase: current state and perspectives." Applied Microbiology and Biotechnology **85**: 1279-1286.

Park, J. H., P. Scheerer, et al. (2008). "Crystal structure of the ligand-free G-protein-coupled receptor opsin." Nature **454**: 183-187.

Park, P. S., S. Filipek, et al. (2004). "Oligomerization of G protein-coupled receptors: Past, present and future." Biochemistry **43** 15643-15656.

Parrish, W., M. Eilers, et al. (2002). "The cytoplasmic end of transmembrane domain 3 regulates the activity of the Saccharomyces cerevisiae G-protein coupled receptor." Genetics **160**: 429-443.

Parton, R. G. and K. Simons (2007). "The multiple faces of caveolae." Nature Reviews Molecular Cell Biology **8**: 185-194.

Partridge, A. W., A. G. Therien, et al. (2004). "Missense mutations in transmembrane domains of proteins: phenotypic propensity of polar residues for human disease." Proteins **54**: 648-656.

Pashkov, V., J. Huang, et al. (2011). "Regulator of G protein signaling (RGS16) inhibits hepatic fatty acid oxidation in a carbohydrate response element-binding protein (ChREBP)-dependent manner." The Journal of Biological Chemistry **286**(17).

Pelkmans, L., J. Kartenbeck, et al. (2001). "Caveolar endocytosis of simian virus 40 reveals a new two-step vesicular transport pathway to the ER." Nature cell biology **3**: 473-483.

Percherancier, Y., A. Yamina, et al. (2005). "Bioluminescence Resonance Energy Transfer Reveals Ligand-induced Conformational Changes in CXCR4 Homo- and Heterodimers." The Journal of Biological Chemistry **280**: 9895-9903.

Pereira, P. S. and N. Jones, C. (2001). "The RGS domain-containing fission yeast protein, Rgs1p, regulates pheromone signalling and is required for mating." Genes to Cells **6**: 789-802.

Pierce, K. L., R. T. Premont, et al. (2002). "Seven-transmembrane receptors." Nature Reviews Molecular Cell Biology **3**: 639-650.

Plo, I., Y. Zhang, et al. (2009). "An activating mutation in the CSF3R gene induces a hereditary chronic neutrophila." The Journal of Experimental Medicine **206**: 1701-1707.

Popot, J. L. and D. M. Engelman (1990). "Membrane protein folding and oligomerization: the two-stage model." Biochemistry **29** 4031-4037.

Popot, J. L., S. E. Gerchman, et al. (1987). "Refolding of bacteriorhodopsin in lipid bilayers. A thermodynamically controlled two-stage process." Journal of Molecular Biology **198**: 655-676.

Promega (2009). "Renilla Luciferase Assay System Technical Manual #TM244."

Promega. (2011). "Which plates should I choose for fluorescence and luminescence measurements?", from http://www.promega.com/resources/articles/pubhub/which-plates-to-choose-for-fluorescence-and-luminescence-measurements/.

Rasmussen, S. G., H. J. Choi, et al. (2007). "Crystal structure of the human beta2 adrenergic G-protein-coupled receptor." Nature **450**: 383-387.

Reiersen, H. and R. A. Rees (2001). "The hunchback and its neighbours: proline as an environmental modulator." TRENDS in Biochemical Sciences **26**: 679-684.

Reis, R. I., E. L. Santos, et al. (2007). "Participation of transmembrane proline 82 in angiotensin II AT1 receptor signal transduction." Regul Pept **140**: 32-36.

Resat, H., T. P. Straatsma, et al. (2001). "The arginine finger of RasGAP helps Gln-61 align the nucleophileic water in GAP-stimulated hydrolysis of GTP." Proceedings of the National Academy of Science USA **98**: 6033-6038.

Ridge, K. D., S. S. Lee, et al. (1995). "In vivo assembly of rhodopsin from expressed polypeptide fragments." Proceedings of the National Academy of Science USA **92**: 3204-3208.

Rocheville, M., D. C. Lange, et al. (2000). "Subtypes of the somatostatin receptor assemble as functional homo- and heterodimers." The Journal of Biological Chemistry **275**: 7862-7869.

Romano, C., W. Yang, et al. (1996). "Metabotropic glutamate receptor 5 is a disulfide-linked dimer." The Journal of Biological Chemistry **271**: 28612-28616.

Rosenbaum, D. M., V. Cherezov, et al. (2007). "GPCR engineering yields high-resolution structural insights into beta2-adrenergic receptor function." Science **318**: 1266-1273.

Rosenbaum, D. M., S. G. Rasmussen, et al. (2009). "The structure and function of G-protein-coupled receptors." Nature **459**.

Roth, M. G. (2006). "Clathrin-mediated endocytosis before fluorescent proteins." Nature Reviews Molecular Cell Biology **7**: 63-68.

Russ, P. W. and D. M. Engelman (1999). "TOXCAT: A measure of transmembrane helix association in a biological membrane." Proceedings of the National Academy of Science USA **96** 863-868.

Russ, P. W. and D. M. Engelman (2000). "The GxxxG motif: a framework for transmembrane helix-helix association." Journal of Molecular Biology **296**: 911-919.

Sambrook, J., E. Fritsch, et al. (1989). Molecular cloning, a laboratory manual, Cold Spring Harbour Laboratory Press.

Sambrook, J. and D. W. Russel (2001). Molecular cloning: a laboratory manual, Cold spring harbor, N.Y.: Cold Spring Harbor Laboratory Press.

Sander, P., S. Grünewald, et al. (1994). "Expression of the human D2S dopamine receptor in the yeasts Saccharomyces cerevisiae and Schizosaccharomyces pombe: a comparative study." FEBS Letters **344**: 41-46.

Sanders, C. R. and J. K. Myers (2004). "Disease-related misassembly of membrane proteins." Annual Review of Biophysics and Biomolecular Structure **33**: 25-51.

Sandvig, K., S. Pust, et al. (2011). "Clathrin-independent endocytosis: mechanisms and function." Current Opinion in Cell Biology **23**: 1-8.

Sato, M., J. B. Blumer, et al. (2006). "Accessory proteins for G proteins: partners in signaling." Annual Review of Pharmacology and Toxicology **46**: 151-187.

Scarselli, M. and J. G. Donaldson (2009). "Constitutive internalization of G protein-coupled receptors and G proteins via clathrin-independent endocytosis." The Journal of Biological Chemistry **284**: 3577-3585.

Scheerer, P., J. H. Park, et al. (2008). "Crystal structure of opsin in its G-protein-interacting conformation." Nature **455**: 497-502.

Schneider, D. and D. Engelman (2004). "Motifs of two small residues can assist but are not sufficient to mediate transmembrane helix interactions." Journal of Molecular Biology **343** 799-804.

Schneider, D. and D. M. Engelman (2003). "GALLEX, a measurement of heterologous association of transmembrane helices in a biological membrane." Journal of Biological Chemistry **278**: 3105-3111.

Schwartz, T. W., T. M. Frimurer, et al. (2006). "Molecular mechanism of 7TM receptor activation - a global toggle switch model." Annual Review of Pharmacology and Toxicology **46**: 481-519.

Seifert, R. and K. Wenzel-Seifert (2002). "Constitutive activity of G-protein-coupled receptors: cause of disease and common property of wild-type receptors." Naunyn-Schmiedeberg's Archives of Pharmacology **366**: 381-416.

Senes, A., M. Gerstein, et al. (2000). "Statistical analysis of amino acid patterns in transmembrane helices: the GxxxG motif occurs frequently and in association with beta-branched residues at neighbouring positions." Journal of Molecular Biology **296**: 921-936.

Serebriiskii, I. G. and E. A. Golemis (2000). "Uses of lacZ to study gene function: evaluation of β-galactosidase assays employed in the yeast two-hybrid system." Analytical Biochemistry **285**: 1-15.

Severin, F. F. and A. A. Hyman (2002). "Pheromone induces programmed cell death in Sc. cerevisiae." Current Biology **12**: 233-235.

Sharifmoghadam, M. R., P. Bustos-Sanmamed, et al. (2006). "The fission yeast Map4 protein is a novel adhesin required for mating." FEBS Letters. **580**: 4457-4462.

Shenoy, S. K., M. T. Drake, et al. (2006). "beta-arrestin-dependent, G protein-independent ERK1/2 activation by the beta2 adrenergic receptor." The Journal of Biological Chemistry **281**: 1261-1273.

Shi, L., G. Liapakis, et al. (2002). "β2 Adrenergic Receptor Activation. Modulation of the proline kink in transmembrane 6 by a rotamer toggle switch " The Journal of Biological Chemistry **277**: 40989-40996.

Shi, C., M. Paige, et al. (2009). "In vitro characterization of ligand-induced oligomerization of the S. cerevisiae G-protein coupled receptor, Ste2p." Biochimica et Biophysica Acta **1790**: 1-7.

Sigismund, S., E. Argenzio, et al. (2008). "Clathrin-mediated internalization is essential for sustained EGFR signaling but dispensable for degradation." Developmental Cell **15**: 209-219.

Sigismund, S., T. Woelk, et al. (2005). "Clathrin-independent endocytosis of ubiquitinated cargos." Proceedings of the National Academy of Science USA **102**: 276-2765.

Singer, S. J. and G. L. Nicolson (1972). "The fluid mosaic model of the structure of cell membranes." Science **175**: 720-731.

Sipiczki, M. (1988). "The role of sterility genes (ste and aff) in the initiation of sexual development in Schizosaccharomyces pombe." Molecular genetics and genomics **213**: 529-534.

Sipiczki, M. (2000). "Where does fission yeast sit on the tree of life?" Genome Biology **1**: Epub.

Skrabanek, L., M. Murcia, et al. (2007). "Requirements and ontology for a G protein-coupled receptor knowledge base." BMC Bioinformatics **8**: 1-20.

Skulachev, V. P. (2002). "Programmed death in yeast as adaptation?" FEBS Letters. **528**: 23-26.

Smith, B. (2009). G Protein-Mediated Signalling in Eukaryotic Cells. PhD, University of Warwick.

Smith, B., C. Hill, et al. (2009). "Dual positive and negative regulation of GPCR signaling by GTP hydrolysis." Cellular Signalling **21**: 1151-1160.

Sodt, A. J. and T. Head-Gordon (2010). "Driving forces for transmembrane alpha-helix oligomerization." Biophysical Journal **99**: 227-237.

Steiner, S., R. Muff, et al. (2002). "The transmembrane domain of receptor-activity-modifying protein 1 is essential for the functional expression of a calcitonin gene-related peptide receptor." Biochemistry **41**: 11398-11404.

Sugimoto, A., Y. Iino, et al. (1991). "Schizosachharomyces pombe ste11+ encodes a transcription factor with an HMG motif that is a critical regulator of sexual development." Genes and Development **5**: 1990-1999.

Sulistijo, E. S., T. M. Jaszewski, et al. (2003). "Sequence-specific dimerization of the transmembrane domain of the "BH3-only" protein BNIP3 in membranes and detergent." Journal of Biological Chemistry **278**: 51950-51956.

Sung, C. H., C. M. Davenport, et al. (1993). "Rhodopsin mutations responsible for autosomal-dominant retinitis-pigmentosa - clustering of functional classes along the polypeptide chain." The Journal of Biological Chemistry **268**: 26645-26649.

Takegawa, K., T. Iwaki, et al. (2003). "Vesicle-mediated protein transport pathways to the vacuole in Schizosaccharomyces pombe." Cell Structure and Function **28**: 399-417.

Tanaka, K., J. Davey, et al. (1993). "Schizosaccharomyces pombe map3+ Encodes the Putative M-Factor Receptor." Molecular and Cellular Biology **13**: 80-88.

Tanford, C. (1978). "The hydrophobic effect and the organization of living matter." Science **200**: 1012-1018.

Tantry, S., F. X. Ding, et al. (2010). "Binding of fluorinated phenylalanine a-factor analogues to ste2p: evidence for a cation-pi binding interaction between a peptide ligand and its cognate g protein-coupled receptor." Biochemistry **49**: 5007-5015.

Terrillon, S. and M. Bouvier (2004). "Roles of G-protein-coupled receptor dimerization. From ontogeny to signalling regulation." Embo rep **5**: 30-34.

Thompson, D. M. and R. Parker (2009). "The RNase Rny1p cleaves tRNAs and promotes cell death during oxidative stress in Saccharomyces cerevisiae." The Journal of Cell Biology **185**: 43-50.

Thomsen, P., K. Roepstorff, et al. (2002). "Caveolae are highly immbole plasma membrane microdomains, which are not involved in constitutive endocytic trafficking." Molecular Biology of the Cell **13**: 238-250.

Tobin, A. B., A. J. Butcher, et al. (2008). "Location, location, location...site-specific GPCR phosphorylation offers a mechanism for cell-type-specific signalling." Trends in Pharmacological Sciences **29**: 413-420.

Towbin, H., T. Staehelin, et al. (1979). "Electrophoretic transfer of proteins from polyacrylamide gels to nitrocellulose sheets: procedure and some applications." Proceedings of the National Academy of Science USA **76**: 4350-4354.

Toyoshima, C., M. Nakasako, et al. (2000). "Crystal structure of the calcium pump of sarcoplasmic reticulum at 2.6 Å." Nature **405**: 647-655.

Traub, L. M. (2005). "Common principles in clathrin-mediated sorting at the Golgi and the plasma membrane." Biochimica et Biophysica Acta **1744**: 415-437.

Tsai, B., Y. Ye, et al. (2002). "Retro-translocation of proteins from the endoplasmic reticulum into the cytosol." Nature Reviews Molecular Cell Biology.

Tsien, R. (1998). "The green fluorescent protein." Annual Review of Biochemistry **67**: 509-544.

Uhlenbrock, K., H. Gassenhuber, et al. (2002). "Sphingosine 1-phosphate is a ligand of the human gpr3, gpr6 and gpr12 family of constitutively active G protein-coupled receptors." Cellular Signalling **14**: 941-953.

Unger, V. M., P. A. Hargrave, et al. (1997). "Arrangement of rhodopsin transmembrane alpha-helices." Nature **389**: 203-206.

van Voorst, F. and B. De Kruijff (2000). "Role of lipids in the translocation of proteins across membranes." Biochemical Journal **347**: 601-612.

Venisnik, K. M., T. Olafsen, et al. (2006). "Bifunctional antibody-Renilla luciferase fusion protein for in vivo optical detection of tumors." Protein Engineering, Design & Selection **19**: 453-460.

Verde, F., D. J. Wiley, et al. (1998). "Fission yeast orb6, a ser/thr protein kinase related to mammalian rho kinase and muotonic dystrophy kinase, is required for maintenance of cell polarity and coordinates cell morphogenesis with the cell cycle." Proceedings of the National Academy of Science USA **95**: 7526-7531.

Vidi, P.-A. and V. J. Watts (2009). "Fluorescent and bioluminescent protein-fragment complementation assays in the study of G protein-coupled receptor oligomerization and signaling." Molecular pharmacology **75**: 733-739.

Vilardaga, J. P., V. O. Nikolaev, et al. (2008). "Conformational cross-talk between alpha2A-adrenergic and mu-opioid receptors controls cell signaling." Nature chemical biology **4**: 126-131.

Violin, J. D. (2006). "G-protein coupled receptor kinase specificity for beta-arrestin recruitment to the beta2-adrenergic receptor revealed by fluorescence resonance energy transfer." The Journal of Biological Chemistry **281**: 20577-20588.

von Heijne, G. (1990). "The signal peptide." Journal of Membrane biology **115**: 195-201.

von Heijne, G. (1999). "Recent advances in the understanding of membrane protein assembly and structure." Quarterly Reviews of Biophysics **32**: 285-307.

Vroling, B., M. Sanders, et al. (2010). "GPCRDB: information system for G protein-coupled receptors." Nucleic Acids Research **D309-19**.

Waldhoer, M., J. Fong, et al. (2005). "A heterodimer-selective agonist shows in vivo relevance of G protein-coupled receptor dimers." Proceedings of the National Academy of Science USA **102**: 9050-9055.

Wang, H. and J. Konopka (2009). "Identification of amino acids at two dimer interface regions of the alpha-factor receptor (Ste2)." Biochemistry **48**: 7132-7139.

Wang, J., U. Golebiewska, et al. (2009). "A self-scaffolding model for G protein signaling." Journal of Molecular Biology **387**: 92-103.

Warne, T., M. J. Serrano-Vega, et al. (2008). "Structure of a beta1-adrenergic G-protein-coupled receptor." Nature **454**: 486-491.

Watson, P., K. Davis, et al. (1999). "An RGS protein regulates the pheromone response in the fission yeast

Schizosaccharomyces pombe." Molecular Microbiology **33**: 623-634.

Welton, R. M. and C. S. Hoffman (2000). "Glucose monitoring in fission yeast via the Gpa2 Gα the git5 Gβ and the git3 putative glucose receptor." Genetics **156**: 513-521.

White, J., A. Wise, et al. (1998). "Heterodimerization is required for the formation of a functional GABA(B) receptor." Nature **396**: 692-630.

White, S. H. (2003). "Translocons, thermodynamics, and the folding of membrane proteins." FEBS Letters **555**: 116-121.

White, S. H. and W. C. Wimley (1999). "Membrane protein folding and stability: physical principles." Annual Review of Biophysics and Biomolecular Structure **28**: 319-365.

Whiteway, M., L. Hougan, et al. (1989). "The STE4 and STE18 genes of yeast encode potential beta and gamma subunits of the mating factor receptor-coupled G protein." Cell **56**: 467-477.

Willingham, M. C. and I. H. Pastan (1982). "Transit of epidermal growth factor through coated pits of the Golgi system." The Journal of Cell Biology **94**: 207-212.

Wood, J., G. Kwon, et al. (2011). An investigation of novel cell cycle transcription factors in fission yeast. The sixth international fission yeast meeting. Boston, MA.

Wood, V. (2006). "Schizosaccharomyces pombe comparative genomics, from sequence to systems." Topics in Current Genetics **15**: 233-285.

Wood, V. (2011). "http://www.pombase.org."

Wu, B., E. Y. Chien, et al. (2010). "Structures of the CXCR4 chemokine GPCR with small-molecule and cyclic peptide antagonists." Science **330**: 1066-1071.

Xu, F., H. Wu, et al. (2011). "Structure of an agonist-bound human A2A adenosine receptor." Science **332**: 322-327.

Xue-Franzen, Y., S. Kjaerulff, et al. (2006). "Genomewide identification of pheromone-targeted transcription in fission yeast." BMC Genomics **303**: 303.

Yamamoto, M. (2004). Initiation of meiosis. The molecular biology of Schizosaccharomyces pombe. R. Egel, Springer**:** 281-296.

Yang, P., Y. Qyang, et al. (2003). "The novel Rho GTase-activating protein family protein, Rga8, provides a potential link between Cdc42/p21-activated kinase and Rho signaling pathways in the fission yeast, *Schizosaccharomyces pombe*." The Journal of Biological Chemistry **278**: 48821-48830.

Yeagle, P. L., M. Bennett, et al. (2007). "Transmembrane helices of membrane proteins may flex to satisfy hydrophobic mismatch." Biochimica et Biophysica Acta **1768**: 530-537.

Yohannan, S., S. Faham, et al. (2003). "The evolution of transmembrane helix kinks and the structural diversity of G protein-coupled receptors." Proceedings of the National Academy of Science USA **101**: 959-963.

Zaugg, M. and M. C. Schaub (2004). "Cellular mechanisms in sympatho-modulation of the heart." British journal of anaesthesia **93**: 34-52.

Zhou, F. X., M. J. Cocco, et al. (2000). "Interhelical hydrogen bonding drives strong interactions in membrane proteins." Nature Structural Biology **7**: 154-160.

Zhou, F. X., H. J. Merianos, et al. (2001). "Polar residues drive association of polyleucine transmembrane helices." Proceedings of the National Academy of Science USA **98**: 2250-2255.

Zimmer, C., B. Zhang, et al. (2006). "On the digital trail of mobile cells." IEEE Signal Processing Magazine **23**: 54-62.